

NEXT GENERATION TRAFFIC SIGNAL PERFORMANCE MEASURES

Leveraging Connected Vehicle Data



Enrique D. Saldivar-Carranza, Howell Li, Jijo K. Mathew, Jairaj Desai, Tom Platte, Saumabha Gayen, James Sturdevant, Mark Taylor, Charles Fisher, and Darcy M. Bullock



NEXT GENERATION TRAFFIC SIGNAL PERFORMANCE MEASURES

Leveraging Connected Vehicle Data

Enrique D. Saldivar-Carranza, Howell Li, Jijo K. Mathew, Jairaj Desai, Tom Platte,
Saumabha Gayen, James Sturdevant, Mark Taylor, Charles Fisher, and Darcy M. Bullock

Recommended Citation

Saldivar-Carranza, E. D., Li, H., Mathew, J. K., Desai, J., Platte, T., Gayen, S., Sturdevant, J., Taylor, M., Fisher, C., & Bullock, D. M. (2023). *Next generation traffic signal performance measures: Leveraging connected vehicle data*. West Lafayette, IN: Purdue University. <https://doi.org/10.5703/1288284317625>

Acknowledgments

This work was supported in part by the Joint Transportation Research Program and Pooled Fund Study (TPF-5(377)) led by the Indiana Department of Transportation (INDOT) and supported by the state transportation agencies of California, Connecticut, Georgia, Minnesota, North Carolina, Ohio, Pennsylvania, Texas, Utah, Wisconsin, plus the City of College Station, Texas, and the FHWA Operations Technical Services Team.

The authors wish to thank the many agencies, practitioners, and colleagues, particularly Margaret Hunter, Benjamin Scholer, and Woosung Kim, that collaborated in the development of the performance measures and different techniques that are summarized in this monograph. The connected vehicle trajectory and event data used in this study was provided by Wejo Data Services, Inc.

The contents of this report reflect the views of the authors, who are responsible for the facts and the accuracy of the data presented herein, and do not necessarily reflect the official views or policies of the sponsoring organizations. These contents do not constitute a standard, specification, or regulation.

Abstract

High-resolution connected vehicle (CV) trajectory and event data has recently become commercially available. With over 500 billion vehicle position records generated each month in the United States, these data sets provide unique opportunities to build on and expand previous advances on traffic signal performance measures and safety evaluation. This report is a synthesis of research focused on the development of CV-based performance measures. A discussion is provided on data requirements, such as acquisition, storage, and access. Subsequently, techniques to reference vehicle trajectories to relevant roadways and movements are presented. This allows for performance analyses that can range from the movement- to the system-level. A comprehensive suite of methodologies to evaluate signal performance using vehicle trajectories is then provided. Finally, uses of CV hard-braking and hard-acceleration event data to assess safety and driver behavior are discussed. To evaluate scalability and test the proposed techniques, performance measures for over 4,700 traffic signals were estimated using more than 910 million vehicle trajectories and 14 billion GPS points in all 50 states and Washington, D.C. The contents of this report will help the industry transition towards a hybrid blend of detector- and CV-based signal performance estimations with rigorously defined performance measures that have been peer-reviewed by both academics and industry leaders.

Authors

Enrique D. Saldivar-Carranza

Graduate Research Assistant
Lyles School of Civil Engineering, Purdue University
(765) 250-1070
esaldiva@purdue.edu
Corresponding Author

Howell Li

JTRP Principal Research Analyst
Lyles School of Civil Engineering, Purdue University

Jijo K. Mathew, PhD

JTRP Transportation Research Engineer
Lyles School of Civil Engineering, Purdue University

Jairaj Desai, PhD

JTRP Transportation Research Engineer
Lyles School of Civil Engineering, Purdue University

Tom Platte

Senior Signal Systems Field Engineer
Indiana Department of Transportation

Saumabha Gayen

Graduate Research Assistant
Lyles School of Civil Engineering, Purdue University

James Sturdevant, PE

Director of Traffic Management
Indiana Department of Transportation

Mark Taylor, PE

Traffic Signal Operations Engineer
Utah Department of Transportation

Charles Fisher, PE

Statewide Traffic Operations Engineer
Ohio Department of Transportation

Darcy M. Bullock, PhD, PE

Lyles Family Professor of Civil Engineering
JTRP Director
Lyles School of Civil Engineering,
Purdue University

EXECUTIVE SUMMARY

Motivation

Traffic signals have significant impacts on mobility. It is therefore important for agencies to have scalable techniques to monitor the performance of traffic signals and prioritize their maintenance and retiming activities.

During the last decade, substantial efforts have been focused on the development and adoption of Automated Traffic Signal Performance Measures (ATSPMs). These detector-based techniques use high-resolution (i.e., tenth-of-a-second) controller event logs and rely on communication equipment to collect data that is used for report generation. The Utah Department of Transportation (UDOT) has taken the lead in the development of an open-source implementation of ATSPMs, and virtually all traffic signal vendors now incorporate high-resolution data logging in their controllers and offer ATSPM capability as an option in their central systems.

ATSPMs require significant capital investments for network-wide deployment and can be a barrier for some agencies to adopt these techniques. Furthermore, depending on the speed limit, volumes, movements at a facility, and the various types of detection technology available, not all traffic use cases may be captured at every approach because of the instrumentation and mode of operation. Connected vehicle (CV) data can complement infrastructure-based ATSPMs.

Connected Vehicle Trajectory-based Traffic Signal Performances Measures

Recently, high-resolution CV trajectory data, comprised of journey-based vehicle trajectories with reporting intervals in the order of seconds, has become commercially available. With over 500 billion vehicle position records generated each month in the United States, and with a spatial accuracy of 3.0 meters (~10 ft.) for each datapoint, this data set provides unique opportunities to build on and expand previous advances in traffic signal performance measures. This report details the work of the multi-state Transportation Pooled Fund (TPF) team to develop a suite of performance measures that estimate split failures, arrivals on green, downstream blockage, travel time, and level of service derived from CV trajectory data.

Throughout this project, the team has produced 14 technical papers that have discussed CV data sets, trajectory processing, derivation of performance measures, and use cases applied to a variety of intersections and configurations. The techniques have been piloted at almost 5,000 signals in all 50 states and Washington, D.C., to demonstrate and confirm scalability. This report summarizes lessons learned and key research findings. The manuscript is designed to complement preceding Pooled Fund Study (TPF-5(258)) reports (1, 2), also known as “blue books”, and is organized in the following chapters.

- Chapter 1 provides context on the current state of traffic signal performance assessment and lists benefits of utilizing commercial CV data.
- Chapter 2 discusses the CV data sets’ attributes, limitations, and management. This chapter includes a discussion of cloud resources and how this approach can be particularly important for the handling of data since it can quickly adapt to various needs and process large volumes of data.

- Chapter 3 presents geographical representations of raw CV data and a technique to linear reference vehicle trajectories along roads. The linear referencing process is a fundamental requirement for efficiently deriving CV-based performance measures since it allows for the mapping of operational conditions in relation to points of interest, such as the far side of an intersection.
- Chapter 4 describes techniques to assign intersection movements to vehicle trajectories, which is necessary for movement-level performance analysis (3).
- Chapter 5 introduces a trajectory-based visualization, called Purdue Probe Diagram (PPD), from which delay, arrivals on green, split failures, and downstream blockage at the movement-level can be estimated (4). This chapter also compares arrivals on green (AOG) derived with the new PPD and the traditional detector-based Purdue Coordination Diagram (PCD) (5).
- Chapter 6 discusses techniques to calculate trajectory-derived arterial travel times (6, 7). Corridor-level travel time gives valuable information for before-after studies and the resiliency of the intersection systems.
- Chapter 7 presents visualizations to evaluate traffic signal performance at the arterial- (8) and system-level. Since the CV-based analysis of four performance measures at a signal generates approximately 3,072 measures for 8 movements over 96 15-minute intervals, a corridor of 10 intersections generates over 30,000 performance datapoints. This chapter describes efficient tools developed to visualize this level of information at-a-glance.
- Chapter 8 provides before-after studies that show corridor performance changes as a result of diversions (9) and signal control upgrades (10). This chapter outlines frameworks that can be used to assess the impacts of increased demand as well as the deployment of any system improvement, ranging from simple retiming to more extensive investments such as added turn lanes, upgraded detection, or the implementation of adaptive signal systems.
- Chapter 9 presents a technique to identify systemwide signal retiming opportunities (11). The technique evaluates all movements at each signalized intersection using CV trajectory data to locate operational challenges and opportunities to reallocate green time to reduce split failures. This approach can help agencies focus engineering resources for retiming activities on locations that have the greatest potential to improve operations.
- Chapter 10 discusses CV-based methodologies to evaluate the performance of tightly-coupled and alternative intersections (12–14). This includes three- and four-phase diamond interchanges, diverging diamond interchanges, and continuous flow intersections.
- Chapter 11 provides a framework to evaluate roundabout performance from CV trajectory data (15). Although roundabouts are not controlled by signals, most of the same performance fundamentals can be applied to roundabouts. These techniques are particularly useful for applying at locations adjacent to signalized corridors in order to provide consistent systemwide operational assessment at a movement- and time-of-day (TOD) level.
- Chapter 12 evaluates the use of CV hard-braking (HB) and hard-acceleration (HA) event data to assess safety (16) and driver behavior change (17) at signalized intersection approaches.
- Chapter 13 discusses the scalability capabilities of the presented techniques.

- Chapter 14 provides a summary of the report.
- Appendix A shows 14 arterial-level performance report summaries derived from approximately 4 million vehicle trajectories and 60 million GPS points passing through 157 signals along 12 corridors in 11 states. This appendix provides a summary of how to read these reports and is also published as a standalone reference (8) on the Purdue Open Access Repository along with print quality PDFs of these poster reports. Additionally, a report published in (18) expands on (8) by providing 58 arterial-level performance reports of corridors located in 14 different states.
- Appendix B provides a list of relevant media files that have been used to explain research concepts, evaluate signal operations, and better understand traffic conditions.

Adoption, Implementation, and Dissemination

The PPD, first proposed in 2020 and published in 2021 (4), is now following a similar adoption evolution as the PCD. INRIX subsequently introduced a variation of their own into their Signal Analytics product in 2022 (19). Similarly, various research efforts have referenced and built upon the developed techniques (20–24).

As with past Purdue traffic signal performance measure work, significant efforts have been made to disseminate findings to agencies and industry concurrent with the research. In addition to the technical papers, the team has shared results in several dozen webinars, professional conference presentations, and poster sessions. For example, the Federal Highway Administration (FHWA) hosts monthly webinars with industry, government, and academia participants to disseminate and discuss advances in the traffic signal performance monitoring space. The Purdue team has partnered with the organizers to share findings on several occasions over the course of this research (see table).

Research Results

Several technical papers were prepared throughout the development of the project to facilitate the dissemination of results and accelerate the implementation of relevant findings. The following is a list of these publications, most of which will be further discussed throughout the report.

- Saldivar-Carranza, E. D., Li, H., & Bullock, D. M. (2021). Identifying vehicle turning movements at intersections from trajectory data. *IEEE Intelligent Transportation Systems* (pp. 4043–4050). <https://doi.org/10.1109/ITSC48978.2021.9564781>
- Saldivar-Carranza, E., Li, H., Mathew, J., Hunter, M., Sturdevant, J., & Bullock, D. M. (2021). Deriving operational traffic signal performance measures from vehicle trajectory data. *Transportation Research Record: Journal of the Transportation Research Board*, 2675(9), 1250–1264. <https://doi.org/10.1177/03611981211006725>

- Saldivar-Carranza, E. D., Li, H., Gayen, S., Taylor, M., Sturdevant, J., & Bullock, D. M. (2023). Comparison of arrivals on green estimations from vehicle detection and connected vehicle data. *Transportation Research Record: Journal of the Transportation Research Board*. <https://doi.org/10.1177/03611981231168116>
- Saldivar-Carranza, E. D., Hunter, M., Li, H., Mathew, J., & Bullock, D. M. (2021). Longitudinal performance assessment of traffic signal system impacted by long-term interstate construction diversion using connected vehicle data. *Journal of Transportation Technologies*, 11(4), 644–659. <https://doi.org/10.4236/jtts.2021.114040>
- Desai, J., Saldivar-Carranza, E., Mathew, J. K., Li, H., Platte, T., & Bullock, D. (2021). Methodology for applying connected vehicle data to evaluate impact of interstate construction work zone diversions. *2021 IEEE International Intelligent Transportation Systems Conference (ITSC)* (pp. 4035–4042). <https://doi.org/10.1109/ITSC48978.2021.9564873>
- Saldivar-Carranza, E., Li, H., Mathew, J., Fisher, C., & Bullock, D. M. (2022). Signalized corridor timing plan change assessment using connected vehicle data. *Journal of Transportation Technologies*, 12(3), 310–322. <https://doi.org/10.4236/jtts.2022.123019>
- Saldivar-Carranza, E. D., Li, H., Platte, T., & Bullock, D. M. (2023). Systemwide identification of signal retiming opportunities with connected vehicle data to reduce split failures. *Transportation Research Record: Journal of the Transportation Research Board*. <https://doi.org/10.1177/03611981231168844>
- Saldivar-Carranza, E., Rogers, S., Li, H., & Bullock, D. M. (2022). Diamond interchange performance measures using connected vehicle data. *Journal of Transportation Technologies*, 12(03), 475–497. <https://doi.org/10.4236/jtts.2022.123029>
- Saldivar-Carranza, E. D., Li, H., & Bullock, D. M. (2021). Diverging diamond interchange performance measures using connected vehicle data. *Journal of Transportation Technologies*, 11(4), 628–643. <https://doi.org/10.4236/jtts.2021.114039>
- Saldivar-Carranza, E., Li, H., Taylor, M., & Bullock, D. M. (2022). Continuous flow intersection performance measures using connected vehicle data. *Journal of Transportation Technologies*, 12(04), 861–875. <https://doi.org/10.4236/jtts.2022.124047>
- Saldivar-Carranza, E., Mathew, J. K., Li, H., & Bullock, D. M. (2022). Roundabout performance analysis using connected vehicle data. *Journal of Transportation Technologies*, 12(01), 42–58. <https://doi.org/10.4236/jtts.2022.121003>
- Hunter, M., Saldivar-Carranza, E., Desai, J., Mathew, J. K., Li, H., & Bullock, D. M. (2021). A proactive approach to evaluating intersection safety using hard-braking data. *Journal of Big Data Analytics in Transportation*, 3, 81–94. <https://doi.org/10.1007/s42421-021-00039-y>

Presentations led during FHWA monthly webinars

Date	Topic
March 22, 2021	Deriving operational traffic signal performance measures from vehicle trajectory data
February 28, 2022	Using commercial connected vehicle data for arterial analysis
October 24, 2022	Multi-modal integrated corridor performance measures

- Saldivar-Carranza, E. D., Mathew, J. K., Li, H., Hunter, M., Platte, T., & Bullock, D. M. (2021). Using connected vehicle data to evaluate traffic signal performance and driver behavior after changing left-turns phasing. *2021 IEEE International Intelligent Transportation Systems Conference (ITSC)* (pp. 4028–4034). <https://doi.org/10.1109/ITSC48978.2021.9564654>
- Mathew, J. K., Li, H., Saldivar-Carranza, E., Duffy, M., & Bullock, D. M. (2022). Integrated performance measures for bus rapid transit system and traffic signal systems using trajectory data. *Journal of Transportation Technologies*, *12*(04), 833–860. <https://doi.org/10.4236/jtts.2022.124046>

TABLE OF CONTENTS

1. INTRODUCTION	1
1.1 State-of-the-Practice of Traffic Signal Evaluation	1
1.2 Connected Vehicle Traffic Signal Performance Measures	1
2. CONNECTED VEHICLE DATA	2
2.1 Trajectories	2
2.2 Events	5
2.3 Data Requirements	6
3. DATA EXPLORATION	8
3.1 Trajectories	8
3.2 Events	13
4. MOVEMENT IDENTIFICATION	15
4.1 Geofencing	15
4.2 Data-Driven Movement Detection	16
5. SIGNAL PERFORMANCE MEASURES: PURDUE PROBE DIAGRAM	22
5.1 Delay Performance Measures	22
5.2 Operational Performance Measures	24
5.3 Temporal Performance Assessment	29
6. ARTERIAL TRAVEL TIME	34
6.1 Trip Chaining	34
6.2 Raw Travel Times	34
6.3 Travel Time Outliers Examples	34
6.4 Travel Time Curation	36
6.5 Travel Time Comparison Before and After Curation	37
7. PERFORMANCE REPORTING VISUALIZATIONS	39
7.1 Arterial-Level Evaluation	39
7.2 System-Level Evaluation	40
8. BEFORE-AFTER STUDIES	46
8.1 Highway Work Zone Impact on a Local Arterial	46
8.2 Change in Performance After Signal System Upgrade	50
9. IDENTIFICATION OF SIGNAL RETIMING OPPORTUNITIES TO REDUCE SPLIT FAILURES	60
9.1 Study Locations	60
9.2 Systemwide Split Failure Assessment	61
9.3 Traffic Signal Retiming Opportunities	62
9.4 Signal Timing Modifications	65
9.5 Results	67
10. CLOSELY-COUPLED INTERSECTIONS	76
10.1 Conventional Diamond Interchanges	76
10.2 Diverging Diamond Interchanges	83
10.3 Continuous Flow Intersections	92
11. ROUNDABOUTS	103
11.1 Control Delay	103
11.2 Data Aggregation and Visualization Graphics	104
11.3 Queue-Length	107
11.4 Origin-Destination Characteristics	107
12. SAFETY EVALUATION	113
12.1 Hard-braking Events as Surrogate for Crashes	113
12.2 Driver Behavior Assessment After Changing Left-Turn Phasing	123
13. SCALABILITY	130
13.1 PM Heatmap Web Dashboard	130
14. SUMMARY	134
14.1 Traffic Signal Performance Measures	134
14.2 Intersection Safety and Driver Behavior Evaluation	134

14.3 Scalability	134
14.4 Future Opportunities	134
REFERENCES	135
APPENDICES	
APPENDIX A. REPORTING FRAMEWORK FOR ARTERIAL-LEVEL TRAFFIC SIGNAL PERFORMANCE MEASURES	141
APPENDIX B. RELEVANT MEDIA	149

LIST OF FIGURES

Figure 1.1 ATSPM technology timeline	2
Figure 2.1 Vehicle trajectory records generated by the state in December 2022	3
Figure 2.2 Passenger CV trajectory penetration across eleven states in August 2021	4
Figure 2.3 Event records generated by the state in December 2022	5
Figure 2.4 Data architecture of an on-demand smart mobility platform	7
Figure 2.5 Query design and efficient partitioning of CV data in a data warehouse	8
Figure 3.1 Trajectory waypoints around a signalized intersection (n: 6,278)	9
Figure 3.2 Trajectory waypoints linear referencing	10
Figure 3.3 Vehicle trajectories along intersections	11
Figure 3.4 Vehicle trajectories along a corridor	12
Figure 3.5 CV events around a signalized intersection (n: 102)	14
Figure 4.1 Turning movements at a signalized intersection	15
Figure 4.2 Waypoint selection with geofences	16
Figure 4.3 Waypoint retrieval radiuses	17
Figure 4.4 Heading-based filtering to identify actively passing vehicles	18
Figure 4.5 Heading-based filtering results	19
Figure 4.6 Entry and exit heading clusters	19
Figure 5.1 Delay definitions	22
Figure 5.2 LOS in a Purdue Probe Diagram	23
Figure 5.3 AOG in a Purdue Probe Diagram	25
Figure 5.4 AOG estimations from different techniques	27
Figure 5.5 AOG estimation comparison	28
Figure 5.6 Queue-length effects on AOG discrepancies	28
Figure 5.7 SF in a Purdue Probe Diagram	30
Figure 5.8 DSB in a Purdue Probe Diagram	31
Figure 5.9 Vehicle trajectories taking the same movement at a signalized intersection during four different TOD plans for all weekdays in a month	33
Figure 6.1 West St. intersections	34
Figure 6.2 Raw travel times of sampled vehicles traveling SB on West St.	35
Figure 6.3 Example trip showing departure from designated corridor as a result of trip chaining (map data: OpenStreetMap)	35
Figure 6.4 Example trip showing departure from designated corridor as a result of detouring (map data: OpenStreetMap)	36
Figure 6.5 Raw travel times for West St. SB colored by match percentage	37
Figure 6.6 Corridor-wide CFD for raw (red) and curated (green) travel times	38
Figure 6.7 Corridor-wide travel time scatter plot	38
Figure 6.8 Corridor-wide weekly travel time plot	39
Figure 7.1 Study arterial	40
Figure 7.2 Signal performance measures for WB-through movements on Eldorado Pkwy	41
Figure 7.3 PPDs for highlighted intersections and time periods in Figure 7.2	42
Figure 7.4 Month-long summary of performance measures on Eldorado Pkwy for all relevant movements	43
Figure 7.5 Geospatial view of intersection performance in downtown Indianapolis	44

Figure 7.6 Intersections in downtown Indianapolis pareto-sorted by their performance	45
Figure 8.1 North Split closure and West St. intersections in downtown Indianapolis	47
Figure 8.2 Signal performance measures for SB-through movements on West St. 1 week before the North Split closure	48
Figure 8.3 Signal performance measures for SB-through movements on West St. 1 week after the North Split closure	49
Figure 8.4 Corridor-wide weekday weekly trajectory counts for SB-through movements from 15:00–18:00 hrs	50
Figure 8.5 SB-through corridor-wide trajectories and intersection performance measures from 15:00–18:00 hrs	51
Figure 8.6 SB-traveling vehicles on West St. from Intersections 4 to 8	52
Figure 8.7 Weekday weekly arterial travel time CFD from 15:00–18:00 hrs	52
Figure 8.8 Corridor-wide weekday weekly performance measures for vehicles traveling SB-through on West St. from 15:00–18:00 hrs	53
Figure 8.9 Weekday weekly median arterial travel time and IQR for vehicles traveling SB-through on West St. from 15:00–18:00 hrs	54
Figure 8.10 Intersections analyzed on US-27	54
Figure 8.11 Signal performance measures for SB-through movements on US-27 during August 2020 weekdays	55
Figure 8.12 Signal performance measures for SB-through movements on US-27 during August 2021 weekdays	56
Figure 8.13 Aerial view of Intersections 6 and 7	57
Figure 8.14 PPDs of vehicles traveling SB-through from 15:00 to 18:00 hrs	58
Figure 8.15 Corridor-wide change in performance by movement	59
Figure 9.1 Analyzed intersections	60
Figure 9.2 May 2022 weekday intersection split failure ratio from 16:00–18:00 hrs	61
Figure 9.3 May 2022 weekday movement split failure ratio from 16:00–18:00 hrs	61
Figure 9.4 Conflicting movement RPD	63
Figure 9.5 Opposite barrier RPD	64
Figure 9.6 Intersection 1: US-421 at W 116th St	65
Figure 9.7 PPDs ring diagrams at Intersection 1 from 16:00–18:00 hrs	66
Figure 9.8 SF before-after assessment at Intersection 1 from 16:00–18:00 hrs	68
Figure 9.9 Intersection 2: US-41 at E Margaret Ave	69
Figure 9.10 PPDs ring diagrams at Intersection 2 from 16:00–18:00 hrs	70
Figure 9.11 SF before-after assessment at Intersection 2 from 16:00–18:00 hrs	71
Figure 9.12 Intersection 3: US-136 at Waterfront Pkwy W Dr	72
Figure 9.13 PPDs ring diagrams at Intersection 3 from 16:00–18:00 hrs	73
Figure 9.14 SF before-after assessment at Intersection 3 from 16:00–18:00 hrs	74
Figure 10.1 I-465 at Michigan Rd. in Indianapolis, Indiana	77
Figure 10.2 George Bush Tpke. at Preston Rd. in Dallas, Texas	77
Figure 10.3 Three-phase diamond interchange signal control in Indiana	78
Figure 10.4 Four-phase diamond interchange signal control in Texas (B1 = barrier 1, B2 = barrier 2, OL = overlap)	79
Figure 10.5 EPPDs for three-phase diamond in Indiana	80
Figure 10.6 EPPDs for four-phase diamond in Texas	81
Figure 10.7 August 2020 weekdays AOG by approach and movement for the three-phase diamond interchange in Indiana (ext = external, int = internal)	82
Figure 10.8 August 2020 weekdays AOG by approach and movement for the four-phase diamond interchange in Texas (ext = external, int = internal)	82
Figure 10.9 August 2020 weekdays SF by approach and movement for the three-phase diamond interchange in Indiana (ext = external, int = internal)	83

Figure 10.10 August 2020 weekdays SF by approach and movement for the four-phase diamond interchange in Texas (ext = external, int = internal)	83
Figure 10.11 August 2020 weekday DSB by approach and movement for the three-phase diamond interchange in Indiana (ext = external, int = internal)	84
Figure 10.12 August 2020 weekday DSB by approach and movement for the four-phase diamond interchange in Texas (ext = external, int = internal)	84
Figure 10.13 August 2020 weekday LOS by approach and movement for the three-phase diamond interchange in Indiana (ext = external, int = internal)	85
Figure 10.14 August 2020 weekday LOS by approach and movement for the four-phase diamond interchange in Texas (ext = external, int = internal)	85
Figure 10.15 Diverging diamond interchange location	87
Figure 10.16 DDI EPPDs	88
Figure 10.17 Source DDI EPPDs	89
Figure 10.18 AOG summary results	90
Figure 10.19 LOS summary results	91
Figure 10.20 SF summary results	92
Figure 10.21 DSB summary results	93
Figure 10.22 Continuous flow intersection location	95
Figure 10.23 Conventional signal phasing for partial CFIs	96
Figure 10.24 EPPDs for major street movements	97
Figure 10.25 PPDs and EPPDs for minor street movements	98
Figure 10.26 SF summary results at all signals at the CFI for August 2021 weekdays	99
Figure 10.27 AOG summary results at all signals at the CFI for August 2021 weekdays	100
Figure 10.28 LOS summary results at all signals at the CFI for August 2021 weekdays	101
Figure 10.29 Initial stops distribution as a percentage of the total sampled trajectories	102
Figure 11.1 Vehicle trajectories traveling EB at Ditch Rd. and W 96th St. during a peak 15-minute period	104
Figure 11.2 Ditch Rd. and W 96th St. trajectories by approach and estimated LOS during a peak 15-minute period between July 12th–16th, 2021	105
Figure 11.3 Ditch Rd. and W 96th St. trajectories by approach and estimated LOS during an off-peak 15-minute period between July 12th–16th, 2021	106
Figure 11.4 LOS by TOD at Ditch Rd. and W 96th St. between July 12th–16th, 2021	107
Figure 11.5 LOS system visualization by approach for all the weekdays in July 2021	108
Figure 11.6 LOS system visualization by approach for all the weekdays in July 2021 during the most congested 15-minute period	109
Figure 11.7 LOS system visualization from the 17:00 to the 17:15 hrs. for all the weekdays in July 2021	110
Figure 11.8 Estimated queue-length by TOD at Ditch Rd. and W 96th St. (ID 2) for weekdays in July 2021	111
Figure 12.1 Studied signalized corridor and July 2019 HB data	114
Figure 12.2 HB event processing	115
Figure 12.3 Number of weekday HB events by intersection and distance to the stop bar	116
Figure 12.4 Heatmap of NB weekday HB events by intersection in July 2019	117
Figure 12.5 Heatmap of SB weekday HB events by intersection in July 2019	117
Figure 12.6 SB approach at Southport Rd. (Intersection 4)	118
Figure 12.7 SB approach at Smith Valley Rd. (Intersection 8)	119
Figure 12.8 Number of weekday crashes by intersection and type on SR-37, between January 1st, 2016, and July 9th, 2020	120

Figure 12.9 Frequency heatmap of weekday crashes between January 1st, 2016, and July 9th, 2020	121
Figure 12.10 Sensitivity analysis for Spearman correlation between HB events and rear-end crashes for 8 weeks in July and August 2019	124
Figure 12.11 Left-turn change from protected-permitted to protected-only at US-40 and German Church Rd.	126
Figure 12.12 Percentage of sampled vehicles turning left that hard-accelerate	127
Figure 12.13 PPDs of vehicle trajectories traveling EB-left between 11:00 and 13:00 hrs.	128
Figure 12.14 EB left-turn traffic signal performance measures before and after the phasing transition	129
Figure 13.1 Trajectory waypoints collected during a 30-minute period in January 2020	130
Figure 13.2 PM Heatmap web dashboard	131
Figure 13.3 PM Heatmap web dashboard showing AOG results for a 9-intersection corridor in Frisco, TX	131
Figure 13.4 PM Heatmap web dashboard showing SF results for a 22-intersection corridor in Cincinnati, OH	132
Figure 13.5 Traffic signals included in the PM Heatmap web dashboard	132
Figure 13.6 Data evaluated in the PM Heatmap web dashboard	133

LIST OF TABLES

Table 4.1	Calculated entry and exit heading limits by movement	20
Table 4.2	Sampled trajectories turning counts	21
Table 4.3	Trajectories identified with a specific movement by method	21
Table 5.1	HCM level of service criteria for signalized intersections	23
Table 5.2	Estimated delays for trajectories in Figure 5.2a	24
Table 5.3	Videos showing the occurrence of relevant operational events	32
Table 6.1	Summary travel time statistics before and after curation	37
Table 7.1	Studied intersection on Eldorado Pkwy	40
Table 7.2	Information included in Figure 7.4	42
Table 8.1	Studied intersection on West St.	47
Table 8.2	Studied intersection on US-27	54
Table 8.3	Volume change from count stations	55
Table 8.4	Performance overview	59
Table 9.1	Performance measure (PM) change at Intersection 1	75
Table 9.2	Performance measure (PM) change at Intersection 2	75
Table 9.3	Performance measure (PM) change at Intersection 3	75
Table 9.4	Overall change in performance from 16:00–18:00 hrs.	75
Table 10.1	Sampled volume distribution at the three-phase interchange in Indiana for August 2020 weekdays from 16:00–18:00 hrs.	79
Table 10.2	Sampled volume distribution at the four-phase interchange in Texas for August 2020 weekdays from 16:00–18:00 hrs.	79
Table 10.3	Timing implementation PM peak performance comparison	86
Table 11.1	HCM-level of service criteria for roundabouts	103
Table 11.2	Highest control delays by approach between 17:00 and 17:15 hrs.	111
Table 11.3	July 2021 weekday sampled vehicle turning counts at Ditch Rd. and W 96th St. (ID 2)	112
Table 12.1	Interpretation of correlation coefficient–Spearman	121
Table 12.2	Spearman’s correlation between intersection rear-end crash counts and number of HB events by distance for NB SR-37	122
Table 12.3	Spearman’s correlation between intersection rear-end crash counts and number of HB events by distance for SB SR-37	122
Table 12.4	Interpretation of correlation coefficient–Pearson and Kendall	122
Table 12.5	Pearson’s correlation between intersection rear-end crash counts and number of HB events by distance for SB SR-37	123
Table 12.6	Kendall’s correlation between intersection rear-end crash counts and number of HB events by distance for SB SR-37	123
Table 12.7	Descriptive statistics for model variables	125
Table 12.8	Estimation results	125
Table 12.9	2020 monthly weekday EB left-turn HA	128
Table 12.10	2020 monthly weekday EB left-turn traffic signal performance measures	129

LIST OF ABBREVIATIONS

AADT	Annual Average Daily Traffic
AOG	Arrival on Green
ATSPM	Automated Traffic Signal Performance Measures
AWS	Amazon Web Services
BOG	Beginning of Green
BOR	Beginning of Red
CDI	Conventional Diamond Interchange
CFD	Cumulative Frequency Distribution
CFI	Continuous Flow Intersection
CL	Confidence Level
CV	Connected Vehicle
DDI	Diverging Diamond Interchange
DLT	Displaced Left-Turns
DOT	Department of Transportation
DSB	Downstream Blockage
EB	Eastbound
EDC	Everyday Counts
EPPD	Extended Purdue Probe Diagram
FFT	Free-Flow Trajectory
FS	Far Side
FYA	Flashing Yellow Arrow
GCS	Google Cloud Storage
GPS	Global Positioning System
HA	Hard-Acceleration
HB	Hard-Brake
HCM	Highway Capacity Manual
HMAC	Hash Message Authentication Code
IAM	Identity and Access Management
ID	Identifier
INDOT	Indiana Department of Transportation
IQR	Interquartile Range
ITS	Intelligent Transportation Systems
JSON	JavaScript Object Notation
LOS	Level of Service
NB	Northbound
ODOT	Ohio Department of Transportation
OEM	Original Equipment Manufacturer
PCD	Purdue Coordination Diagram
POG	Percentage on Green
PPD	Purdue Probe Diagram
RAID	Redundant Array of Independent Disk
RAM	Random Access Memory
RDBMS	Relational Database Management System
RPD	Relative Performance Diagram
SB	Southbound
SF	Split Failure
SFTP	Secure File Transfer Protocol
SPaT	Signal Phase and Timing
SQL	Structured Query Language
SR	Split Rebalance
SSD	Solid-State Drive
TMMS	Traffic Monitoring Management System
TOD	Time-of-Day
TPF	Transportation Pooled Fund
TRB	Transportation Research Board
UDOT	Utah Department of Transportation
VPD	Vehicles per Day
VPN	Virtual Private Network
WB	Westbound

1. INTRODUCTION

The 2019 *Traffic Signal Benchmarking and State of the Practice Report* indicates that traffic signals contribute up to 10 percent of all traffic delay on the National Highway System. This represents a cost of \$22.9 billion in urban areas (25). With over 400,000 traffic signals across the United States, it is important for agencies to systematically evaluate signal performance with the objective of identifying locations where operations could be improved (26).

An approach to improve signal operations that has proven to be effective is signal retiming. During the signal retiming process, timing parameters, phasing sequences, and control strategies are implemented or modified to better serve current demand (27). Properly managed traffic signals can reduce congestion, improve mobility and safety, and decrease vehicle stops and delays (28). For these reasons, it is important to determine when and where signal retiming is warranted.

Traditionally, agencies have retimed signals every 3–5 years, with motorist complaints as the main performance measure (29). During this process, a traffic engineer goes to the field to collect vehicle counts and assess operations. Then, models are created to attempt to replicate observed conditions from which timing adjustments are tested and then implemented (26). This methodology is reactive as traffic patterns may have changed dramatically even before the complaint. Further, the proposed timing changes are usually based on observations obtained during short periods of time which may not properly caption operational conditions.

During the last two decades, significant efforts focused on the development of systematic techniques to evaluate signal performance. The first in-cabinet high-resolution traffic signal performance measures were developed in Indiana in 2005, and subsequently in 2007 in Minnesota. A consensus among traffic controller manufacturers on data logging and enumerations convention was reached in 2012 (30). In 2014, the Utah Department of Transportation (UDOT) released the first version of the Automated Traffic Signal Performance Measures (ATSPMs) dashboard that incorporated the signal metrics into an open-source web platform. ATSPMs have surged in popularity as an effective data-driven proactive approach to assess signal operations (29). Figure 1.1 provides an approximate chronology of ATSPMs and its identification as an implementation-ready technology in Every Day Counts (EDC)-4 (31).

1.1 State-of-the-Practice of Traffic Signal Evaluation

ATSPMs are enriched data, visualizations, and tools that use traffic signal controller high-resolution (tenth-of-a-second) event data (i.e., changes in signal outputs and detector states) to evaluate signal performance (33). Through modern communication and data infrastructure, these performance measures continuously assess signal operations with enough resolution to allow for a prompt identification of challenges and needed changes

(26). During a previous Pooled Fund Study (TPF-5(258)), a report titled *Performance Measures for Traffic Signal Systems: an Outcome-oriented Approach* was produced which presents a collection of ATSPMs (1) and another report titled *Integrating Traffic Signal Performance Measures into Agency Business Processes* was published which discusses the uses and requirements to implement ATSPMs from an agency's perspective (2).

By 2019, agencies within 31 states had demonstrated, assessed, or institutionalized implementation of ATSPMs. Even though that is significant progress, the number of states with some level of ATSPM implementation fell short from the original EDC-4 goal of 35 (29). One challenge of deploying controller-based high-resolution data collection is the significant initial capital investment and communication costs. In 2014, the 10-year cost of implementing high-resolution data collection at a traffic signal was estimated to be \$7,320, without considering maintenance (1).

Though developed around the same timeframe as ATSPMs in its infancy, the use of crowdsourced data to evaluate signal systems in recent years has significantly increased with greater vehicle penetration. These data sets have historically provided corridor-level travel times reflecting the overall user experience while traversing a system of intersections. A major benefit of utilizing crowdsourced data is that no infrastructure investment and maintenance is required. By 2021, 38 states had demonstrated, assessed, or institutionalized implementation of crowdsourced data to evaluate transportation operations, two more states than the EDC-5 goal at the time (34).

A crowdsourced data set that has been used to evaluate signal performance is segment-based probe vehicle data, usually comprised of aggregated minute-by-minute average speeds and travel times for a given road segment (35). This data set has extensively been used to evaluate highway mobility (36, 37) and signalized arterial progression (35, 38, 39). However, vendor-defined segments often differ from queueing and deceleration boundaries at signalized intersection approaches, and 1-minute aggregations do not provide enough temporal fidelity to discern platoons within a cycle. Evaluations derived from segment-based probe vehicle data usually make some compromises when intersection-level assessments are made. This makes pinpointing sources of operational challenges a difficult task (35, 38).

1.2 Connected Vehicle Traffic Signal Performance Measures

Recently, crowdsourced high-resolution connected vehicle (CV) trajectory and event data have become commercially available. These data sets provide positional and descriptive information on individual vehicles as they traverse through road networks. With over 500 billion trajectory records and over 1 billion event records generated each month in the United

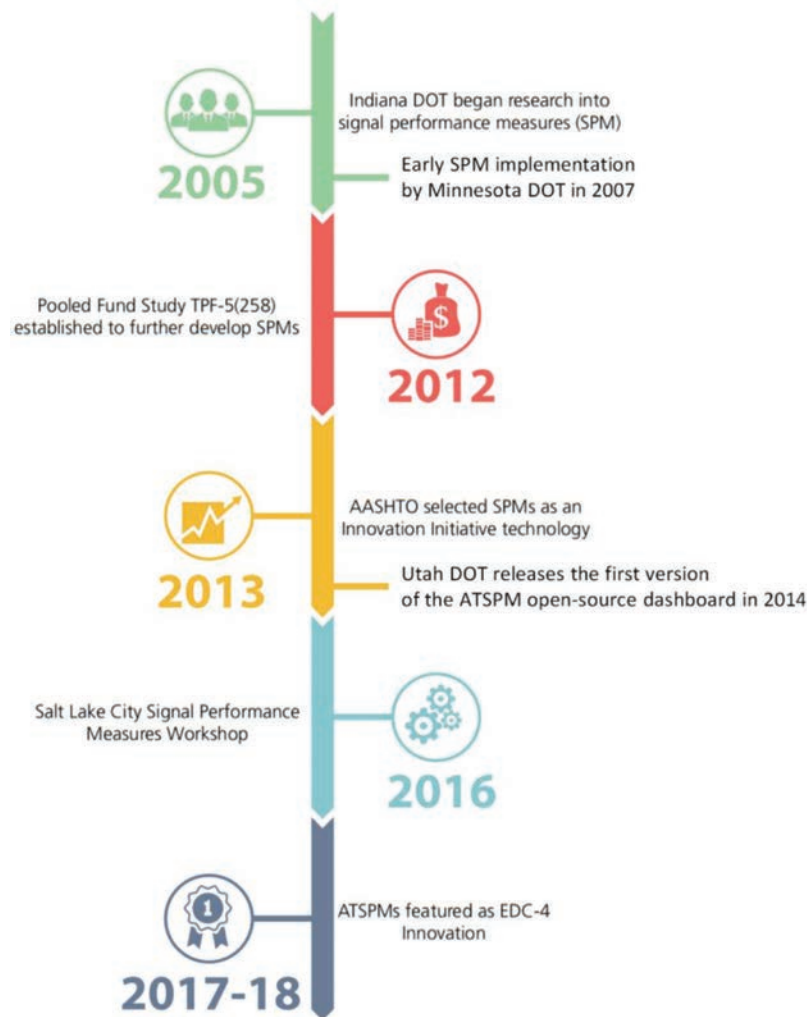


Figure 1.1 ATSPM technology timeline (31, 32).

States, unique opportunities arise to make use of these data sets to systematically evaluate signal efficiency and safety. Some of the benefits of utilizing CV data to evaluate traffic signal performance are the following.

- No detection or communication equipment is required.
- Practitioners have access to entire vehicle trajectories and are not constrained to limited detection areas or segments.
- Performance analysis at the movement-, approach-, intersection-, arterial-, and system-levels are possible due to the resolution and ubiquity of the data.
- Evaluation techniques are scalable to any location where CV data is available due to the homogeneity of the data attributes.

2. CONNECTED VEHICLE DATA

One in every 28 vehicles in the United States provides telematics-based CV data through one of the commercial data vendors (40). With 276 million registered vehicles in the country in 2020, there are nowadays an estimated 9.85 million connected vehicles on the roads

(41). Furthermore, this number is expected to grow significantly as 470 million connected vehicles are anticipated to be in operation in the United States, Europe, and China by 2025 (42).

This chapter explains the composition of the CV trajectory and event data sets that are used in the different studies presented in this report, as well as data requirements and best practices. CV data is obtained from a third-party data vendor that works directly with original equipment manufacturers (OEMs). Both data sets are generated from passenger vehicles that are factory-equipped with the required technology for sampling and transmission. It is important to mention that only vehicle information is available from the CV data sets and no infrastructure attributes, such as Signal Phase and Timing (SPaT) or MAP messages (43, 44), are provided.

2.1 Trajectories

CV trajectory data consists of a set of waypoints for an entire (i.e., from on to off) vehicle trajectory with a

reporting interval of 3 seconds and a spatial accuracy of 3 meters (~10 ft.). Every waypoint contains the following information: GPS location, timestamp, speed, heading, and anonymous unique trajectory identifier. The range of heading values is $[0^\circ, 360^\circ)$, where 0° is the true north and it increases clockwise.

By linking individual waypoints with the same trajectory identifier and sorting them by timestamp, a complete chronological vehicle journey can be obtained. Therefore, a trajectory τ is defined as the set of its waypoints w_i , with $i = 1, 2, \dots, n$ where $i = 1$ is the first sample collected after the vehicle is turned on and $i = n$ is the last sample collected before the vehicle is turned off. That is:

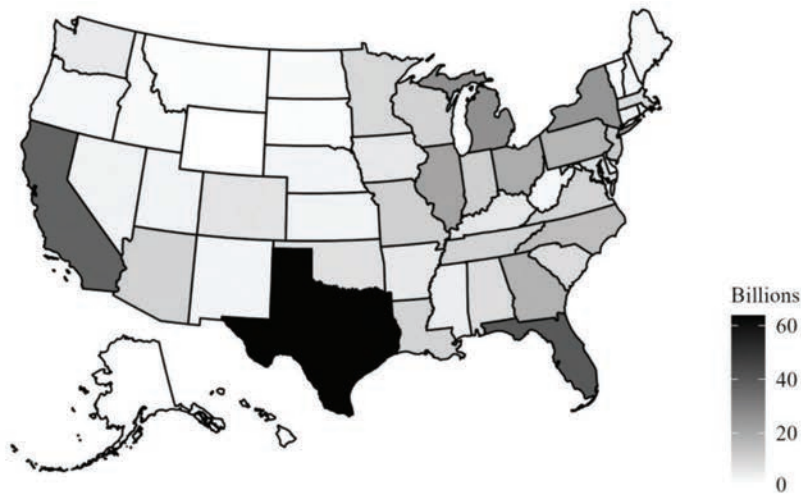
$$\tau = \{w_i\}_{i=1}^n \quad (\text{Eq. 2.1})$$

$$w_i = \{\text{identifier}, \text{latitude}_i, \text{longitude}_i, \text{timestamp}_i, \text{speed}_i, \text{heading}_i\} \quad (\text{Eq. 2.2})$$

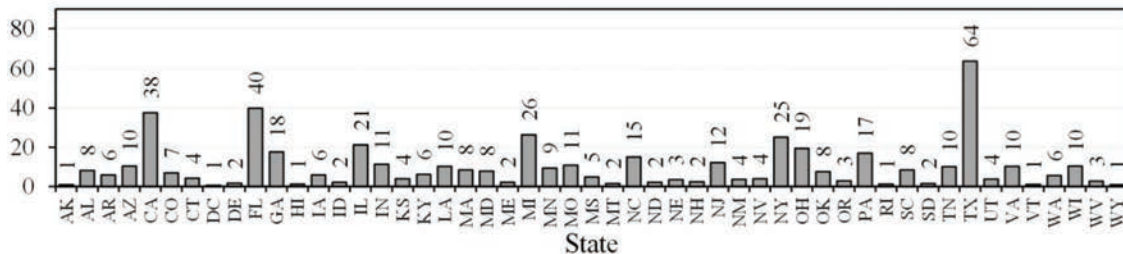
Figure 2.1 shows the number of trajectory waypoints generated during 1 month by state. In total, 503 billion records were produced nationwide in December 2022. Texas is the state with the most records (64 billion), and Washington, D.C., is the entity with the fewest records (0.69 billion).

2.1.1 Market Penetration

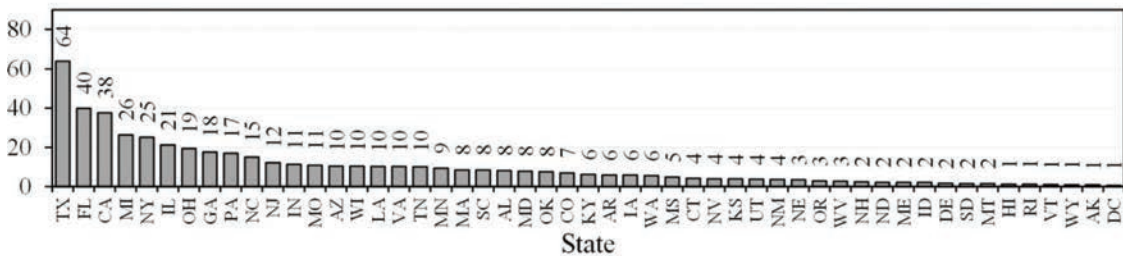
A relevant characteristic of CV trajectory data that must be considered is its level of representativeness. This is often measured by calculating the CV market



(a) Map



(b) Billions of records alphabetically-sorted



(c) Billions of records pareto-sorted

Figure 2.1 Vehicle trajectory records generated by the state in December 2022.

penetration as the ratio of sampled vehicles to all vehicles (obtained either by a roadway sensor or manual counting). The market penetration percentage is important because it provides a level of confidence on whether a CV-based study sufficiently characterizes on-the-ground conditions.

Several studies have looked at the market penetration required for assessing traffic signal performance measures. Waddell et al. concluded that penetration percentages smaller than 0.04% can be enough to estimate signal performance (45). Day et al. used CV trajectory data with penetration rates ranging from 0.09% to 0.80% to optimize signal offsets on two different corridors. It was concluded that only 2 weeks of trajectory data are required to obtain positive results (46). Argote-Cabañero et al. estimated minimum CV penetration percentages to obtain accurate performance measures at signalized arterials under different traffic conditions. The authors concluded that penetrations between 5.6% and 29.89% are required for average speed estimations, between 4.92% and 15% for average unitary delay, and between 2.68% and 13.01% for average number of stops (47).

A useful technique to increase the level of confidence on whether the CV data sufficiently characterizes on-the-ground conditions is to aggregate samples. For example, if 10% penetration is required for a particular study, but only 2% is available from a given data set, then five days of CV data can be aggregated to comply with the requirements. This practice assumes that the CV data represents random samples and that similar traffic conditions are exhibited over the multiple days within the time periods from which data is aggregated.

The penetration percentage of the CV trajectory data for eleven states is calculated by comparing data from Departments of Transportation (DOT) permanent count stations and unique CV trajectory counts.

Permanent count stations make use of vehicle detection technology, such as inductive loop detectors, piezoelectric sensors, or magnetic sensors to count the number of vehicles that traverse a specific section of the roadway (48). Over 340 continuous count stations are selected to be geographically distributed, represent varied operational conditions, and provide information on interstate and non-interstate roadways as well as urban and rural areas (49).

The unique CV trajectory counts are obtained from quarter-mile-long geofenced regions near the count stations that cover the entire width of the road. All waypoints found within the geofenced regions are selected and the unique vehicle identifiers are counted (49).

Considering vehicle counts obtained from the permanent count stations as ground truth, the statewide CV trajectory monthly penetration percentage S_p can be calculated using:

$$S_p = \left(\frac{\sum V_m}{\sum C_m} \right) 100 \quad (\text{Eq. 2.3})$$

where V_m is the monthly count of unique vehicle trajectory identifiers within a geofence, and C_m is the monthly count of vehicles that pass a count station within that same geofence. The sum of both counts across all geofences and all count stations within the same state is performed and the percentage is calculated. Figure 2.2 shows estimated penetration percentages for California, Connecticut, Georgia, Indiana, Minnesota, North Carolina, Ohio, Pennsylvania, Texas, Utah, and Wisconsin in August 2021 (49).

2.1.2 Limitations

Even though CV trajectory data provides unique benefits for traffic signal performance estimation, it has some limitations that need to be considered.

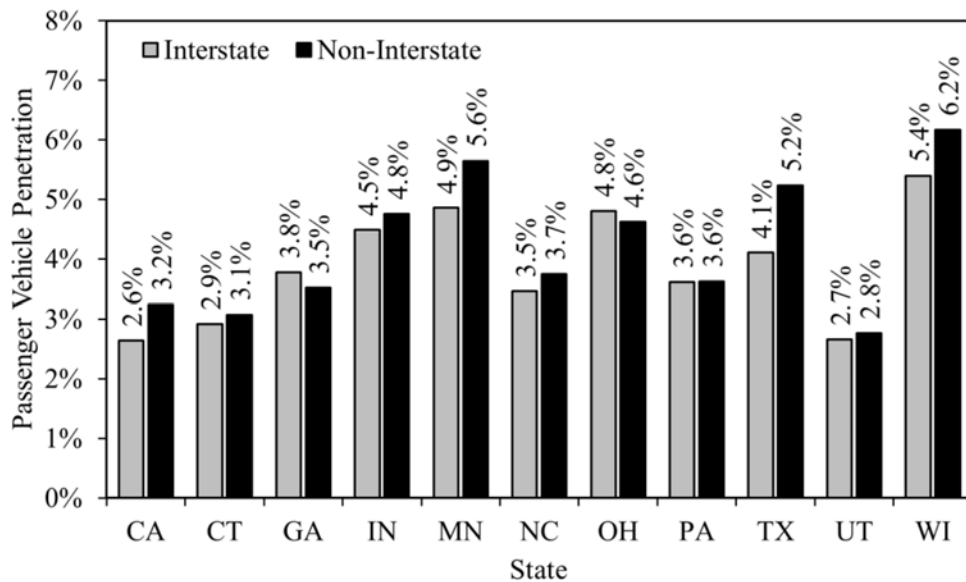


Figure 2.2 Passenger CV trajectory penetration across eleven states in August 2021 (49, 50).

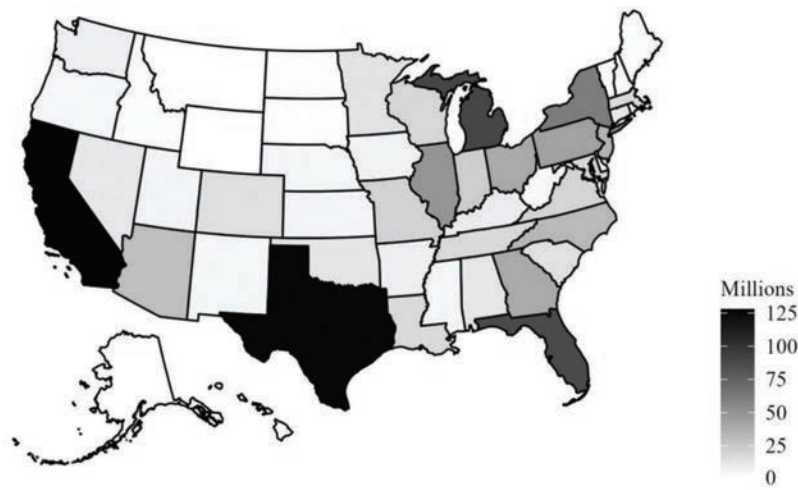
The CV trajectory data used for these series of studies has a latency from 30 to 60 seconds, which is not low enough to be used in real-time signal control (51). Furthermore, the level of confidence on whether CV data characterizes on-the-ground conditions can be increased only when the analysis aims at evaluating performance trends rather than operational singularities. For this reason, cycle-by-cycle performance evaluations are still not feasible with the current data penetration rates.

Additionally, given the large volume of data, its storage and analysis can be challenging with traditional, on-premise, relational database management systems (RDBMS). For example, 1 month of data for the state of Georgia is comprised of over 14 billion records and is over 1.8 terabytes of storage.

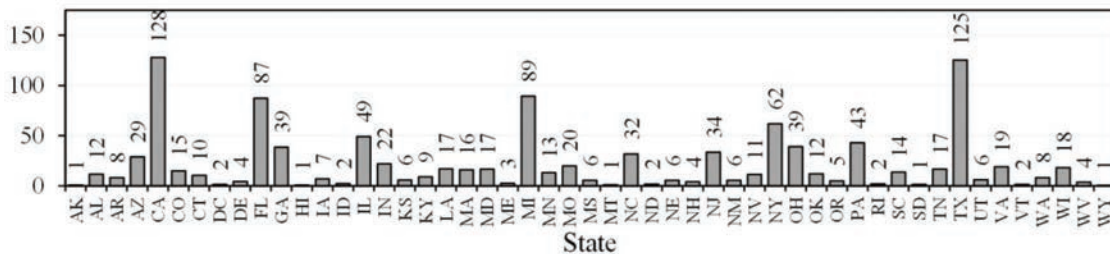
2.2 Events

CV event data consists of individual hard-acceleration (HA) and hard-braking (HB) records that include the vehicle's GPS location within a spatial accuracy of 3 meters (~10 ft.), timestamp, speed, and heading. HA and HB events are recorded as soon as a vehicle's on-board accelerometer experiences an acceleration (or deceleration) greater in magnitude than 8.76 ft/s² (0.272 g), as defined by the data supplier. The range of heading values is [0°, 360°), where 0° is the true north and it increases clockwise.

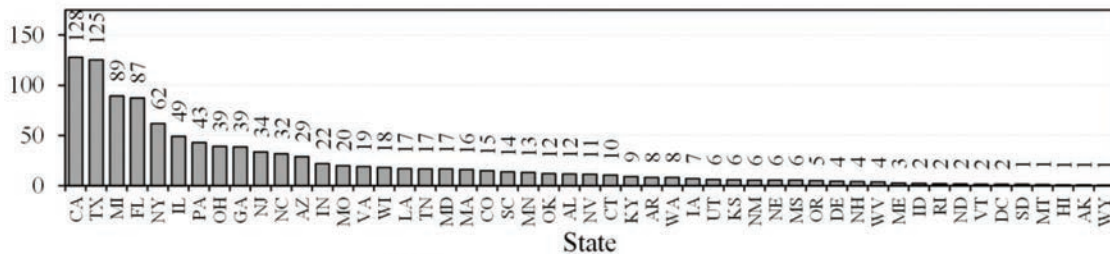
Figure 2.3 shows the number of event records generated during 1 month by state. In total, 1.09 billion records were produced nationwide in December 2022. California is the state with the most records



(a) Map



(b) Millions of records alphabetically-sorted



(c) Millions of records pareto-sorted

Figure 2.3 Event records generated by the state in December 2022.

(128 million) and Wyoming has the fewest records (0.76 million). The next subsection discusses data requirements and techniques to manage CV data sets.

2.3 Data Requirements

There are a few approaches for managing large data sets such as CV data. The current research has explored leveraging cloud-based data warehouse technology. Large amounts of CV data can be challenging not only to store, but also difficult to access and query due to its temporal and spatial nature. For many agencies this can be a barrier for creating reports and dashboards from the raw data for stakeholder consumption. Traditional RDBMS typically would require extensive upgrades and high-performance components to ensure that large data sets can be effectively leveraged. Cloud providers can give organizations flexibility in terms of a usage fee-based model that incurs charges based on the size of the data stored and the amount of querying and extracting performed. However, it may be difficult to estimate expenditures accurately prior to procuring such a system as costs vary based on different management practices, unforeseen query complexities, and uncertainty of the demand by users accessing the system.

2.3.1 Acquisition

Secure File Transfer Protocol (SFTP) and cloud storage services have been widely accepted as two data delivery methods for acquiring CV data. On-premise systems with an SFTP endpoint can be made accessible to the data vendor for sending files. For cloud platforms, the vendor can provide access or send data to an agency-owned web storage “bucket”, such as Google Cloud Storage (GCS) or Amazon Web Services (AWS) S3. Using buckets, the vendor’s data is passed between cloud systems and would not be transferred through on-premise systems unless specific Virtual Private Network (VPN) rules or data governance policies are in place. In some cases, the execution of commands for the initiation of transfers may be performed at an on-premise workstation. An important distinction between on-premise and cloud storage systems is the speed of the network and disk bandwidth that determines the rate of data uptake. This can be a limiting factor on some on-premise systems, but usually not for cloud platforms. Typically, a state similar to Indiana (average for the United States) would amass 2.5 GB of compressed CV trajectory data in a peak hour of a weekday.

The raw data is provided compressed in flat-file or binary-packed format. Data files can come in various formats, including compressed JavaScript Object Notation (JSON) or parquet (52). For conventional systems that are hosted on-premise, using applications such as Apache Spark (53), or developing data extraction code on platforms such as Python or .NET C# by making use of pre-existing extraction libraries, the data from the files can be unpacked and prepared for processing

into a database. For cloud platforms, many data warehouses natively support the staging of flat-file data from a bucket directly in the database store, such as Google’s BigQuery. Other systems may require additional data transformation steps, such as setting up a data pipeline, to process the flat-file data into a database store.

The data can be acquired or delivered in batches or in real-time, depending on the needs of the agency. Depending on the size of the data delivered, real-time processing performance of the system must be adequate to sustain the ingress rate of the data, especially while running queries and backups simultaneously.

2.3.2 Storage

CV data stored in databases enables running queries, generating dashboards, and creating reports. Traditional RDBMS platforms can be hosted either on-premise or in the cloud, and consist of tabular stores of rows and columns. RDBMS stores are often used to host traffic-related data, such as high-resolution controller logs (2), because of its structured nature.

The challenge of using RDBMS for large CV data sets is that scaling capacity and performance as the data set grows becomes more difficult over time. Increasing the number of disks or adding servers to accommodate a quickly growing database may be viable options but are time-intensive and cost-prohibitive in many cases. RDBMS that are not hosted as a service, such as on-premises systems, may quickly run into a situation where a server chassis has been outgrown (i.e., no more slots available for additional disk drives). Additionally, a performant system requires fast disks for random access, such as multiple solid-state drives (SSD), to improve query speed. Other considerations include having a redundant array of independent disks (RAID) to combine multiple disk drives into a single volume to protect against failures and increase performance; having one or more high-speed hard-drive controller cards to ensure the data streams reach the memory and processor quickly; having fast and abundant random-access memory (RAM); and having enough processing power.

A cloud data warehouse is an alternative database system where data storage and queries are provided as a service. The data is not stored at an agency’s data center but at a remote location such as a server farm or cluster. For redundancy and depending on the availability of options for storage regions or zones, the data may be replicated across different geographic areas around the world to protect against single-point failures.

Cloud data warehouse products are provided by many vendors and have different architectures, though the common purpose of these products is to produce aggregated data metrics from a large volume of underlying disaggregated data, such as developing traffic signal performance metrics from uncategorized CV trajectory data. Typically, systems that use structured

data schemas work well with CV data as the underlying data attributes are strictly typed with expected ranges, and do not often change. Many cloud data warehouse platforms also conform to the familiar SQL standard that has been common in traditional RDBMS to access and manage the data, which allow users to quickly immerse in the platform and minimize workforce training. A few examples of cloud data warehouses include DataBricks, Azure Synapse Analytics, Amazon Redshift, Google BigQuery, and Snowflake.

2.3.3 Data Access

There are numerous ways that an agency and stakeholders can be provided access to the data, whether for ad hoc querying, report generation, application services, backups, or auditing purposes. Depending on the platform, the data can be made accessible using a specific set of authentication schemes. For on-premise databases, a centralized directory of access-enabled users, groups, or roles can be applied to most database authenticators. In some cases, typically for testing environments, manually-generated usernames and passwords are used. As all agencies are behind private networks, access from outside of the network would require VPN connectivity.

For cloud data warehouses, identity, and access management (IAM) can be delegated using dedicated principals (i.e., user accounts, service accounts, groups, or domains). Each principal may be assigned one or more roles that allow a specific type of access to a resource, or to groups where a predefined set of roles may apply. User accounts permit access for end users, while service accounts enable access via automated means, such as for dashboard applications, data processes, or automated report generators. Service account requests are verified and granted by a dedicated security key in JSON format or hash message authentication code (HMAC). Extreme precaution must be taken in the generation, dissemination, and storage of these keys since they are tied to the underlying principle, which has enabled permissions to use resources that would incur costs.

2.3.4 Best Practices

For the efficient analysis of large data sets, steps to optimize the structure of the data should be considered to ensure the platform is performant and to reduce

costs. For instance, read and write operations in real-time while running backups on the same data set would often stress a database if there were a large volume of transactions occurring in parallel. In the data pipeline, additional sets of procedures to aggregate the raw data into key performance metrics may be helpful to reduce the size of the resulting data set. This could also be leveraged by user-facing dashboards that report more efficiently than having applications process the raw data for each query. Figure 2.4 shows an example of how data can be brought into a cloud data warehouse, enriched, and aggregated for web applications.

Compared with traditional on-premise architectures where the server hardware and software are purchased up-front and additional costs are incurred for the maintenance and operation of the systems, cloud-based platforms typically charge per use, or with a pre-negotiated cost for committed use of selected amount of resources. A key design element for ensuring the data warehouse performs as efficiently and as cost-effectively as possible is the partitioning of data.

As an example, Figure 2.5 shows 192 trajectories stored over a 24-hour period, partitioned in 1-hour blocks. Since charges are incurred by the amount of data analyzed in a query, if a report requests metrics to be generated for a 3-hour period, design the query to only target the interested hours to maximize efficiency and minimize cost. Similar methods to cluster and index the data can be applied to the spatial domain, where only a subset of the data is analyzed over a geographic boundary, such as on a route or town, to further reduce costs. While the cost structure is different, these methods can also be applied to traditional RDBMS to improve operational efficiency of queries.

2.3.5 Cost

Traditional server procurement involves specifying how much storage is required, type of storage, processing power, memory, database software licensing, and backups. Recent advancements allow storage and database management to be done in the cloud. While there are no upfront costs associated with this approach, the pricing depends on how much data is stored, how long it is stored for, and what analytics are performed against the data set.

There are several major cloud data providers available for an agency to choose from. A representative cloud cost for the Indiana CV data is \$20 per

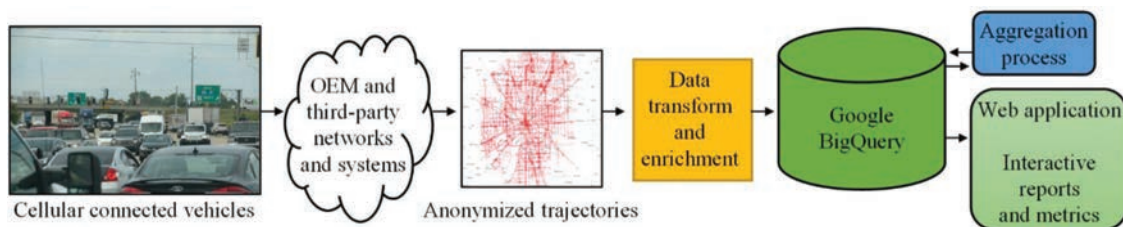


Figure 2.4 Data architecture of an on-demand smart mobility platform.

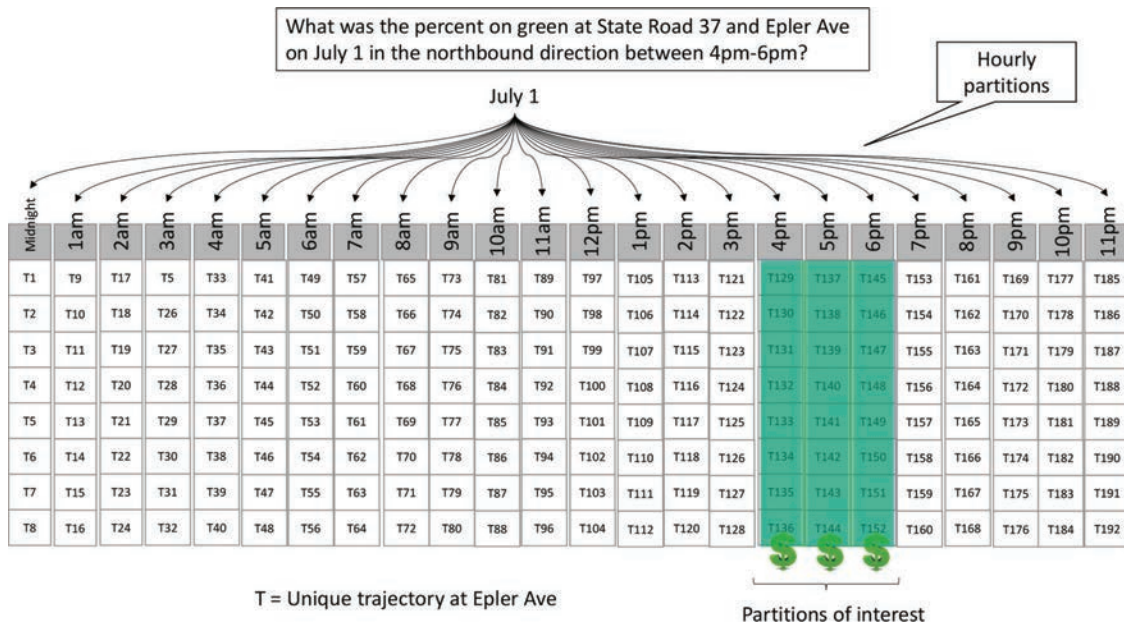


Figure 2.5 Query design and efficient partitioning of CV data in a data warehouse.

month per terabyte to store the data and \$5 to analyze each terabyte. To put it in perspective, running an analysis on a corridor with 100 million waypoints, or about 10 gigabytes, would cost five cents (54). Depending on the use case and data retention policy, agencies now have several options between cloud platforms and infrastructure maintained on-premise. In many cases, the data architecture and retention policies will have the most significant impact on cloud computing costs.

3. DATA EXPLORATION

In this chapter, examples of raw CV trajectory and event data at signalized intersections and corridors are given. Additionally, a technique to perform necessary linear referencing of trajectory waypoints in relation to a point of interest is presented.

The CV trajectory and event data sets are independent from each other, and a HA or HB event cannot be directly linked to a particular vehicle trajectory. If necessary, this could be estimated by matching locations, timestamps, and headings. However, this approach assumes that the same vehicle that provides event data also provides its trajectory information. If this is not the case, results would be erroneous. Regardless of this limitation, each data set can provide valuable information separately.

3.1 Trajectories

Figure 3.1 shows 6,278 trajectory waypoints sampled during one day near a signalized intersection. Since trajectory waypoints are available every 3 seconds if a connected vehicle is online, there is data available far upstream from the intersection (callout i), at the stop

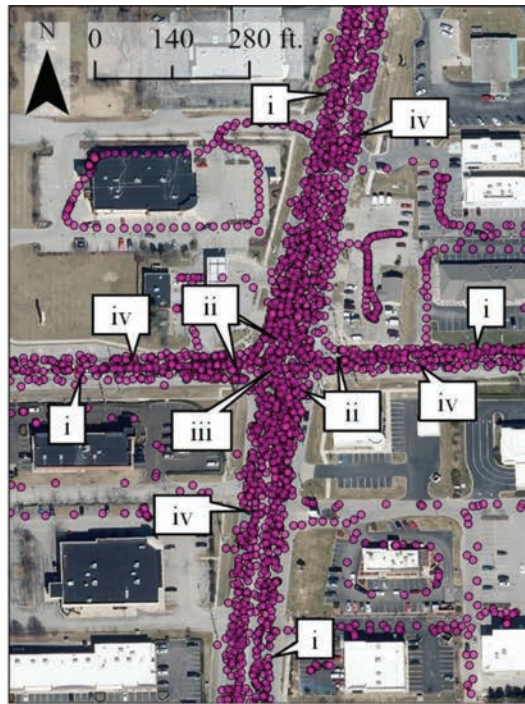
bar (callout ii), within the intersection (callout iii), and at the exiting approach (iv). With such a wide coverage, CV trajectory data provides flexibility to develop different types of traffic signal studies and performance metrics.

Figure 3.1b and Figure 3.1c show vehicle speeds and headings, respectively, of each trajectory waypoint record. As expected for this uncongested intersection, speeds are faster farther away from the intersection (callout v) as vehicles approach, and slower near the intersection (callout vi) as some vehicles must stop or turn. It can also be observed that vehicles approach the intersection northbound (NB) with headings near 0° (callout vii), eastbound (EB) with headings around 90° (callout viii), southbound (SB) with headings neighboring 180° (callout ix), and westbound (WB) with headings near 270° (callout x).

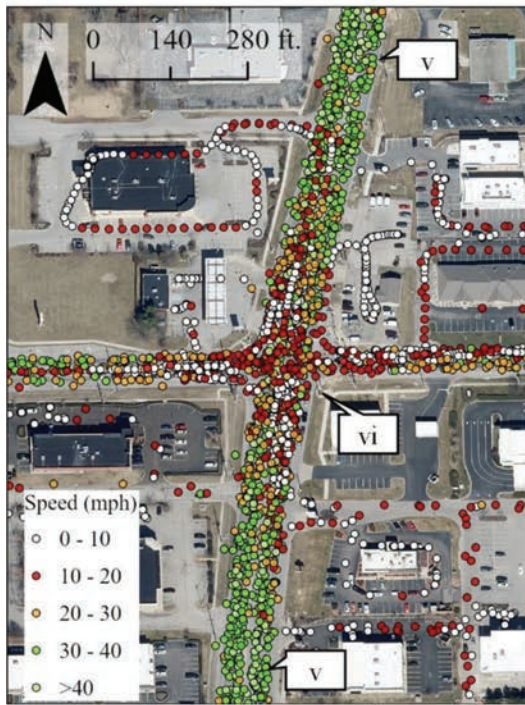
Even though showing the geospatial location of trajectory waypoints by its attributes may provide some insights into the operational conditions at an intersection (Figure 3.1), it is difficult to estimate signal performance from raw data. By stitching individual vehicle trajectories by their unique identifiers, and by linear referencing their waypoint locations to a point of reference, it is possible to meticulously evaluate vehicle experience while traversing an area of interest.

3.1.1 Linear Referencing

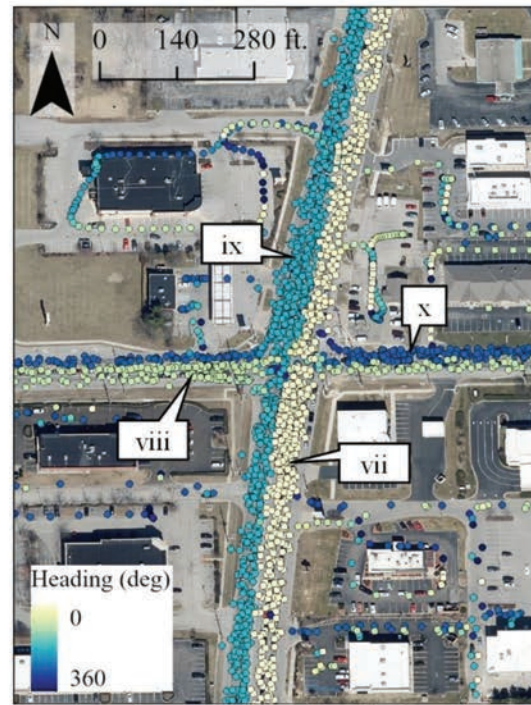
Linear referencing is the process by which the linearized location of CV waypoints along a route is calculated. This allows to situate and report performance within the route of interest as well as the estimation of operational conditions. Before accomplishing the linear referencing of vehicle trajectory waypoints, the following steps need to be observed.



(a) Trajectory waypoints



(b) Trajectory waypoints by speed



(c) Trajectory waypoints by heading

Figure 3.1 Trajectory waypoints around a signalized intersection (n: 6,278) (map data: Indiana Geographic Information Council).

1. Identify a route of interest. This can be any road segment for which a direction of travel is defined. The end of the route of interest is the reference r , which is the reference point from which road distances are measured.
2. Obtain the waypoints found within the route of interest.
3. Obtain individual vehicle trajectory segments by grouping all waypoints by their trajectory identifier.
4. Chronologically sort all waypoints for each trajectory grouping.

Once individual vehicle trajectories that traversed the route of interest are acquired, grouped, and sorted, the linear referencing of their waypoints can be estimated.

Given the set of waypoints w_1, \dots, w_n from trajectory τ that lie within the route of interest, where w_1 is the last sampled waypoint within the route, therefore closest to r , and w_n is the first sampled waypoint, hence farthest from r , the linear distance γ of the i -th waypoint is given by:

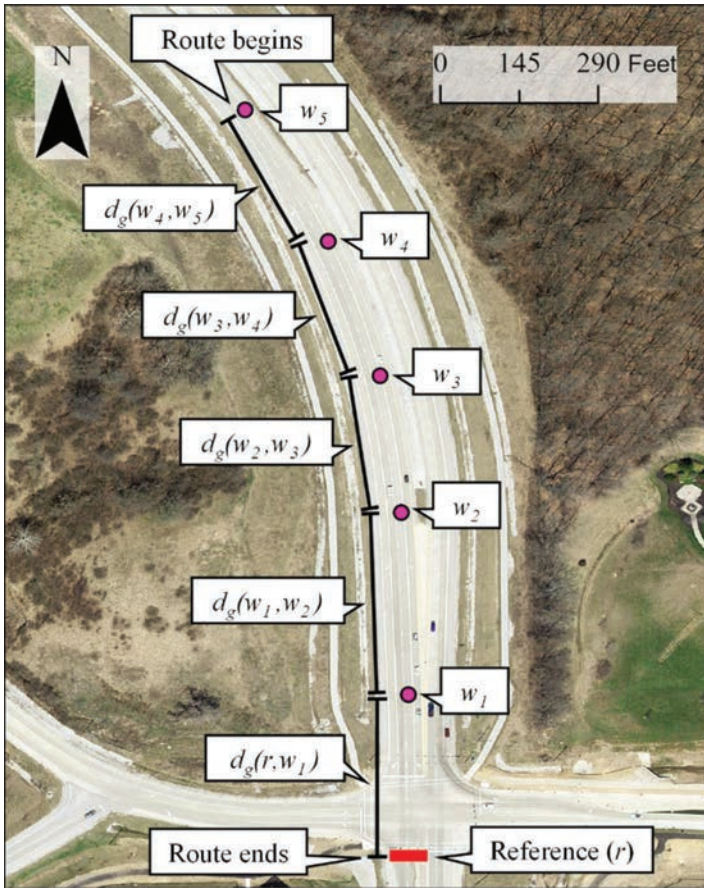
$$\gamma_{\tau}(i) = d_g(r, w_1) + \sum_{k=1}^{i-1} d_g(w_k, w_{k+1}) \quad (\text{Eq. 3.1})$$

where d_g is the geodesic distance (55) between two points and can be calculated with popular open-source geospatial analysis computation packages, such as

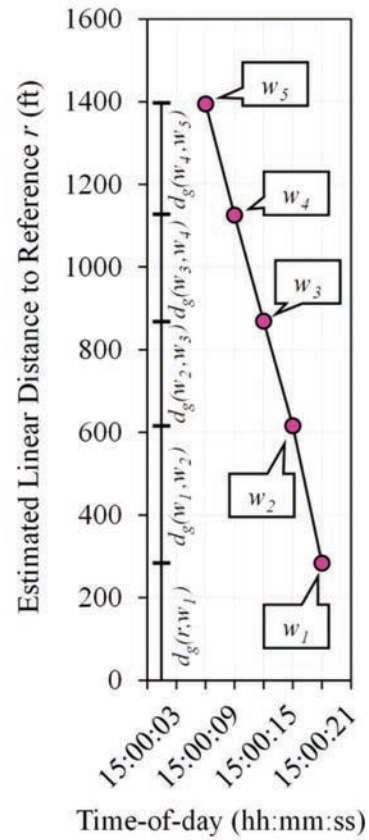
Python's *geopy* (56) or R's *sf* (57). The units of γ are the same as the units for d_g .

Figure 3.2 is a graphical representation of Equation 3.1. Figure 3.2a shows the route of interest where linear referencing is required. The beginning of the route is upstream of the SB approach of a signalized intersection and the end of the route is located at the far side (FS) of the intersection, designated by r . Within this route, five waypoints of the same trajectory are obtained, where w_5 is sampled first and w_1 last. Therefore, using Equation 3.1, the linear distance of w_1 within the route is $d_g(r, w_1)$, for w_2 is $d_g(r, w_1) + d_g(w_1, w_2)$, and so on. Figure 3.2b shows a time-space diagram of the linear referenced progression of the vehicle trajectory segment shown in Figure 3.2a.

The presented linear referencing technique, in which a particular linear waypoint location is based on the cumulative distance to a reference point, provides the ability to estimate a number of metrics when working on studies at the intersection- and corridor-level. However, for studies where the route of interest is several miles long, for example, when analyzing mobility at the interstate-level, the linear distance error accumulated from a much greater number of samples may add up to a significant quantity. In these scenarios, an alternative



(a) Geospatial location (map data: Indiana Geographic Information Council)



(b) Linear referenced waypoints

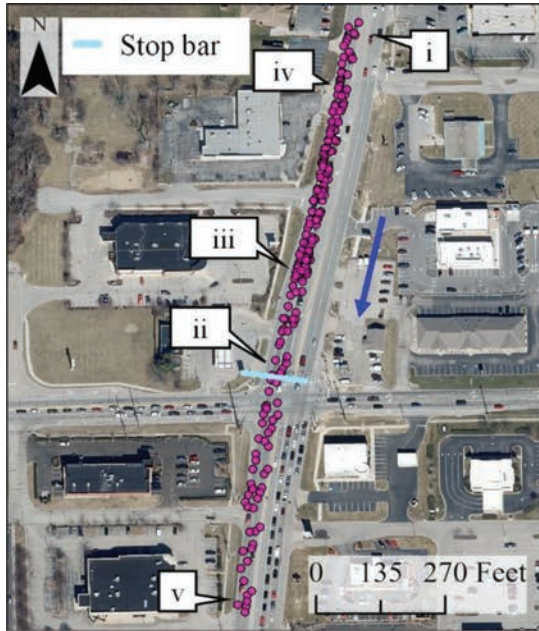
Figure 3.2 Trajectory waypoints linear referencing.

approach could be to create closely spaced geospatial references along the route of interest for which each linear distance along the route is known. Then, to linear reference a trajectory waypoint, the closest geospatial reference is found, and its linear distance assigned to the waypoint.

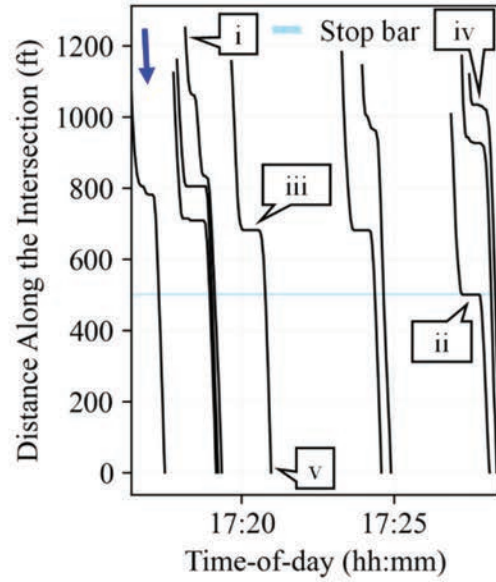
Once vehicle trajectories are linear referenced, their progression along routes of interest can be assessed.

3.1.2 Trajectories Along Intersections

Figure 3.3a displays 301 waypoints that belong to ten different vehicles that traveled SB-through at a signalized intersection. Figure 3.3b shows a time-space diagram of the ten linear referenced trajectories where the route of interest begins upstream and ends downstream of the intersection. One can distinguish how



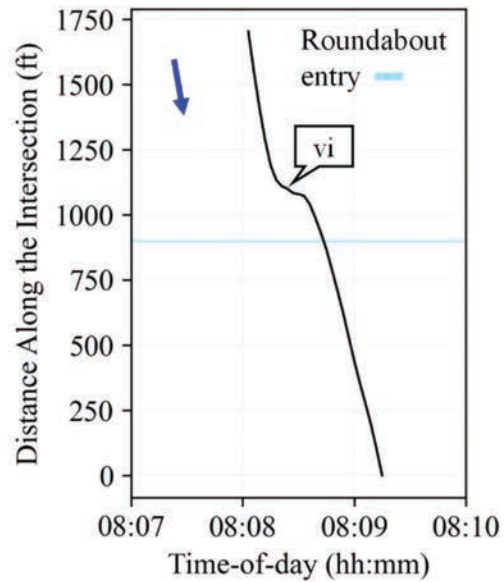
(a) Waypoints along a signalized intersection (n: 301)



(b) Linear-referenced trajectories along a signalized intersection



(c) Waypoints along a roundabout (n: 25)



(d) Linear-referenced trajectory along a roundabout

Figure 3.3 Vehicle trajectories along intersections (map data: Indiana Geographic Information Council).

these vehicle trajectories start approaching the intersection over 500 ft. upstream from the stop bar (callout i). Then, before crossing the intersection, some of these trajectories become completely horizontal. This means that they have come to a full stop since the distance does not change as time advances (which can be verified by reviewing the speed). For example, callout ii points to a vehicle trajectory segment that stopped just before the stop bar. Additionally, callouts iii and iv point to vehicle trajectory segments that stopped behind queues 200 and 500 ft. upstream from the stop bar, respectively. Finally, vehicles are discharged, and their trajectories track downstream from the intersection (callout v).

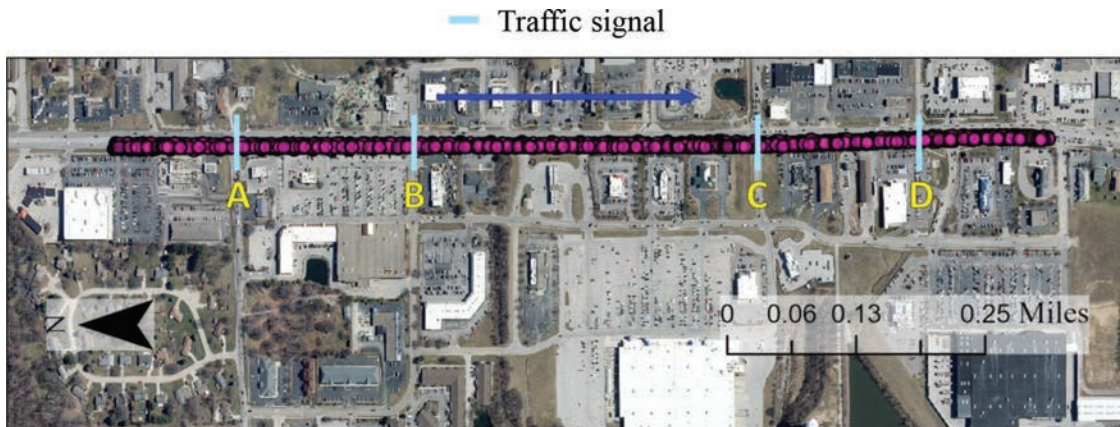
Depending on the type of intersection analyzed, vehicle behavior may vary significantly. For example, Figure 3.3c shows 25 waypoints from a vehicle that traveled NB-through at a roundabout. In a roundabout, vehicles entering the intersection may modulate their speed to avoid conflicts and coming to a full stop. Figure 3.3d shows a time-space diagram of the

linear referenced trajectory from Figure 3.3c where the route of interest begins upstream and ends downstream of the roundabout. In this case, the vehicle slows down, denoted by a shift in the slope of the trajectory (Figure 3.3d, callout vi), but does not come to a full stop.

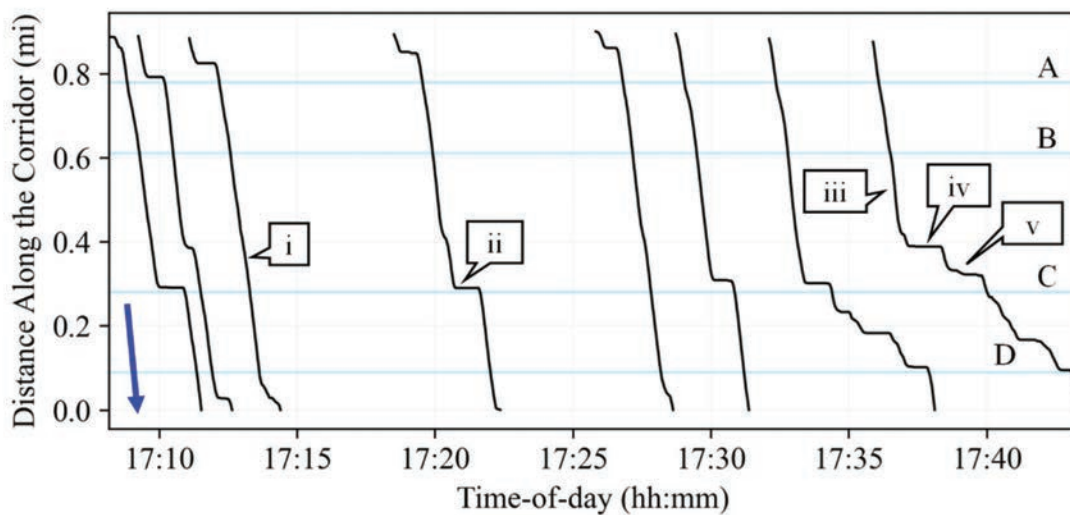
A more thorough assessment of vehicle experience while traversing intersections, from which signal performance measures are estimated, is presented in Chapter 5.

3.1.3 Trajectories Along Corridors

Vehicle progression can be evaluated by expanding the above analysis across several intersections. Figure 3.4a displays 663 waypoints that belong to eight different vehicles that traversed SB-through for the entirety of the route of interest which encompasses four signalized intersections marked A to D. Figure 3.4b shows a time-space diagram of the eight linear referenced trajectories where the route of interest begins upstream and ends downstream of the roundabout.



(a) Trajectory waypoints (n: 663) (map data: Indiana Geographic Information Council)



(b) Linear-referenced trajectories

Figure 3.4 Vehicle trajectories along a corridor.

upstream of intersection A and ends downstream of the intersection D.

From Figure 3.4b, the number of vehicles that stop before passing a particular intersection can be determined. For example, all eight vehicles passed through intersection B without stopping. However, different operational conditions are shown for intersection C. Before crossing through this location, a few vehicles did not stop (such as callout i), a few vehicles stopped once (such as callout ii), and a vehicle stopped twice (vehicle pointed by callout iii stops first at callout iv and then at callout v).

Figure 3.4b provides a framework from which corridor performance can be estimated. Additional assessments of vehicle experience while traversing arterials are presented throughout the report.

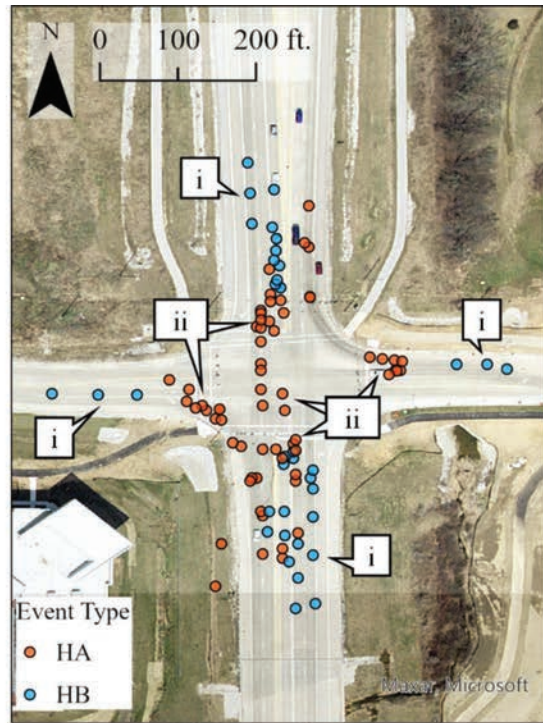
3.2 Events

Figure 3.5 shows 102 recorded CV events that occurred during one day near a signalized intersection.

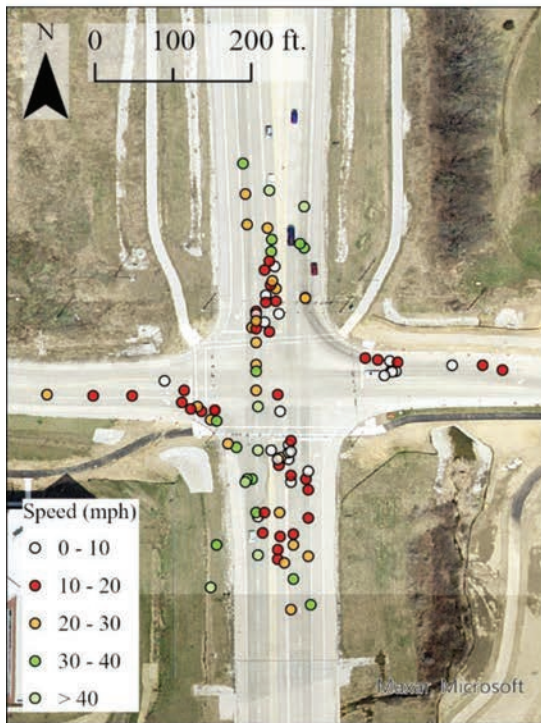
HA and HB events are differentiated on Figure 3.5a. It becomes apparent how HB events mostly occur upstream from the intersection (callout i) as vehicles may decelerate quickly during their approach for the left turn movement or upon entering the dilemma zone (58, 59). On the other hand, HA events mainly occur near the stop bar or inside the intersection (callout ii) as vehicles may try to promptly proceed after an onset of yellow or rapidly accelerate after the onset of green.

Figure 3.5b and Figure 3.5c show vehicle speeds and headings, respectively, at the moment when samples were collected. From a qualitative evaluation, it can be determined that both types of events can occur at different speeds. It can also be identified that vehicles approach the intersection NB with headings near 0° and 360° (callout iii), EB with headings around 90° (callout iv), SB with headings neighboring 180° (callout v), and WB with headings near 270° (callout vi).

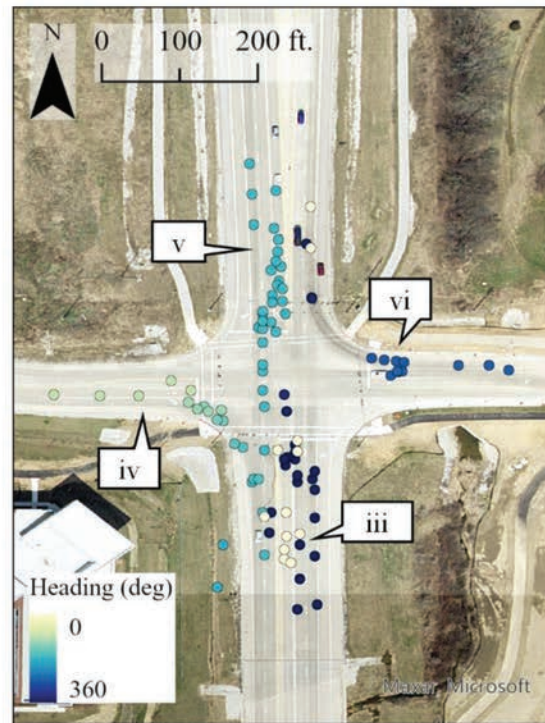
The use of CV events to evaluate safety and driver behavior is discussed in Chapter 12.



(a) Events by type



(b) Events by speed



(c) Events by heading

Figure 3.5 CV events around a signalized intersection (n: 102) (map data: Indiana Geographic Information Council).

4. MOVEMENT IDENTIFICATION

A movement describes the course undertaken by a vehicle at an intersection (60). It usually entails the combination of approaching directions (e.g., NB, EB, SB, and WB) and turn types (e.g., through, left, and right). For example, a vehicle approaching an intersection NB and continuing through is described as a NB-through movement, a vehicle approaching EB and turning right is described as an EB-right movement, and a vehicle approaching WB and turning left is described as a WB-left movement.

Practitioners need the ability to evaluate the performance of their managed intersections at the movement-level because traffic signal phases serve one or more movements at the same time (60). Therefore, by analyzing the performance of specific movements, practitioners can identify the signal phase that may have operational challenges. Once a poor-performing movement is pinpointed, the signal phase parameters and its associated detection hardware can be evaluated to determine a possible remedy (e.g., maintenance, split rebalance, offset modification, or changes in cycle length).

Figure 4.1 shows all trajectory waypoints sampled over a day at a typical four-legged, bidirectional, signalized intersection and the 12 different movements a vehicle can take when proceeding, except U-turns. Conventional traffic signal phase and overlap identifiers are used to differentiate the movements, where through movements are even numbers, left movements are odd numbers, and right movements are assigned a letter.

The objective of the movement identification is to assign one of the 12 movement identifiers to trajectories that proceed through an intersection of interest. This chapter provides two different techniques to accomplish this task—one using geofences and the other using CV data itself.

4.1 Geofencing

Geofencing is a technique that uses virtual boundaries, called geofences, over geographical areas of interest to monitor mobile objects equipped with GPS devices (61). Geofences can be used to assign movements to vehicle trajectories that traverse an intersection.

First, geofences that encompass the route that specific movements would follow need to be manually defined. Figure 4.2a and Figure 4.2b show sets of geofences to capture NB-through and NB-left movements at a signalized intersection, respectively. Each movement requires the following three different geofences.

1. A geofence upstream of the intersection (callout i) to retrieve waypoints that approach the intersection on the lanes used by the movement of interest.
2. A geofence downstream of the intersection (callout ii) to retrieve waypoints that leave the intersection on the lanes used by the movement of interest.
3. A geofence to link upstream and downstream geofences (callout iii) to retrieve waypoints passing the intersection following the movement of interest.

Vehicle trajectories that lie within the geofences for the movement of interest, which waypoints are found both in the upstream (callout i) and downstream (callout ii) sections, are retrieved and assigned the movement. Figure 4.2c and Figure 4.2d show the selected trajectory waypoints from the geofences created to identify NB-through and NB-left traversing vehicles, respectively.

Another important application for the created geofences is to use them as route of interest to perform linear referencing. With this approach, the geofences can provide a framework to evaluate traffic signal performance.

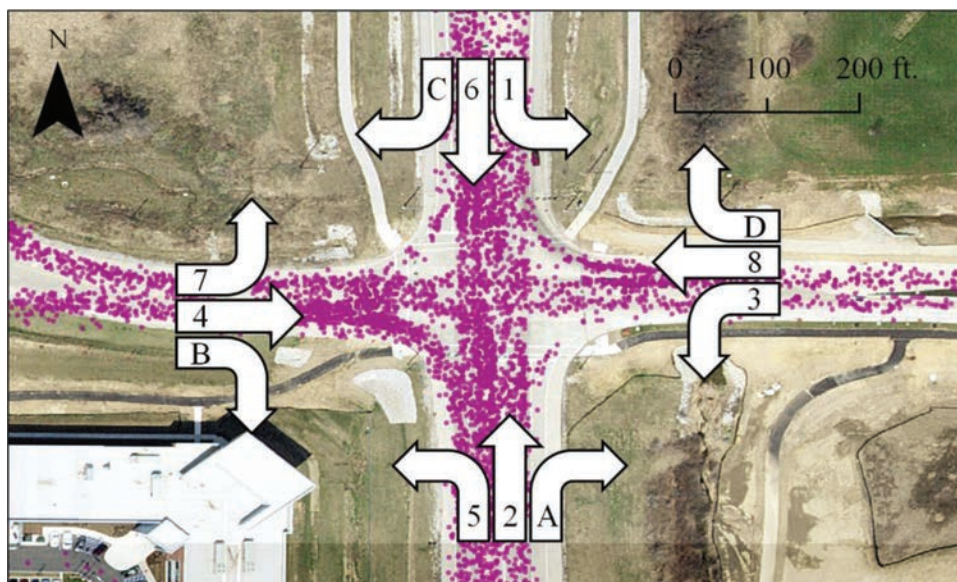


Figure 4.1 Turning movements at a signalized intersection (map data: Indiana Geographic Information Council).



Figure 4.2 Waypoint selection with geofences (map data: Indiana Geographic Information Council).

However, the 12 movements of a conventional four-legged, bidirectional, intersection would require 36 different geofences. Manually defining these geofences is cumbersome and labor-intensive. For example, if 100 intersections are to be evaluated, the geofencing required to produce such a study could take up to 13 entire working days. Therefore, it is important to develop movement identification techniques that scale without significant manual input.

4.2 Data-Driven Movement Detection

A scalable approach of associating vehicle trajectories with intersection movements uses the heading information from the vehicle waypoints (3). The method consists of classifying trajectory movements based on the entry and exit vehicle headings at the intersection. This technique relies on the notion that vehicles following the same movement would also have similar

headings when entering and exiting the intersection. This process broadly consists of the following three steps.

1. Obtain waypoints located in the vicinity of the intersection.
2. Acquire entry and exit headings of waypoints.
3. Evaluate entry and exit heading clusters to identify movements.

A detailed explanation of these steps is provided below.

4.2.1 Trajectory Waypoint Selection

The first step in the data-driven movement identification process is to obtain CV waypoints located near the intersection. These waypoints will eventually be used to estimate signal performance, and a subset of those will be used to acquire entry and exit heading boundaries.

Relevant trajectory waypoints of vehicles passing an intersection are obtained by selecting the waypoints that lie within a buffered intersection center that can be manually defined. Figure 4.3a shows all the vehicle waypoints located within 1,250 ft. from the defined center at a signalized intersection. As the retrieval radius increases, the number of trajectory waypoints that can be evaluated also increases. This is relevant when, for example, it is desired to assess how far away from an intersection vehicles stop. If the retrieval radius is too short, then stops may be missed. Nevertheless, the longer the retrieval radius, the more noise is included in the data set. For example, callouts i highlight waypoints outside the approaches that were also retrieved but are not directly affected by the traffic signal.

To limit the amount of noise included in the waypoint data set, a subset of the initially retrieved data near the intersection is used. Figure 4.3b shows a subset area (callout ii) used to identify entry and exit headings. The inner radius (175 ft. long) filters out waypoints that are passing the center of the intersection and the outer radius (350 ft. long) provides enough coverage to capture entry and exit headings as vehicles approach and depart the intersection. Even though the subset area provides a good compromise between noise and coverage, further processing is required to determine the entry and exit waypoints of vehicle trajectories that actively pass the intersection.

4.2.2 Entry and Exit Waypoint Identification

The second step in the data-driven movement identification process is to obtain the entry and exit headings of vehicle trajectories that pass the intersection.

From the previous step, a subset of waypoints near the intersection is made available (Figure 4.3b). However, this data set still contains waypoints of vehicles that are not actively approaching or leaving the intersection (Figure 4.3b, callout iii). These waypoints would generate miscalculations when estimating entry and exit headings. For this reason, further filtering is needed.

Based on the assumption that vehicles' headings entering an intersection point towards the center and headings exiting point away, vehicles that actively proceed through the intersection can be determined. From the waypoint subset acquired in Figure 4.3b, only the first (entry) and last (exit) samples of each unique trajectory are analyzed. An entry waypoint is deemed correct if its heading value is within $\pm 20^\circ$ from the

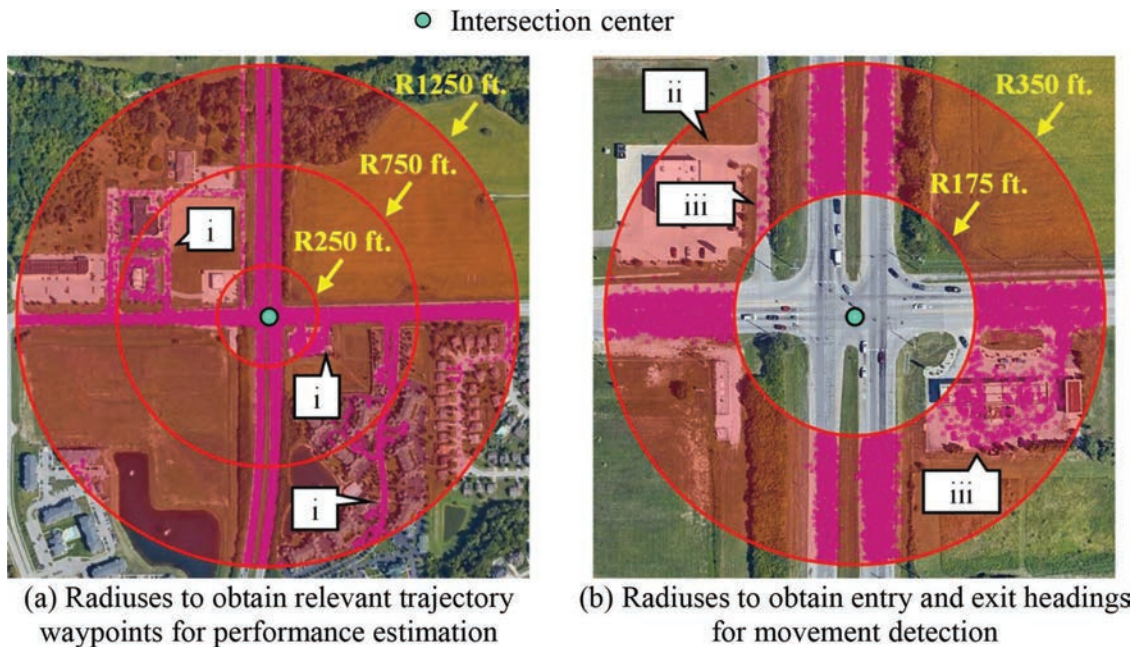


Figure 4.3 Waypoint retrieval radiuses (map data: Google).

direction of a vector that goes from the waypoint to the center of the intersection. An exit waypoint is deemed correct if its heading value is within $\pm 20^\circ$ from the direction of a vector that goes from the center of the intersection to the waypoint. If either the entry or exit waypoint heading is incorrect, the trajectory is rejected.

Figure 4.4a shows an example of a trajectory's entry and exit waypoints deemed correct. The entry waypoint has a heading of 90° (callout i). Similarly, a vector that goes from the entry waypoint to the center of the intersection also has a 90° direction (callout ii). Since these two values are within $\pm 20^\circ$ (callout iii), the entry waypoint is accepted. Meanwhile, the exit waypoint has a heading of 0° (callout iv) and a vector that goes from the center of the intersection to the exit waypoint has a 5° direction (callout v). Since these two values are within $\pm 20^\circ$, the exit waypoint is also accepted. Because both the entry and exit headings are accepted, the waypoints are kept.

In comparison, Figure 4.4b shows an example of a trajectory's entry and exit waypoints that are deemed incorrect. The entry waypoint has a heading of 180° (callout vi) and a vector that goes from the entry waypoint to the center has a 145° direction (callout vii). Because these values are not within $\pm 20^\circ$, the entry waypoint is rejected. Similarly, the exit waypoint is also rejected since it has a 180° heading (callout viii) and the vector that goes from the center to the exit waypoint is 135° (callout ix). Because at least one waypoint is rejected, both points are eliminated.

Figure 4.5 shows the filtering impact on entry and exit waypoint selection. Almost 16,000 waypoints are initially acquired from the entry and exit collection boundaries (Figure 4.5a). This data set includes a significant number of datapoints that belong to vehicles

that are not actively passing through the intersection (callout i). Figure 4.5b shows the results of the filtering technique explained previously. The trajectory waypoints that are not approaching or leaving the intersection are eliminated (callout ii) and only under 5,000 waypoints are deemed as entry or exit datapoints. This reduced waypoint data set can be further evaluated to determine intersection movement heading boundaries.

4.2.3 Movement Identification from Heading Clusters

Once entry and exit waypoints are identified, the next step to determine the heading boundaries is to group entry and exit heading clusters.

Figure 4.6a shows a scatterplot where each datapoint represents the entry and exit heading values, from the waypoints selected in Figure 4.5b, that belong to individual vehicle trajectories. Various clusters are formed for which vehicles' approaching directions (e.g., NB, EB, SB, and WB) can be determined by evaluating entry headings. Additionally, cluster turn types (e.g., left through right) can be identified by comparing entry and exit headings. When combining the estimated approach directions and turn types, intersection movements can be assigned to each cluster.

Figure 4.6a also indicates which movement identifiers, shown in Figure 4.1, belong to the different heading clusters. For example, movement B (EB-right) belongs to the heading cluster with entries around 90° and exits near 180° .

To automate the intersection movement identification process, the number of clusters and their centroids need to be estimated. Then, entry and exit movement heading boundaries can be calculated. However, before this can be accomplished, the results obtained in

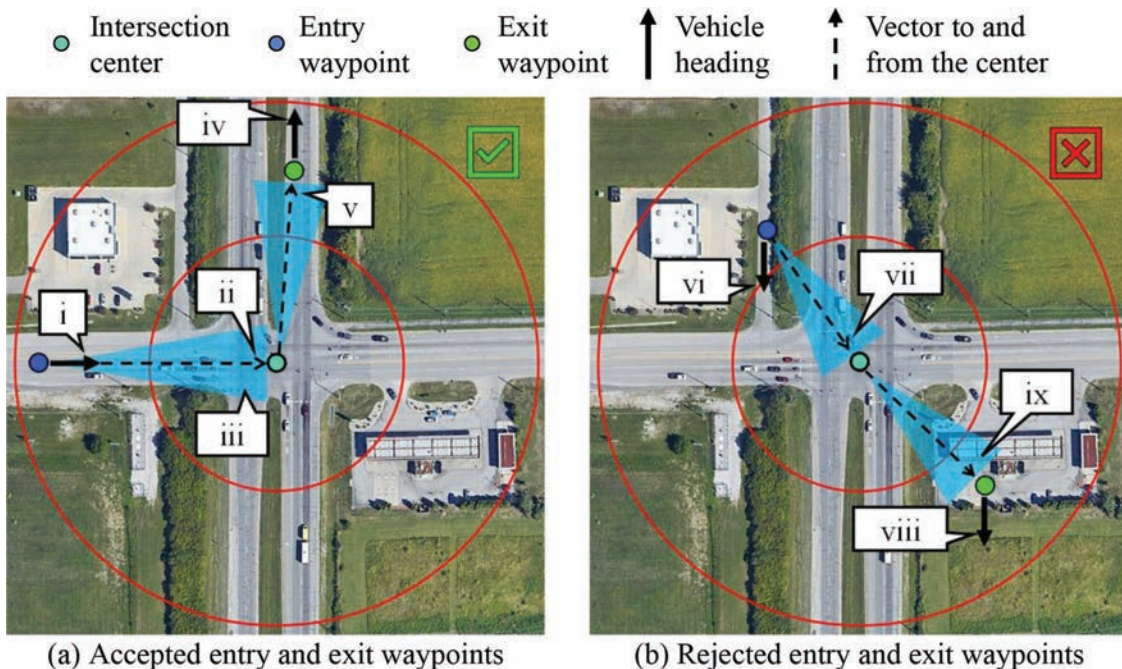


Figure 4.4 Heading-based filtering to identify actively passing vehicles (map data: Google).

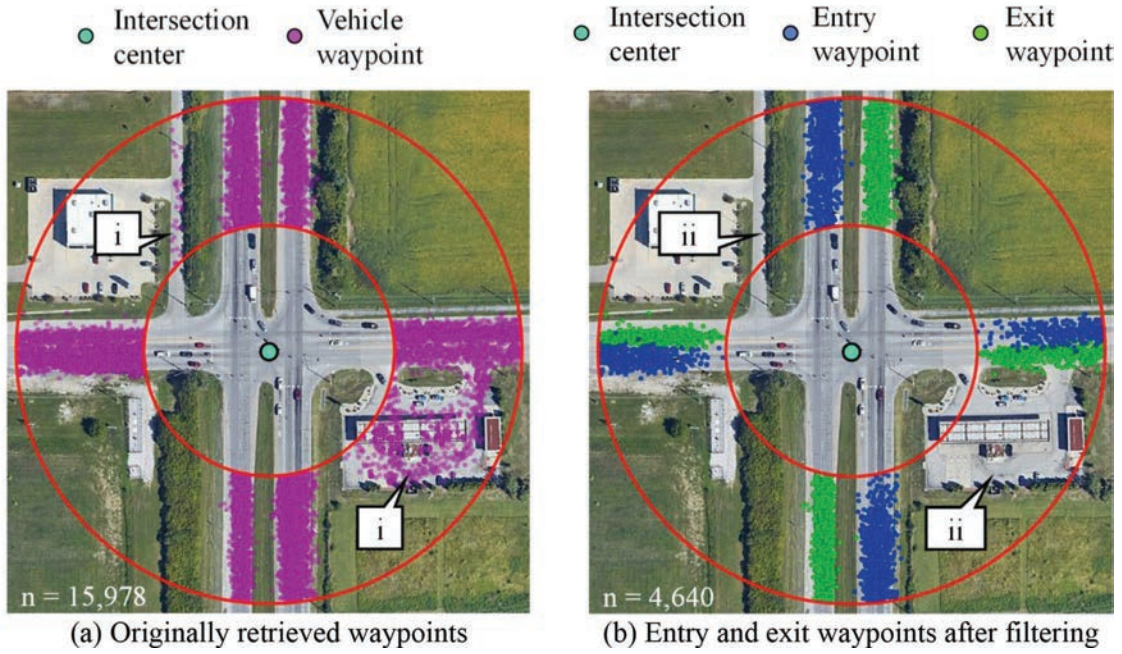


Figure 4.5 Heading-based filtering results (map data: Google).

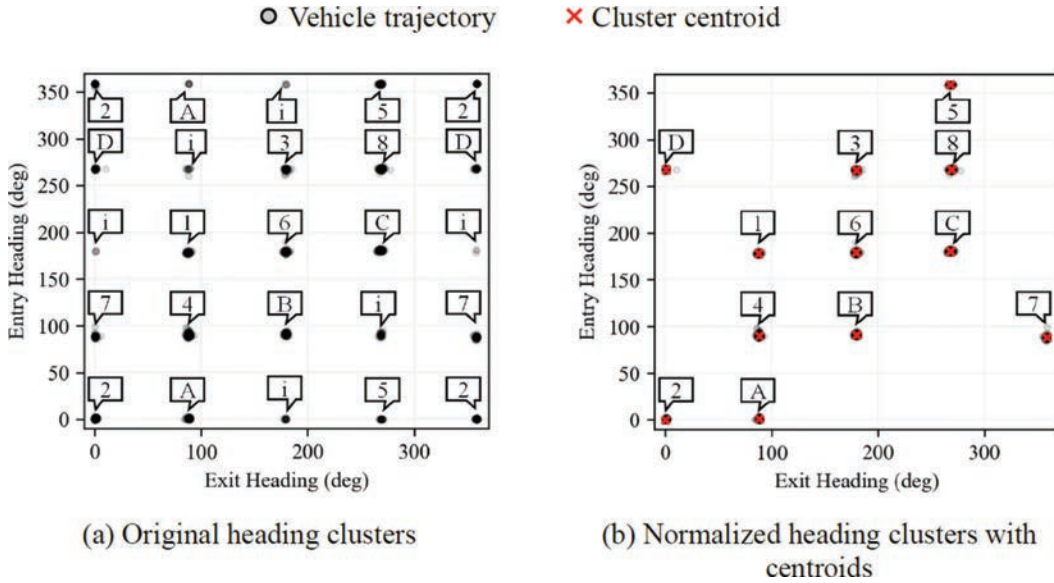


Figure 4.6 Entry and exit heading clusters.

Figure 4.6a need to be normalized by eliminating clusters of vehicles making U-turns (callouts i) since the performance of those movements is usually not evaluated. Additionally, trajectory clusters that have a certain movement and appear more than once (e.g., movement identifier 2 appears four times), due to the heading values wrapping around after crossing 360° , are consolidated with the cluster with the most trajectory points. The result of normalizing Figure 4.6a is shown in Figure 4.6b.

After the heading clusters are normalized, the *k-means* clustering method (62) is used to detect the

number of clusters and their centroids. In *k-means*, for any set C of k clusters, and any set of centroids m_1, \dots, m_k , the error sum of squares is defined as:

$$ESS(C, m_1, \dots, m_k) = \sum_{j=1}^k \sum_{i=1}^{n_j} \|x_{ij} - m_j\|^2 \quad (\text{Eq. 4.1})$$

where n_j is the number of observations in the j -th cluster and x_{ij} is the i -th observation in the j -th cluster. The objective of *k-means* is to find the set C and set of centroids that would minimize *ESS*. To accomplish this, the following steps are taken.

1. Provide an initial set of k centroids.
2. Create k clusters by grouping the datapoints nearest to each centroid.
3. Calculate the centroids for each cluster.
4. Re-assign datapoints to the closest calculated centroid.
5. Repeat steps 3 and 4 until no datapoints are reassigned.

To select a proper value of k clusters (or k movements), the k -means algorithm is run for k values from 1 to 12 to account for all the possible movements at intersections with different number of legs up to a four-legged bidirectional intersection. The k value that has the highest reduction in ESS is selected for further analysis. Then, the average Euclidean distance d_j between the n_j observations and the m_j centroid for all the k clusters in C are calculated as:

$$d_j = \frac{1}{n_j} \sum_{i=1}^{n_j} \|x_{ij} - m_j\| \quad (\text{Eq. 4.2})$$

If an average distance d_j is greater than 10° (threshold selected by testing the method for various locations), k is increased by one and the k -means algorithm is run again. This is done to avoid clustering more than one intersection movement together.

For the normalized scatterplot shown in Figure 4.6b, a k value of 12 is estimated. This means that the analyzed intersection has 12 different movements. The calculated cluster centroids are also shown with red crosses.

Then, entry and exit heading boundary limits can be mapped to the different movements identified by assessing the range of each cluster. Table 4.1 shows the estimated heading boundaries for the 12 movements identified at the evaluated intersection.

At this point, entire vehicle trajectories can be assigned a particular movement by analyzing their entry and exit headings in relation to the intersection. However, movement assignments could include vehicles that trip-chained between the first time they entered and the last time they exited. To filter out these trajectories, the distance traveled by all vehicles assigned with

a particular movement within the retrieval radius can be evaluated. Once the distance traveled distribution is available, outliers that likely performed trip chaining can be identified and filtered (3).

Other useful results for practitioners that can be obtained after assigning movements to sampled trajectories are turning counts. Table 4.2 shows turning counts from a month of data at the analyzed intersection. The heaviest volumes are the mainline through movements with Identifiers 2 and 6, each with 30% of the sampled trajectories. The side-street through movements 4 and 8 follow with 9% and 8% respectively. Even though the trajectory counts are just a sample of vehicles that pass through the location, the distribution of movements can provide insight on which approaches have the highest demands.

4.2.4 Comparison with Geofencing

To assess the performance of the data-driven movement identification method, CV trajectories that passed through eight signalized intersections, located in a south segment of SR-37 in Indianapolis, Indiana, during the month of July 2020 are analyzed. The presented technique is used to assign intersection movements and the results are compared to those obtained from geofencing, which is used as baseline.

Table 4.3 shows the number of trajectories identified with a particular movement by retrieval radius and by method used. The percentage of trajectories identified with a specific movement by the data-driven method that match the selection by the geofencing technique is shown. The matching ratio is calculated by dividing the number of trajectories identified with a particular movement with the data-driven method that are also identified with the same movement by the geofencing technique, by the total number of trajectories identified with the same movement by the data-driven method. The geofencing method typically captures more trajectories because it employs no filters to assure the accuracy of the traversal.

TABLE 4.1
Calculated entry and exit heading limits by movement

Mov ID	Dir	T-Type	Entry Lower Limit (deg)	Entry Upper Limit (deg)	Exit Lower Limit (deg)	Exit Upper Limit (deg)
2	NB	T	0	3	0	2
4	EB	T	87	98	85	93
6	SB	T	177	190	176	184
8	WB	T	263	271	265	278
5	NB	L	357	359	265	271
7	EB	L	84	99	355	359
1	SB	L	177	181	85	91
3	WB	L	261	269	177	185
A	NB	R	0	4	84	89
B	EB	R	89	95	177	182
C	SB	R	179	183	265	272
D	WB	R	265	270	0	10

Note: Mov = movement, Dir = direction, T-type = turn-type, T = through, L = left, and R = right.

Even though a higher matching percentage does not necessarily mean better results, since the data-driven technique can potentially identify more trajectories than with geofences, high values still reassure the

TABLE 4.2
Sampled trajectories turning counts

Mov ID	Trajectory Count	Percentage of All Movements
2	23,616	30
4	7,063	9
6	23,741	30
8	6,498	8
5	2,526	3
7	2,857	4
1	2,130	3
3	1,672	2
A	1,428	2
B	2,391	3
C	2,647	3
D	2,259	3

Note: Mov = movement.

accuracy of the methodology. Matching trajectories range between 88% and 98%. Further, the longer the trajectory retrieval radius is (Figure 4.3a), the more trajectories that are evaluated and assigned a movement. However, as this radius increases, more trajectories can be filtered based on their distance traveled, as it is more likely that vehicles will take different paths or perform trip chaining.

The data-driven movement identification technique can enhance scalability of any analysis that uses CV trajectory data that must be referenced by intersection movements. This is because the only manual labor required is the identification of the intersection's center and retrieval radius, which usually only takes under 5 minutes. For example, if 100 intersections are to be evaluated, under 9 hours of manual labor would be needed.

The automated classification of movements is critical for systematically analyzing traffic signal performance of thousands of signalized intersections necessary to efficiently manage surface street networks.

TABLE 4.3
Trajectories identified with a specific movement by method

Retrieval Radius (ft.)	Movement	Number of Trajectories by Method		Match (%)
		Geofencing	Data-Driven (Heading Cluster)	
250	Through	424,485	84,950	91
750	Through	424,485	446,110	88
1,250	Through	424,485	418,137	88
250	Left	46,488	16,652	92
750	Left	46,488	31,067	93
1,250	Left	46,488	28,613	93
250	Right	50,450	15,037	88
750	Right	50,450	31,067	98
1,250	Right	50,450	27,767	98

5. SIGNAL PERFORMANCE MEASURES: PURDUE PROBE DIAGRAM

Once CV trajectories are linear referenced and assigned an intersection movement, movement-level signal performance can be calculated. This chapter discusses the use of a developed trajectory-based visualization tool, called Purdue Probe Diagram (PPD), to estimate the following traffic signal performance measures (4):

- traditional Highway Capacity Manual (HCM) level of service (LOS),
- number of vehicles experiencing arrivals on green (AOG), sometimes also presented as the percentage on green (POG),
- percentage of vehicles experiencing split failures (SF), and
- percentage of vehicles experiencing downstream blockage (DSB).

Additionally, a comparison between AOG calculations from detector-based techniques and the PPD is presented. Finally, a temporal performance evaluation of a movement at a signalized intersection is conducted to identify time-of-day (TOD) periods where challenges exist.

5.1 Delay Performance Measures

The two most popular delay definitions used to evaluate intersections are stopped and control delay (Figure 5.1) (1, 63). Stopped delay (d_s) is defined as the amount of time that a vehicle has a speed of zero while approaching an intersection and is given by:

$$d_s = t_3 - t_2 \quad (\text{Eq. 5.1})$$

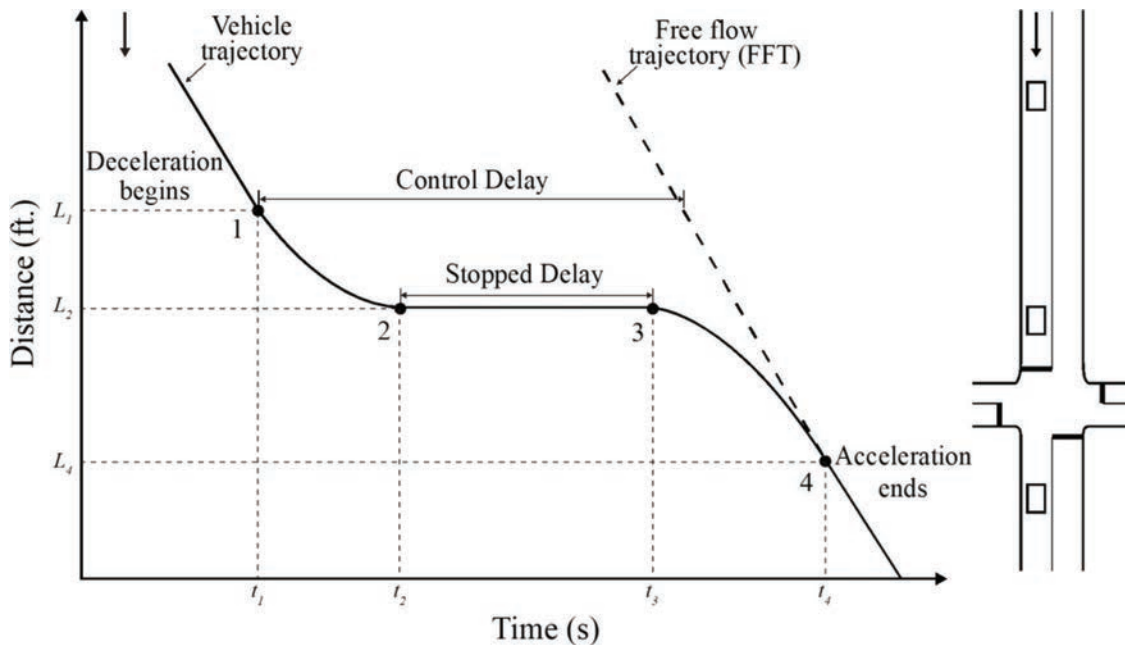


Figure 5.1 Delay definitions (63).

where t_2 is the time when the vehicle speed initially became zero and t_3 is the time when the speed became non-zero after stopping. Control delay (d_c) includes the delay caused by deceleration, stopped delay, and the delay caused by acceleration. It can be calculated as:

$$d_c = (t_4 - t_1) - \frac{L_1 - L_4}{s_f} \quad (\text{Eq. 5.2})$$

where t_1 is the time when the vehicle started decelerating, t_4 is the time when the vehicle stopped accelerating, L_1 is the distance where deceleration started, L_4 is the distance where acceleration ended, and s_f is the speed of a free-flow trajectory (FFT) (i.e., trajectory of a vehicle traveling at the posted speed limit without stopping). Control delay is particularly important as the HCM bases its LOS estimations on this value.

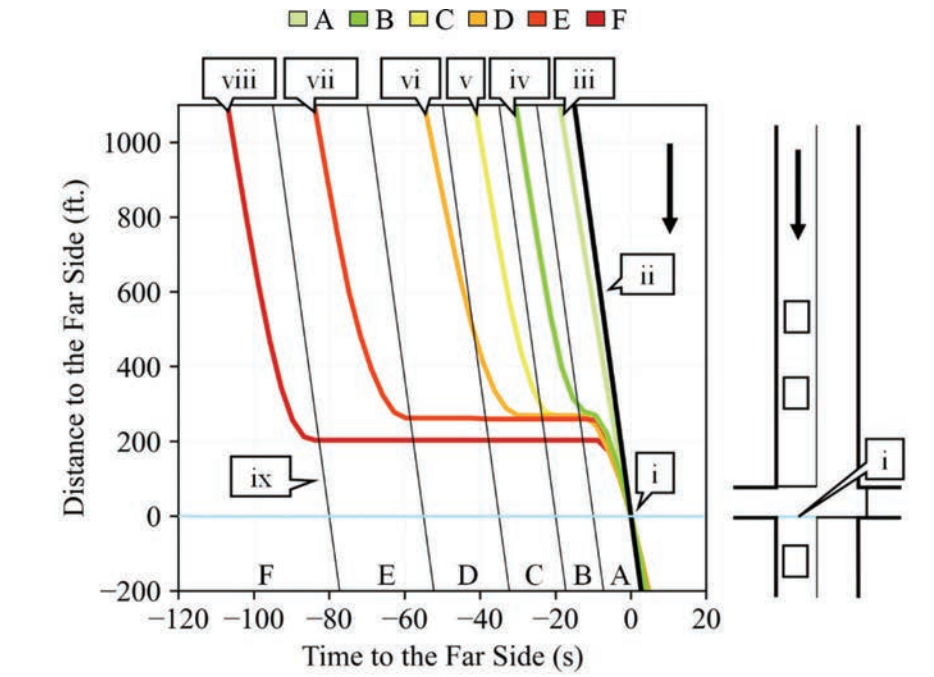
5.1.1 Control Delay Level of Service

LOS is a qualitative description of the operating conditions at an intersection. It is based on the control delay experienced by vehicles (64). Table 5.1 shows the different LOS ratings with their respective range of control delay.

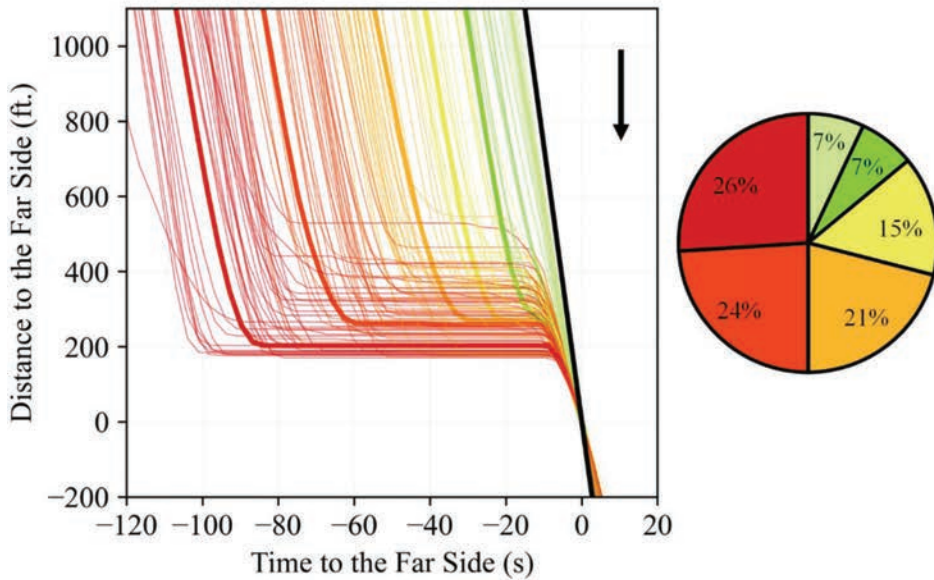
By utilizing Equation 5.2 and the criteria presented in Table 5.1, individual trajectories can be assigned a LOS rating. Figure 5.2a depicts a LOS PPD. A PPD is a time-space diagram where the vertical axis is the distance to the intersection's FS (callout i) and the horizontal axis is the time in seconds relative to when a vehicle crosses the same FS. Therefore, the PPD pivots on the time and space where vehicles exit the intersection. Additionally, an FFT is included for reference

TABLE 5.1
HCM level of service criteria for signalized intersections (64)

Level of Service	Average Control Delay (s/veh)	Description
A	≤10	Free flow
B	>10–20	Stable flow (slight delay)
C	>20–35	Stable flow (acceptable delays)
D	>35–55	Approaching unstable flow (tolerable delay)
E	>55–80	Unstable flow (intolerable delay)
F	>80	Forced flow (congested and queues fail to clear)



(a) Six trajectories with different LOS classifications



(b) All trajectories sampled over a week during the same TOD period (n: 137)

Figure 5.2 LOS in a Purdue Probe Diagram.

(callout ii). Callouts iii–viii are a series of CV trajectories of vehicles following the same movement color-coded by their different LOS classifications. The farther to the left a trajectory approaches the FS from the FFT, the greater its delay is.

Further, callout ix points to a segregation line that helps to visually separate trajectories by their LOS (in this case, the boundary between LOS E and F). It is important to note that the objective of the segregation lines is merely to help set visual boundaries since they are only based on the deceleration and d_s components of control delay, neglecting some of the acceleration delay.

Figure 5.2a is a subset of Figure 5.2b, which shows all 137 trajectories of vehicles following the same movement during the same TOD over 5 weekdays. Additionally, Figure 5.2b shows a pie chart of what percentage of the trajectories are categorized with the different LOS ratings. Only 7% of the trajectories sampled during the analysis period are classified as LOS A, while a considerable number of trajectories are LOS E or F (24% and 26%, respectively). It is worth stating that because of the 3-second frequency of the waypoints, some individual vehicle trajectories may be misclassified by one LOS (e.g., C instead of B, or vice-versa). Nevertheless, the distribution of this error is uniform; therefore, on average, no statistical bias is introduced.

Table 5.2 shows the estimated stopped and control delay values for the trajectories called out in Figure 5.2a. The distinction between these two delay definitions is clear when trajectories do not stop while approaching the intersection but slow down due to a discharging queue or to modulate their speed approaching at the end of red (callouts iii and iv). It is evident that control delay is always greater than stopped delay.

5.2 Operational Performance Measures

Apart from experiencing minimum delay, motorists' general expectations while traversing traffic signals are the following.

- Well-coordinated signals so that vehicles arrive during the green interval and do not stop. The degree to which this occurs can be evaluated by AOG.
- Sufficient green time so they can proceed through after having to stop. The degree to which this does not occur can be assessed by estimating the percentage of vehicles that have to wait for more than one cycle length before proceeding. These events are known as split failures.

TABLE 5.2
Estimated delays for trajectories in Figure 5.2a

Callout	Stopped Delay (s)	Control Delay (s)	LOS
iii	0	6	A
iv	0	18	B
v	9	30	C
vi	18	44	D
vii	51	72	E
viii	78	95	F

- Sufficient storage and not oversaturated at a downstream signal so they can proceed through an intersection unimpeded by downstream queues. The degree to which this does not occur can be evaluated by calculating the proportion of vehicles that experience downstream blockage.

The use of CV-based trajectory data provides an opportunity to look holistically at these three performance measures from the perspective of individual vehicles. For example, AOG is based on whether each evaluated vehicle passes the intersection without stopping; SF is based on whether each assessed vehicle stops more than once during its approach; and DSB is based on whether each evaluated vehicle is significantly obstructed by a downstream queue after exiting. In order to normalize by demand, these operational performance measures are usually presented as a percentage given by:

$$\text{Operational Performance Measure} = \frac{100}{n} \sum_{i=1}^n \varphi(\tau_i) \quad (\text{Eq. 5.3})$$

where τ_i is the i -th trajectory out of n analyzed and φ is an indicator function that denotes whether the event being evaluated by the particular performance measure occurred. That is:

$$\varphi(\tau_i) = \begin{cases} 0, & \text{if } \tau_i \text{ does not experience the event} \\ 1, & \text{if } \tau_i \text{ experiences the event} \end{cases} \quad (\text{Eq. 5.4})$$

To obtain performance results as ratios rather than percentages, calculations obtained from Equation 5.3 are divided by 100.

5.2.1 Arrivals on Green

AOG indicates the number of vehicles that arrive at a signal during the green phase of the cycle and POG indicates the percentage of vehicles that do the same. For simplicity, AOG and POG are used interchangeably for the rest of the report. AOG is calculated from Equations 5.3 and 5.4 with $\varphi(\tau_i) = 1$ when τ_i does not have to stop before exiting and $\varphi(\tau_i) = 0$ when it must stop. This measurement gives valuable information on the performance of coordinated intersections, where low AOG values indicate that vehicle platoons are not progressing as intended (65).

Figure 5.3a shows a PPD with two vehicle trajectories color-coded based on their number of stops. The first time a vehicle's speed goes to zero when approaching an intersection, the trajectory is assigned one stop and the location where this occurs is regarded as the queue-length at that time. After this, every time a vehicle's speed goes from non-zero to zero, after traveling for at least 100 ft. following the previous stop, it is attributed an additional stop. The 100 ft. filtering is done to avoid counting extra stops when vehicles are just inching forward when waiting for green in a queue and can be adjusted depending on the approach.

Callout i points to a green trajectory that does not stop before exiting the intersection, therefore categor-

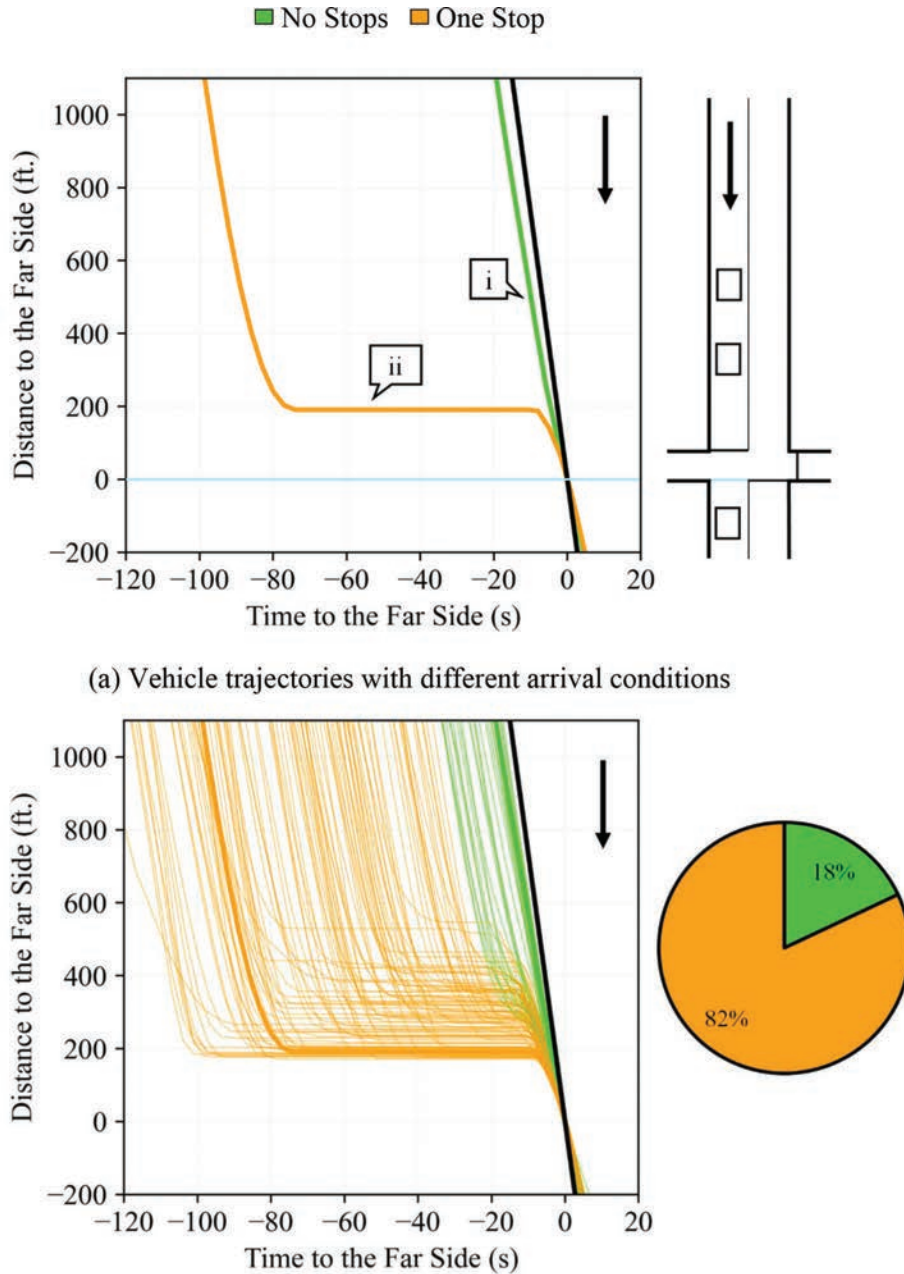
ized as having arrived on green (i.e., $\varphi(\tau_i) = 1$). Callout ii points to an orange trajectory that stopped 200 ft. upstream from the FS, therefore categorized as not having arrived on green (i.e., $\varphi(\tau_i) = 0$), also known as arrival on red. The trajectory that does not stop during the approach is closer to the FFT; hence, it has a smaller delay than the trajectory with one stop.

Figure 5.3a is a subset of Figure 5.3b, which shows all 137 trajectories of vehicles following the same movement during the same TOD over 5 weekdays. Additionally, Figure 5.3b shows a pie chart of what percentage of the trajectories are categorized as having

arrived on green. The movement analyzed at this intersection has an AOG value of only 18%, which indicates that 82% of all vehicles following this movement must stop before exiting.

5.2.1.1 Comparison with detector-based techniques.

Discrepancies between detector-based ATSPMs and actual traffic conditions vary depending on the type, placement, and size of detection, and the traffic operational regime (66). Qualitatively, these discrepancies have been known by experienced practitioners for some time. CV data now provides an opportunity for a more



(b) All trajectories sampled over a week during the same TOD period (n: 137)

Figure 5.3 AOG in a Purdue Probe Diagram.

thorough comparison using real vehicle data. This subsection compares AOG estimations obtained from CV-based and detector-based (ATSPM) techniques under different queue-length conditions (5).

Detector-based techniques estimate AOG by identifying the presence of vehicles with an advance detector upstream of the stop bar. When a vehicle is detected, its arrival time at the intersection is projected and the signal state is evaluated to determine if the vehicle arrived on green (65). This method may not provide an accurate estimation under conditions that affect vehicle arrivals either upstream or downstream from the advance detector since arrival projections usually assume that vehicles travel in undersaturated and unimpeded conditions (66).

In contrast, AOG calculations from CV trajectory data are based on whether vehicles stop at some point during their entire approach towards a signalized intersection without the need for projections or assumptions, as illustrated on the PPDs in Figure 5.3. This is possible because trajectory data reports where a CV vehicle traverses. As long as there is sufficient CV penetration in the traffic stream, CV-based AOG estimations reflect more accurately the impacts from oversaturation, residual queues, and speed modulation than those derived from advance detection. Therefore, it is assumed that similar AOG estimations from both techniques indicate accurate detector-based results, whereas distinct estimations suggest detector-based errors.

Detector-based AOG estimations are usually obtained and visualized from Purdue Coordination Diagrams (PCDs) (67). Figure 5.4a shows a PCD of a movement at a traffic signal. In a PCD, the vertical axis represents the time-in-cycle of the analyzed movement, and the horizontal axis is the TOD. Once the end of the cycle is reached on the vertical axis, the value is reset to zero to start the next cycle. Therefore, time moves diagonally from bottom to top and left to right. Further, a green line represents the beginning of green (BOG) and a red line indicates the beginning of red (BOR) of the analyzed movement. Finally, markers (i.e., dots and crosses) show the estimations of vehicle arrivals at the signal (1).

AOG values are derived by calculating the percentage of vehicles that are estimated as having arrived during the green interval of the phase (i.e., markers above the green line and below the red line). However, accurate AOG estimations depend on whether the projection of arrivals reflect the behavior of vehicles and traffic conditions.

Figure 5.4b shows a PPD for the same movement and time as the PCD in Figure 5.4a. Callout i points to the location of the stop bar and callout ii to the location of the advance detector (295 ft. upstream from the stop bar). In both subfigures, vehicles correctly identified by the detector-based technique as having arrived on green are color-coded in green and vehicles correctly categorized as having to stop are color-coded in orange. Vehicles that stopped which are incorrectly categorized

as arrived on green by the PCD are color-coded in red and marked with a cross in Figure 5.4a.

The reason for the PCD misclassifications in Figure 5.4 is because those vehicles stopped before the advance detection due to queues longer than 295 ft. Once the vehicles pass through the advance detector (callout iii) they are projected to arrive on green. This overestimates AOG by 22% using the detector-based technique. Figure 5.4 compares AOG estimations at one movement; however, it is important to contrast AOG calculations at the system-level to obtain a complete picture of estimation differences.

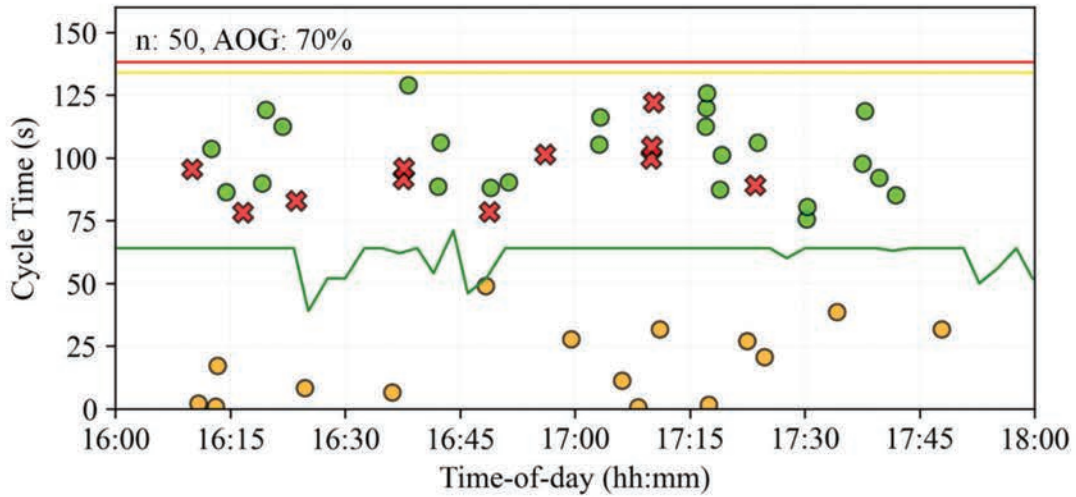
Figure 5.5 shows a scatterplot comparing AOG estimations from both techniques for 52 intersections that operate under different traffic conditions. Each point represents an AOG estimation for a particular movement and timing plan of a signal. There is a total of 272 points corresponding to 43 unique timing plans deployed at the evaluated intersections. The analysis period is from August 16th to August 20th, 2021. Since the ATSPM tool from which AOG estimations are obtained (68) only provides results for entire TOD plans and no raw data is available, the median value of the evaluated week for each TOD plan is taken as the detector-based result.

A blue line with no offset and a slope of one is plotted for reference. Points near the blue line indicate a smaller discrepancy between the AOG estimation methods. Points above the blue line are locations where detector-based estimations are higher than those from CV data, such as the case analyzed in Figure 5.4, where long-queues created a significant discrepancy between calculations. Points below the blue line are locations where detector-based estimations are lower than those obtained from CV data.

A linear least-squares regression line is plotted in black to show the overall trend of the relation. With an R^2 value of 0.81, it can be stated that, in general, there is close correlation between measurements. However, one can also observe that for CV-based AOG values below 30%, detector-based AOG results can be highly overestimated for some outliers. As queue-length is the main factor that cause discrepancies on AOG estimations (5), their impact is further analyzed.

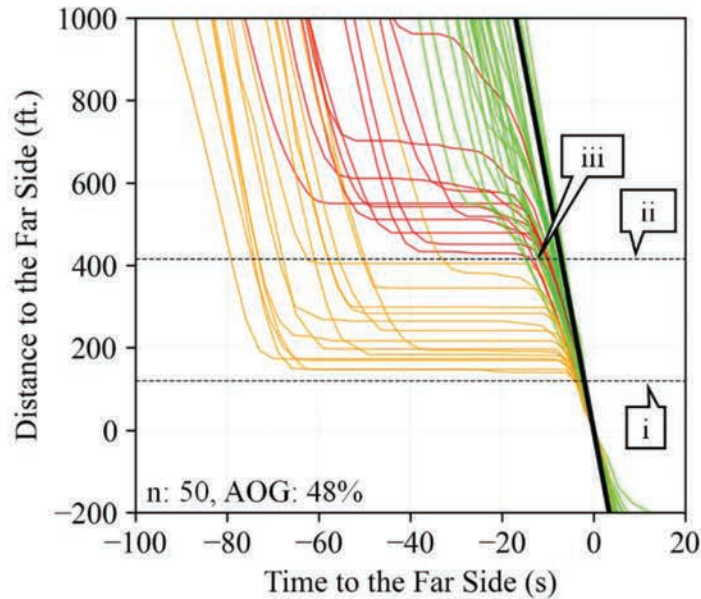
Figure 5.6 shows a negative trend between the median queue-length and the difference of AOG estimations. Each point represents a particular intersection, movement, and period for locations where the advance detector is located between 350 and 400 ft. upstream of the signal (most popular distances due to prevailing speed limits). For long queues, as in Figure 5.4, detector-based AOG results are overestimated. For short queues, some detector-based AOG results are underestimated. This is because approaching vehicles may pass the advance detection at a time when they are projected to not arrive on green but may modulate their speed due to a short standing queue, or to avoid stopping, which allows them to arrive on green (5).

— Change to Green — Change to Yellow — Change to Red
● Correct AOG Projection ● Correct non-AOG Projection ✘ Incorrect AOG Projection



(a) Detector-based PCD

■ No Stops ■ One Stop ■ One Stop (Incorrectly Projected by PCD)



(b) CV-based PPD

Figure 5.4 AOG estimations from different techniques.

The effects that queue-length have on detector-based AOG estimation reliability is shown in Figure 5.6. Detector-based AOG estimation accuracy considera-

tions during long (i.e., past the advance detector) and short (i.e., not past the advance detector) queue-length conditions are (5) the following.

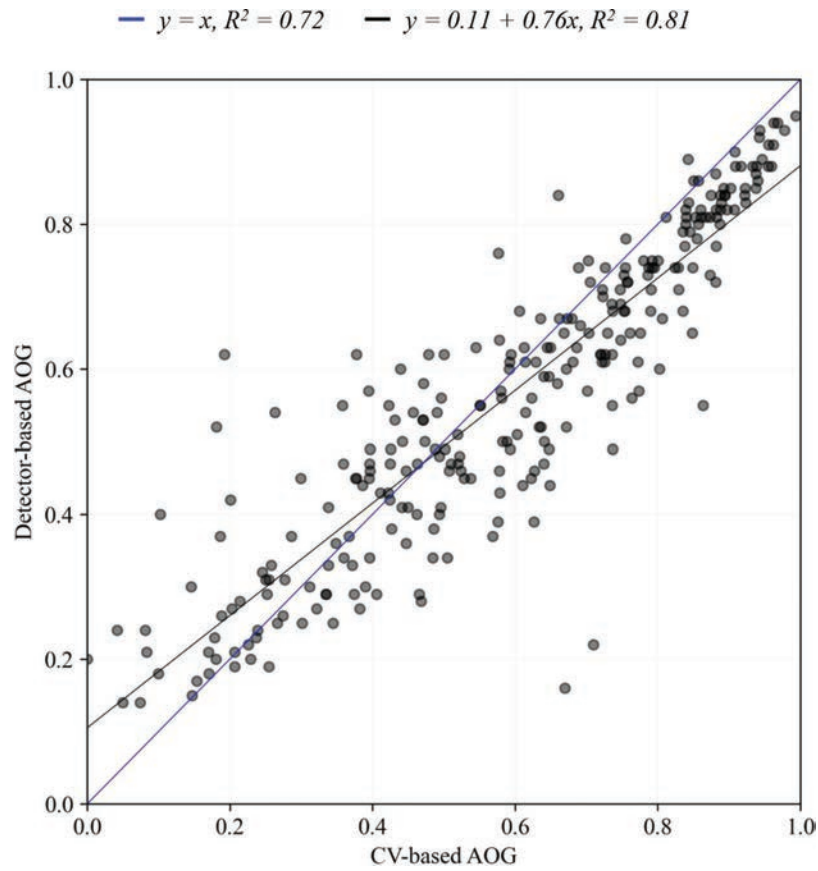


Figure 5.5 AOG estimation comparison.

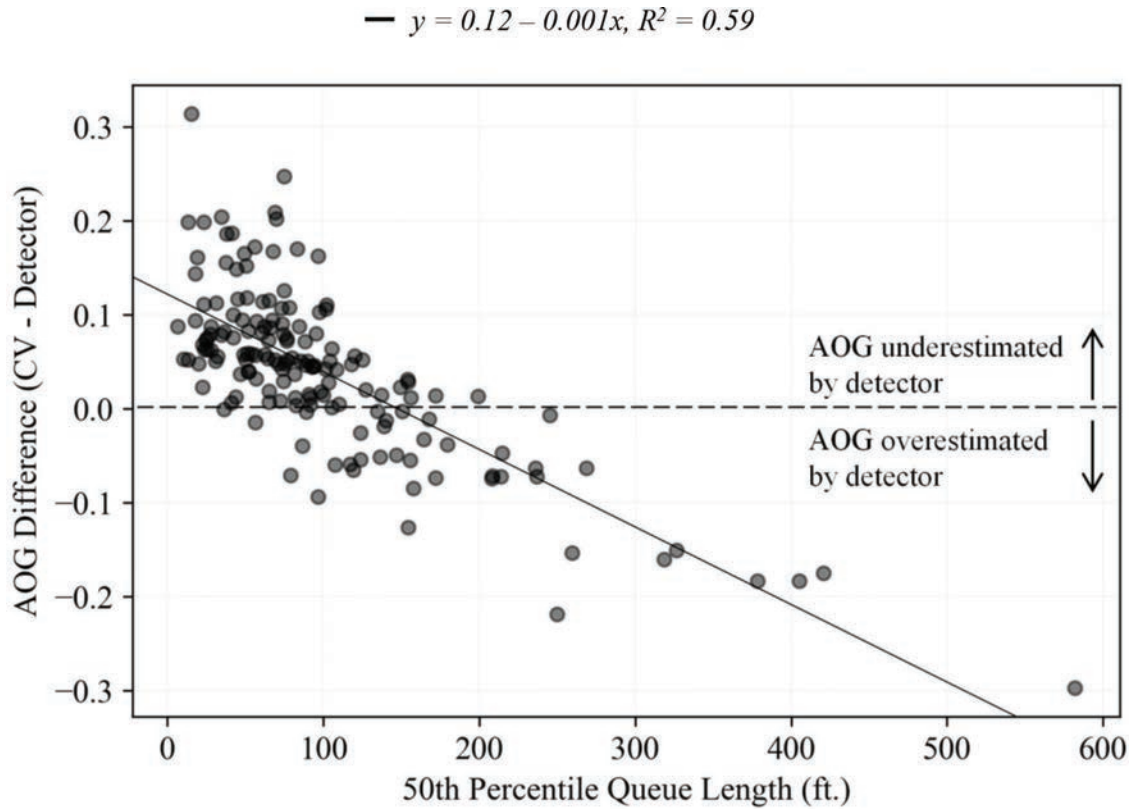


Figure 5.6 Queue-length effects on AOG discrepancies.

- Long queues: During this condition, detector-based results tend to be significantly overestimated. This is because vehicles may stop before the advance detection and the queue discharge dynamics are unpredictable, making the detector-based arrival time projections inaccurate. Figure 5.4 illustrates this situation quite clearly.
- Short queues: Under this scenario arriving platoons may not be significantly affected by the discharging queue. In this case, detector-based calculations tend to be accurate. Nevertheless, if the speed of the arriving platoon is affected by the discharging queue or to avoid red, then the detector-based AOG results may not reflect real conditions.

5.2.2 Split Failures

A split failure occurs when a traffic signal does not provide enough green time to allow previously stopped vehicles to proceed through the intersection, thus making them wait for longer than one cycle. Split failures occurring for a movement is an indication of that movement operating at overcapacity. Detecting time and location of split failures can help agencies to systematically identify opportunities to reallocate green time to improve operations (69).

SF is a performance measure that provides the percentage of vehicles that experience a split failure during their approach to a traffic signal. From CV trajectory data, a split failure is identified when a vehicle stops more than once before exiting the intersection. The first stop is the arrival at the back-of-queue and subsequent stops are failed attempts to clear the intersection. SF is calculated from Equations 5.3 and 5.4 with $\varphi(\tau_i) = 1$ when τ_i stops more than once and $\varphi(\tau_i) = 0$ when it does not.

Figure 5.7a shows a PPD that illustrates the trajectory of a vehicle that experiences a split failure (i.e., $\varphi(\tau_i) = 1$). It first stops almost 500 ft. upstream from the far side (callout i) and then again 200 ft. upstream from the far side (callout ii). Figure 5.7a is a subset of Figure 5.7b, which shows all 114 trajectories of vehicles following the same movement during the same TOD over 5 weekdays. Additionally, Figure 5.7b shows a pie chart of what percentage of the trajectories experienced a certain number of stops. For the movement and time analyzed at this intersection, only 8% of the vehicles arrived during green, 57% stopped once, 23% stopped twice, and 12% stopped more than twice. Therefore, there is a 35% SF.

5.2.3 Downstream Blockage

Downstream blockage occurs when the downstream intersection has a queue that obstructs the progression of vehicles exiting the current intersection. Identifying downstream blockage is important as a means to pinpoint oversaturated intersections (probably with high SF values) where challenges are caused by an adjacent location. Hence, the source of congestion may be the downstream intersection and not the location being analyzed. In some cases, an adjustment of the

downstream green may address the problem; in other cases, an agency must make a policy decision on how to manage those oversaturated conditions (e.g., change a two-way street into a one-way street) and the impact on the overall network.

Downstream blockage has been quite difficult to assess from traditional high-resolution data as most detection equipment focuses on the upstream segments of an intersection, with the exception of some radar and camera systems. By contrast, CV-based performance measures enable trajectory segments both upstream and downstream of the intersection. Downstream blockage is identified from CV data when a trajectory has at least a 10-second delay compared to the FFT after passing the far side of the intersection (4).

DSB is a performance measure that provides the percentage of vehicles that experience downstream blockage after exiting the intersection. DSB is calculated from Equations 5.3 and 5.4 with $\varphi(\tau_i) = 1$ when τ_i experiences downstream blockage and $\varphi(\tau_i) = 0$ when it does not.

Figure 5.8a shows a PPD that illustrates two trajectories with different downstream blockage classifications. Callout i points to a division line located 10 seconds apart from the FFT. Any vehicle that crosses this line is categorized as having experienced downstream blockage. For example, the vehicle indicated with callout ii does not experience downstream blockage as its downstream segment (gray) does not have more than a 10-second delay in relation to the FFT (i.e., $\varphi(\tau_i) = 0$). On the other hand, the vehicle indicated with callout iii experiences downstream blockage as its downstream segment (blue) has a delay greater than 10 seconds compared to the FFT (i.e., $\varphi(\tau_i) = 1$).

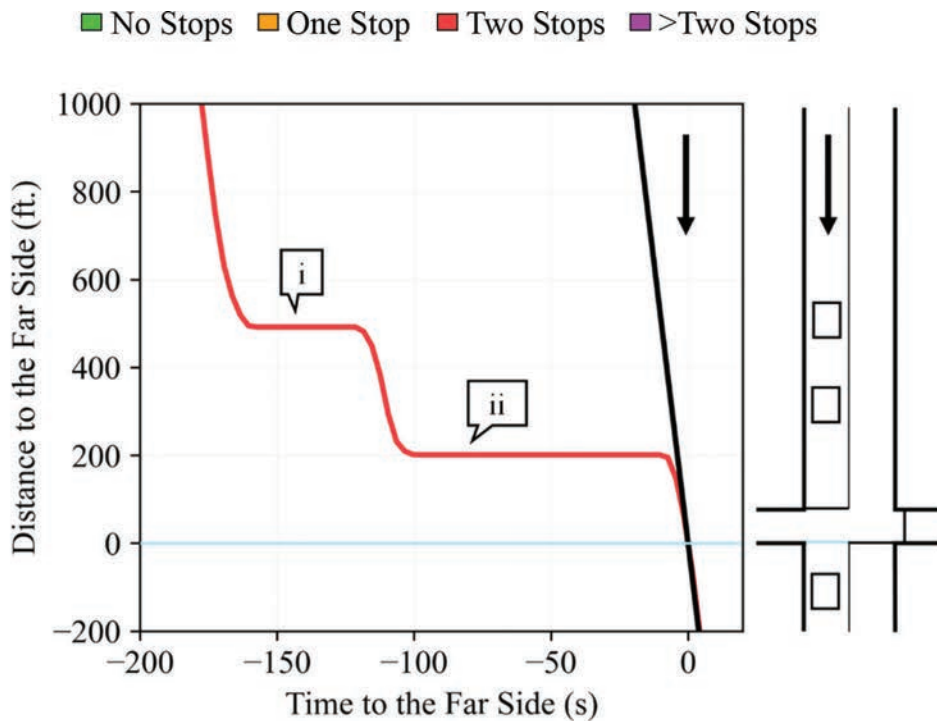
Figure 5.8a is a subset of Figure 5.8b, which shows all 236 trajectories of vehicles following the same movement during the same TOD over 5 weekdays. Additionally, Figure 5.8b shows a pie chart of what percentage of vehicles experienced downstream blockage. For the movement and time analyzed at this intersection, 15% of vehicles experienced DSB.

5.2.4 Concepts Examples

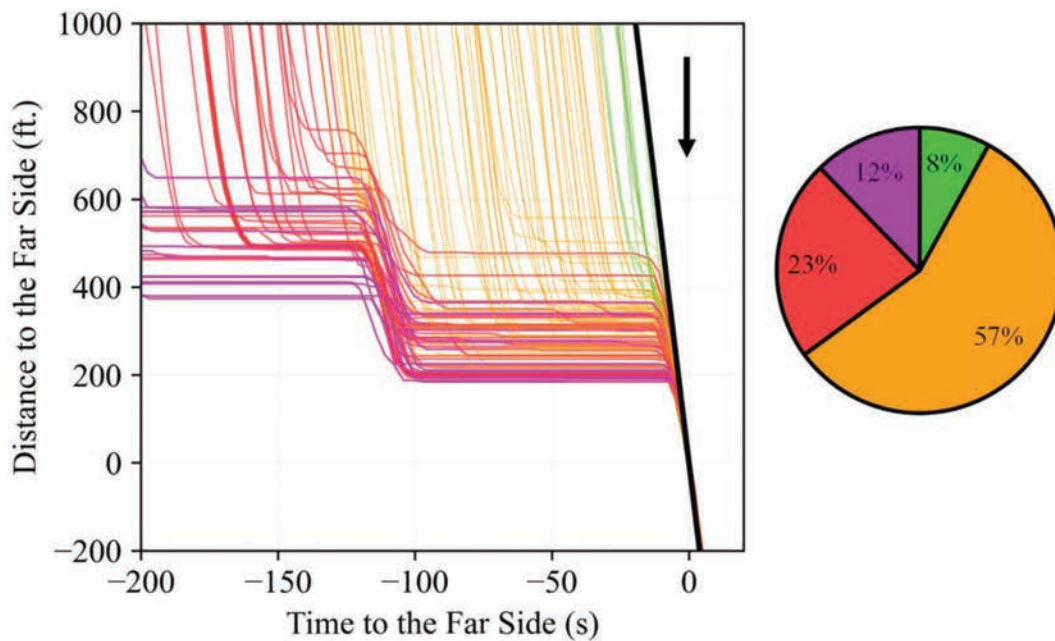
The AOG, SF, and DSB concepts have been explained above in the context of the PPD. However, it is often useful to see physical examples of these scenarios. Table 5.3 provides links and QR codes to short video clips of the occurrence of the relevant operational events discussed in this chapter.

5.3 Temporal Performance Assessment

The PPD provides a framework to evaluate delay, AOG, SF, and DSB for a specific movement and time period. However, practitioners need visualizations to quickly assess signal performance by TOD to identify when challenges exist. To address this need, vehicle trajectories can be color-coded based on their number



(a) Vehicle trajectory that experiences a SF



(b) All trajectories sampled over a week during the same TOD period (n: 114)

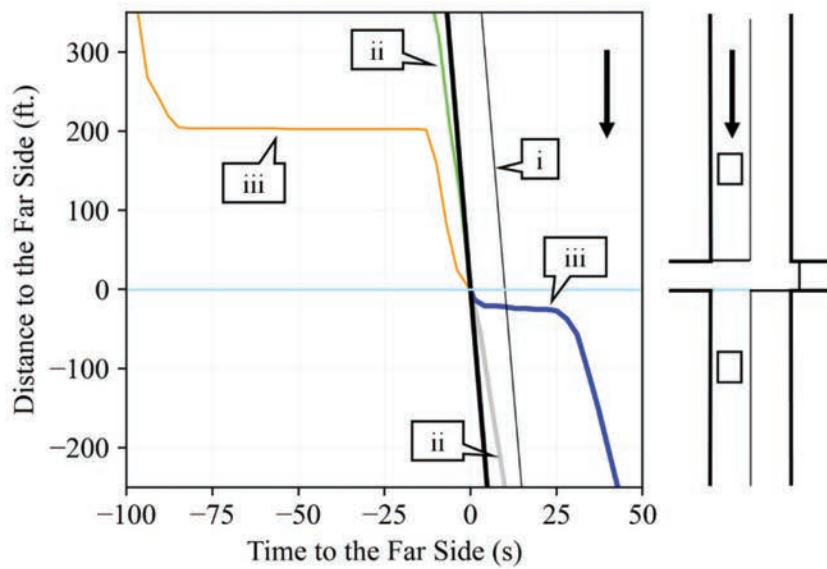
Figure 5.7 SF in a Purdue Probe Diagram.

of upstream stops and based on the occurrence of downstream blockage (as in Figure 5.3, Figure 5.7, and Figure 5.8) with the horizontal axis as the TOD when the waypoints are sampled.

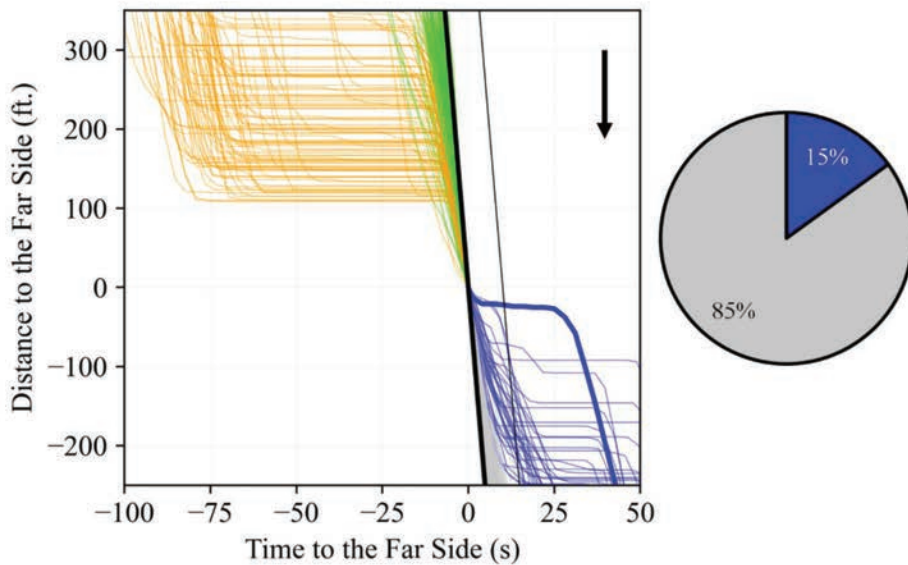
Figure 5.9a shows all trajectories passing a signalized intersection color-coded by their number of stops and

occurrence of downstream blockage. The analyzed period is segmented into four timing plans: AM peak (AM, 06:00–09:00 hrs.), midday (MD, 09:00–15:00 hrs.), PM peak (PM, 15:00–18:00 hrs.), and evening (EV, 18:00–22:00 hrs.). From a qualitative evaluation of Figure 5.9a, it can be determined that no downstream

■ No Stops ■ One Stop ■ Two Stops ■ >Two Stops ■ DSB ■ No DSB



(a) Vehicle trajectories that experience DSB and no DSB



(b) All trajectories sampled over a week during the same TOD period (n: 236)

Figure 5.8 DSB in a Purdue Probe Diagram.

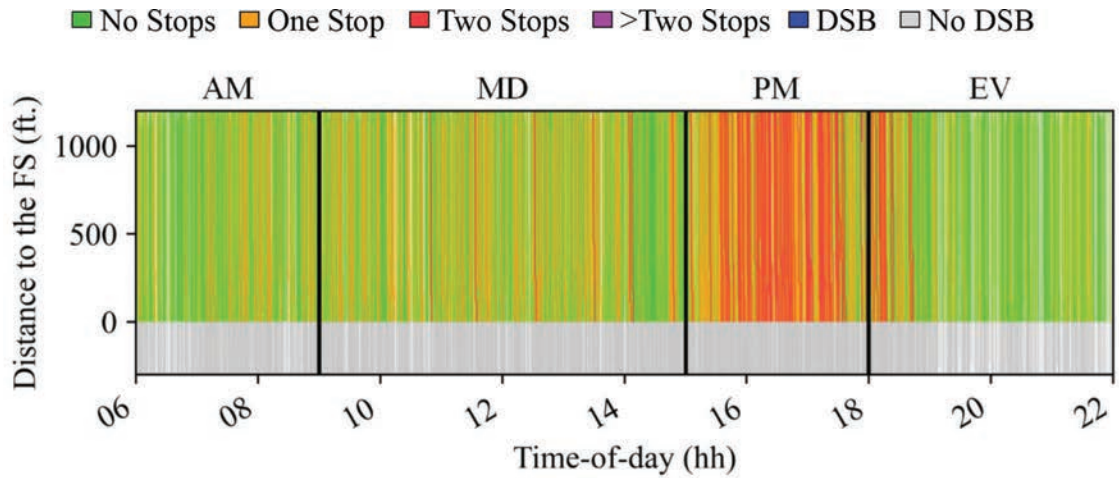
blockage occurs. Furthermore, it becomes evident that the PM period presents some challenges as some vehicles experienced split failures. These operational conditions seem to spill into the beginning of the EV period.

Figures 5.9b, 5.9c, 5.9d and Figure 5.9e show the PPDs for the four TOD periods with their respective

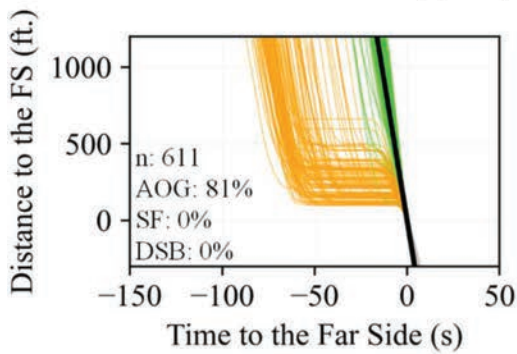
AOG, SF, and DSB estimations. During the AM peak period the highest AOG value exists, with 81% of vehicles arriving on green. In contrast, the PM peak period has the lowest AOG value (47%) and the highest SF estimation, with 12% of the vehicles experiencing a split failure before exiting the intersection.

TABLE 5.3
Videos showing the occurrence of relevant operational events

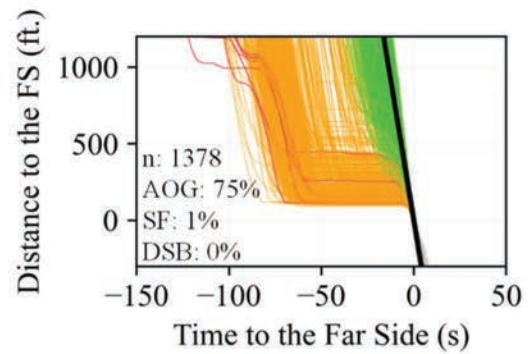
Operational Event	PPD Reference	Video Link	Video QR Code
Arrival on Green	Figure 5.3a callout i	https://tinyurl.com/arrivalOnGreen	
Arrival on Red	Figure 5.3a callout ii	https://tinyurl.com/arrivalOnRed	
Split Failure	Figure 5.7a	https://tinyurl.com/splitFailure	
Downstream Blockage	Figure 5.8a callout iii	https://tinyurl.com/downstreamBlockage	
No Downstream Blockage	Figure 5.8a callout ii	https://tinyurl.com/noDownstreamBlockage	



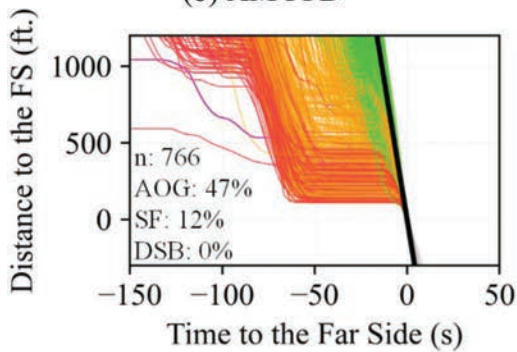
(a) Trajectories by TOD



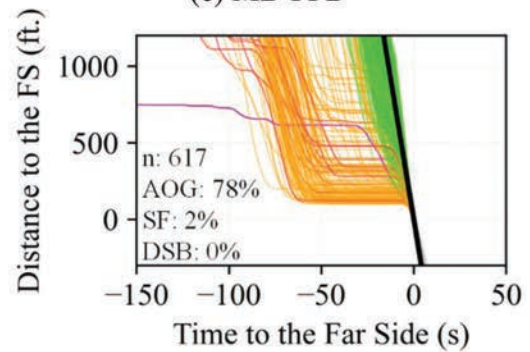
(b) AM PPD



(c) MD PPD



(d) PM PPD



(e) EV PPD

Figure 5.9 Vehicle trajectories taking the same movement at a signalized intersection during four different TOD plans for all weekdays in a month.

6. ARTERIAL TRAVEL TIME

Travel time has long been used by practitioners as a metric for evaluating roadway mobility. Traditional techniques leveraged floating car methods, license-plate matching, and Bluetooth detectors in addition to aerial videos to record, compute, and track travel times along a study corridor (70–74). These techniques, while reliable, are labor, cost, and time intensive and do not easily scale as some require equipment to be deployed to ensure reliable and continuous data collection.

On the other hand, emerging CV data provides a unique opportunity in this respect to compute travel time through a corridor without the need of sensors. Additionally, it affords researchers the freedom and scalability to implement travel time data collection on any corridor provided CV data is available. The near real-time availability of these data sets also provides stakeholders with an opportunity for more dynamic travel time tracking and implementing maintenance of traffic changes during construction or roadway closures. CV waypoint-level information additionally reveals lane-level effects on travel times as opposed to link or segment-level analysis which may mask some local effects due to the inherent aggregation involved.

6.1 Trip Chaining

Trip chaining is defined by multiple characterizations, with the overarching theme being any trip that involves a short stop on the way from an origin to a destination either for leisure or work. This is an important aspect to consider when performing travel time studies and evaluating locations where vehicles may enter or leave an approach to a signal mid-block. Household travel surveys and theoretical modeling have been the primary methods for identifying and analyzing trip chaining activities in the past (75, 76). However, trip chaining can be identified more precisely and at scale using CV data.

When computing travel time performance, it is important to only include relevant trips that do not detour or trip chain through the corridor, which otherwise may lead to unnecessary bias in travel time

estimates. As CV data provides waypoint information for each trajectory, methodologies have thus been developed to filter out instances of trip chaining or detouring at scale. This removes outliers and focuses on travel time estimates for the core of travelers.

Nonetheless, there might be some instances where trip chaining activities need to be analyzed, for example, when evaluating mode choice (77, 78). For these cases, vehicles performing trip chaining should be included in the study.

6.2 Raw Travel Times

To demonstrate the curation technique, an 11-intersection segment of West St. (Figure 6.1) running north-south in the heart of Indianapolis, Indiana, is evaluated.

Figure 6.2 shows a scatter plot of raw travel times obtained from 287 CV trajectories passing through the corridor in the SB direction of travel on February 27th, 2023. The CV trajectories are filtered out by performing virtual detection at the start (north-end) and end (south-end) of the corridor and only picking those trajectories which are observed to have passed through both ends of the corridor. Travel times are then calculated from the selected vehicle trajectories by computing the difference between their last and first recorded timestamps.

Travel time values for this nearly 2-mile stretch of roadway are seen to be varying from 2.9 minutes up to 69.1 minutes. The nominal expected travel time for this corridor would range from 5–7 minutes, pending variations introduced by TOD. While a majority of the travel time values under 15 minutes are within realistic expectations, a number of trips showing higher travel times (e.g., callouts i, ii, and iii) appear to be obvious outliers and should ideally be filtered out of any aggregate travel time performance measurements to sidestep bias in the data.

6.3 Travel Time Outliers Examples

Figure 6.3 shows an example of one such outlier travel time where the vehicle trip deviates from the analysis corridor just prior to South St. (Intersection 10)



Figure 6.1 West St. intersections (map data: OpenStreetMap).

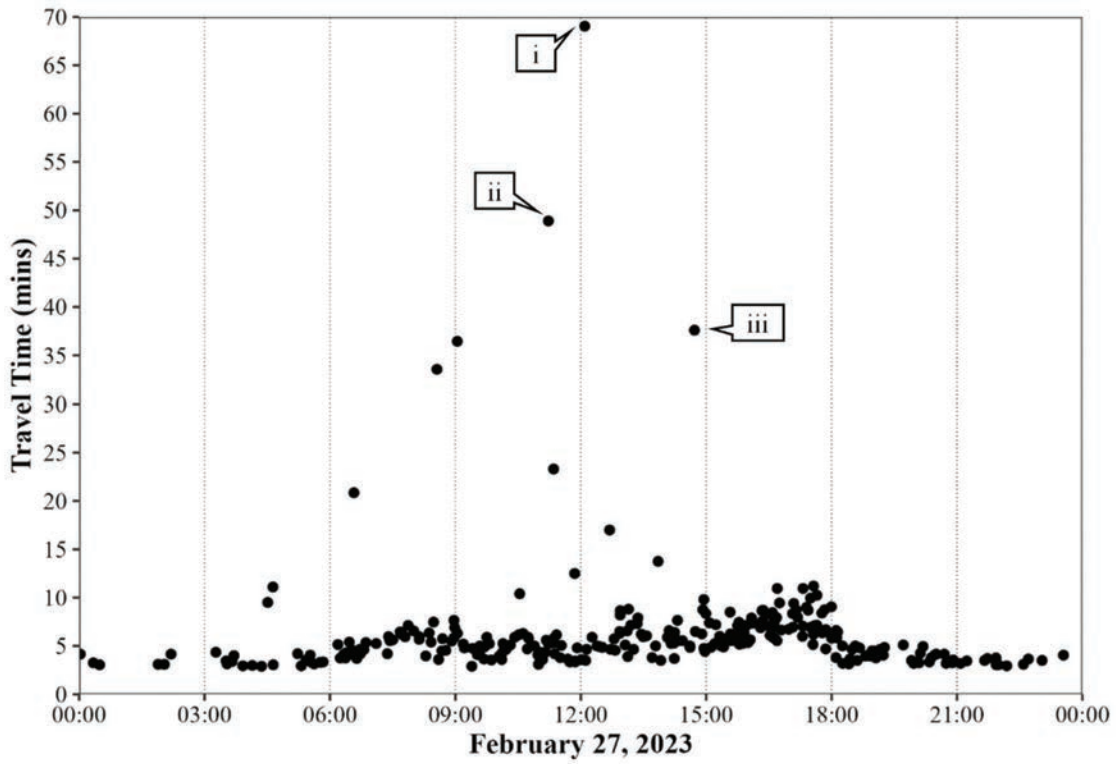


Figure 6.2 Raw travel times of sampled vehicles traveling SB on West St.



(a) All waypoints for a trip

(b) Trip waypoints for designated corridor

Figure 6.3 Example trip showing departure from designated corridor as a result of trip chaining (map data: OpenStreetMap).

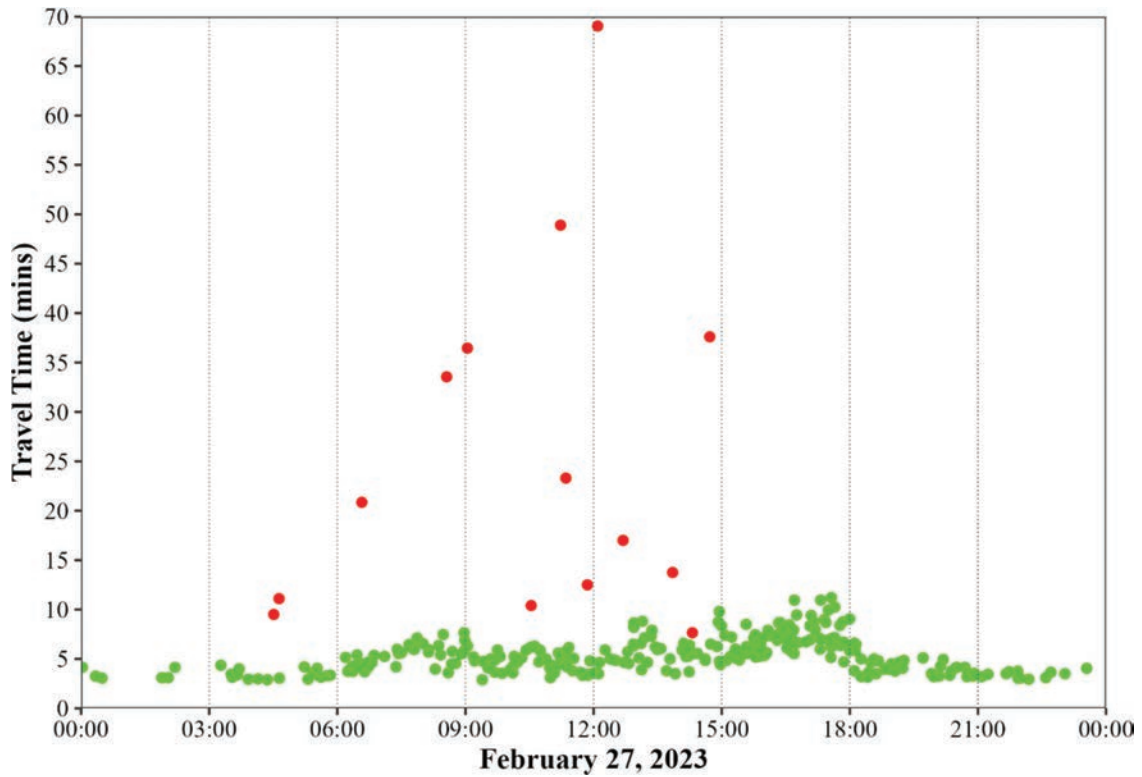


Figure 6.5 Raw travel times for West St. SB colored by match percentage.

TABLE 6.1
Summary travel time statistics before and after curation

Summary Travel Time Measure (min)	Raw Travel Times (289 trips)	Curated Travel Times (275 trips)
Minimum	2.9	2.9
1st Quartile	4.1	4.0
Median	5.2	5.1
Mean	6.3	5.4
3rd Quartile	6.6	6.3
Maximum	69.1	11.2

percentage thresholds allows for the same technique to be adopted for computing curated travel times at the arterial-level.

6.5 Travel Time Comparison Before and After Curation

Table 6.1 shows a summary statistics comparison of travel times on the corridor in the SB direction of travel using raw values as well as curated travel times. Notably, after the curation procedure, almost 5% of trips are filtered out (14 trips) due to their waypoints not matching or lying on the designated corridor exactly. Median travel time after curation reduces from 5.2 to 5.1 minutes while mean travel time reduces from 6.3 to 5.4 minutes. This points to a more realistic and tighter bound on the travel time estimates obtained from CV trajectories.

Figure 6.6 shows a cumulative frequency distribution (CFD) diagram of the same sets of raw (red) and curated (green) travel time values where curated travel times depict a cropping of the tail of the distribution due to the outlier and high travel times being filtered out by the preceding analysis techniques. Figure 6.7 thus shows a resulting scatter plot of curated travel times for the chosen corridor for Monday February 27th, 2023, making it much easier to visualize trends in travel time rise and falls around the morning and evening commuter peaks between 06:00–09:00 hrs. and 15:00–18:00 hrs. respectively, which would have possibly been difficult to discern earlier using raw travel time values.

A final visualization is presented in Figure 6.8 showing a scatter plot of travel times on the analysis corridor for a 1-week period from February 27th–

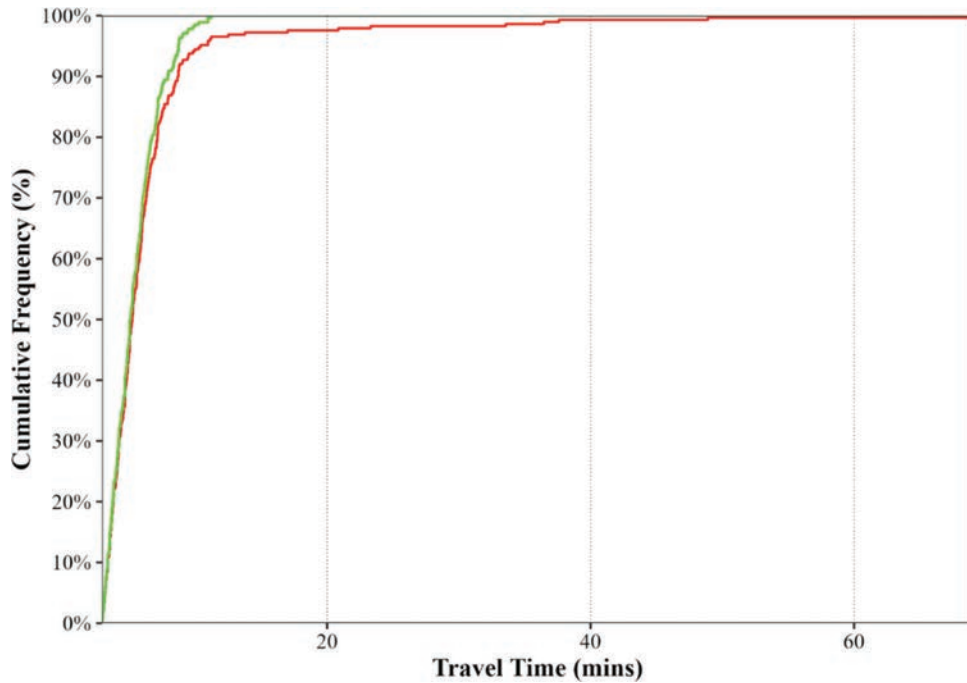


Figure 6.6 Corridor-wide CFD for raw (red) and curated (green) travel times.

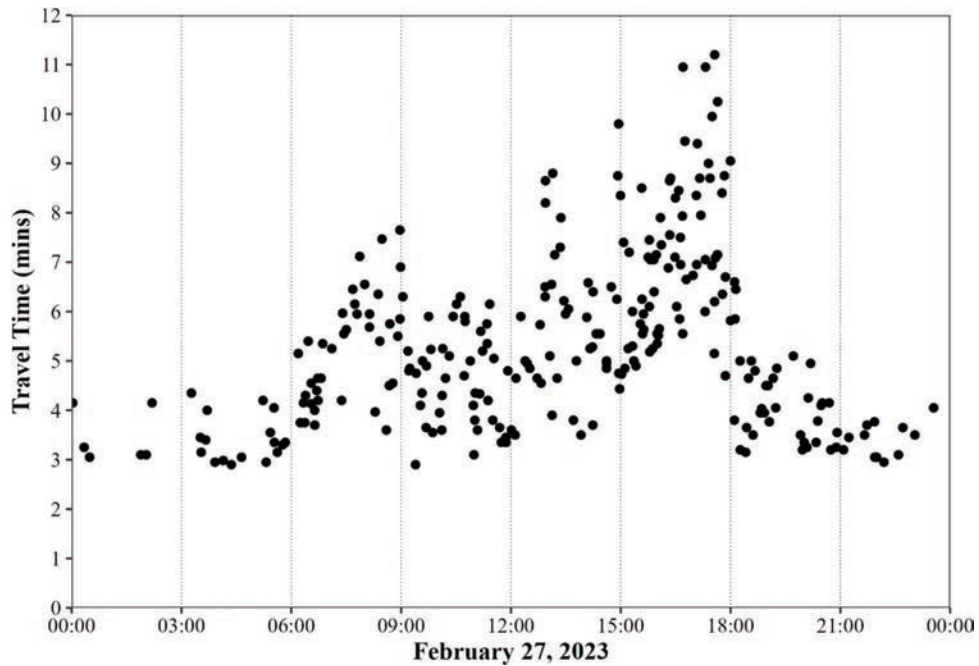


Figure 6.7 Corridor-wide travel time scatter plot.

March 5th, 2023. Weekly visualizations such as these document travel time trends varying from day-to-day. Morning and evening peaks lining up with commuter times are easily discernible Monday through Friday

while Saturday and Sunday show singular peaks for travel times potentially corresponding with recreational travel among CV trajectories passing through the corridor.

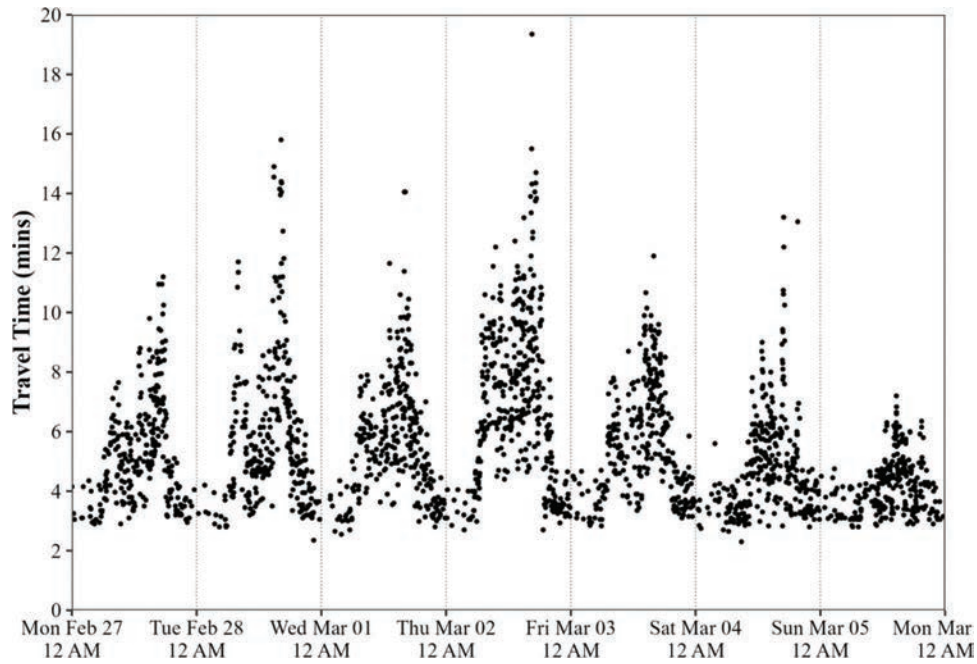


Figure 6.8 Corridor-wide weekly travel time plot.

7. PERFORMANCE REPORTING VISUALIZATIONS

Agencies need performance visualization tools to quickly assess system-level operations to identify challenges and opportunities. Chapter 5 presented the CV-based PPD, from which intersection performance at the movement-level can be derived. Even though the discussed PPD can provide practitioners valuable insights into the operational state at an intersection, the scope of analysis is too specific to report performance estimations at scale.

This chapter provides effective visualization frameworks to analyze traffic signal performance at the arterial- and system-levels. Both approaches aim at using trajectory-based performance estimations and reporting techniques to aid practitioners understand high-level operational conditions.

7.1 Arterial-Level Evaluation

An arterial-level performance assessment for December 2022 weekdays is presented for a corridor located in a suburban area north of Frisco, Texas (Figure 7.1, callout i). The intersections evaluated are listed in Table 7.1 and the traffic volumes range from 42,000 to 57,000 vehicles per day (VPD).

Figure 7.2 show heatmaps summarizing LOS, AOG, SF, and DSB, and a scatterplot displaying the arterial travel time by TOD for vehicles traveling WB-through on the studied corridor. Heatmaps' results are shown for every 15-minute period, an interval useful for traffic studies and signal controller timing plans.

The LOS (Figure 7.2a) 15-minute classification (Table 5.1) is assigned based on the calculated movement average control delay, given by:

$$\text{Average Control Delay} = \frac{1}{n} \sum_{i=1}^n d_{ci} \quad (\text{Eq. 7.1})$$

where d_{ci} is the control delay of the i -th trajectory out of n analyzed during the evaluated period. AOG (Figure 7.2b), SF (Figure 7.2c), and DSB (Figure 7.2d) estimations are obtained from Equation 5.3. Arterial raw travel times (Figure 7.2e) are calculated based on the techniques presented in Chapter 6.

In general, green indicates good operational conditions, whereas red and purple indicate challenges. From 06:00–15:00 hrs. most intersections are estimated to function without major problems, resulting in arterial travel times mostly below 5 minutes. During this time, no intersection presents significant SF or DSB, and only Intersections 4 and 9 show low AOG and consistent LOS D.

In comparison, from 15:00–19:00 hrs. some significant challenges arise. LOS E and F appear at Intersections 4, 5, 6, and 9. Additionally, SF values above 25% occur at Intersections 4 and 5. Further, DSB above 25% are estimated for Intersections 5 and 6. These conditions result in arterial travel times that range from under 5 to over 10 minutes.

During the most challenging period between 17:00 and 18:00 hrs., interesting operational conditions exist. For example, Intersection 8 (callout i) seems to function without major problems, while Intersection 5 (callout ii) shows significant delay, medium AOG, and high SF

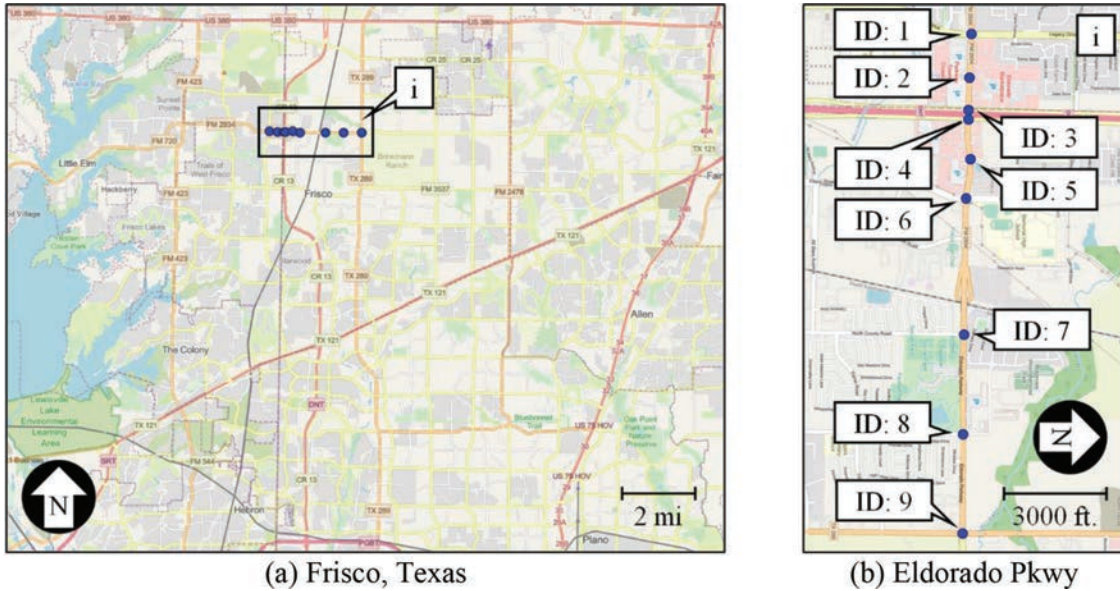


Figure 7.1 Study arterial (map data: OpenStreetMap).

TABLE 7.1
Studied intersection on Eldorado Pkwy

Intersection ID	Intersection Name
1	Eldorado Pkwy at Legacy Dr.
2	Eldorado Pkwy at Towne Xing
3	Eldorado Pkwy at Dallas Pkwy S
4	Eldorado Pkwy at Dallas Pkwy N
5	Eldorado Pkwy at Woodsboro Way
6	Eldorado Pkwy at Frisco St.
7	Eldorado Pkwy at N County Rd.
8	Eldorado Pkwy at Rogers Rd.
9	Eldorado Pkwy at Preston Rd.

and DSB values. The PPDs for these two intersections are shown in Figure 7.3.

Even though the level of granularity presented in Figure 7.2 can provide clear indications on which intersections require further attention, the analysis is still limited to a single movement. Ideally, arterial-level reporting would provide practitioners with information on the operational state of all movements at all signals being evaluated. This would help determinate possible mitigation strategies (e.g., split rebalance, offset modification, or changes in cycle length).

To present a holistic view of a corridor's performance measures to stakeholders and operators, a template that displays relevant information for all intersections and movements is provided. The template is shown in Figure 7.4, which displays Eldorado Pkwy (Figure 7.1, callout i) signal performance measures derived from over 340,000 trajectories and 9.4 million waypoints during December 2022 weekdays. Table 7.2 provides an explanation of the information included in Figure 7.4.

The reporting template can provide up to 3,072 measures per intersection since it gives information for eight different movements and four performance measures for every 15-minute period over 24 hours. Following the practices presented in Chapter 2, the queries to generate such a visualization incurred a cloud cost just under \$0.80. A document reporting performance estimations with the provided framework for 14 different arterials was produced (8). Additionally, (18) expands on (8) by providing 58 arterial-level performance reports of corridors located in 14 different states.

7.2 System-Level Evaluation

The framework presented above provides an effective approach to evaluating arterials. However, agencies sometimes require extended analyses to gather information on the performance of various signals, regardless of whether they are located on the same road. This section presents visualization techniques to do the following.

- Identify the geospatial location of intersections with challenges that may affect each other.
- Identify the worst performing intersections in a system.

7.2.1 Geographical Representation of Results

A geographical representation of performance results can show effects that certain intersection may have on adjacent locations.

Figure 7.5 shows LOS, AOG, SF, and DSB estimations at the intersection-level for 132 signals in downtown Indianapolis, Indiana, for all weekdays in December 2022 from the 17:00 to the 18:00 hrs. From the presented results, the group of intersections located

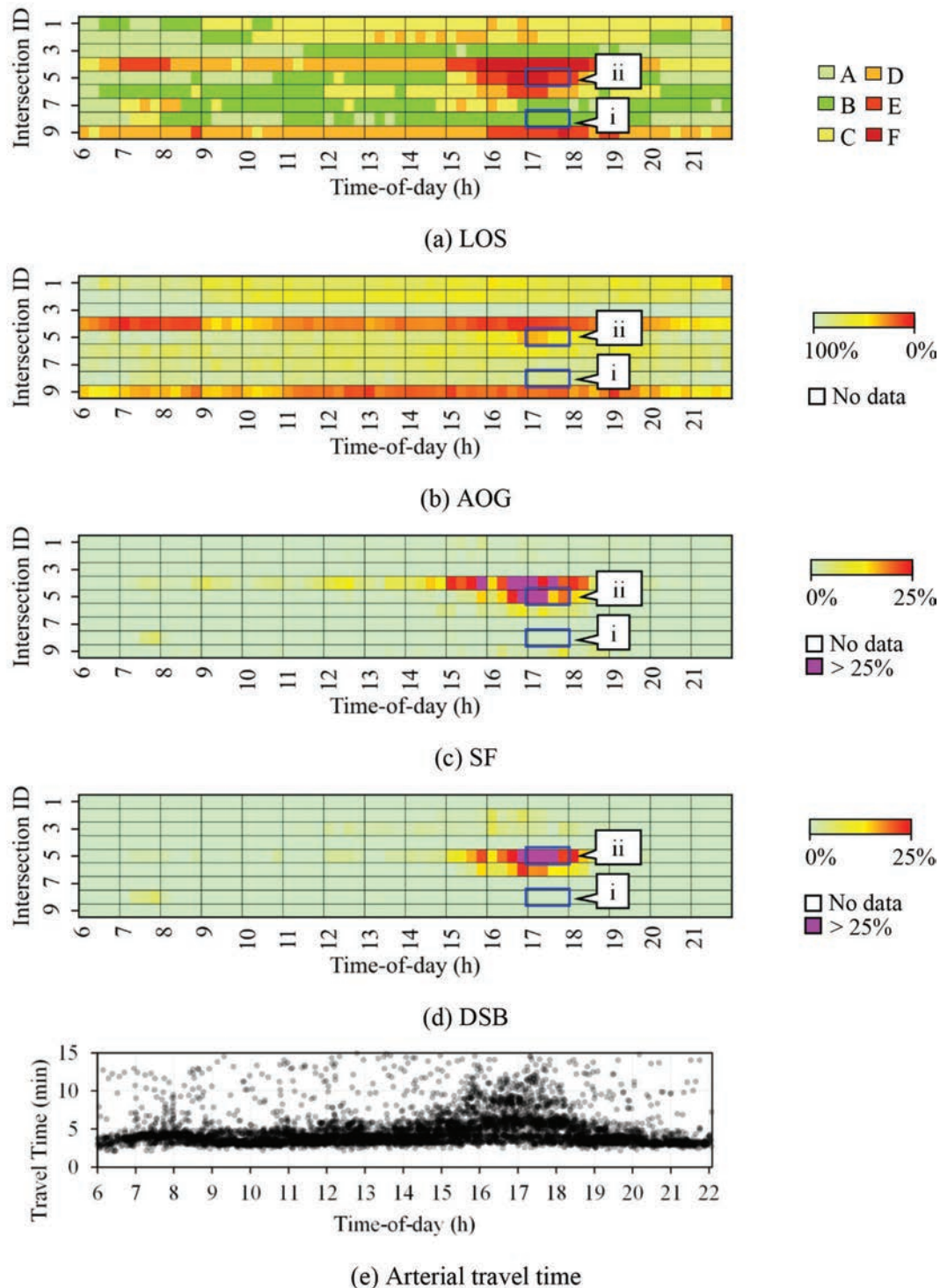


Figure 7.2 Signal performance measures for WB-through movements on Eldorado Pkwy.

north of downtown (callout i) operate without major problems. In contrast, the center section of downtown (callout ii) shows some challenges as high DSB percentages (>25%) may be causing long delays (LOS D and E). A video presenting a LOS evaluation of these signals by TOD was created (79).

Furthermore, the eight-intersection corridor of West St., located west of downtown (callout iii), is of particular interest as these closely located intersections present some of the longest delays (LOS D, E, and F) and have significant SF and DSB estimations. It is likely that operational challenges at some of these

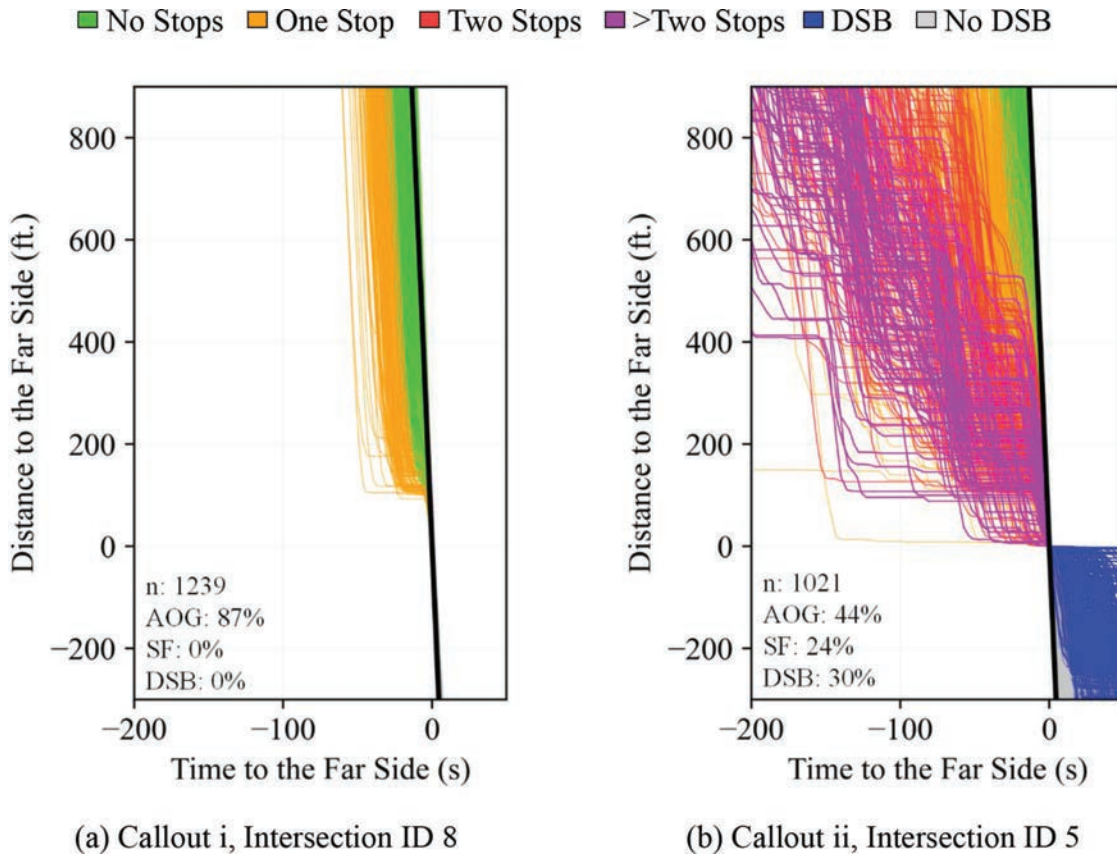


Figure 7.3 PPDs for highlighted intersections and time periods in Figure 7.2.

intersections propagate and affect the rest. An in-depth analysis of this arterial is presented in the next chapter.

7.2.2 Pareto-Sorted Representation of Results

When analyzing the performance of a significant number of traffic signals in a system, it is useful to identify the locations that operate in the most challenging conditions. Not only does this help locate the intersections that require further attention, but it also provides valuable information on the overall health of the system.

Figure 7.6 shows all 132 intersections analyzed in Figure 7.5 pareto-sorted by their overall performance. Intersections on the left side of the graphic are the worst performing for each category. All signals have an average control delay lower than 90 s/veh, AOG values above 15%, and SF and DSB below 21% and 42%, respectively. This means that at the worst performing intersections vehicles experience 90 seconds of control delay on average, only 15% arrive on green, one out of

TABLE 7.2
Information included in Figure 7.4

Callout	Description
i	Study location
ii	Trajectory counts at the different analyzed intersections
iii	Study period
iv	Column with LOS results
v	Column with AOG results
vi	Column with SF results
vii	Column with DSB results
viii	Row with mainline through movements
ix	Row with mainline left movements
x	Row with side street through movements
xi	Row with side street left movements

five vehicles experience a split failure, and almost half experience downstream blockage. Once these locations are identified, further analysis can be performed to determine if mitigation strategies could be implemented to improve operations.

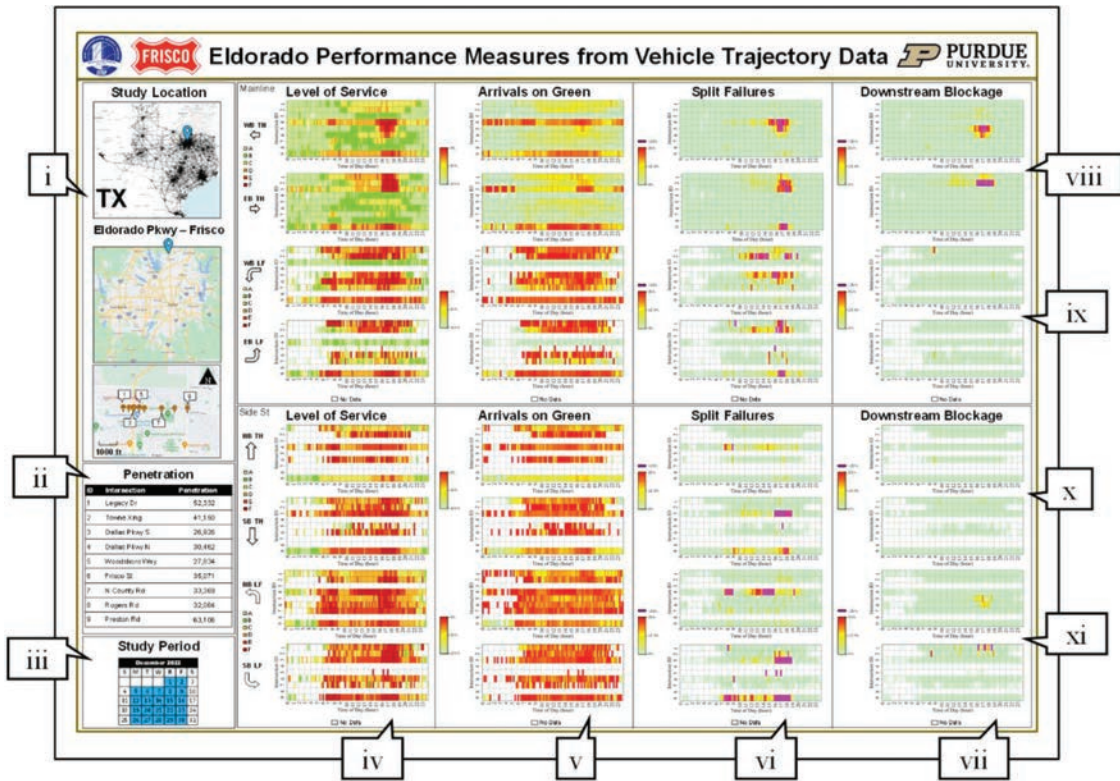


Figure 7.4 Month-long summary of performance measures on Eldorado Pkwy for all relevant movements.

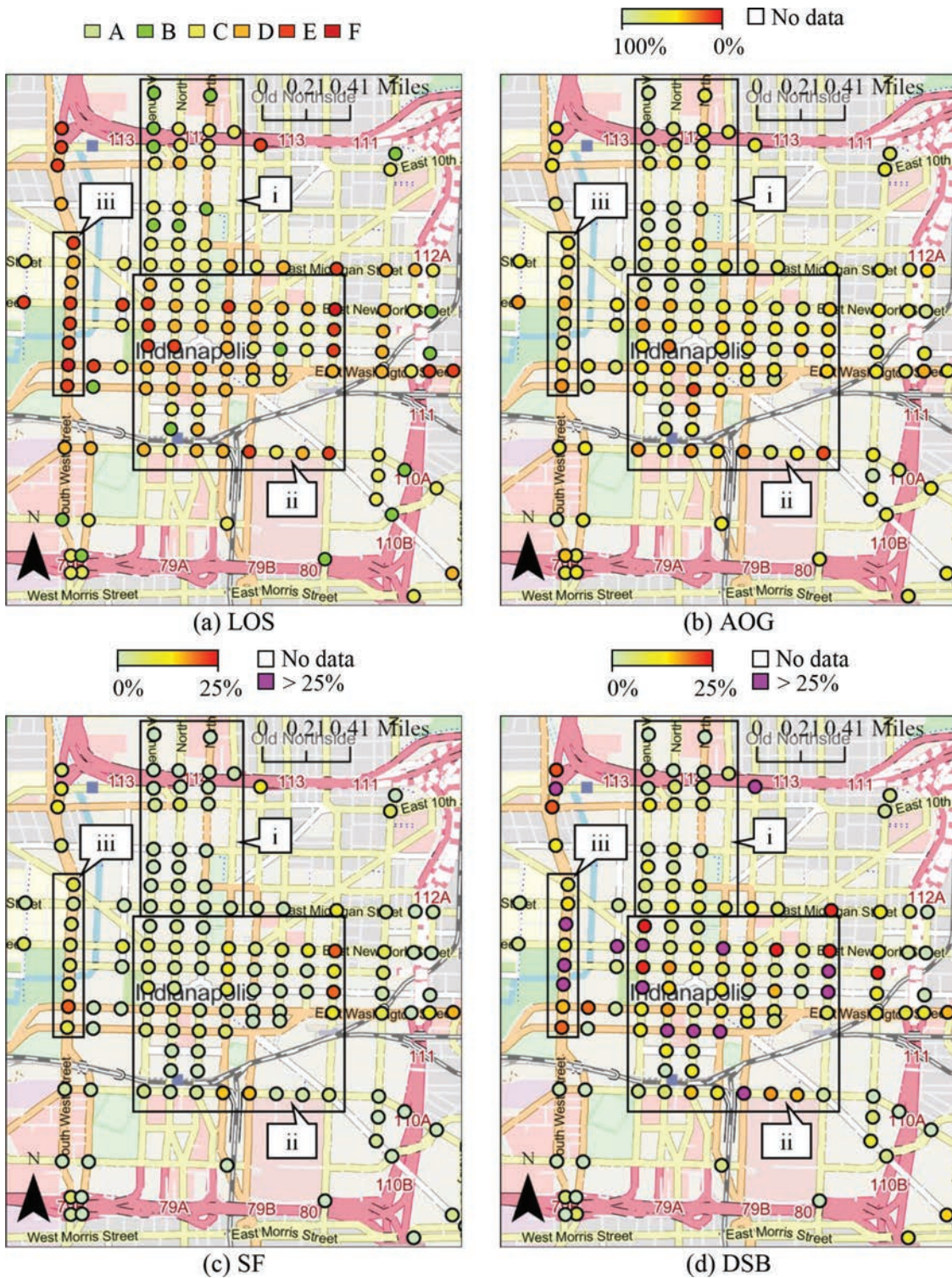
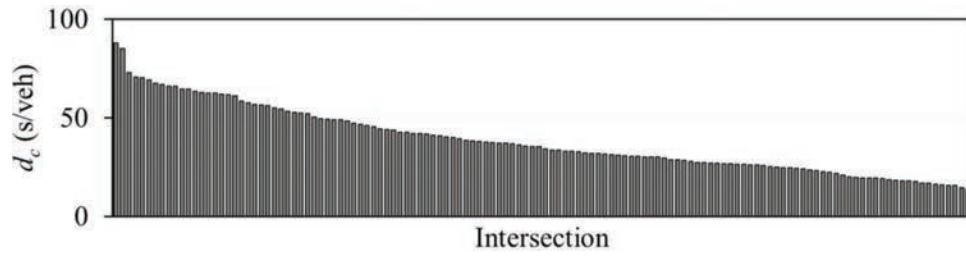
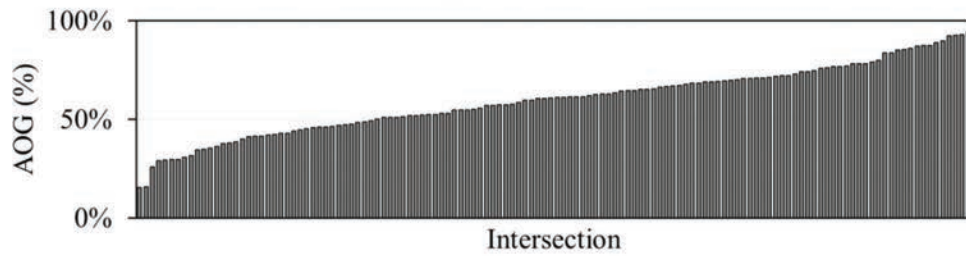


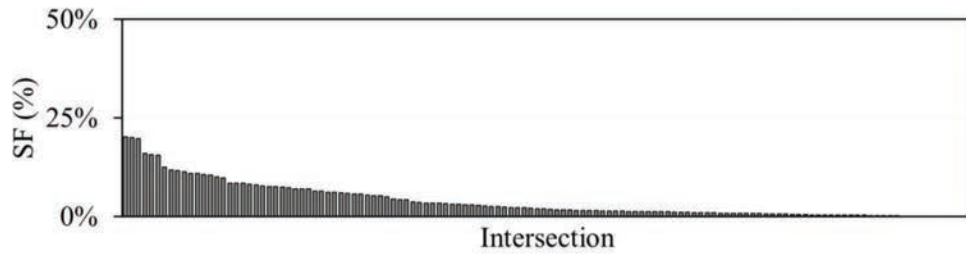
Figure 7.5 Geospatial view of intersection performance in downtown Indianapolis (map data: OpenStreetMap).



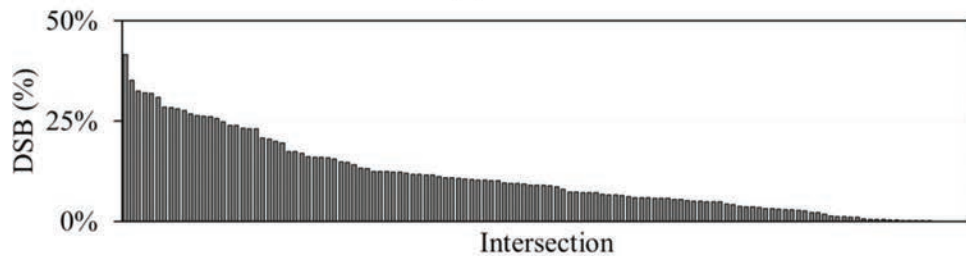
(a) Average control delay



(b) AOG



(c) SF



(d) DSB

Figure 7.6 Intersections in downtown Indianapolis pareto-sorted by their performance.

8. BEFORE-AFTER STUDIES

Before-after traffic studies are evaluation techniques that facilitate the analysis of the effects that particular events have on the performance of transportation systems. For example, by conducting before-after studies, practitioners are able to assess and communicate the impact that highway work zone diversions have on local arterials (9, 80) or the effectiveness of upgraded timing techniques (10). These results provide agencies with data-driven decision tools to mitigate degrading conditions, or to further improve operations.

This chapter presents two CV-based before-after studies (9, 10) that serve as frameworks for agencies to systematically evaluate traffic signal performance impacted by particular events.

8.1 Highway Work Zone Impact on a Local Arterial

Highway maintenance and construction can significantly impact the surrounding network by creating an influx of diverting vehicles that can saturate local streets. This can lead to significant congestion and delays. According to the *2021 Urban Mobility Report* (81), in 2019 there were 8.7 billion hours of congestion-related travel delay, which represented a \$190 billion cost in time and wasted fuel. The Federal Highway Administration (FHWA) indicates that 10% of all congestion, and 24% of non-recurring congestion, are caused by work zones (82, 83). Therefore, it is important for agencies to monitor the impact of work zones on arterials and local streets.

This subsection demonstrates that current CV trajectory data can be used to assess the impact that work zone diversions have on local arterials (9). A case study was developed based upon an 11-intersection segment impacted by a long-term closure of the I-65/70 interchange in Indianapolis, Indiana. The case study performs a longitudinal assessment of the changes in sampled volumes, LOS, AOG, SF, DSB, and travel times. Locations that are under-performing are identified and insights on the type of problems being experienced (saturation and/or coordination) is provided, which aids in the identification of potential solutions.

8.1.1 Study Location and Analysis Period

The I-65/I-70 interchange, located in downtown Indianapolis, Indiana (Figure 8.1), also known as North Split, was closed on May 15th, 2021. Therefore, all analyses presented in this subsection are derived from 2021 CV trajectory data and focus on the weeks immediately before and after the closure event.

The North Split usually served approximately 214,000 VPD before being closed (84). As this volume of vehicles utilizes local streets as detour, the overall network performance gets degraded. Eleven of the most affected intersections are studied. They are all located on West St., a parallel arterial to the North Split

(Figure 8.1) and their names are shown in Table 8.1. It is important to mention that, as an outlier, Intersection 7 (West St. at Robert D. Orr Plaza) has a constant green light for vehicles traveling SB-through.

8.1.2 Performance Evaluation

Figure 8.2 and Figure 8.3 show the summary of 5 performance measures by TOD derived from over 47,000 unique trajectories and 500,000 waypoints for vehicles traveling SB-through on West St. 1 week before (Figure 8.2, May 10th–14th, 2021) and 1 week after (Figure 8.3, May 17th–21st, 2021) the North Split closure. Additional details on how to interpret the graphics are provided below.

- Figure 8.2a and Figure 8.3a: Traditional HCM LOS (Table 5.1). Even though LOS does not provide actionable information by itself, it provides practitioners with an understanding on the levels of delay. Comparing these two figures, one can see a very large increase in experienced delay during the period between the 15:00 and 18:00 hrs. (PM peak period).
- Figure 8.2b and Figure 8.3b: AOG. Comparing these two figures, one can see a substantial decrease in AOG during the PM peak period.
- Figure 8.2c and Figure 8.3c: SF. Comparing these two figures, one can see an important increase in the occurrence of split failures during the PM peak period, particularly at Intersection 8.
- Figure 8.2d and Figure 8.3d: DSB. Comparing these two figures, one can see a significant increase in DSB during the PM peak period. Interestingly, the block of Intersections 3 to 7 shows high DSB ratios (Figure 8.3d). This is an indication that queues formed at Intersection 8 affect the progression of upstream platoons all the way until reaching Intersection 3. This can also be considered as one long queue that extends from intersection 8 to 3.
- Figure 8.2e and Figure 8.3e: Arterial travel time. Longer trips are seen during the PM peak period a week after the North Split closure.

As expected, all the presented performance measures worsened after the North Split closure, especially from the 15:00 to the 18:00 hrs. As this period seems the most critical, further analysis will focus on that time-range.

8.1.2.1 Sampled volumes. As the 214,000 vehicles that used the North Split on a daily basis have to travel using alternative routes, a significant increase in the studied location's volumes is expected. Figure 8.4 shows the weekday weekly change in sampled CV volumes of vehicles that traveled SB through the entire arterial during the PM peak period. Sampled volumes just after the start of the North Split closure increased 148% (from 54 to 134). With such a significant increase in demand, and with no added capacity, operational performance is expected to degrade.

Callouts i and ii are the weeks in which Memorial Day and Independence Day were observed, respectively. Even though these weeks present decreased demands compared to previous and following weeks,

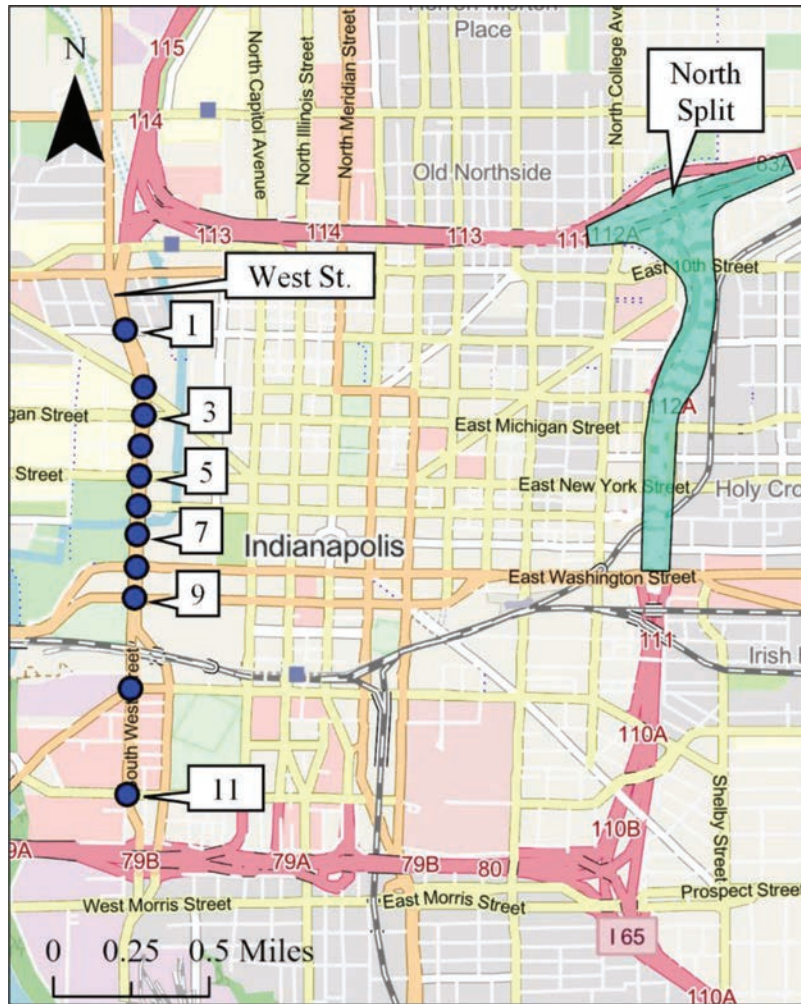


Figure 8.1 North Split closure and West St. intersections in downtown Indianapolis (map data: OpenStreetMap).

TABLE 8.1
Studied intersection on West St.

Intersection ID	Intersection Name
1	West St. at Clair St.
2	West St. at Indiana Ave.
3	West St. at Michigan St.
4	West St. at Vermont St.
5	West St. at New York St.
6	West St. at Ohio St.
7	West St. at Robert D. Orr Plaza
8	West St. at Washington St.
9	West St. at Maryland St.
10	West St. at South St.
11	West St. at McCarty

they still have higher traffic volumes than pre-closure conditions.

8.1.2.2 Arterial trajectories and performance measures by intersection. To better illustrate the operational dynamics at the studied intersections, trajectories of

vehicles traveling SB-through are plotted in Figure 8.5a (week before the closure) and Figure 8.5b (week after the closure). Next to the trajectories, DSB, SF, and AOG results are displayed. The performance measures are placed in such a way that they match the segment of the trajectories which they represent (AOG and SF for the upstream section, and DSB for the downstream section). From performing a before and after qualitative comparison, the following can be stated.

- By comparing the trajectories, not only is the increase in demand noticeable, but also in the number of stops and the time required to traverse the corridor.
- By contrasting DSB, significant increments occurred from Intersections 3 to 7, which means that long queues at Intersections 4 to 8 affect upstream locations. However, this seems to abruptly end after Intersection 8. This suggests that the downstream blockage identified at upstream locations may be a consequence of Intersection 8 having queue spillback. If that is the case, by fixing the congestion at Intersection 8, the state of operation at the upstream locations may improve.
- By comparing SF, it is clear that an important increase occurred at Intersections 2, 4, and 8. However, as Intersection 4 also showed significant downstream

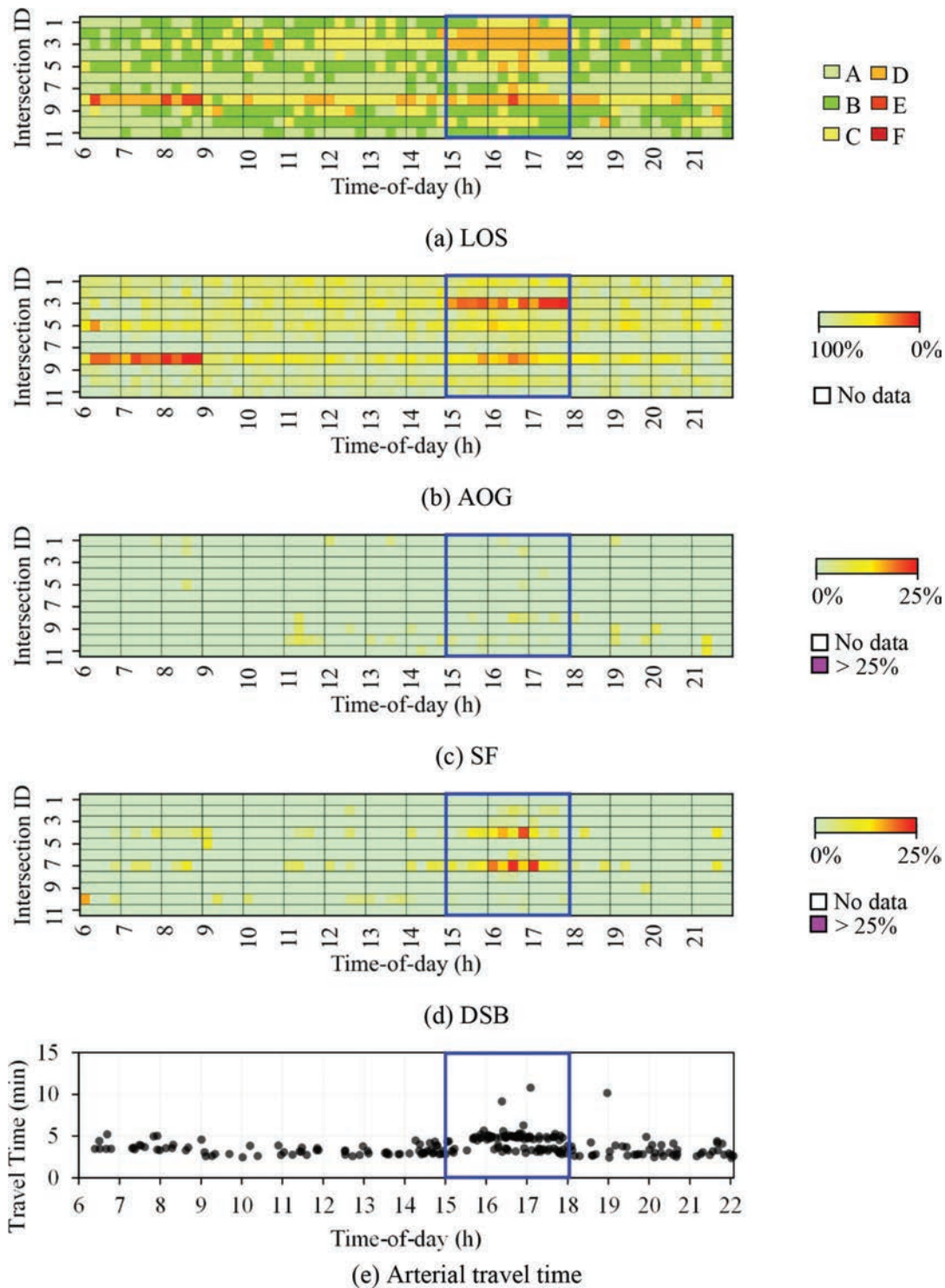


Figure 8.2 Signal performance measures for SB-through movements on West St. 1 week before the North Split closure.

blockage, this is not necessarily an indication that this location is operating at overcapacity, but there is a possibility that its split failures are a result of downstream queue spillback.

- By contrasting AOG, a general decline is appreciated.

Figure 8.6 shows an image of vehicles traveling SB through Intersections 4 to 8, which were identified as

having significant operations challenges in Figure 8.5b (callout i). It is interesting to note that the queue length at Intersection 8 stretches over a significant segment of the roadway, and results in vehicles experiencing split failures, downstream blockage, and long delays. A video provided here (85) shows a vehicle experiencing a split failure at Intersection 8.

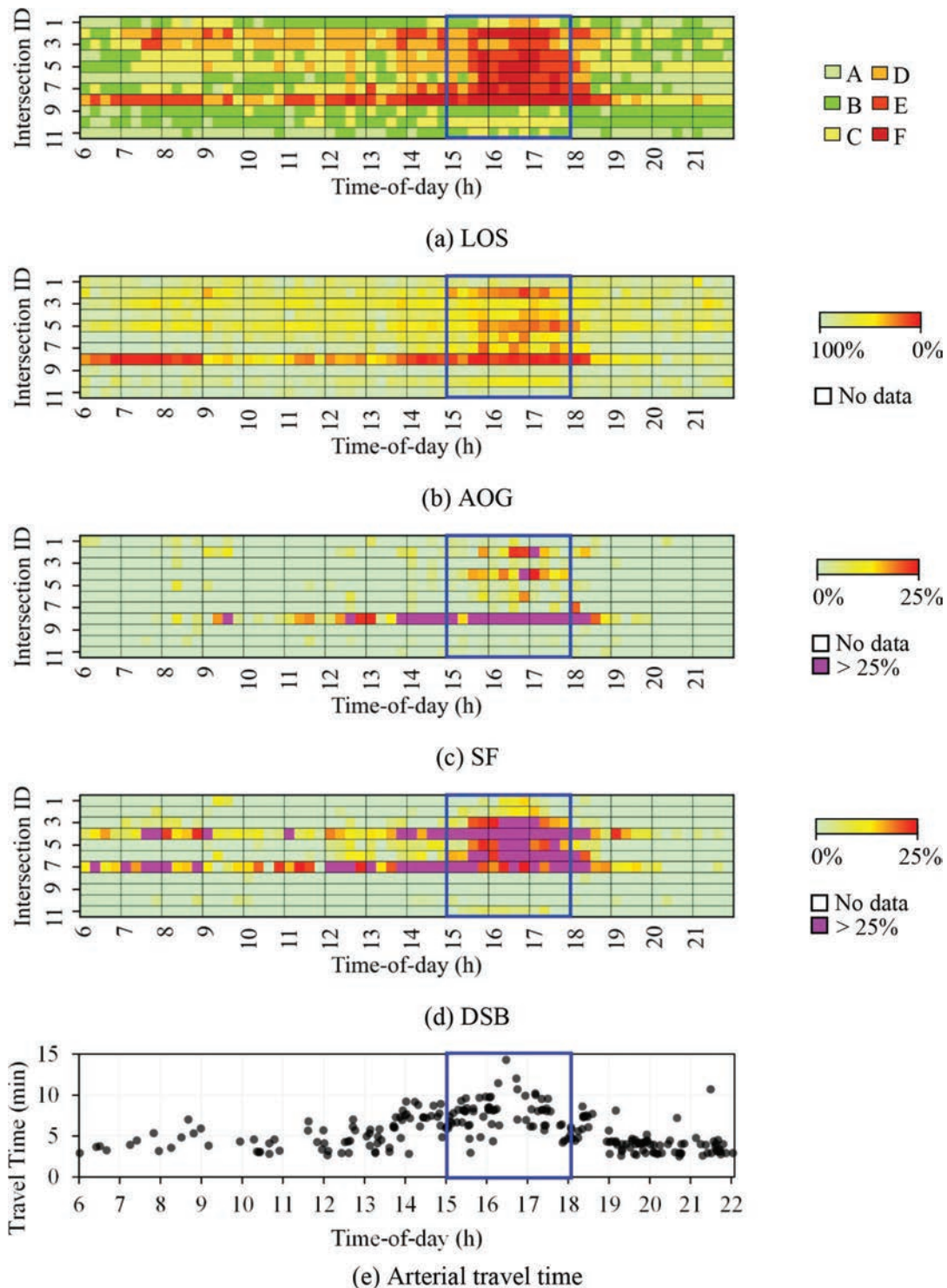


Figure 8.3 Signal performance measures for SB-through movements on West St. 1 week after the North Split closure.

8.1.2.3 Travel times. A valuable and commonly used metric to assess the performance of a corridor is travel time. An effective way of analyzing the travel time experienced by traversing vehicles is by generating CFD plots. In general, a good-performing arterial will show a vertical line (which is an indication of reliability) with the minimum possible travel time (near free flow).

Figure 8.7 shows corridor travel time CFDs for SB-traveling trajectories during the analysis period. Travel times for the 2 weeks before the closure are indicated by callout i. Travel time increased noticeably since the May 17th week (callout ii, right after the start of the closure). In fact, the median travel time increased from 5.4 to 8.5 minutes. Furthermore, a reduction in travel

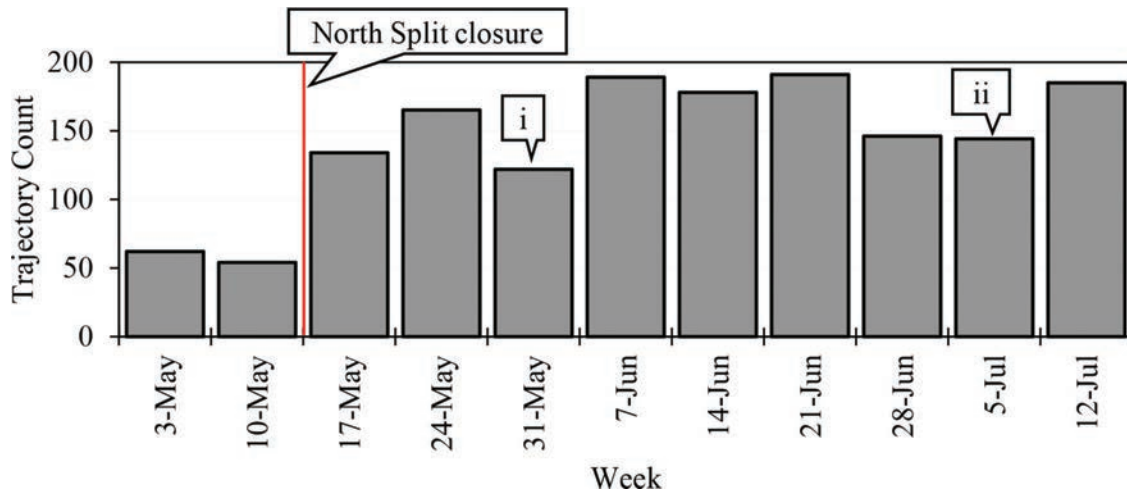


Figure 8.4 Corridor-wide weekday weekly trajectory counts for SB-through movements from 15:00–18:00 hrs.

time reliability is shown by the reduction in the slope of the lines, indicating an increase in travel time variation.

8.1.3 Results

Average corridor-wide AOG, SF, and DSB results are shown in Figure 8.8. As expected, all performance measures significantly worsened after the North Split closure. The maximum changes in performance are a 10% increase in DSB, 7% increase in SF, and a 17% decrease in AOG.

Results for the corridor travel time are presented in Figure 8.9. The Interquartile Range (IQR) increased by up to 140%, and the median travel time rose 74% when comparing weeks before and after the closure.

8.1.4 Summary

In summary, current CV trajectory data is used to estimate the before-after performance for an 11-intersection segment of West St. affected by the North Split closure. The following results are observed:

- a 148% increase in sampled volumes, which indicates a significant increase in demand on the arterial;
- a 17% decrease in AOG, indicating the existence of potential opportunities to improve coordination;
- a 7% increase in SF, indicating an increment of traffic signals operating at overcapacity;
- a 10% increase in DSB, indicating growing queues; and
- a 74% increase in median travel time.

From Figure 8.5, Intersection 8 (Washington St.) is identified as a location that influences the operational state at upstream intersections. This is an example of how agencies can use these frameworks to identify critical intersections that affect entire systems.

8.2 Change in Performance After Signal System Upgrade

Updates to traffic signal timing plans are expected to either improve operations or mitigate the effects of

increased demand. Longitudinal before-after studies are important when validating changes to traffic signal systems, but they have historically required field data collection as well as deployment of extensive detection and communication equipment (1).

This subsection describes how current CV trajectory data can be used to conduct before-after evaluations of corridor-wide traffic signal timing and system upgrades (10). A 22-intersection corridor with a recent implementation of a semi-automated adaptive system to update timing plans is used to demonstrate these techniques.

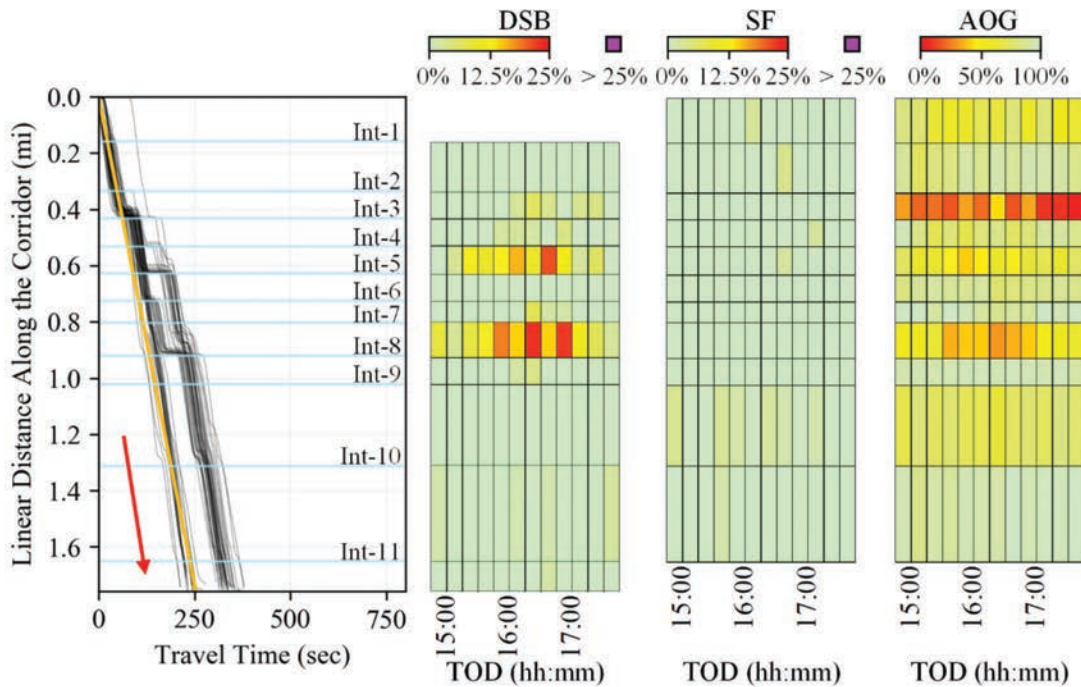
8.2.1 Study Location and Analysis Period

The operation of a 22-intersection segment of US-27, located north of Cincinnati, Ohio (Figure 8.10), was upgraded in 2021 from a coordinated-actuated control to a semi-automated adaptive implementation of the Purdue Link Pivot Algorithm (86). The new system suggests timing changes based on traffic conditions and an operator approves or rejects the recommendations. To validate the efficiency of the implemented system, a before-after analysis based on August 2020 and August 2021 CV trajectory data is performed.

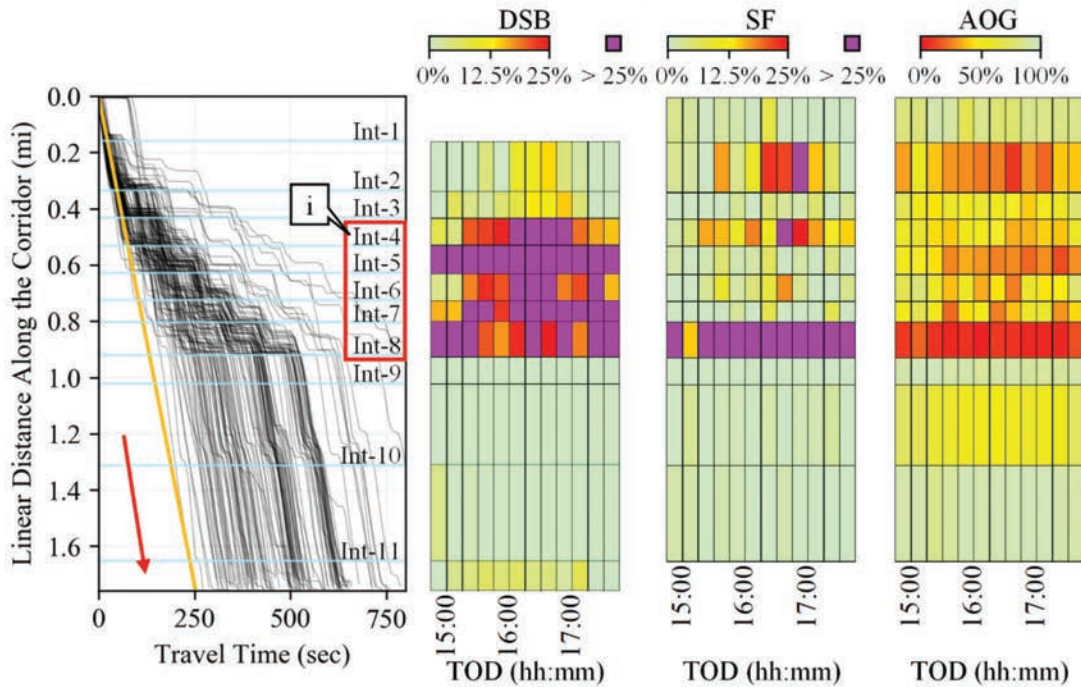
The intersections studied are listed on Table 8.2. It is important to note that Intersection ID 2, US-27 at Generation Dr., was installed between the two analysis periods. Therefore, movement performance measures at this location are only computed for the after analysis. However, corridor travel times implicitly capture the operational performance of the entire corridor.

To have a consistent before-after comparison of performance measures, CV trajectory data for the same duration is used to carry out the analysis.

- For the before period, trajectory data from August 3rd, 2020, to August 28th, 2020, weekdays (20 days) are used. This period will be referenced as August 2020 (weekdays), where 152 intersection movements are analyzed.
- For the after period, trajectory data from August 2nd, 2021, to August 27th, 2021, weekdays (20 days) are



(a) Before North Split closure: May 10th–14th, 2021



(b) After North Split closure: May 17th–21st, 2021

Figure 8.5 SB-through corridor-wide trajectories and intersection performance measures from 15:00–18:00 hrs.

used. This period will be referenced as August 2021 (weekdays), where 160 intersection movements are analyzed (eight more since the implementation of Intersection 2).

8.2.2 Traffic Volume Change

Annual average daily traffic (AADT) for road segments on the studied corridor in 2020 and 2021 were



Figure 8.6 SB-traveling vehicles on West St. from Intersections 4 to 8.

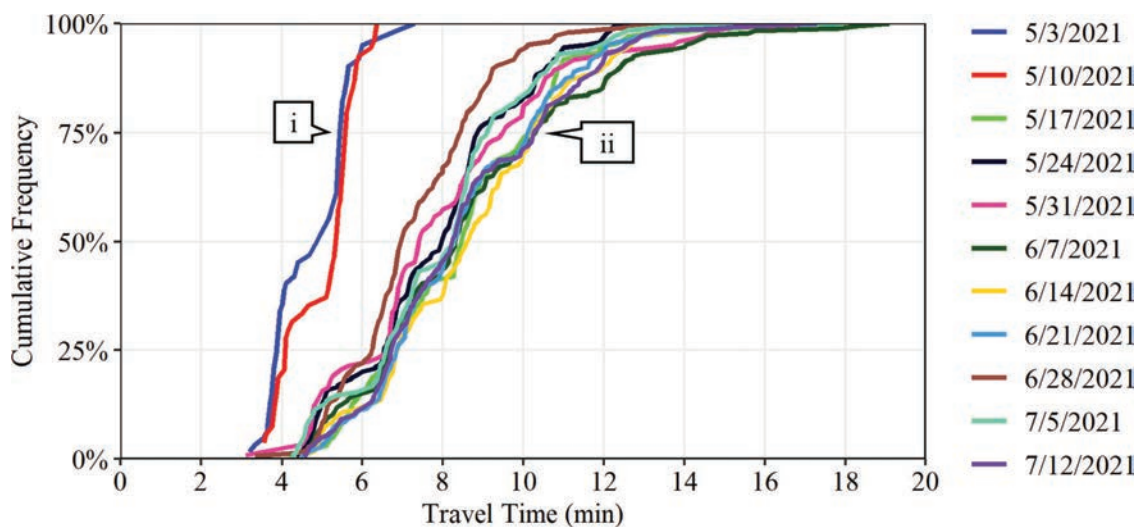


Figure 8.7 Weekday weekly arterial travel time CFD from 15:00–18:00 hrs.

obtained from the Ohio Department of Transportation (ODOT) Traffic Monitoring Management System (TMMS) (87) and are shown in Table 8.3. For the four segments for which data is available, there was a significant total increase of 35% on traffic volume between 2020 and 2021, which can be attributed to post COVID-19 rebound of travel.

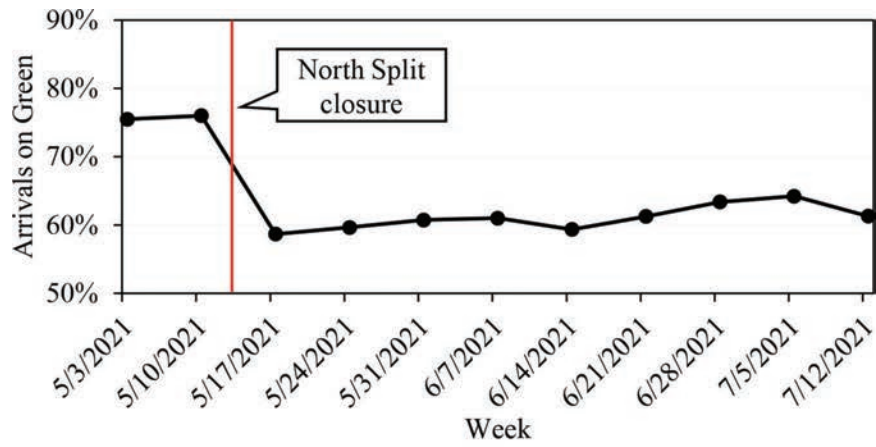
8.2.3 Performance Evaluation

Figure 8.11 and Figure 8.12 show the estimated performance measures by TOD of vehicles traveling SB-through for an 11-intersection section of the studied corridor. Results are based in August 2020 weekday trajectories (before timing upgrade) for Figure 8.11 and

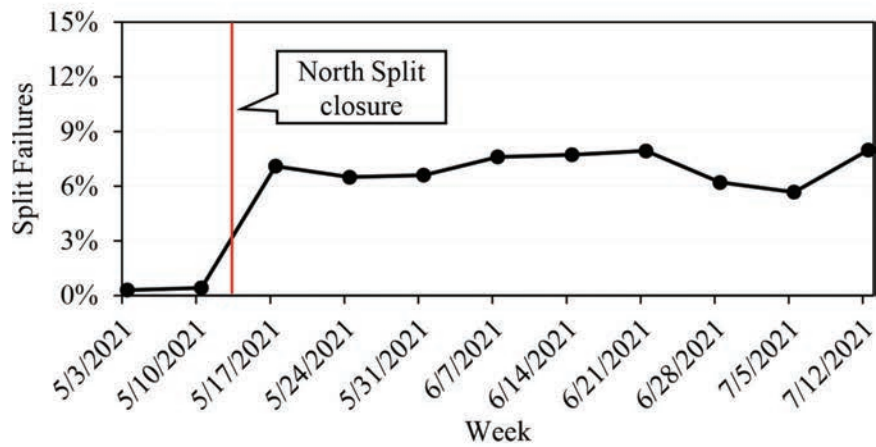
in August 2021 weekday trajectories (after retiming upgrade) for Figure 8.12. Performance measure estimations by TOD for all relevant movements over the entire corridor are available here (8).

Qualitatively, it can be observed that AOG improved for most locations, which indicates a more efficient progression through this corridor’s section. SF and travel time have no significant change. Regarding DSB and LOS, some locations have improvements and others saw degraded conditions.

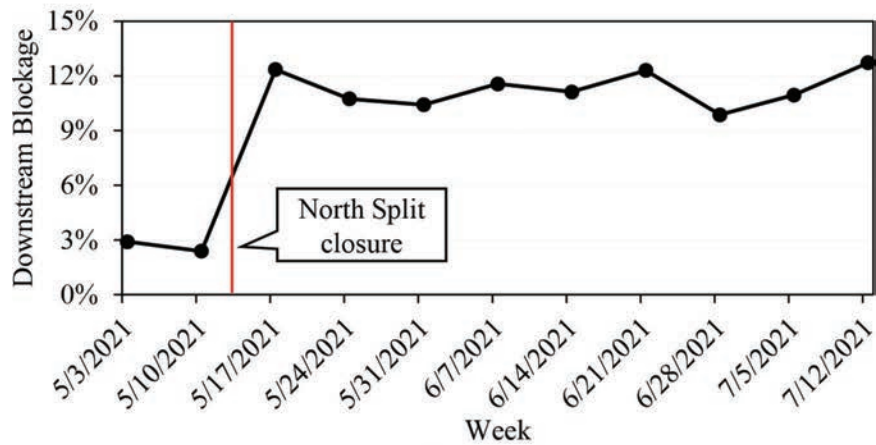
Considering that traffic volumes increased approximately by 35%, a significant worsening of performance would have been expected. The fact that there is only a modest change in performance suggests that the signal timing plan updates and adaptive link pivot implemen-



(a) AOG



(b) SF



(c) DSB

Figure 8.8 Corridor-wide weekday weekly performance measures for vehicles traveling SB-through on West St. from 15:00–18:00 hrs.

tation effectively diminished the impact of increased demand and even improved operations in specific cases.

8.2.3.1 Intersection operational improvements and influence on adjacent locations. By closely analyzing the graphics presented on Figure 8.11 and Figure 8.12,

it is possible to obtain insights not only on the operational changes, but also on the influence between adjacent intersections.

For example, Intersections 6 and 7 are closely spaced with a separation of 630 ft. (192 m.), as shown in Figure 8.13; hence, their operation is highly dependent on each

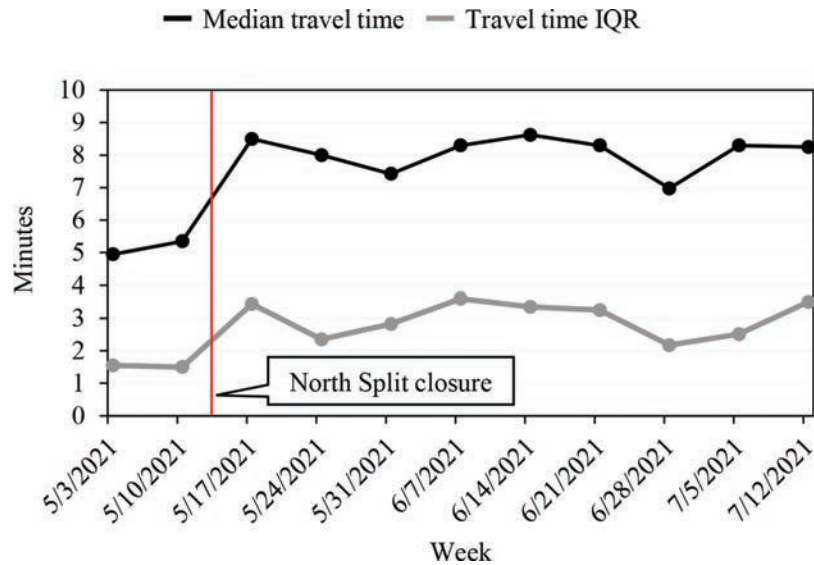


Figure 8.9 Weekday weekly median arterial travel time and IQR for vehicles traveling SB-through on West St. from 15:00–18:00 hrs.

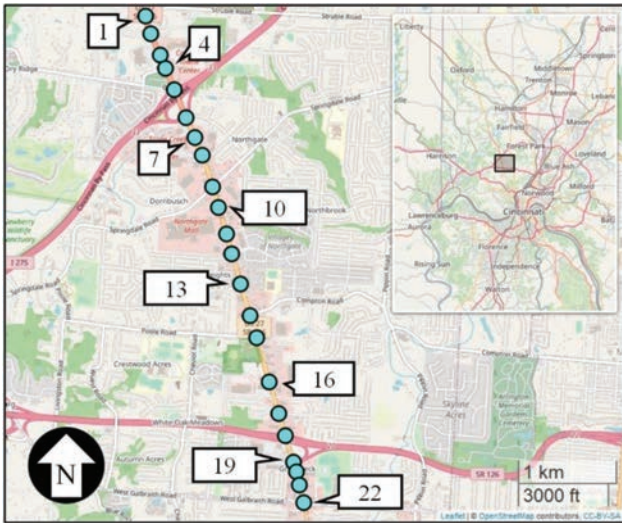


Figure 8.10 Intersections analyzed on US-27 (map data: OpenStreetMap).

TABLE 8.2
Studied intersection on US-27

Intersection ID	Intersection Name
1	US-27 at Struble Rd.
2	US-27 at Generation Dr.
3	US-27 at Dry Ridge C Rd.
4	US-27 at Dry Ridge Rd.
5	US-27 at IR 275 WB
6	US-27 at IR 275 EB
7	US-27 at Stone Creek
8	US-27 at Redskin Dr.
9	US-27 at Springdale Rd.
10	US-27 at Marshall Square
11	US-27 at Mall Dr.
12	US-27 at Commons Circle
13	US-27 at Round Top
14	US-27 at Compton Rd.
15	US-27 at Poole Rd.
16	US-27 at Joseph Rd.
17	US-27 at Sovereign Dr.
18	US-27 at Cross Cty. WB
19	US-27 at Cross Cty. EB
20	US-27 at Colerain
21	US-27 at Salvage Auto
22	US-27 at Galbraith Rd.

other, particularly with regards to queue storage. Callouts i in Figure 8.11 and Figure 8.12 highlight the performance of these two intersections during the PM peak period (15:00–18:00 hrs.). As shown, there are substantial improvements in LOS, AOG, and DSB in the after period.

The PPDs from which the performance measures are estimated for Intersections 6 and 7 are shown in Figure 8.14. Before the new semi-automated adaptive system was implemented, Intersection 7 had 31% AOG, which is noticeable by a lack of non-stopping (green) trajectories at its approach (Figure 8.14c, callout i). This low level of progression had negative effects on the upstream Intersection 6 since vehicles at this location experienced queued traffic soon after exiting the

intersection, which is reflected by a high percentage of DSB (Figure 8.14a, callout ii).

In contrast, after the semi-automated adaptive system was implemented, Intersection 7 had an improved AOG value of 78% (Figure 8.14d, callout iii). This enhanced progression had positive effects on Intersection 6 since the percentage of DSB was significantly reduced (Figure 8.14b, callout iv).

This analysis can also be performed solely from Figure 8.11 and Figure 8.12 by understanding the

TABLE 8.3
Volume change from count stations (87)

North Intersection ID	South Intersection ID	2020 AADT	2021 AADT	Difference (%)
2	3	29,837	47,535	+59
4	5	30,092	41,405	+38
6	7	34,436	38,969	+13
13	14	29,852	39,504	+32
<i>Total</i>		<i>124,217</i>	<i>167,413</i>	<i>+35</i>

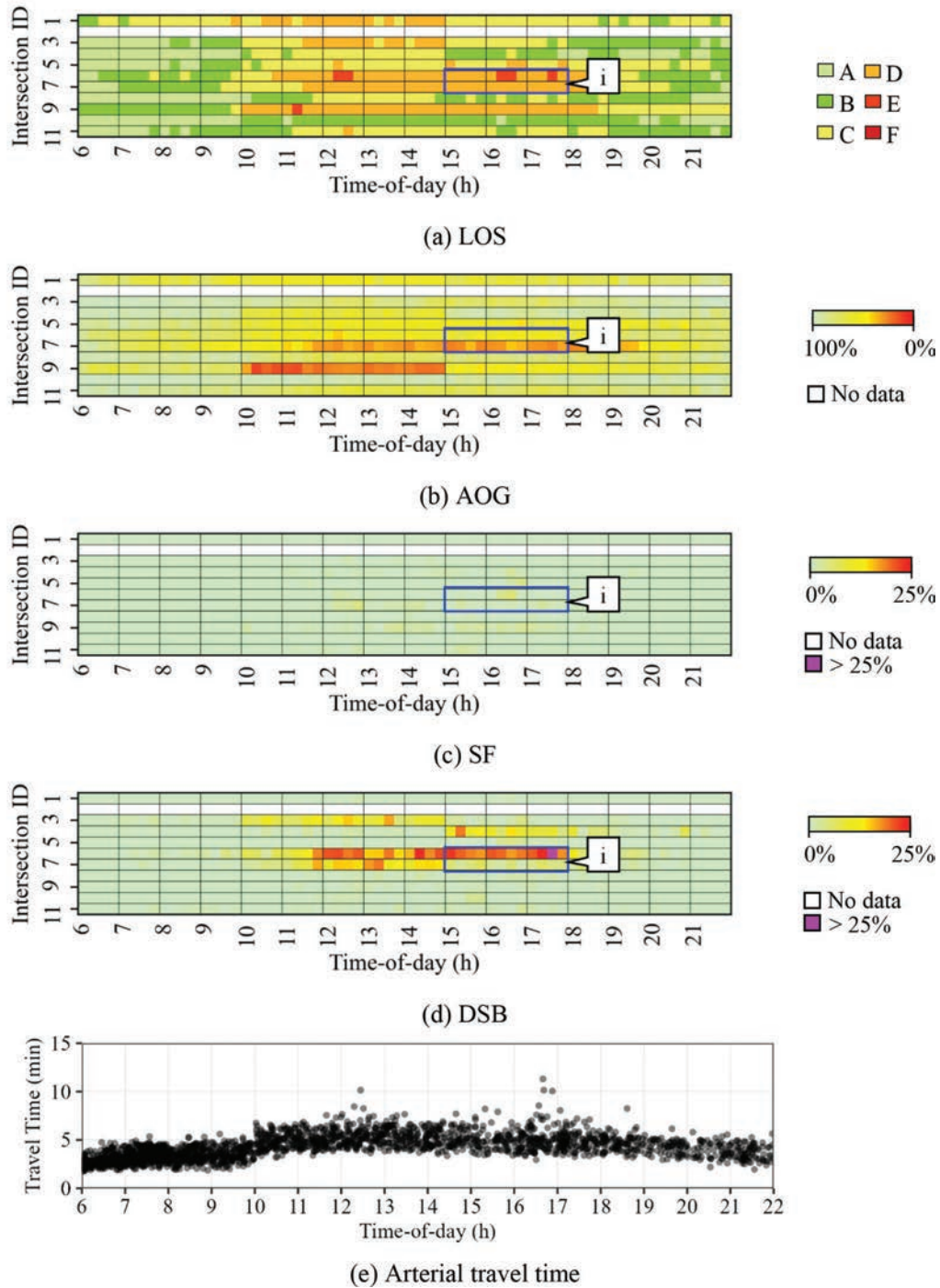


Figure 8.11 Signal performance measures for SB-through movements on US-27 during August 2020 weekdays.

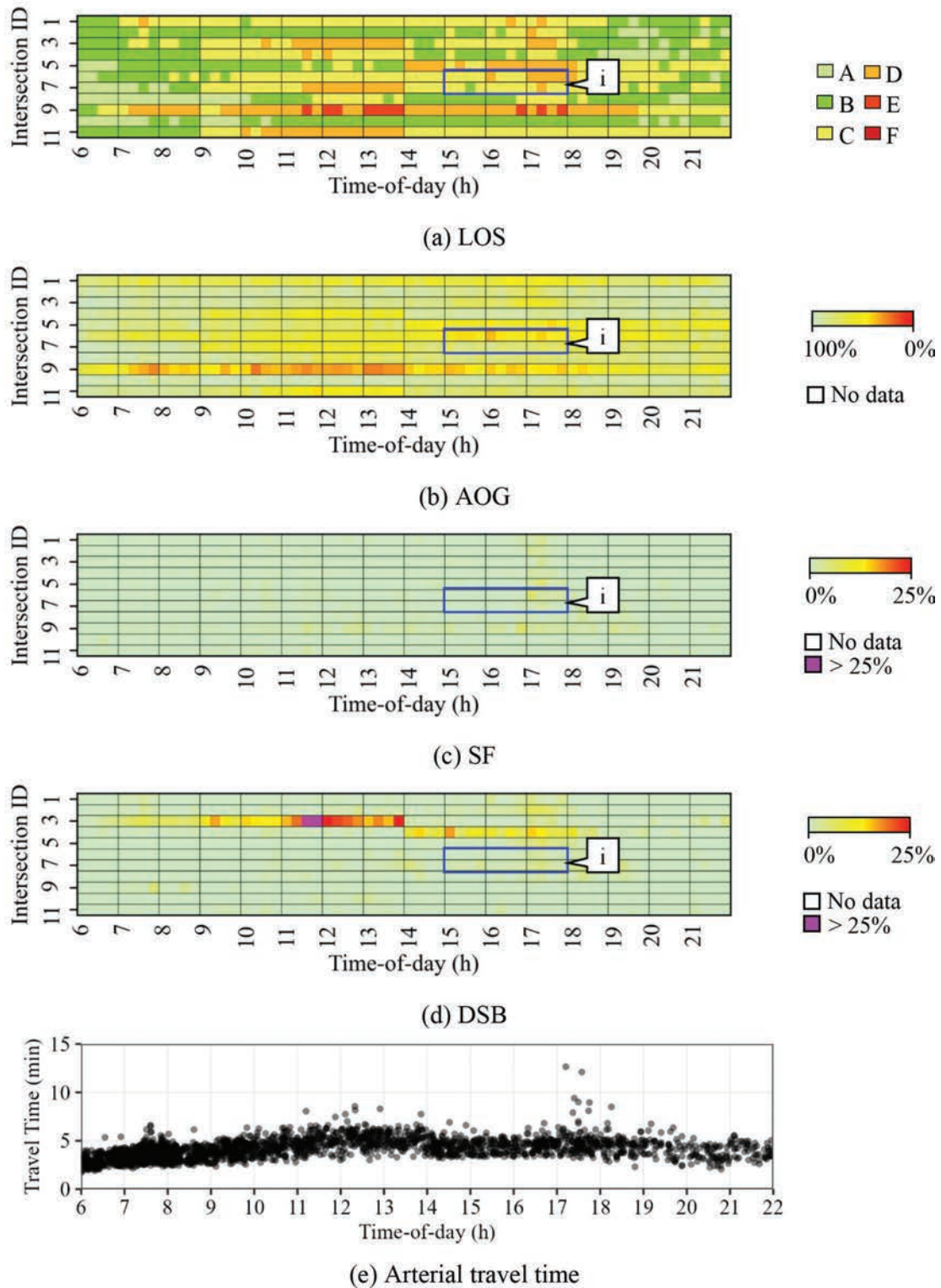


Figure 8.12 Signal performance measures for SB-through movements on US-27 during August 2021 weekdays.

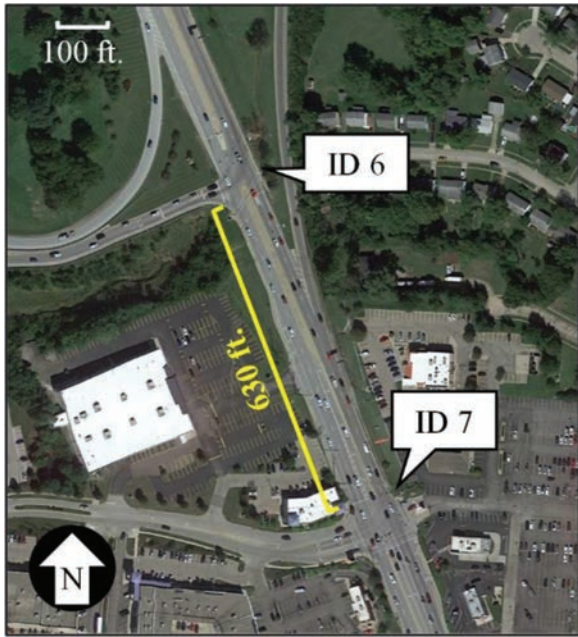


Figure 8.13 Aerial view of Intersections 6 and 7 (map data: Google).

location of the intersections on the corridor and the correlation between CV-based performance measures.

8.2.4 Results

August 2020 and August 2021 average corridor-wide AOG, SF, DSB, and control delay, by movement, are shown on Figure 8.15. No significant changes are

observed for AOG. SF increased for EB- and WB-through movements and decreased for EB-left. DSB improved for EB-through movements but worsened for NB-through and EB-left. Average control delay increased for the WB-through movement and the NB-, EB-, and WB-left movements.

Table 8.4 shows the change in aggregated performance measure results for all the intersections and movements on the studied corridor. Overall, there is a 1% AOG improvement and a 2-second increase of average control delay. SF, DSB, and LOS did not see any changes.

Based on the small differences in operational performance and considering the significant increase in traffic volume of 35%, it is clear that the semi-automated adaptive signal system is effective on diminishing the effects of an increased demand on the entire corridor.

8.2.5 Summary

Approximately 1 million trajectories and 13.5 million waypoints are analyzed from August 2020 (before timing upgrade) and August 2021 (after timing upgrade) CV data to generate corridor-wide (Figure 8.11 and Figure 8.12) and approach-level (Figure 8.14) visualizations. Further, the presented technique is shown to be capable of providing insight into the influence between adjacent intersections.

Figure 8.15 and Table 8.4 illustrate only very minor changes in system performance after a 35% traffic volume increase. The average control delay increased by only 2 seconds and the overall system level of service remained as “C”.

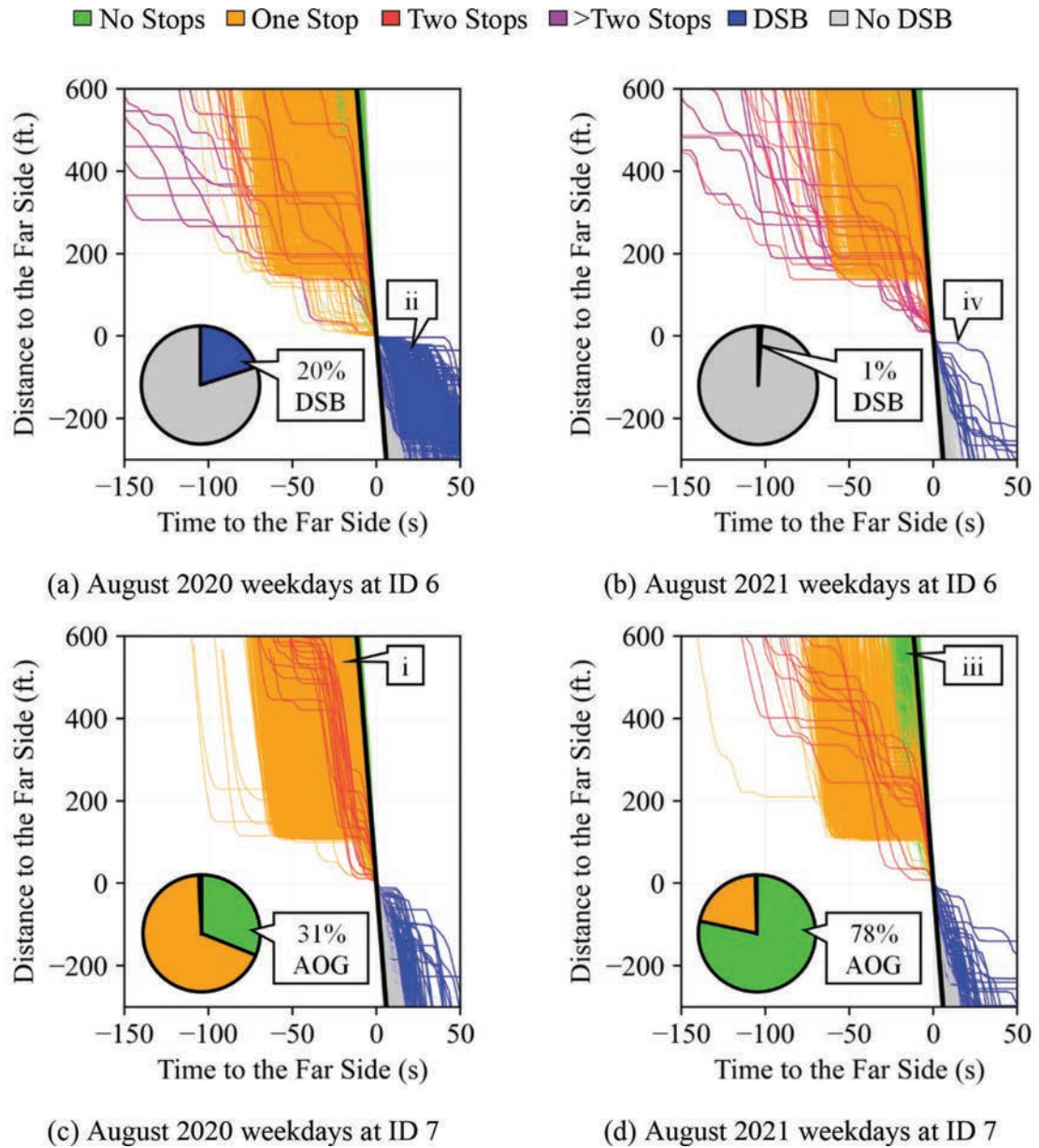


Figure 8.14 PPDs of vehicles traveling SB-through from 15:00 to 18:00 hrs.

TABLE 8.4
Performance overview

Measurement	Analysis Period	
	August 2020	August 2021
Count Station Traffic Volume	124,217	167,413
AOG	70%	71%
SF	1%	1%
DSB	2%	2%
Average Control Delay (s/veh)	25	27
LOS	C	C

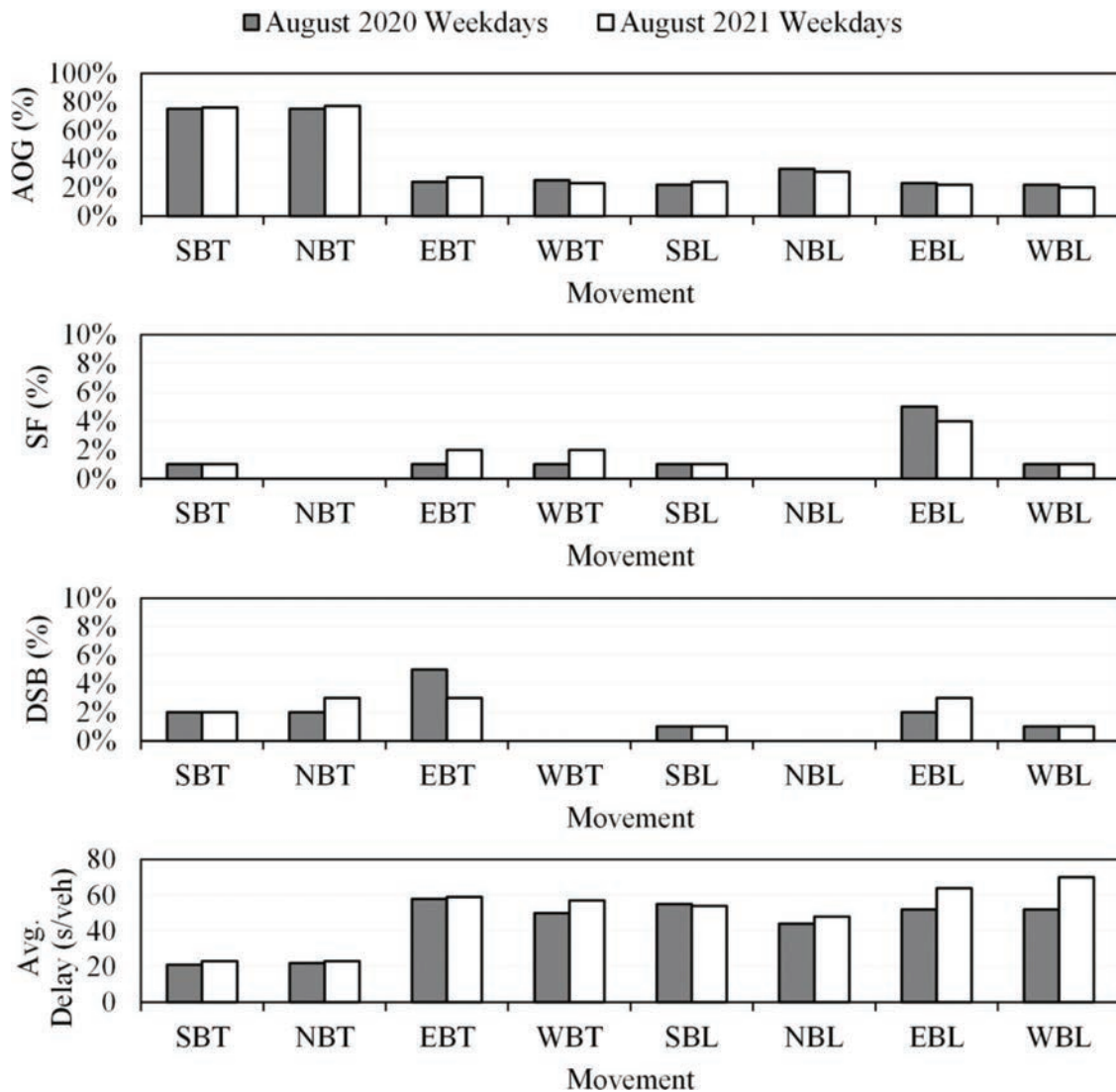


Figure 8.15 Corridor-wide change in performance by movement.

9. IDENTIFICATION OF SIGNAL RETIMING OPPORTUNITIES TO REDUCE SPLIT FAILURES

Traffic signal operations have a significant impact on road networks. The state-of-the-practice traffic signal management had a national result of C+ in the *2019 Traffic Signal Benchmarking and State of the Practice Report* (25). With over 400,000 traffic signals in operation nationwide, it is crucial for agencies to monitor signal performance and identify locations where timing improvements could reduce congestion, enhance mobility, decrease delays, and reduce the number of stops (28).

The implementation and modification of signal timing parameters, phasing sequences, and control techniques enables efficient operations to service vehicle demand (27). To maximize benefits, FHWA recommends agencies to focus resources to maximize favorable measures such as progression and throughput and minimize unfavorable measures such as delay and split failures (88). The benefit-to-cost ratio of signal retiming has been estimated to be around 40:1 (27).

The identification of oversaturated movements and whether green time can be redistributed has previously been studied using ATSPMs, probe data, and aggregated data (88–91). Achieving this analysis agency-wide using sensor infrastructure methods typically require robust and accurate detection (66), which can be costly to install and maintain (92). Furthermore, analyses derived from probe data can constrain practitioners due to the limited spatial and temporal fidelity of segments.

This chapter presents a scalable methodology by which CV-based performance measures can be used to

identify critical split-failing movements where additional green time could be provided from either within or across ring diagram barriers at the intersection (11). To present the technique, signal retiming is prioritized for 112 intersections in a Relative Performance Diagram (RPD) by evaluating SF and DSB of all traffic movements. Over 400,000 trajectories and 6.8 million waypoints are analyzed. Three intersections are identified as having opportunities for tactical operational improvement by adjusting the timing plan. A post-retiming review of the traffic signal performance measures is provided at the end of the chapter.

Using the discussed methodology, agencies can proactively identify systemwide where there are not only capacity challenges, but where tactical deployment of retiming resources is likely to result in an improvement.

9.1 Study Locations

In this chapter, 112 intersections in central and west Indiana, shown in Figure 9.1, are analyzed to identify locations where signal timing modifications could potentially reduce SF at a particular movement. These intersections function in a wide variety of conditions (e.g., different volumes and geometries) and are operated and maintained by INDOT. Most of the intersections are located in suburban areas with low pedestrian demand. Figure 9.1b shows the intersections chosen for retiming with callouts 1 to 3 which will be discussed in detail in a subsequent section.

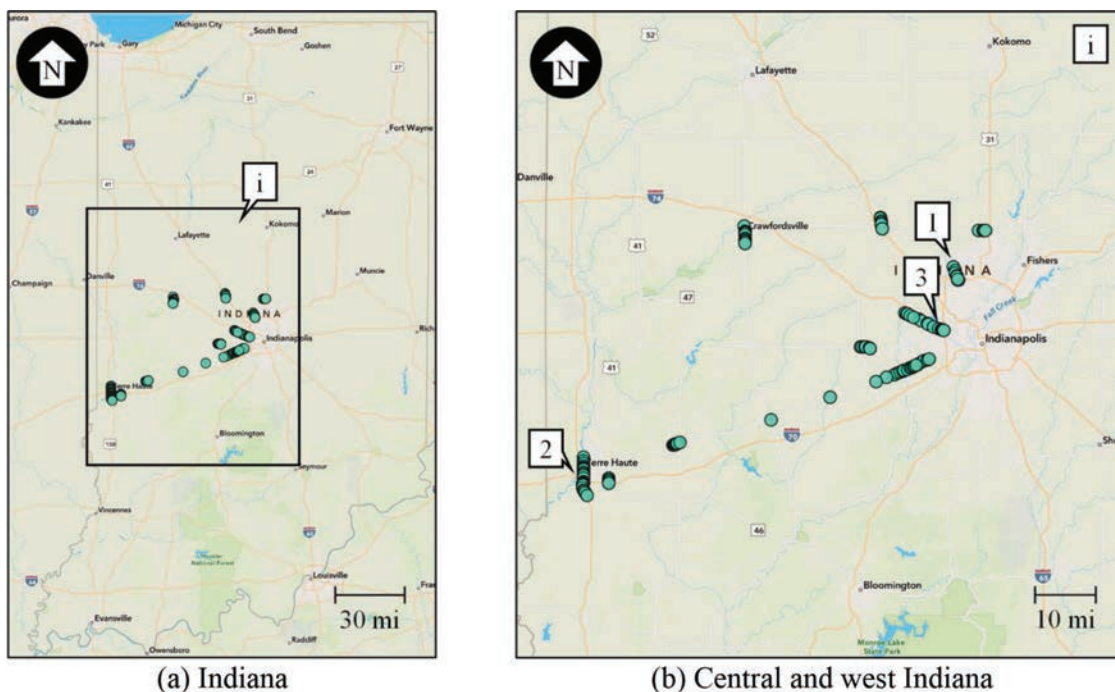


Figure 9.1 Analyzed intersections (map data: Esri, HERE, Garmin, FAO, NOAA, USGS, EPA, and NPS).

9.2 Systemwide Split Failure Assessment

As discussed in Chapter 7, when analyzing the performance of a significant number of traffic signals, it is useful to identify the locations that operate in the most challenging conditions. Not only does this help locate the intersections that require further attention, but it also provides valuable information on the overall health of the system.

Figure 9.2 shows all 112 intersections sorted by their overall SF ratio during the PM peak (16:00–18:00 hrs.). This is calculated by dividing the count of all vehicles that experienced a split failure over the total number of sampled vehicles that passed the intersection regardless

of movement. All signals have a value below 0.2, which shows that, at the worst case (left-most intersection), roughly one out of five sampled vehicles passing the intersection experienced a split failure.

Although it is valuable to assess the overall SF ratio of traffic signals, from an operational perspective, it is more useful to evaluate systemwide performance by movement. With this approach, practitioners can identify the source of congestion. Figure 9.3 shows the movements of the 112 intersections sorted by their SF ratio. Through movements are shown in Figure 9.3a and left movements in Figure 9.3b. These enable practitioners to identify which movements are the most challenged in the system.

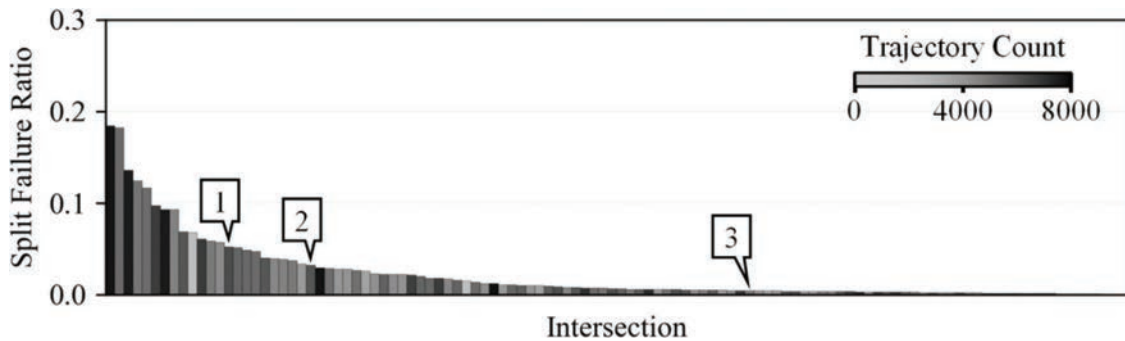
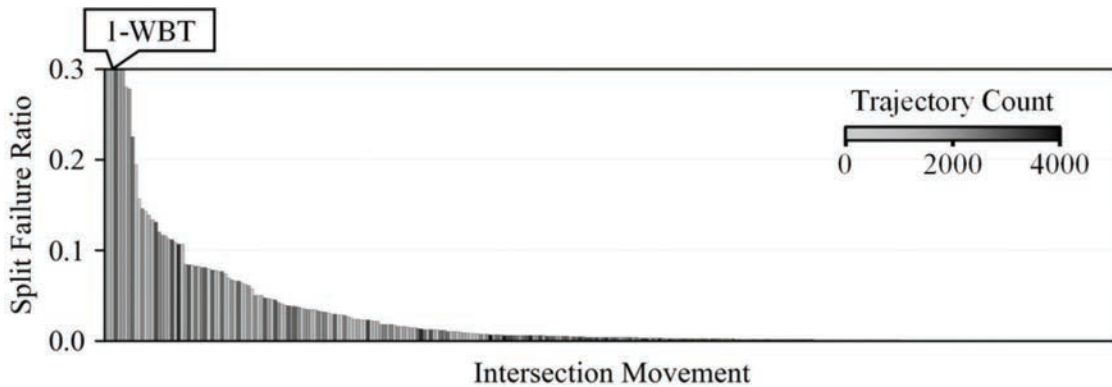
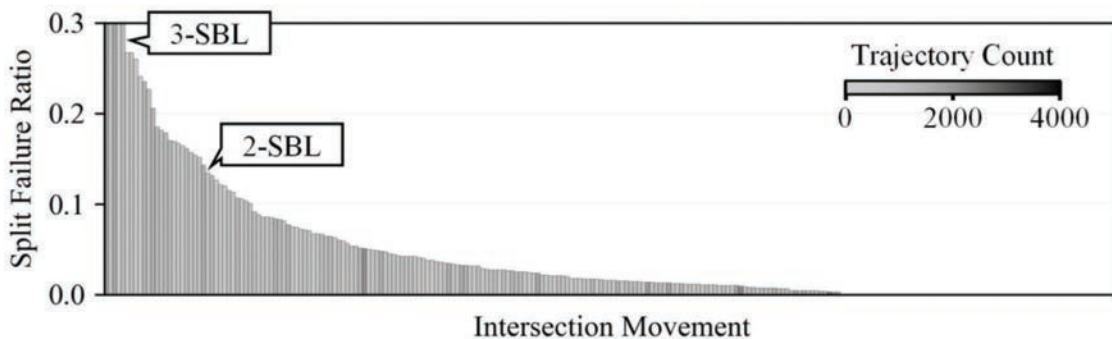


Figure 9.2 May 2022 weekday intersection split failure ratio from 16:00–18:00 hrs.



(a) Through movements (n: 306)



(b) Left movements (n: 240)

Figure 9.3 May 2022 weekday movement split failure ratio from 16:00–18:00 hrs.

It is of interest to not only be aware of the worst performing movements, but also the movements that can be improved by reallocating green time. The following section discusses a CV-based technique to identify which signals are good candidates for signal retiming.

9.3 Traffic Signal Retiming Opportunities

Signals where potential retiming opportunities exist are identified based on the following two criteria (90).

- The movement at the signal that has the highest SF level needs to be identified. This movement will be referred to as the “critical movement” and it is the target where additional split (green time) is desired.
- Movements that could distribute split to the critical movement need to be evaluated. These movements will be referred to as “donor movement(s)”. If the donor movements are also saturated, then split rebalance (i.e., the practice of taking split from one phase and giving it to another) cannot be performed. On the other hand, if the donor movements are undersaturated, there is potential to reduce SF by reallocating split from the donor movement to the critical movement.

There are two types of donor movements. The first is the conflicting movement of the critical movement within the same barrier and ring. The second considers movements on the opposite side of the barrier. Depending on which donor is used to identify retiming candidates, different signals may appear as having retiming options.

To determine retiming candidates, RPDs, which are visualization tools based on the points discussed above (11), can be used. RPDs differ depending on which donor movements are evaluated and are further explained below.

9.3.1 Conflicting Movement Relative Performance Diagram

Conflicting Movement RPDs are based on the analysis of conflicting movements as donor movements. After identifying the critical movement, the conflicting movement is evaluated to assess split rebalance (SR) opportunities.

The conflicting movement is easily identifiable as it is located next to the critical movement within the same barrier in the ring diagram. Figure 9.4a shows how this concept works. In this hypothetical case, the SB-left movement (Phase 1) is identified as having the highest level of SF in the intersection; hence, it is the critical movement. Then, the NB-through movement (Phase 2) is the potential donor as it is next to the critical movement and is located within the same barrier and ring. Therefore, if Phase 2 is undersaturated there might be opportunities for a split rebalance.

Figure 9.4b shows the Conflicting Movement RPD for the analyzed locations. Each marker represents an intersection. The horizontal axis displays the SF ratio of the critical movement. The vertical axis shows the SF ratio of the conflicting (donor) movement. Only

intersections where at least 30 trajectories are sampled for the donor and critical movement are plotted. Dashed lines located at the global SF ratio (i.e., total number of split failures divided by the total number of sampled trajectories on the analyzed movements) are plotted for reference (callout i). These dashed lines divide the RPD in four quadrants.

- Top-left (0 intersections): This quadrant should always be empty as there is no case in which the donor movement has a higher SF value than the critical movement.
- Bottom-left (32 intersections): This quadrant shows the intersections where both the critical and donor movements have relatively small SF ratios; hence, no concerns are raised.
- Top-right (6 intersections): This quadrant shows the intersections where both movements have significant SF and split rebalancing is not feasible. Nonetheless, these intersections could potentially be good candidates to evaluate for capital investments that would increase capacity.
- Bottom-right (26 intersections): This quadrant shows the intersections where the critical movement has significant SF while the donor movement has values below the global average. Here is where the locations with retiming opportunities are found. The closer the donor movement is to zero, the more likely it can provide split time to the critical phase with no detrimental impact to itself.

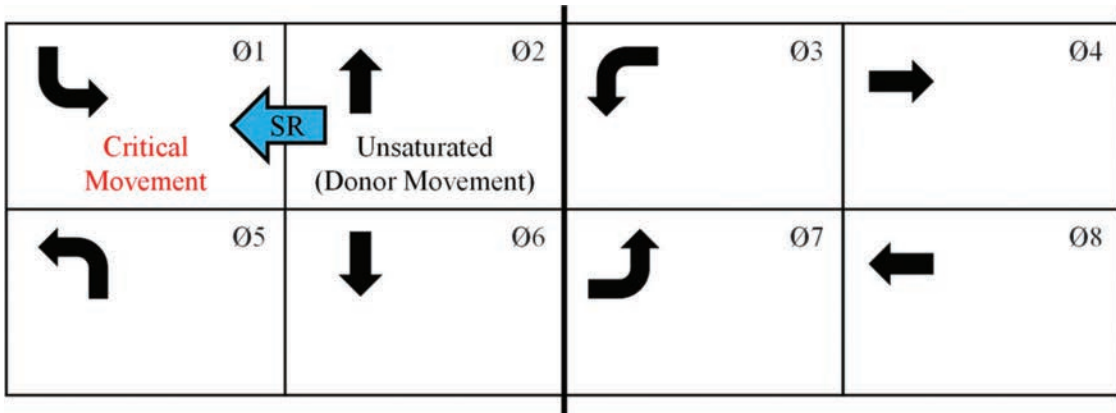
Additionally, each datapoint is color-coded based on the level of DSB of the critical movement. This is done because even if an intersection seems like a good candidate for retiming, if vehicles are being blocked by a downstream intersection, then the source of split failures would not be at the analyzed location and additional green time would not alleviate congestion (90).

Two intersections are identified as being good candidates for signal retiming by analyzing Figure 9.4b. Intersection 1, US-421 at W 116th St., has a critical and donor movement with 0.35 and 0.01 SF, respectively. This intersection is selected for its significant difference in SF levels between the critical and donor movements. Intersection 2, US-41 at E Margaret Ave., has a critical and donor movement with 0.13 and 0.00 SF, respectively. This intersection is selected for having the highest level of SF on the critical movement with non-existent split failures on the donor movement. Furthermore, both intersections have no DSB on the critical movement, which indicates that the source of congestion is not a downstream intersection and signal retiming may improve operations.

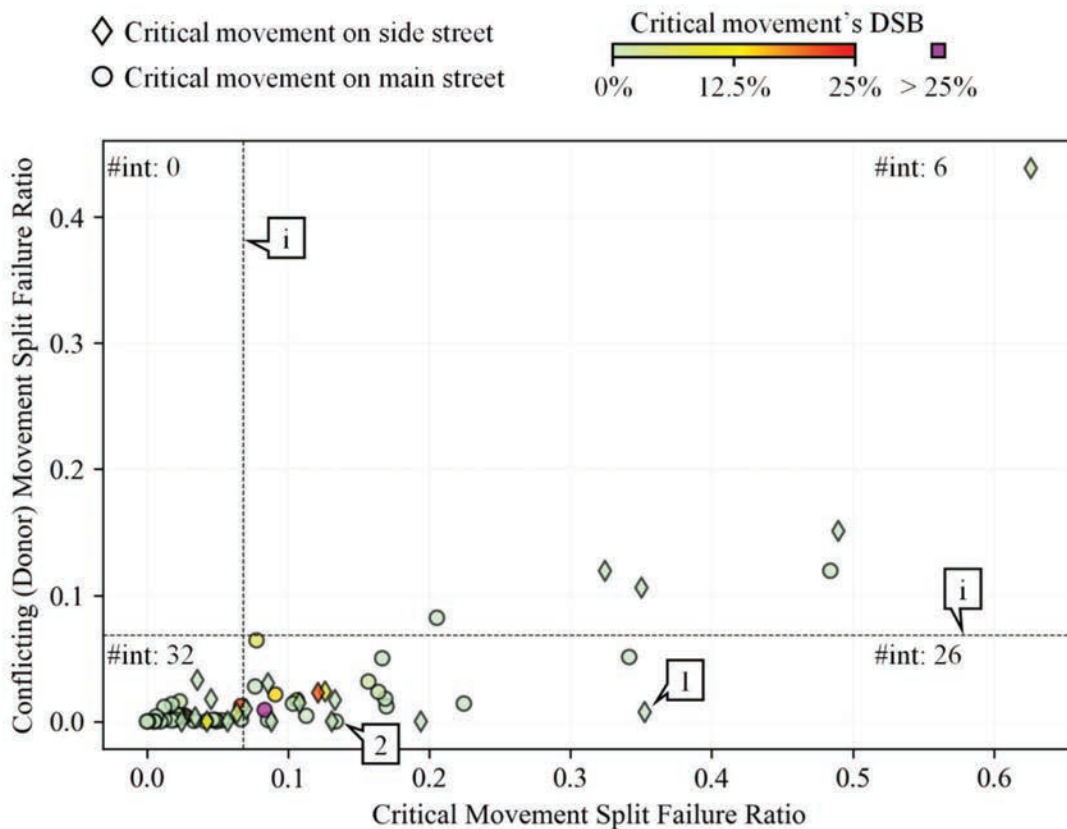
9.3.2 Opposite Barrier Relative Performance Diagram

Opposite Barrier and Conflicting Movement RPDs are similar, with the only difference being that the vertical axis on the former is based on the maximum SF value from the movements on the opposite barrier.

Figure 9.5a shows how this concept works. In this hypothetical case, the EB-through movement (Phase 4) is identified as having the highest level of SF in the intersection; hence, becoming the critical movement.



(a) Split rebalance concept



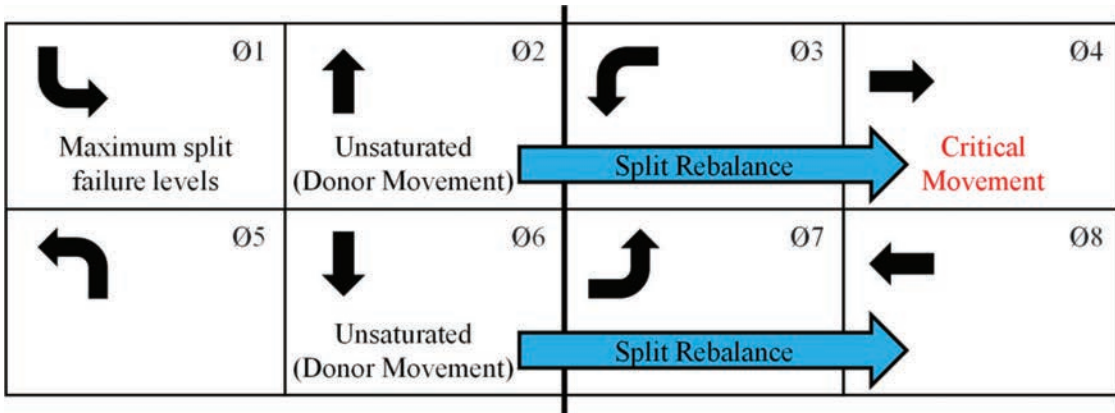
(b) May 2022 weekday system RPD from 16:00–18:00 hrs.

Figure 9.4 Conflicting movement RPD.

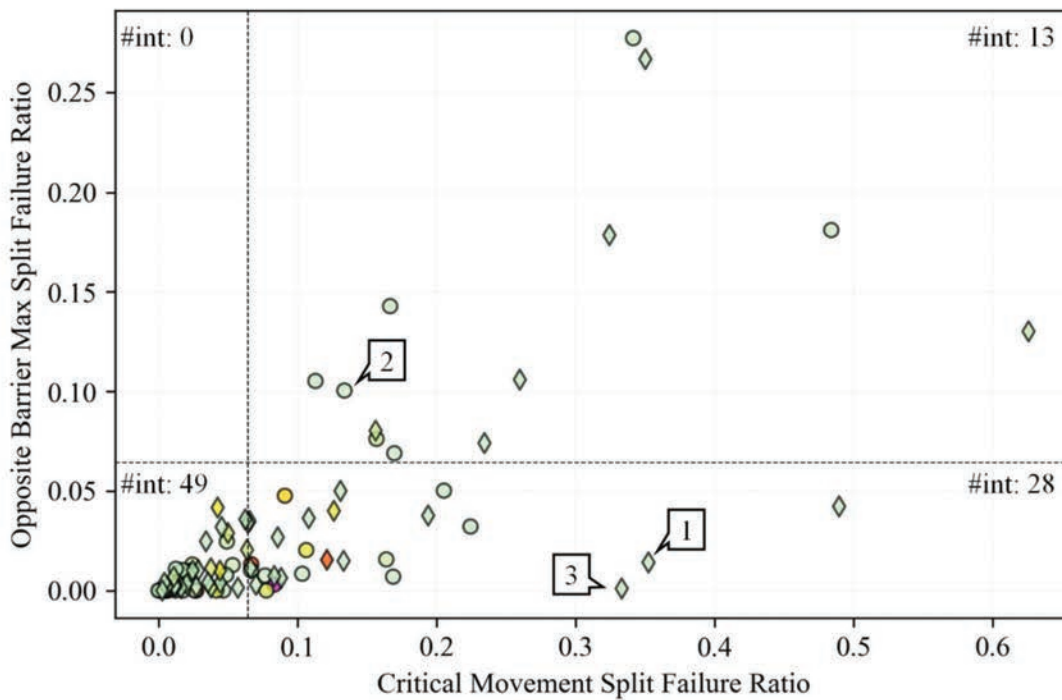
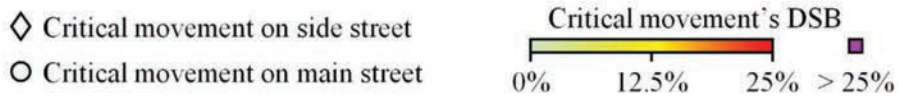
Then, all the SF values of the movements on the opposite barrier (Phases 1, 2, 5, and 6) are evaluated and the maximum is plotted on the RPD. The maximum is used because any other combination would underestimate the level of congestion at a movement within that block. In the example, the SB-left movement (Phase 1) has the maximum SF value. If the maximum is low, the block opposite the critical movement is a viable option for further analysis. In

this case, Phases 2 and 6 are undersaturated and opportunities for split rebalance are available. Since this technique requires inter-barrier split distribution, the same amount of time modified on one ring must be modified on the other.

Figure 9.5b shows the Opposite Barrier RPD of the signals analyzed. Two intersections are identified as being good candidates for retiming. Intersection 1, which is also identified as a good option from the



(a) Split rebalance concept



(b) May 2022 weekday system RPD from 16:00–18:00 hrs.

Figure 9.5 Opposite barrier RPD.

Conflicting Movement RPD (Figure 9.4b), has a critical movement and opposite maximum with 0.35 and 0.01 SF, respectively. Intersection 3, US-136 at Waterfront Pkwy W Dr., has a critical movement and opposite maximum with 0.33 and 0.00 SF, respectively. This intersection is selected for having the highest level of SF and no DSB on the critical movement with almost non-existent split failures on the opposite maximum. Interestingly, Intersection 2 does not appear to be a good candidate when analyzing the Opposite Barrier

RPD, which is why it is important to assess both versions of the RPD, so no retiming opportunities are missed.

It is important to note that the movements at Intersections 1 through 3 are not the worst performing in the system, as shown in Figure 9.2 and Figure 9.3. The highest split-failing intersections may not be good retiming candidates due to lack of underutilized green available for reallocation, and therefore are not highlighted by the RPDs as such.

9.3.3 Relative Performance Diagram Limitations

Current limitations of RPD-based identification of retiming opportunities are that the method assumes a sequence at each intersection and that signals use fixed force-offs (i.e., every movement can receive unused time from previous phases). For the first point, it is important to distinguish leading phases that have been identified as donors but may already be running efficiently due to gap out. Additionally, timing plans that run floating force-offs do not allow non-coordinated movements to inherit unused green time and may be preventing the controller from efficiently allocating additional green to those movements that may be split-failing. Confirmation of timing plans remotely or via field visits are necessary before any adjustments are made.

Another limitation is that RPDs do not take into consideration pedestrian phase timing requirements. Under-utilized green splits may run concurrent with pedestrian movements and split time cannot be reduced. Future research would incorporate pedestrian volumes (93) at pertinent intersections.

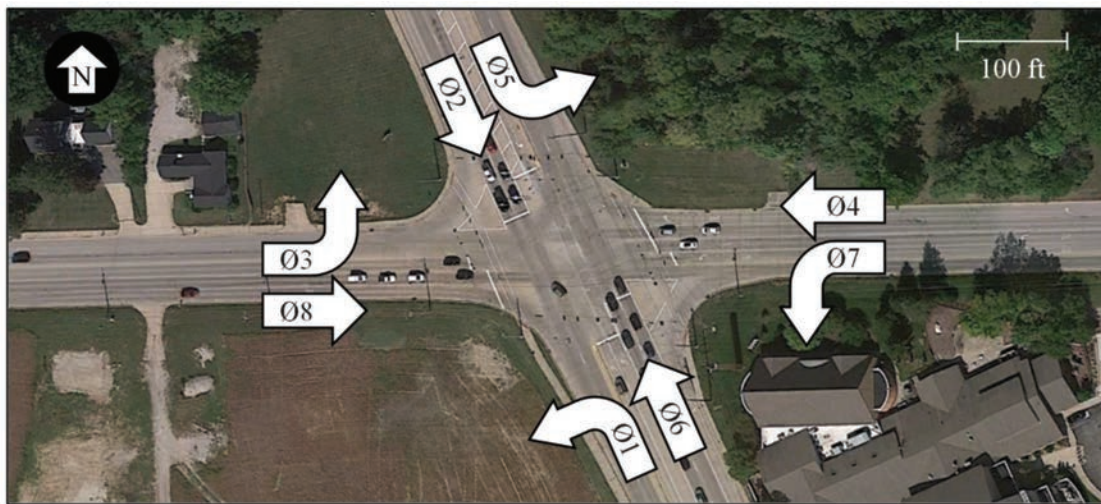
9.4 Signal Timing Modifications

In this section, the intersections selected from the RPDs in Figure 9.4b and Figure 9.5b are further evaluated. For each location, a deeper analysis of the operational state of the different movements is performed. Then, from the estimated performance and insights gained from site-visits, signal timing modifications are implemented. Finally, a before-after analysis is provided.

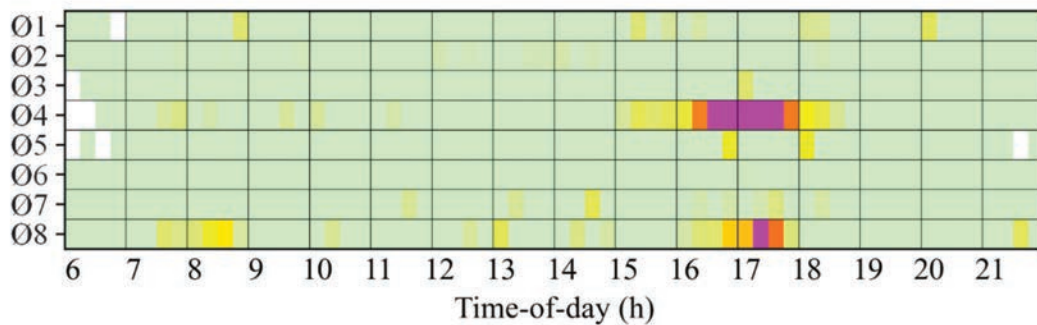
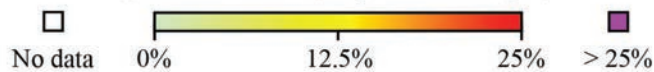
9.4.1 Intersection 1: US-421 at W 116th St.

Figure 9.6a shows an aerial view of the intersection with its respective movements and phases. The coordinated phases are 2 (SB-through) and 6 (NB-through). Figure 9.6b shows a heatmap with the SF estimations for all movements by TOD.

The critical movement is WB-through (Phase 4). However, the EB-through movement (Phase 8) also experiences significant levels of SF. Both phases have lagging left-turns and do not inherit time from previous



(a) Aerial view (map data: Google)



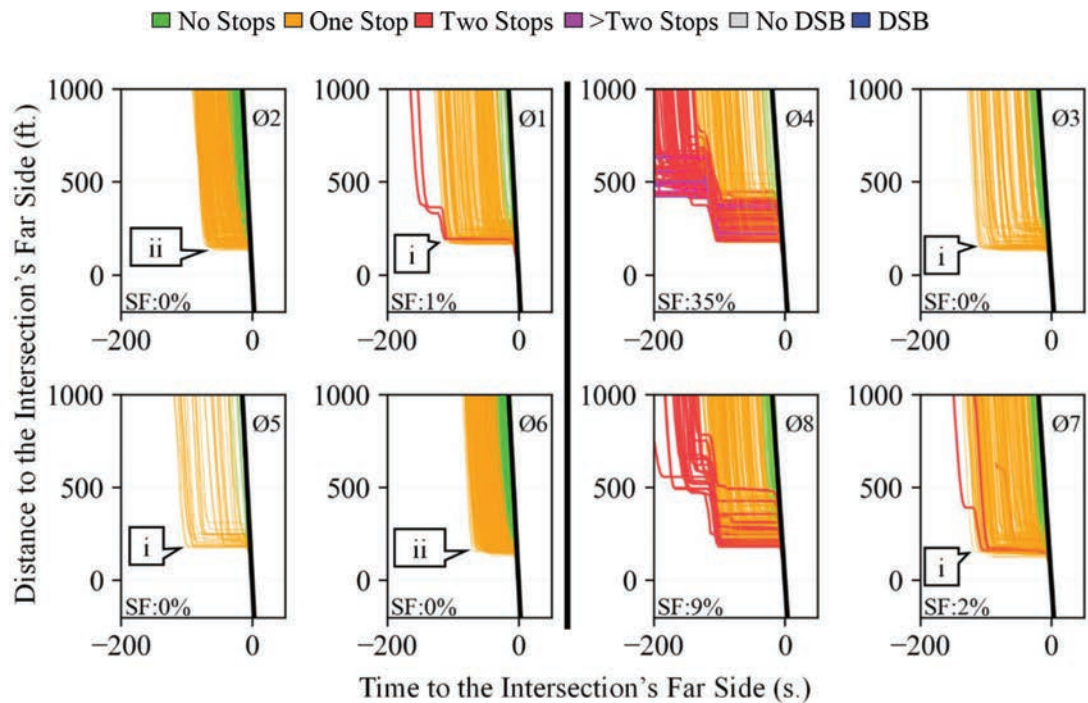
(b) May 2022 weekday SF by movement

Figure 9.6 Intersection 1: US-421 at W 116th St.

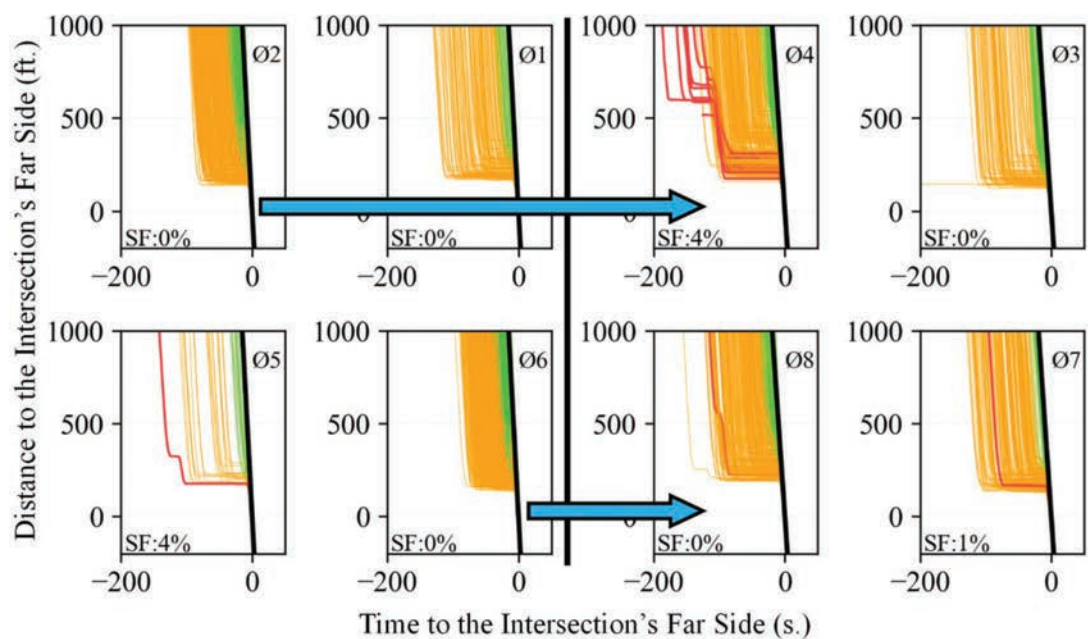
phases in the sequence due to floating force-offs. Therefore, it is desired to provide both phases (4 and 8) additional split time and adjust the force-off option to allow them to receive unused green.

Since this intersection appears as a good candidate on both RPDs (Figure 9.4b and Figure 9.5b), time could potentially be rebalanced from either conflicting

movements (Phases 3 and 7) or the opposite barrier (Phases 1, 2, 5, and 6). However, since Phases 1, 3, 5, and 7 already have delays close to the cycle length of 120 seconds (Figure 9.7a, callout i), it is decided to use Phase 2 and 6 as donor movements as those vehicles have significantly shorter delays (Figure 9.7a, callout ii). Thus, the changes implemented for the PM peak



(a) Before signal retiming: May 27th to June 9th, 2022, weekdays



(b) After signal retiming: June 10th to June 23rd, 2022, weekdays

Figure 9.7 PPDs ring diagrams at Intersection 1 from 16:00–18:00 hrs.

period based on the performance estimations, field visits, and engineering judgment are the following.

- Donor phases (2 and 6): 4.8 seconds reduction of split time and 1.8 seconds reduction of minimum gap time. Further, set actuated-coordinated (split extension) to 7% and 10%, respectively, to allow the phases to gap out.
- Critical phases (4 and 8): Additional 4.8 seconds of split time and receive any additional unused time from Phases 2 and 6 by changing operations to simulate fixed force-offs.
- Left-turn phases (1, 3, 5, and 7): Changed maximum selection to be limited to the split time to allow Phases 4 and 8 to inherit all unused time by 2 and 6.

Figure 9.7 shows the ring diagrams representing the sequence and barriers of this intersection with the PPDs of each movement before and after the timing changes. Figure 9.7b shows blue arrows indicating from which phases time is taken and which phases time is given. The benefits of the implemented changes can be qualitatively observed.

Figure 9.8 shows an in-depth before-after SF assessment of Intersection 1. Figure 9.8a shows the before period, Figure 9.8b shows the timing changes implemented, Figure 9.8c shows the after period, and Figure 9.8d shows the difference in split failures. Positive results are shown on Figure 9.8d for the modified phases with significant reduction of SF on the critical phases (4 and 8) and no changes on the donors (Phases 2 and 6). Additionally, from field observations, it is found that queues at the critical movement went from having up to 20 vehicles during the before period to only up to 8 vehicles during the after period.

9.4.2 Intersection 2: US-41 at E Margaret Ave.

Figure 9.9a shows an aerial view of the intersection with its respective movements and phases. The coordinated phases are 2 (NB-through) and 6 (SB-through). Figure 9.9b shows a heatmap with the SF estimations for all movements by TOD.

The critical movement is SB-left (Phase 1). This location is identified as having retiming opportunities from the Conflicting Movement RPD (Figure 9.4b) with the donor movement NB-through (Phase 2). The identification is corroborated by the heatmap showing that this movement is not split-failing. Thus, the changes implemented for the PM peak period based on the performance estimations, field visits, and engineering judgment are the following.

- Donor phase (2): Reduced split time up to 5 seconds between 16:00 and 16:15 hrs. and up to 3 seconds between 16:15 and 18:00 hrs. if there is demand on Phase 1.
- Critical phase (1): Additional split time up to 5 seconds between 16:00 and 16:15 hrs. and up to 3 seconds between 16:15 and 18:00 hrs. if there is demand.

Figure 9.10 shows the ring diagrams used at this intersection with the PPDs of each movement before (Figure 9.10a) and after (Figure 9.10b) the timing changes. Figure 9.10b shows a blue arrow indicating the

effectuated split rebalance. The benefits of the implemented changes can be qualitatively observed.

Figure 9.11 shows an in-depth before-after SF assessment of Intersection 2. Figure 9.11a shows the before period, Figure 9.11b the timing changes implemented, Figure 9.11c the after period, and Figure 9.11d the difference in SF. Positive results are shown on Figure 9.11d for the modified phases with significant reduction of SF at the critical phase with no changes on the donor (Phase 2).

9.4.3 Intersection 3: US-136 at Waterfront Pkwy W Dr.

Figure 9.12a shows an aerial view of the intersection with its respective movements and phases. The coordinated phases are 2 (EB-through) and 6 (WB-through). Figure 9.12b shows a heatmap with the SF estimations for all movements by TOD.

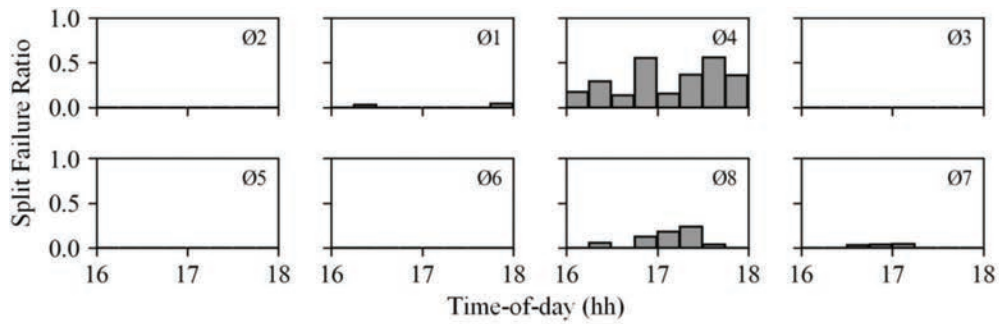
The critical movement is SB-left (Phase 7). Interestingly, this movement presents high SF values throughout the day, regardless of time. This indicates that split failures occur during all levels of demand experienced at this intersection, which points at the issue not being lack of capacity. After a field-visit, it was discovered that the split failures were caused by the phase gapping-out prematurely. This occurred due to the farthest back loop at the stop bar being broken (Figure 9.12a). It was found that detection had already been adjusted to work with the rest of the loop detectors but the gap out time was not increased to accommodate a reduced detection area causing vehicles to experience split failures. Thus, the change implemented based on the performance estimations, field visits, and engineering judgment, is an increase of the extension time at Phase 7 from 2.0 to 3.5 seconds to accommodate for the shorter detection area.

Figure 9.13 shows the ring diagrams used at this intersection with the PPDs of each movement before (Figure 9.13a) and after (Figure 9.13b) the timing changes. The benefits of the implemented changes can be qualitatively observed.

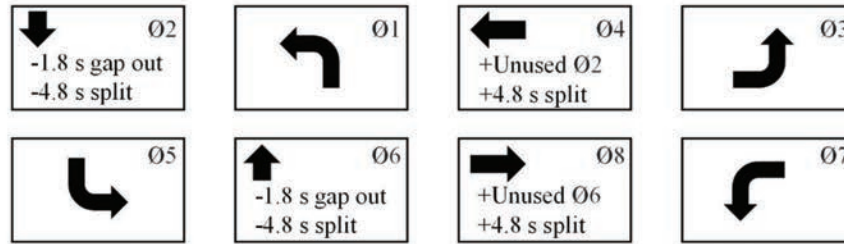
Figure 9.14 shows an in-depth before-after SF assessment of Intersection 3. Figure 9.14a shows the before period, Figure 9.14b the timing change implemented, Figure 9.14c the after period, and Figure 9.14d the difference in SF. Positive results are shown for Phase 7 with reductions on split failures.

9.5 Results

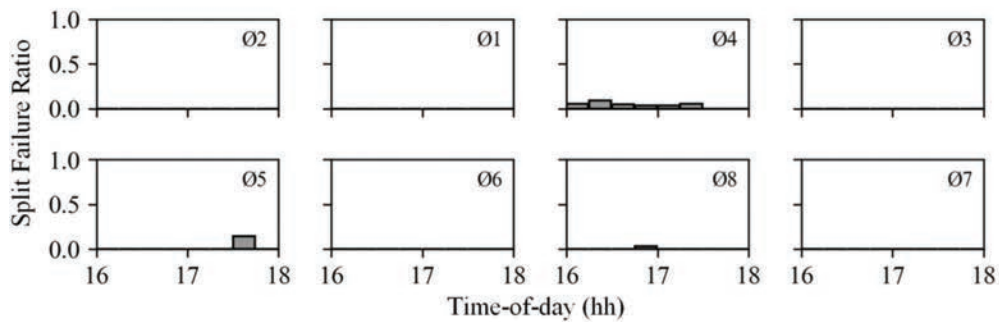
In this section, the aggregated change in performance from 2 weeks before and after timing modifications are implemented is presented for Intersections 1 to 3 on Table 9.1 to Table 9.3, respectively. Levels of SF, AOG, and average control delay are assessed for each movement. Results for each 2-week period are calculated by dividing the count of vehicles that experienced a SF, arrived on green, and the total delay of all sampled vehicles combined by the number of sampled vehicles.



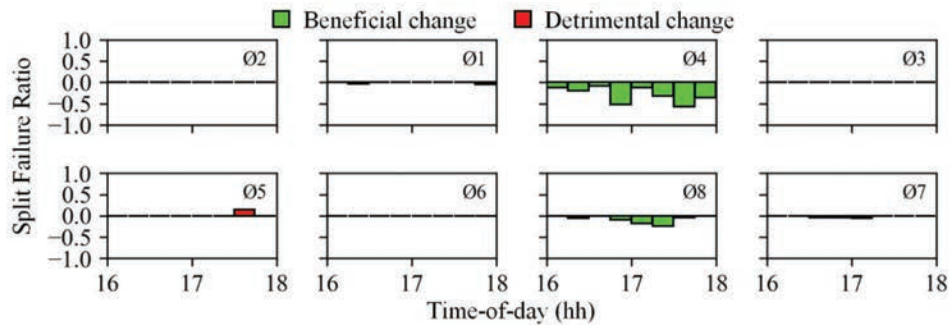
(a) Performance before the timing change: May 27th to June 9th, 2022, weekdays



(b) Timing changes implemented the morning of June 10th, 2022



(c) Performance after the timing change: June 10th to June 23rd, 2022, weekdays

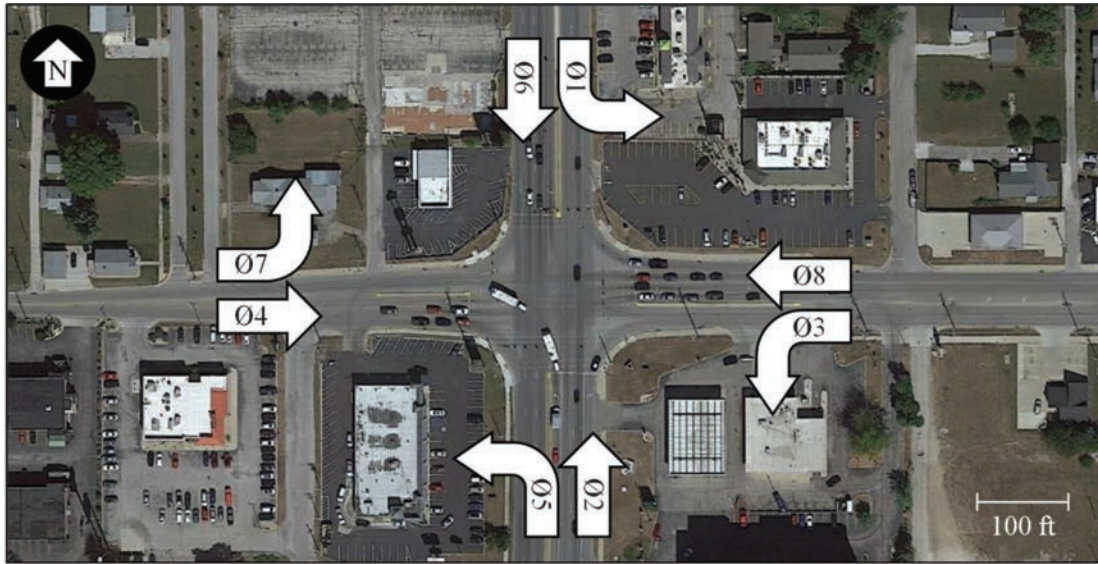


(d) Split failure ratio difference

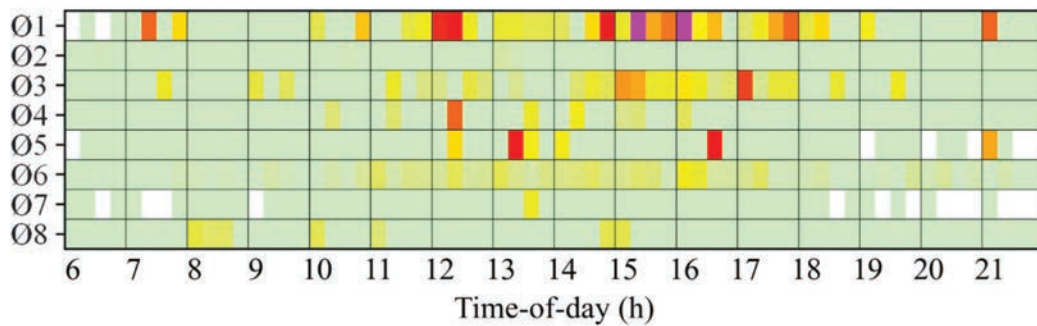
Figure 9.8 SF before-after assessment at Intersection 1 from 16:00–18:00 hrs.

Intersection 1 showed 30% and 9% reductions in SF, 15% and 8% increase in AOG, and 53 and 19 s/veh reduction in delay for the benefited critical phases 4 and 8, respectively. Simultaneously, the donor phases 2 and 6 experienced no change in SF, 7% and 3% decrease on AOG, and 7 and 3 s/veh growth in delay, respectively. Intersection 2 showed a 12% reduction on SF, a 9%

increase on AOG, and a 17 s/veh reduction on delay for the critical phase 1. Concurrently, the donor phase 2 had no changes in SF, a 7% decrease in AOG, and a 5 sec increase in delay. Intersection 3 showed a 9% decrease in SF, a 21% increase in AOG, and a 3 s/veh increase in delay for the critical movement, and negligible changes for the donor movements.



(a) Aerial view (map data: Google)



(b) May 2022 weekdays SF by movement

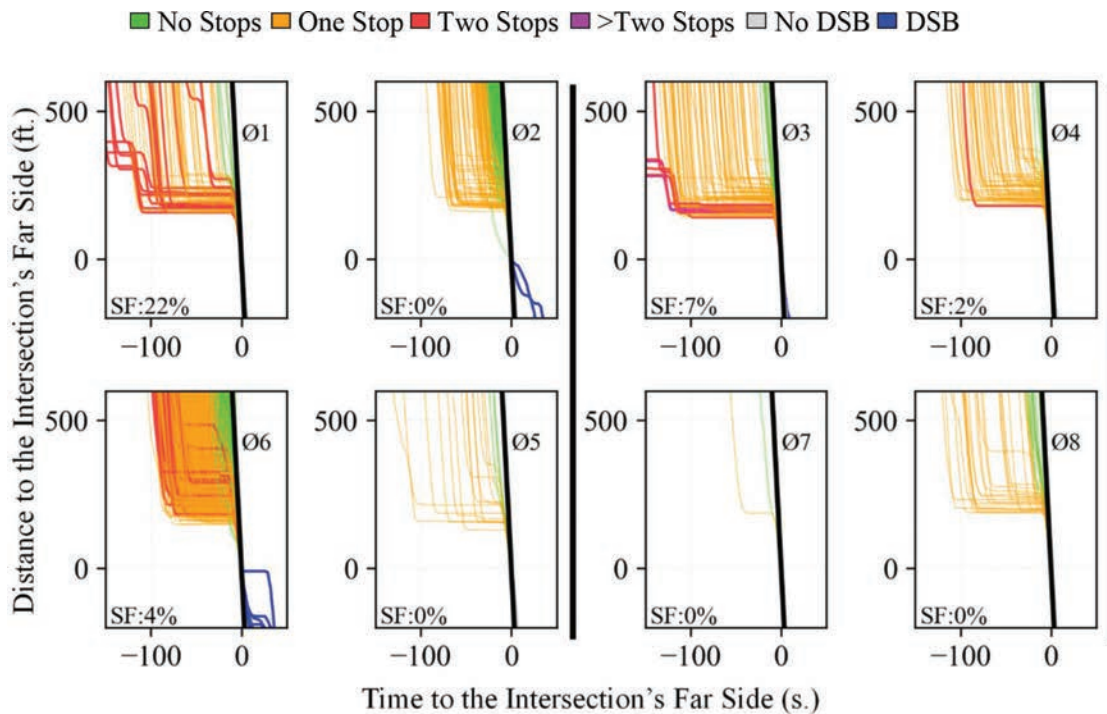
Figure 9.9 Intersection 2: US-41 at E Margaret Ave.

In general, SF is significantly reduced at the critical movements without increasing the ratio of SF occurring at the donor movements. At adjacent intersections from the modified locations, the largest changes in performance at the movement-level are only a 1% decrease in SF, a 4% increase in AOG, and a 1.9 s/veh reduction in delay. Thus, adjacent intersections are not negatively impacted by the timing changes.

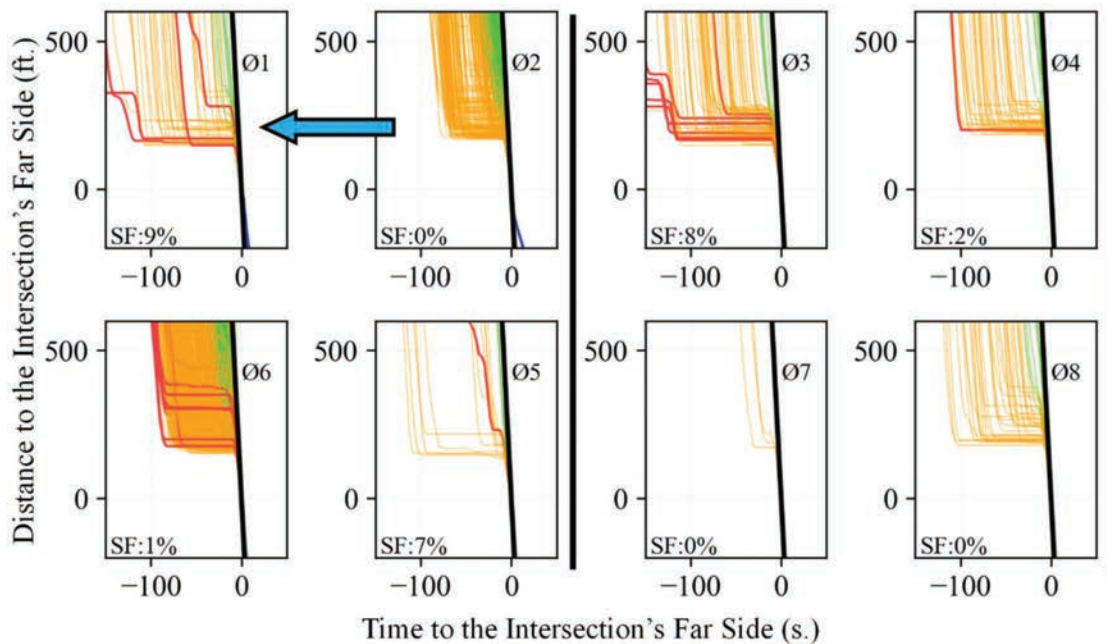
Additionally, changes in performance at the intersection-level considering all sampled vehicles regardless of movement choice at each location are presented in

Table 9.4. All intersections have reductions in SF and average control delay.

The presented techniques scale well for agencies to apply to hundreds of intersections to prioritize locations and TOD where traffic signal timings can be improved. Since these techniques and associated RPD summary graphics are based exclusively on CV data, they can be applied to any traffic signal system where CV data is available without the need for vehicle detection or communication infrastructure.

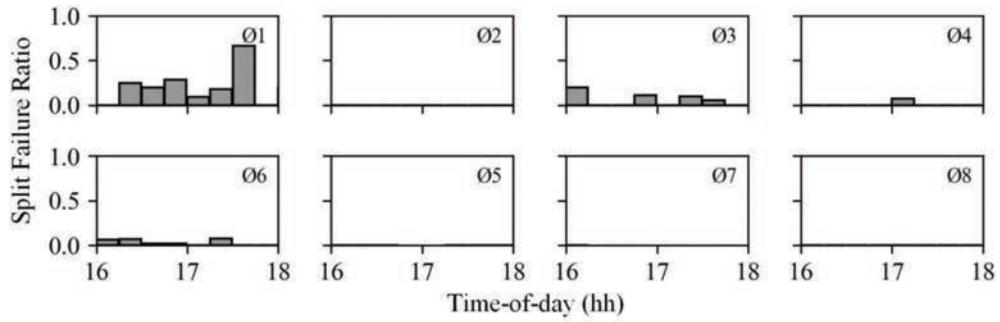


(a) Before signal retiming: May 30th to June 10th, 2022, weekdays

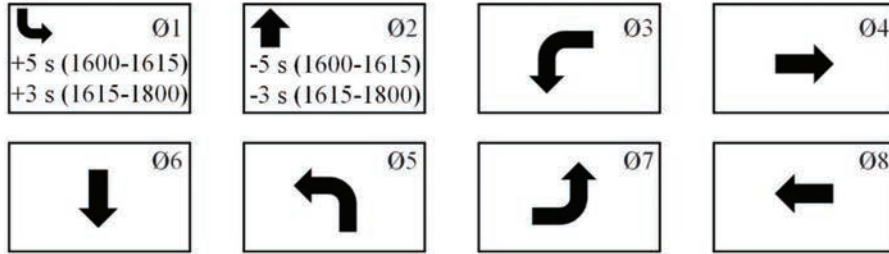


(b) After signal retiming: June 13th to June 24th, 2022, weekdays

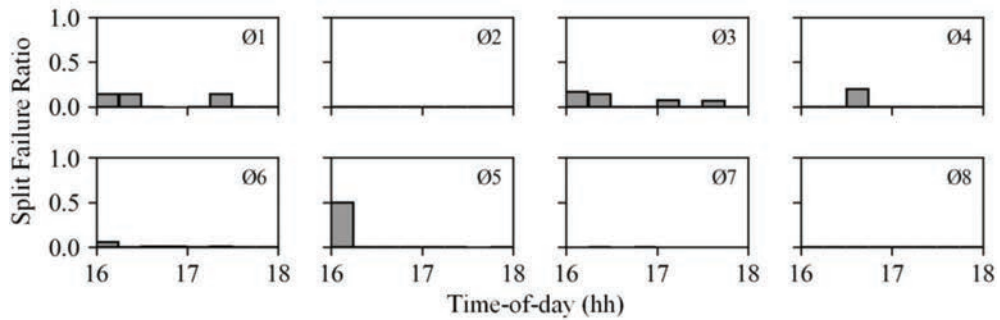
Figure 9.10 PPDs ring diagrams at Intersection 2 from 16:00–18:00 hrs.



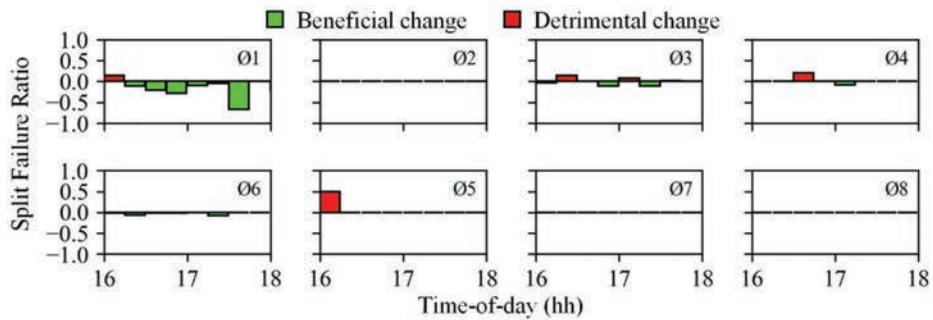
(a) Performance before the timing change: May 30th to June 10th, 2022, weekdays



(b) Timing changes implemented the morning of June 13th, 2022

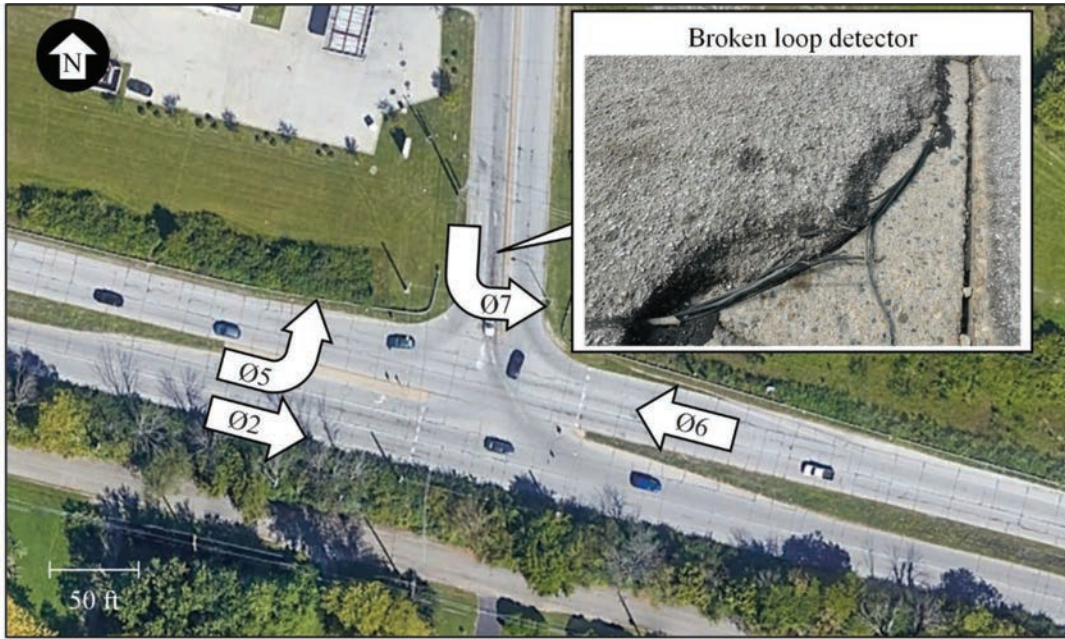


(c) Performance after the timing change: June 13th to June 24th, 2022, weekdays

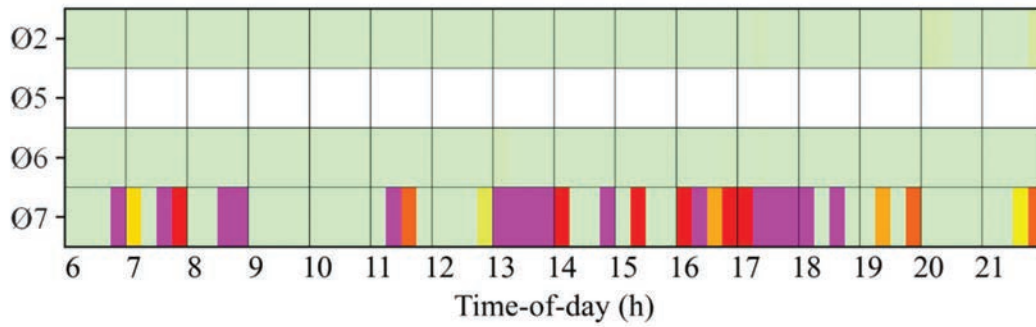
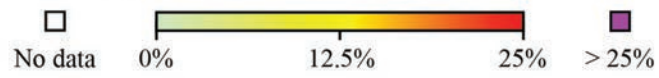


(d) Split failure ratio difference

Figure 9.11 SF before-after assessment at Intersection 2 from 16:00–18:00 hrs.

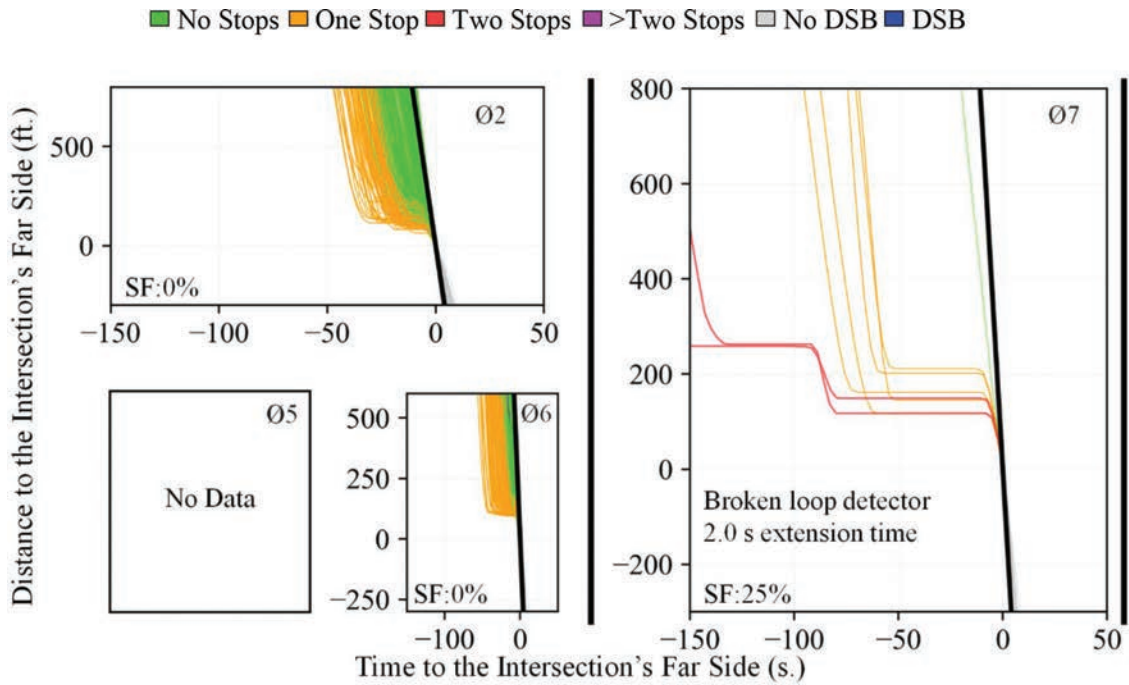


(a) Aerial view (map data: Google)

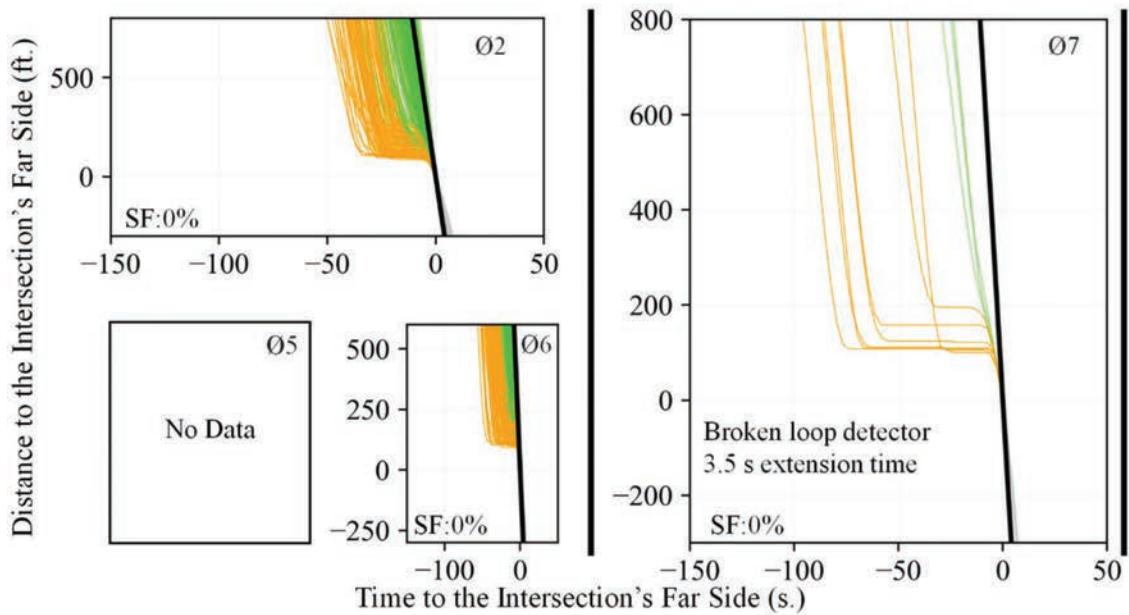


(b) May 2022 weekday SF by movement

Figure 9.12 Intersection 3: US-136 at Waterfront Pkwy W Dr.

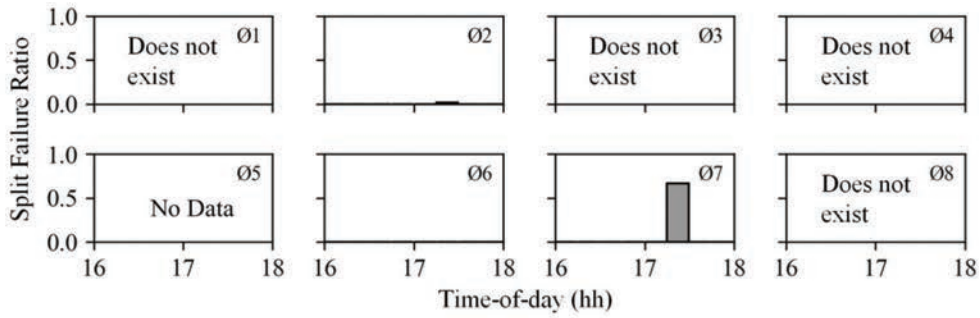


(a) Before signal retiming: May 16th to May 27th, 2022, weekdays

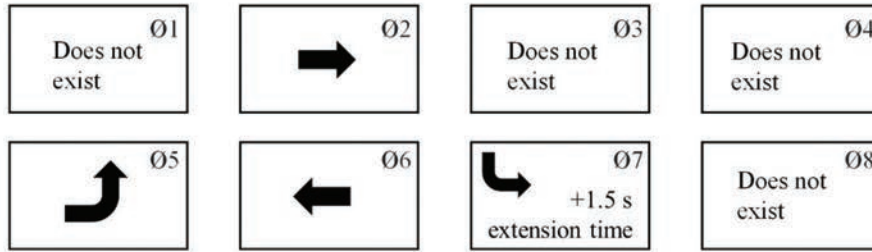


(b) After signal retiming: June 13th to June 24th, 2022, weekdays

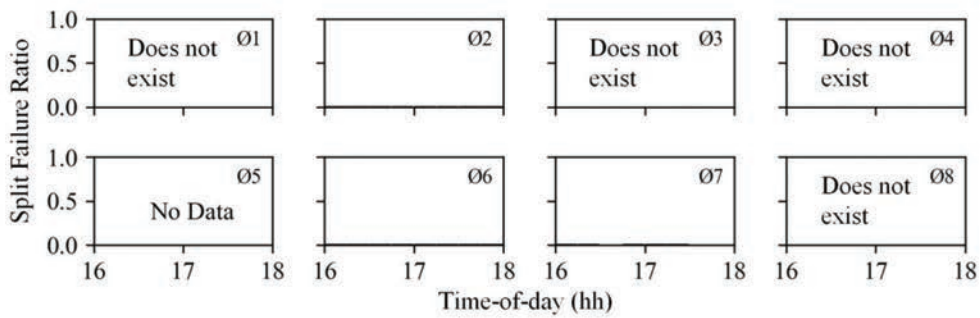
Figure 9.13 PPDs ring diagrams at Intersection 3 from 16:00–18:00 hrs.



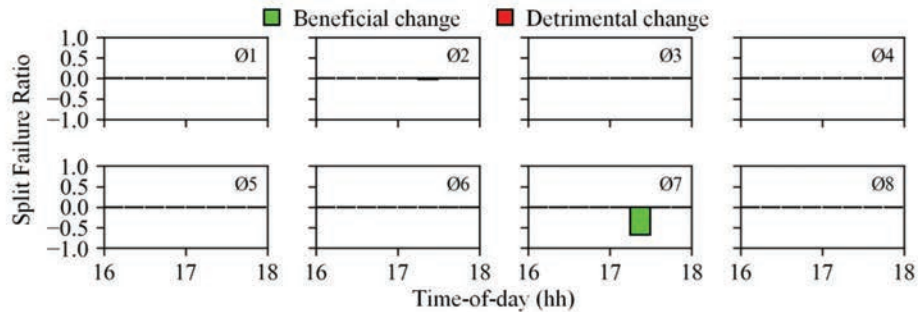
(a) Performance before the timing change: May 30th to June 10th, 2022, weekdays



(b) Timing changes implemented the morning of June 13th, 2022



(c) Performance after the timing change: June 13th to June 24th, 2022, weekdays



(d) Split failure ratio difference

Figure 9.14 SF before-after assessment at Intersection 3 from 16:00–18:00 hrs.

TABLE 9.1
Performance measure (PM) change at Intersection 1

PM	Period	Phase							
		1	↓ 2 ¹	3	↑ 4	5	↓ 6 ¹	7	↑ 8
SF	Before	1%	0%	0%	35%	0%	0%	2%	9%
	After	0%	0%	0%	4%	4%	0%	0%	0%
	Difference	-1%	0%	0%	-30%	4%	0%	-2%	-9%
AOG	Before	7%	49%	21%	3%	11%	57%	13%	12%
	After	12%	42%	23%	18%	29%	54%	12%	20%
	Difference	5%	-7%	2%	15%	17%	-3%	-1%	8%
Avg. Delay (s/veh)	Before	67	37	52	113	63	34	64	73
	After	62	44	57	60	54	36	56	55
	Difference	-5	7	5	-53	-9	3	-8	-19

¹Coordinated phases.

Note: ↑ = additional green time, ↓ = reduced green time.

TABLE 9.2
Performance measure (PM) change at Intersection 2

PM	Period	Phase							
		↑ 1	↓ 2 ¹	3	4	5	6 ¹	7	8
SF	Before	18%	0%	7%	2%	0%	4%	0%	0%
	After	7%	0%	7%	2%	7%	1%	0%	0%
	Difference	-12%	0%	0%	0%	7%	-2%	0%	0%
AOG	Before	8%	85%	11%	8%	18%	31%	50%	33%
	After	18%	77%	7%	22%	20%	41%	0%	22%
	Difference	9%	-7%	-4%	14%	2%	10%	-50%	-11%
Average Delay (s/veh)	Before	88	20	85	67	48	53	-36	56
	After	70	25	85	61	61	44	31	55
	Difference	-17	5	0	-6	13	-9	67	-1

¹Coordinated phases.

Note: ↑ = additional green time, ↓ = reduced green time.

TABLE 9.3
Performance measure (PM) change at Intersection 3

PM	Period	Phase							
		1	2 ¹	3	4	5	6 ¹	↑ 7	8
SF	Before	–	0%	–	–	–	0%	9%	–
	After	–	0%	–	–	–	0%	0%	–
	Difference	–	0%	–	–	–	0%	-9%	–
AOG	Before	–	77%	–	–	–	92%	9%	–
	After	–	84%	–	–	–	85%	30%	–
	Difference	–	6%	–	–	–	-7%	21%	–
Average Delay (s/veh)	Before	–	24	–	–	–	20	49	–
	After	–	17	–	–	–	22	52	–
	Difference	–	-7	–	–	–	2	3	–

¹Coordinated phases.

Note: ↑ = additional extension time.

TABLE 9.4
Overall change in performance from 16:00–18:00 hrs.

Intersection	Sampled Vehicles	SF (%)	AOG (%)	Average Delay (s/veh)
1	+6	-3.7	+1.3	-5.5
2	+77	-1.6	+5.5	-5.5
3	-101	-0.2	-0.7	-0.9

10. CLOSELY-COUPLED INTERSECTIONS

Traditional closely-spaced intersections are often challenged by ever-increasing traffic demand due to their tight coupling, structured phase timings, and storage limitations. Alternative intersection designs have been proposed over the years with the objective of improving mobility and have been selectively implemented at locations where an assessment of traffic flow patterns may lead to increased efficiencies (94–96).

The proposed alternative designs often aim at improving operations while incurring lower costs and with greater flow than traditional configurations (94–96). It is therefore important to systematically assess the efficiency of such designs to compare operations with traditional approaches and document the benefits of the implementation. Previous performance analyses have been done by means of simulation (94, 97–100) and from ATSPMs (101, 102).

Estimating performance measures from simulation requires traffic signal timing plans, peak factors, volumes, and model configuration. Usually, this information requires time-consuming data collection efforts to develop an accurate model. With regards to data from point sensors to derive ATSPMs, capital and maintenance costs remain a barrier for widespread implementation. Depending on the type and placement of sensors deployed, origin-destination flows, and overcapacity periods have been challenging to assess.

Additionally, closely-coupled signalized intersections have their own operational challenges where the timing at one location significantly affects others (94–96). Therefore, it is important to assess interactions between each intersection as a system. However, even if comprehensive sensing infrastructure is implemented, at a minimum, floating car data is needed to measure the performance of a single vehicle travelling through a set of adjacent signals holistically. This limitation hinders the analysis of closely-coupled intersection systems such as conventional diamond interchanges (CDIs).

The advantages of CV trajectory data are its wide coverage and short reporting intervals. With said characteristics, it is possible to determine vehicle experience by traveled path in an intersection system. Thus, it is of interest to count with CV-based techniques to evaluate the performance of closely-coupled intersections. This chapter discusses the use of CV trajectory data, particularly a PPD variation called Extended Purdue Probe Diagram (EPPD), to evaluate signal performance at the following conventional and alternative closely-coupled intersection systems:

- three- and four-phase CDIs (12),
- diverging diamond interchanges (DDIs) (13), and
- continuous flow intersections (CFIs) (14).

10.1 Conventional Diamond Interchanges

CDIs transfer traffic between freeways or service roads and two-way surface streets (103). Full CDIs

consist of a pair of closely-coupled ramp intersections with relatively close interlocked left-turns, four entry points, and four exit points (104–106). CDIs are crucial for urban transportation networks experiencing high volumes; hence, their efficient operation is critical.

Due to the close proximity of the intersections at a CDI, coordinating the ramp signals to manage the internal queues is critical to ensure they do not spill back and block upstream movements. To effectively manage a CDI, practitioners must evaluate the progression of vehicles traversing the interchange system and their effect on each approach (104). Although there are design procedures for developing this signal phasing, variations in demand and driver behavior can significantly impact operations.

With the available high-resolution CV data, it is possible to measure a sample of vehicles' experience traversing a CDI on a movement-by-movement basis. This section discusses CV-based methodologies to measure AOG, SF, DSB, and movement-based control delay at CDIs (12). The application of these techniques is presented by analyzing operations at two diamond interchanges with three- and four-phase control.

10.1.1 Study Locations

Two CDIs with different control schemes are evaluated. Figure 10.1 shows the studied diamond interchange at I-465 and Michigan Rd. located in Indianapolis, Indiana. Figure 10.2 shows the analyzed CDI at George Bush Turnpike and Preston Rd. located north of Dallas, Texas. Each intersection at the CDIs has been marked as *X*, *Y*, *W*, and *Z* to facilitate their reference. The most relevant difference between these two locations for the purposes of this analysis is the proximity of their intersections since it significantly affects operations. For the location in Indiana, the internal distance between stop bars is 500 ft. (152 m.). In contrast, the CDI in Texas has only 240 ft. (73 m.) of separation between the internal stop bars.

10.1.2 Signal Phasing

There are two main signal control techniques implemented at CDIs: three-phase and four-phase (105–107). Depending on the chosen scheme, operations can significantly vary. Each control's implementation is briefly described below.

10.1.2.1 Three-phase control. Three-phase control is commonly used at diamonds where the intersections are located more than 400 ft. (121 m.) apart (106). Such is the case of the study location in Indiana (Figure 10.1), where the intersections are 500 ft. away from each other. Figure 10.3 illustrates the three-phase control implemented at this location. Figure 10.3a shows a common representation of the phases on a simplified geometry diagram of the CDI. Figure 10.3b shows the ring structure for the left intersection (*X*) and



Figure 10.1 I-465 at Michigan Rd. in Indianapolis, Indiana (map data: Google).



Figure 10.2 George Bush Tpk. at Preston Rd. in Dallas, Texas (map data: Google).

Figure 10.3c shows the ring structure for the right intersection (*Y*).

The three phases are the entering arterial, the internal left-turn, and the ramp movement at each signal. The distance between *X* and *Y* provides storage for ramp traffic. If no queue spillback occurs, three-phase operation usually generates less delay than four-phase control and facilitates two-way progression on the arterial when the offsets between the two signals are close to zero (*106, 107*).

10.1.2.2 Four-phase control. Four-phase control is typically used where interior left-turn volumes are high and the spacing between intersections is less than 400 ft. (122 m.) (*106, 107*). Such is the case of the study

location in Texas (Figure 10.2), where the intersections are 240 ft. apart. Figure 10.4 illustrates the four-phase control implemented at this location. Figure 10.4a shows a typical phase numbering scheme. Figure 10.4b shows the ring structure for the left (*W*, top ring) and right (*Z*, bottom ring) intersections.

Both intersections of the interchange are tightly coordinated and are operated as if they were one large intersection. The four phases are the two arterial movements and the two ramp movements. If proper cycle length, splits, and offsets are set and volumes are manageable, this type of control provides progression through the interchange to major movements while efficiently managing the queues within the limited internal storage (*106, 107*).

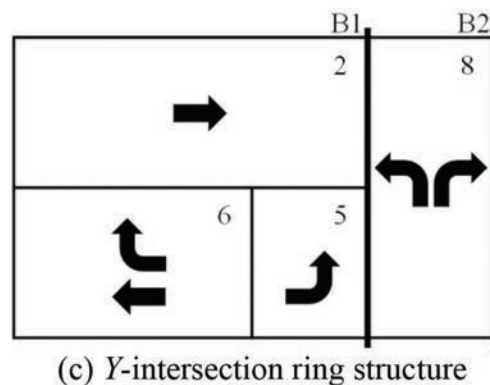
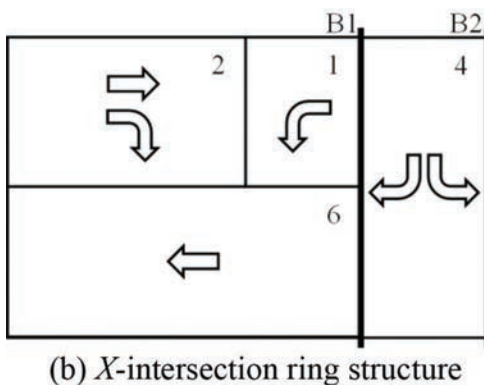
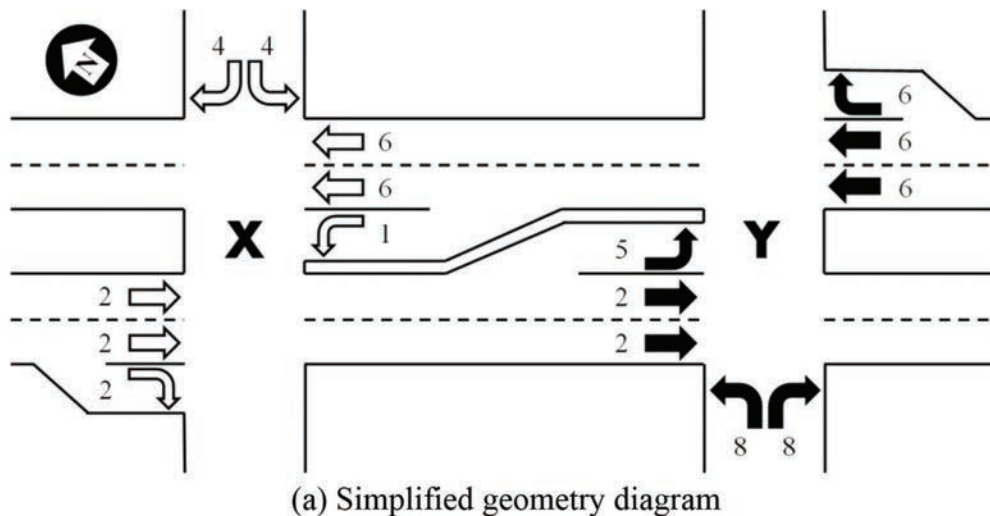


Figure 10.3 Three-phase diamond interchange signal control in Indiana.

10.1.3 Extended Purdue Probe Diagram

As the critical objective for CDI operation is to keep the internal storage free of long queues to avoid spillback that blocks adjacent arterial and ramp movements, the progression of vehicles needs to be evaluated. Even though a PPD (Figure 5.8b) provides insight into the quality of progression at an intersection, it does so for each internal movement in isolation and does not discern the origin of vehicles from adjacent signals. To overcome this limitation, EPPDs can be utilized.

An EPPD is a visualization tool that shows the queue and progression quality for a travel path through multiple signals in a system to help assess performance based on the origin of vehicles. EPPDs characterize the complete movement of vehicles through a system of signals. This is accomplished by linear-referencing the distinct trips and pivoting at the last intersection's FS of a complete origin-destination path. Each approach is independently color-coded based on the number of stops. A trajectory's transition segment from one intersection to the next is colored black. Additionally, the location of every signal's FS is indicated by horizontal lines for spatial referencing. Finally, an FFT is included to allow for delay estimations.

In the case of CDIs, only two intersections need to be included in an EPPD. The sampled volume distributions for the eight main origin-destination paths of the three- and four-phase controlled interchanges are provided in Table 10.1 and Table 10.2, respectively. This information helps identify which paths have the highest demands and are more likely to congest the storage area.

Figure 10.5 shows EPPDs for four paths of August 2020 weekdays vehicle trajectories that traversed the three-phase CDI in Indiana from 16:00–18:00 hrs. The image in the lower left corner of all the subfigures has a movement arrow that graphically illustrates the path of vehicles analyzed in each EPPD. All EPPDs reveal significant number of vehicles stopping before entering the interchange (callout i) and most of them show internal stops (callout ii), except for Figure 10.5d. From this subfigure, it is apparent that the CDI is timed with the objective of serving and progressing vehicles coming off the WB ramp to SB as efficiently as possible, with essentially none of those vehicles having to stop internally. By connecting the trajectories across the two signals, the EPPD is able to shed light on efficiency trade-offs made in the signal timing plan.

Figure 10.6 shows EPPDs for four paths of August 2020 weekdays vehicle trajectories that traversed the

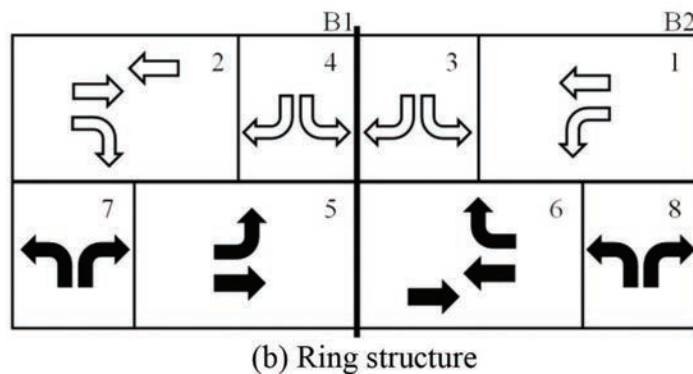
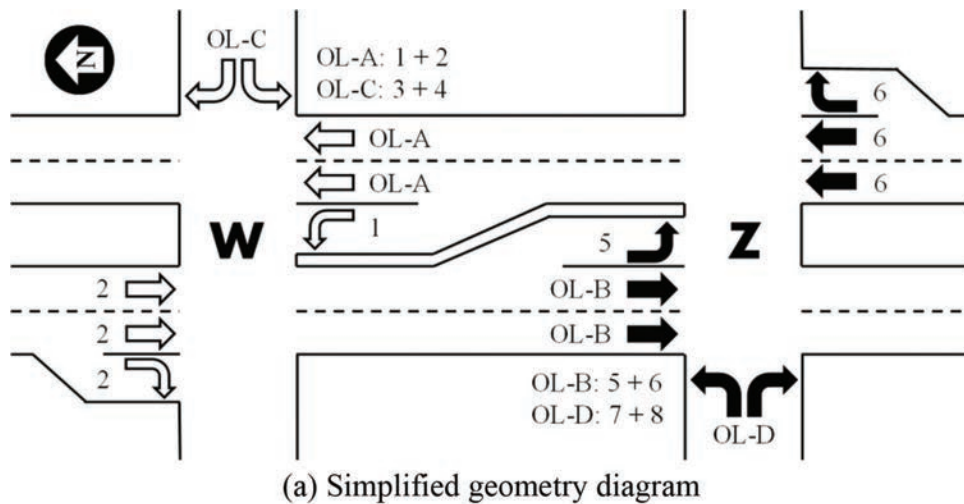


Figure 10.4 Four-phase diamond interchange signal control in Texas (B1 = barrier 1, B2 = barrier 2, OL = overlap).

TABLE 10.1
Sampled volume distribution at the three-phase interchange in Indiana for August 2020 weekdays from 16:00–18:00 hrs.

Origin (external movements)	Destination (internal movements)			
	Y SB-through	Y SB-left	X NB-through	X NB-left
X SB-through	14%	22%	–	–
X WB-left	8%	0%	–	–
Y NB-through	–	–	23%	11%
Y EB-left	–	–	22%	0%

TABLE 10.2
Sampled volume distribution at the four-phase interchange in Texas for August 2020 weekdays from 16:00–18:00 hrs.

Origin (external movements)	Destination (internal movements)			
	Z SB-through	Z SB-left	W NB-through	W NB-left
W SB-through	21%	18%	–	–
W WB-left	4%	0%	–	–
Z NB-through	–	–	29%	15%
Z EB-left	–	–	13%	1%

four-phase CDI in Texas from 16:00–18:00 hrs. Similar to the interchange in Indiana, the CDI in Texas shows significant number of vehicles stopping before entering

the system. However, once vehicles enter the interchange, they continue their progression unimpeded (callout i), which is the main benefit of properly

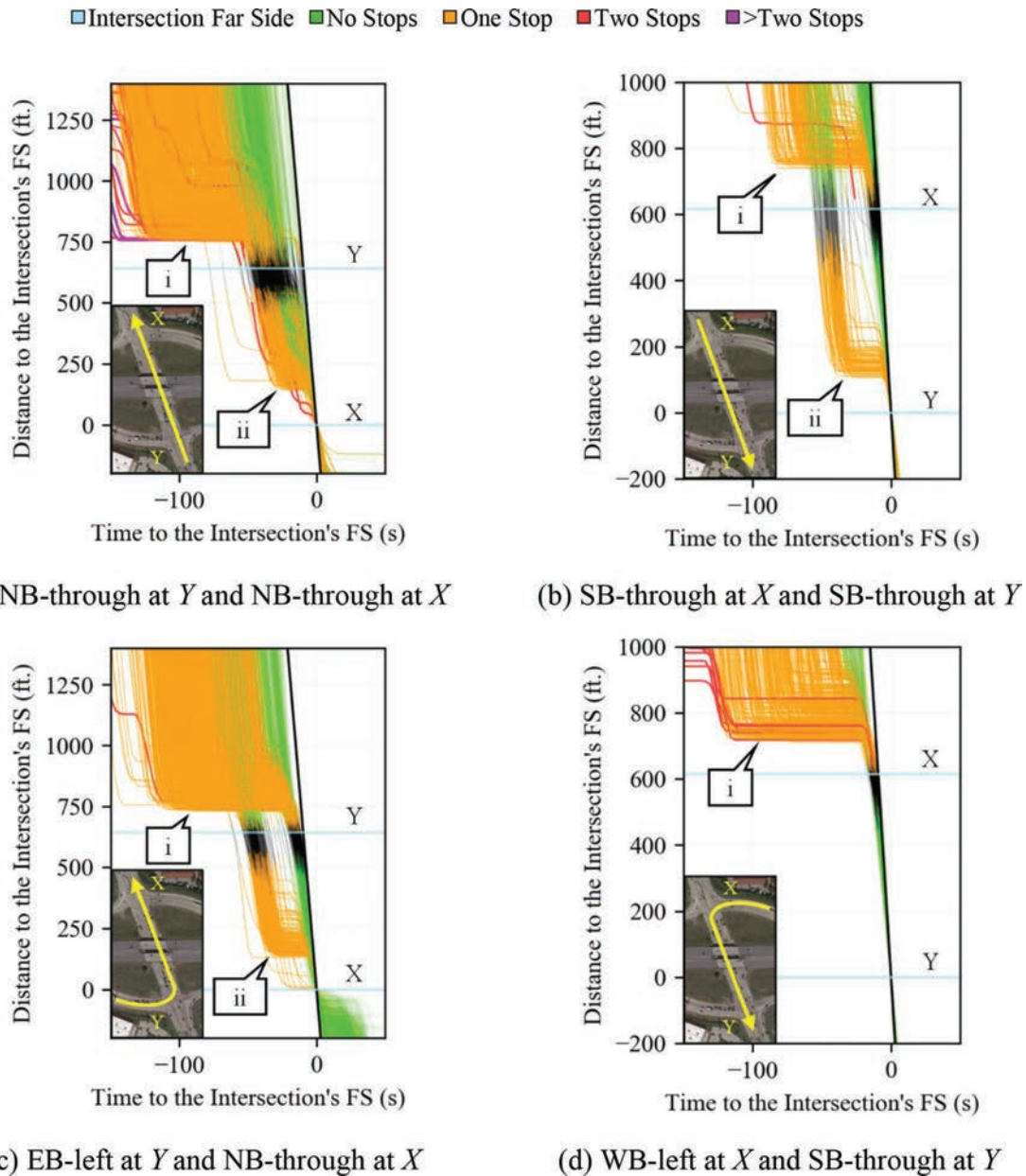


Figure 10.5 EPPDs for three-phase diamond in Indiana (map data: Google).

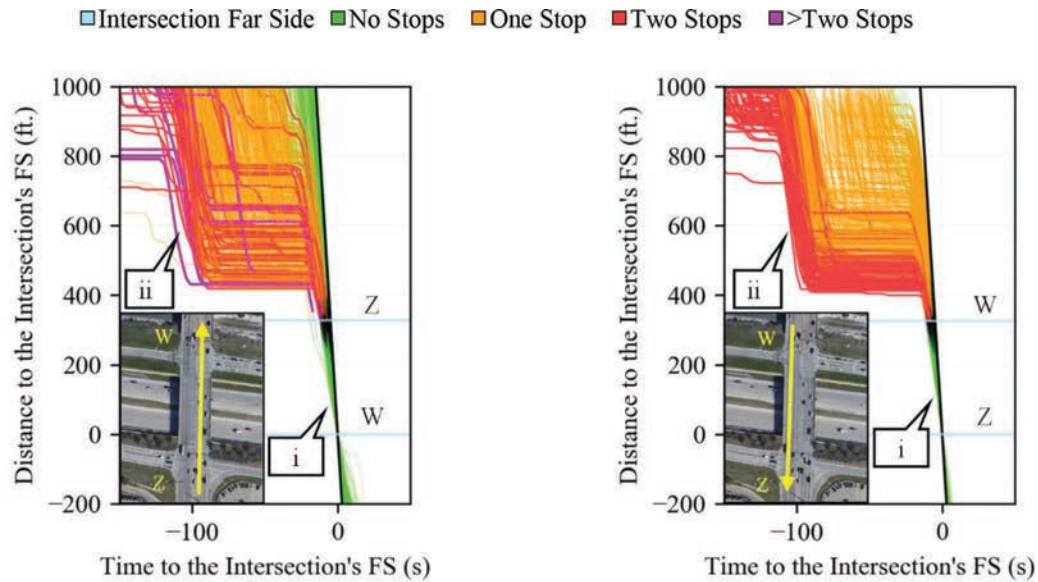
implemented four-phase control. This is an important characteristic as closely spaced intersections have a higher risk of getting blocked by internal queues. However, the four-phase CDI operates similarly as a split-phased signal, which contributes to increased congestion on the movements entering the CDI (callout ii) shown by vehicles stopping more than once.

10.1.4 Summary Performance by TOD

The EPPDs provide a graphical characterization of progression, stops, split failures, downstream blockage, and delay for a specific time period. However, it is important to have an overview of how all the movements perform by TOD to effectively evaluate all

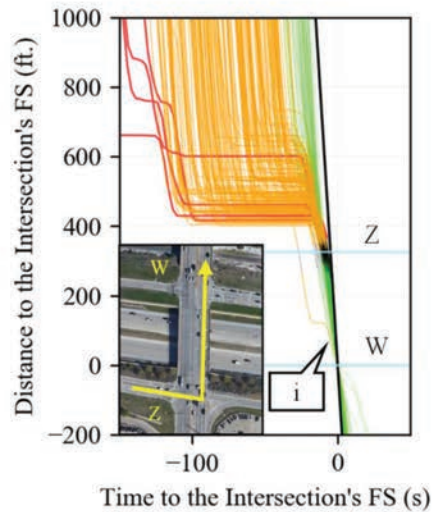
timing plans. To address this need, graphical heat maps summarizing performance by movement and by TOD are generated.

Figure 10.7 and Figure 10.8 show heatmaps with 15-minute resolution indicating the percentage of vehicles arriving on green at the eight external and internal movements. For the three-phase controlled interchange (Figure 10.7), it is shown how some internal movements have AOG around 50% (callout i), with NB-left having poor progression (callout ii, ~0% AOG) and SB-through having good progression (callout iii, ~100% AOG). For the four-phase controlled interchange (Figure 10.8), all internal movements have efficient progression as vehicles do not have to stop before exiting the CDI (callout iv).

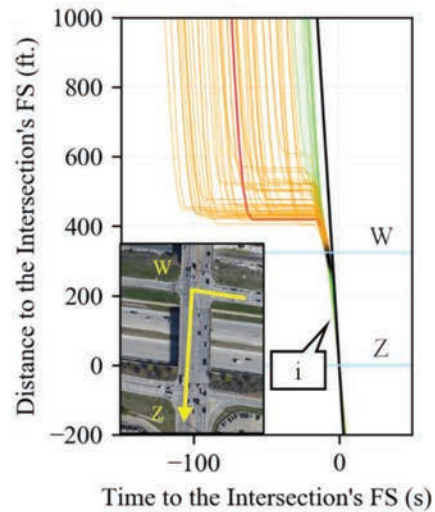


(a) NB-through at *Z* and NB-through at *W*

(b) SB-through at *W* and SB-through at *Z*



(c) EB-left at *Z* and NB-through at *W*



(d) WB-left at *W* and SB-through at *Z*

Figure 10.6 EPPDs for four-phase diamond in Texas (map data: Google).

Figure 10.9 and Figure 10.10 show the percentage of sampled vehicles that experienced split failures at the three- and four-phase CDI intersections, by TOD. The three-phase controlled CDI (Figure 10.9) has few split failures throughout the day. The four-phase controlled CDI (Figure 10.10) has significant split failures at most of the external movements during different TOD (callout i) but no split failures on the internal movements.

Figure 10.11 and Figure 10.12 show heatmaps indicating the level of DSB at different movements. For the CDI in Indiana (Figure 10.11), the NB-through movements are being significantly obstructed soon after they pass each intersection during the PM peak period between the 15:00 and the 18:00 hrs. (callout i). This is of particular interest as DSB is a consequence of long downstream

queues. In the case of the external NB-through movement (Figure 10.11b), this means that the internal CDI queue is long enough to affect progression. In contrast, four-phase control (Figure 10.12) has minimal number of vehicles experiencing downstream blockage.

Finally, Figure 10.13 and Figure 10.14 show the LOS based on control delay (Table 5.1) for the relevant movements at the three- and four-phase CDI intersections, respectively. The effects that poor progression and congestion have on delay are illustrated.

10.1.5 Results and Discussion

Table 10.3 shows a summary of the evaluated performance measures for the PM peak period (16:00–

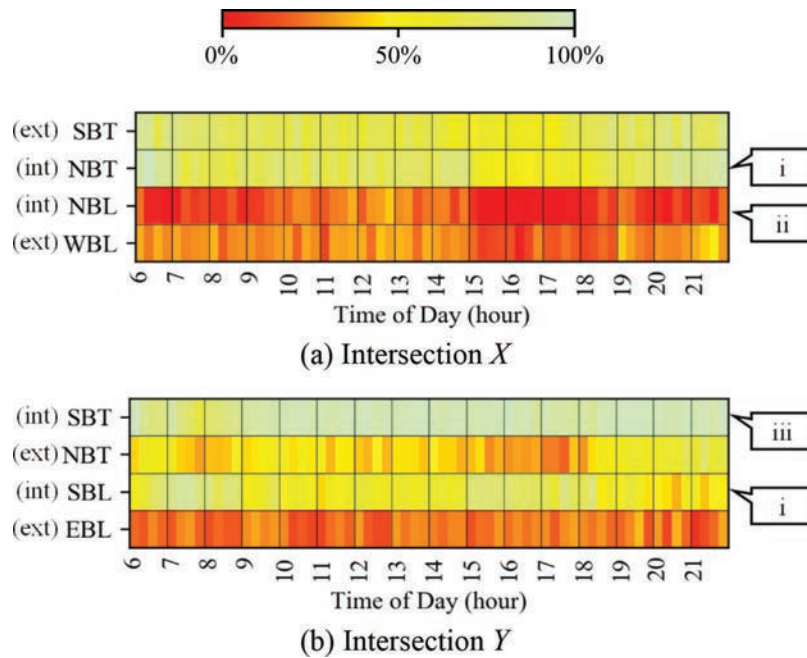


Figure 10.7 August 2020 weekdays AOG by approach and movement for the three-phase diamond interchange in Indiana (ext = external, int = internal).

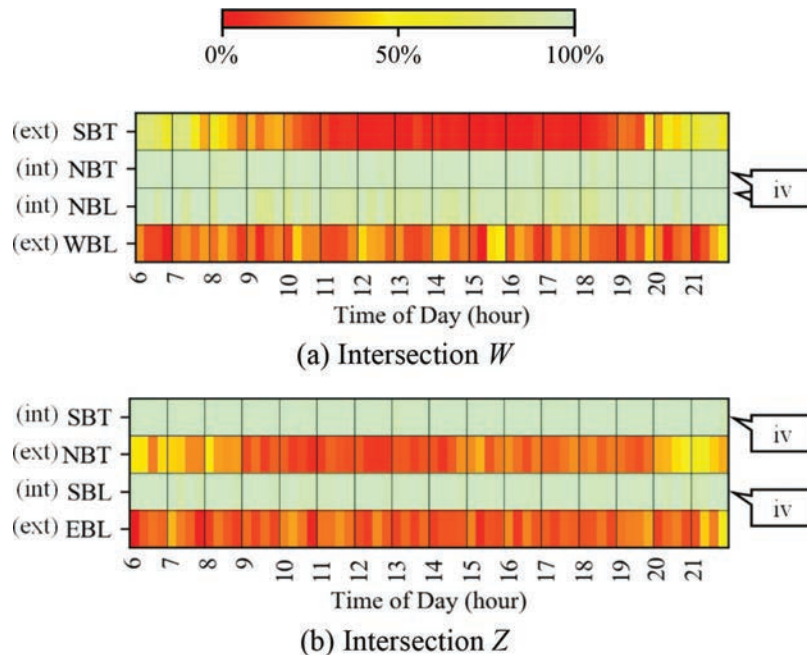


Figure 10.8 August 2020 weekdays AOG by approach and movement for the four-phase diamond interchange in Texas (ext = external, int = internal).

18:00 hrs.). Although these intersections have different demand volumes and configuration, it is interesting to compare their operation as they illustrate tradeoffs between three- and four-phase control. Trajectory data for the four-phase CDI demonstrated high internal progression (99% AOG), as is intended by its signal control. In contrast, the three-phase control showed only moderate internal progression (64% AOG). Regarding downstream blockage, the operation of the four-phase

signal resulted in 1% of internal DSB despite having saturated external movements that have approximately 11% SF. The three-phase control has substantially higher internal DSB (7%), despite having a much smaller percentage of SF on the exterior movements (2%).

The ability to have performance measures such as those shown in Table 10.3 provides quantitative information for an agency to tune their TOD schedule. Further, EPPDs (Figure 10.5 and Figure 10.6) provide

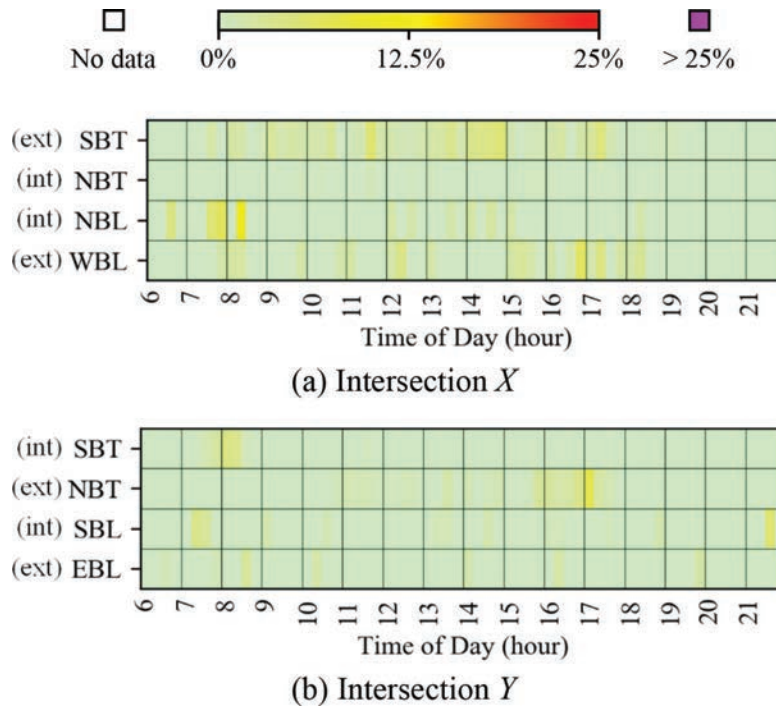


Figure 10.9 August 2020 weekdays SF by approach and movement for the three-phase diamond interchange in Indiana

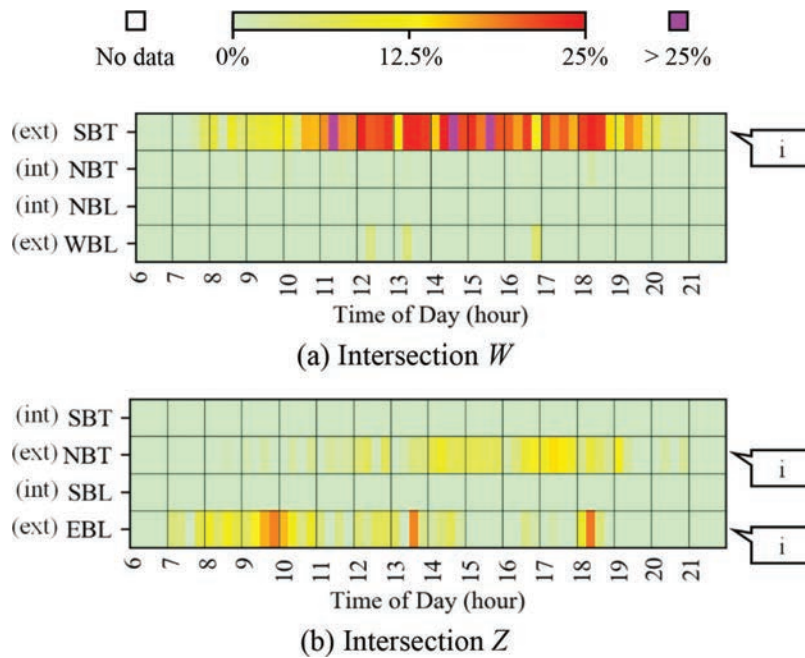


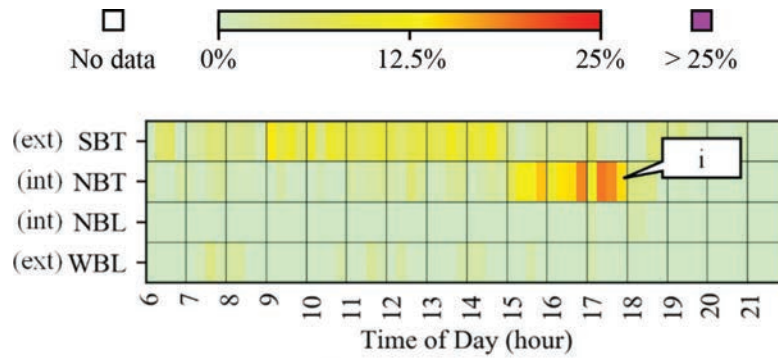
Figure 10.10 August 2020 weekdays SF by approach and movement for the four-phase diamond interchange in Texas (ext = external, int = internal).

a holistic view of origin-destination dynamics to support or reinforce signal timing objectives.

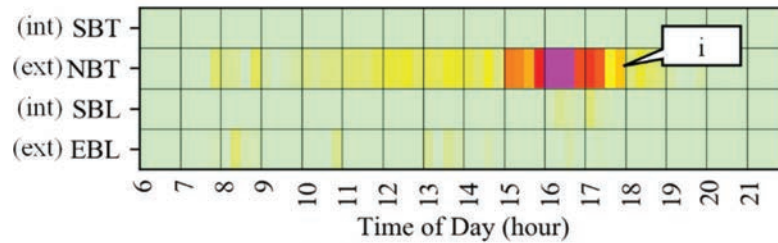
10.2 Diverging Diamond Interchanges

Over the past decade, several DDIs have been built in the United States with the objective of reducing

construction costs, improving safety, and enhancing traffic operations (95). A DDI is an alternative interchange in that it implements directional crossovers on each end of the crossing street. By switching through movements to the left side of the road within the interchange, conflicts between left-turning vehicles and opposing through traffic from the crossing street are eliminated (95, 108).

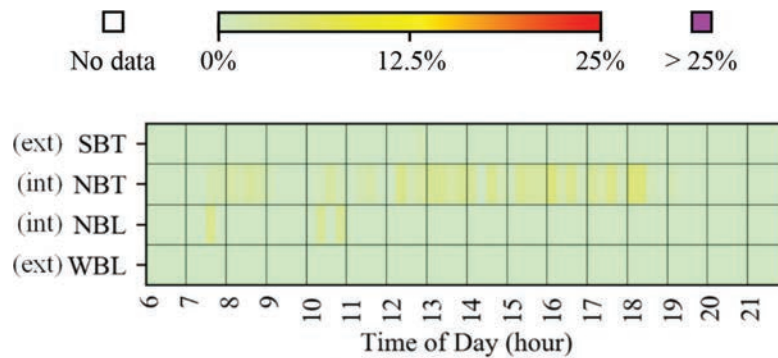


(a) Intersection *X*

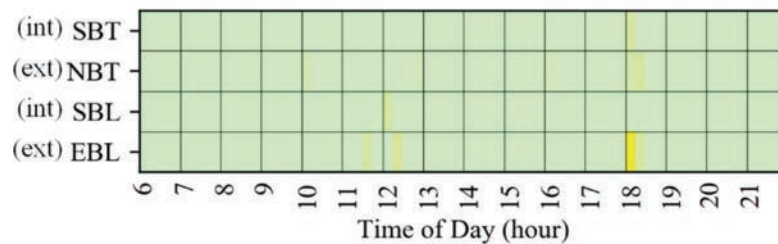


(b) Intersection *Y*

Figure 10.11 August 2020 weekday DSB by approach and movement for the three-phase diamond interchange in Indiana (ext = external, int = internal).



(a) Intersection *W*

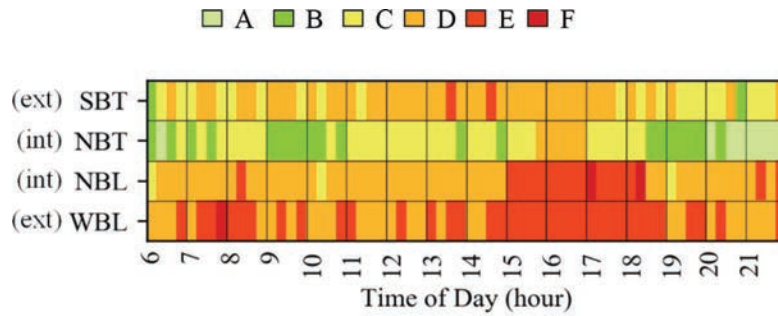


(b) Intersection *Z*

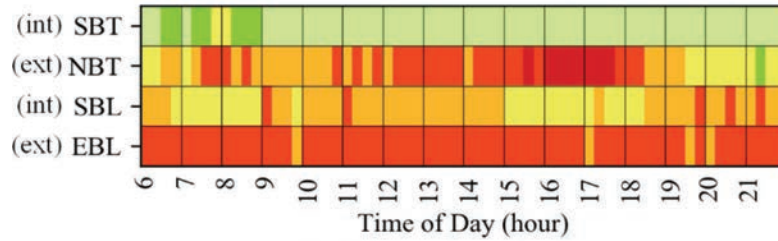
Figure 10.12 August 2020 weekday DSB by approach and movement for the four-phase diamond interchange in Texas (ext = external, int = internal).

This section uses CV trajectory data to generate performance measures for a DDI in Indiana (13). EPPDs are generated and a variation to evaluate critical queue dynamics within the crossover (i.e., internal) storage by vehicle origin is discussed. Further, AOG, SF, DSB, and

traditional LOS are calculated for different segments of the DDI. By utilizing the presented techniques, agencies can evaluate the performance of any DDI in their jurisdiction to identify movements and TOD periods that require timing adjustments.

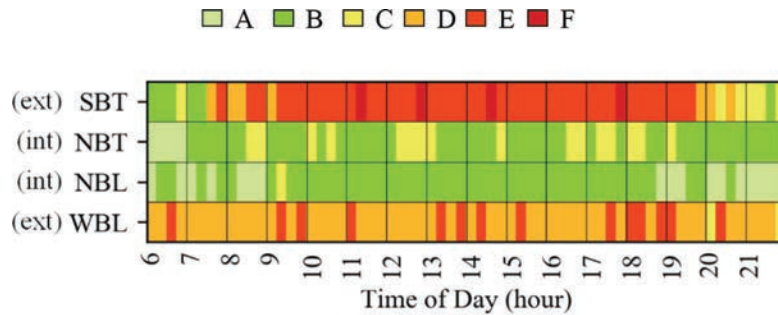


(a) Intersection *X*

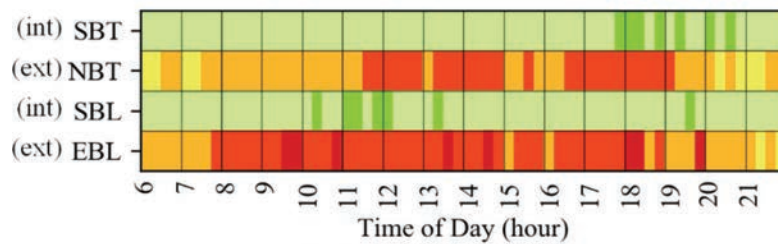


(b) Intersection *Y*

Figure 10.13 August 2020 weekday LOS by approach and movement for the three-phase diamond interchange in Indiana (ext = external, int = internal).



(a) Intersection *W*



(b) Intersection *Z*

Figure 10.14 August 2020 weekday LOS by approach and movement for the four-phase diamond interchange in Texas (ext = external, int = internal).

10.2.1 Study Location

Over 7,000 trajectories and 130,000 waypoints are analyzed to evaluate the performance at the DDI located at I-69 and E Dupont Rd. in Fort Wayne, Indiana, from the 7th to the 11th of June 2021 (Figure 10.15). This DDI was opened to traffic in 2014 and has an AADT of 56,000 VPD on the interstate and 21,000 VPD on the crossing road.

Figure 10.15c shows the analyzed DDI. The most critical segment of a DDI is the crossover storage. If vehicles in this area fail to be discharged efficiently, delays and saturation at the approaches of the entry crossover could significantly increase (102). The crossover storage can receive vehicles from the external street and from the interstate exit ramps. Therefore, the performance of both approaches and the crossover storage needs to be monitored.

TABLE 10.3
Timing implementation PM peak performance comparison

Performance Measure	Three-Phase Control (%)	Four-Phase Control (%)
Internal Movements AOG	64	99
Internal Movements SF	0	0
Internal Movements DSB	7	1
External Movements AOG	38	16
External Movements SF	2	11
External Movements DSB	8	0

When presenting DDIs’ performance results, it is important to differentiate two attributes: the source of vehicles, and which crossover signal is being evaluated. To differentiate these attributes throughout the analysis, the following naming format is employed: source-direction-turn_type-intersections_crossed. Usage is as follows.

- Source: The source of traffic before entering the DDI. If coming from the external crossing street, *E*; if coming from the interstate’s ramp, *R*.
- Direction: Direction of approach entering the DDI: SB, WB, NB, and EB.
- Turn type: if through, *T*; if left, *L*.
- Intersections crossed: Which crossover area signals are crossed for the presented results. If only signals in area 1 are crossed, then *1*; if signals in area 1 and then 2 are crossed, then *12*; if only signals in area 2 are crossed, then *2*; if signals in area 2 then 1 are crossed, then *21*.

For example, results for traffic traveling NB at the exit ramp, turning left into the DDI, and passing traffic signals on crossover areas 2 and 1 will be labeled *R-NB-L-21*.

10.2.2 Phasing Schemes

The utilized phasing schemes at DDIs are based on the number of critical movements at each location. Critical movements are those prioritized by an agency (normally based on demand). The following are three common phasing scenarios (95).

- Two-critical-movement: Focuses on progression for either the external cross-street movements or the off-ramp movements. It is most useful for DDIs with one dominant movement.
- Three-critical-movement: Focuses on progression for the external cross-street movements and the off-ramp left-turn movements. It is most useful for DDIs with one or multiple dominant movements.
- Four-critical-movement: Focuses on progression for both the cross-street movements and the off-ramp movements. It is most useful for DDIs with low to moderate volumes, either dominant through or left-turn movements, and short to medium crossover storage.

Depending on each agency’s objectives, CV-based performance measures provide insights on whether the phasing scheme being employed manages operations as desired.

10.2.3 Extended Purdue Probe Diagram

Since the signals’ dynamics between crossover areas 1 and 2 (Figure 10.15c) are crucial for the efficient operation of DDIs, it is important to provide analytical performance measures (and graphics) that provide insight on the operational status at both locations simultaneously. This can be accomplished with EPPDs.

Figure 10.16 shows EPPDs for the four different traffic sources shown on Figure 10.15c from the 16:00 to the 18:00 hrs. between the 7th and 11th of June 2021. The location of the traffic signals’ far side are indicated with blue lines and labelled 1 and 2. In an EPPD, as with a conventional PPD (Figure 5.8b), vehicle delay can be assessed by analyzing how far away from the FFT a trajectory approaches the first signalized intersection. The farther away from the FFT a trajectory starts, the longer the experienced delay at the DDI. AOG can be evaluated by comparing the amount of green-colored (no-stops, arrived on green) and non-green-colored (one or more stops) trajectories. The larger the proportion of green trajectories is, the better the progression. Saturation can be assessed by calculating SF and downstream blockage can be identified by looking at the vehicle’s progression immediately after crossing the FS of each intersection (blue lines).

Some interesting insights provided by the EPPDs in Figure 10.16 are that vehicles following most movements have to stop before entering the DDI (callout i), with the exception of Figure 10.16c (callout ii). Similarly, a significant number of vehicles following most movements have to stop before exiting the DDI (callout iii), with the exception of Figure 10.16d (callout iv). Further, the following qualitative statements can be derived from Figure 10.16.

- Vehicle trajectories going EB from the external street (Figure 10.16a) and SB from the ramp (Figure 10.16b) experience the most delay since they approach the intersections the farthest away from the FFT.
- Vehicle trajectories traveling EB from the external street (Figure 10.16a) are experiencing split failures when approaching both intersections.
- Vehicles trajectories traveling NB from the ramp (Figure 10.16b) are experiencing split failures when approaching Intersection 2.

10.2.3.1 EPPD by source. The most critical segment of a DDI is its crossover storage. To facilitate the

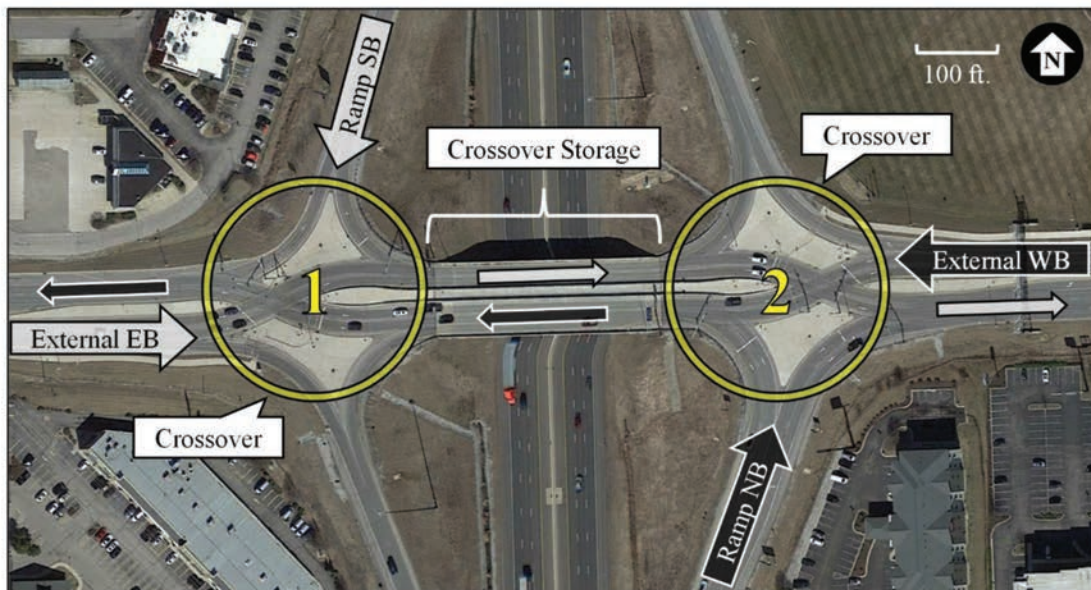
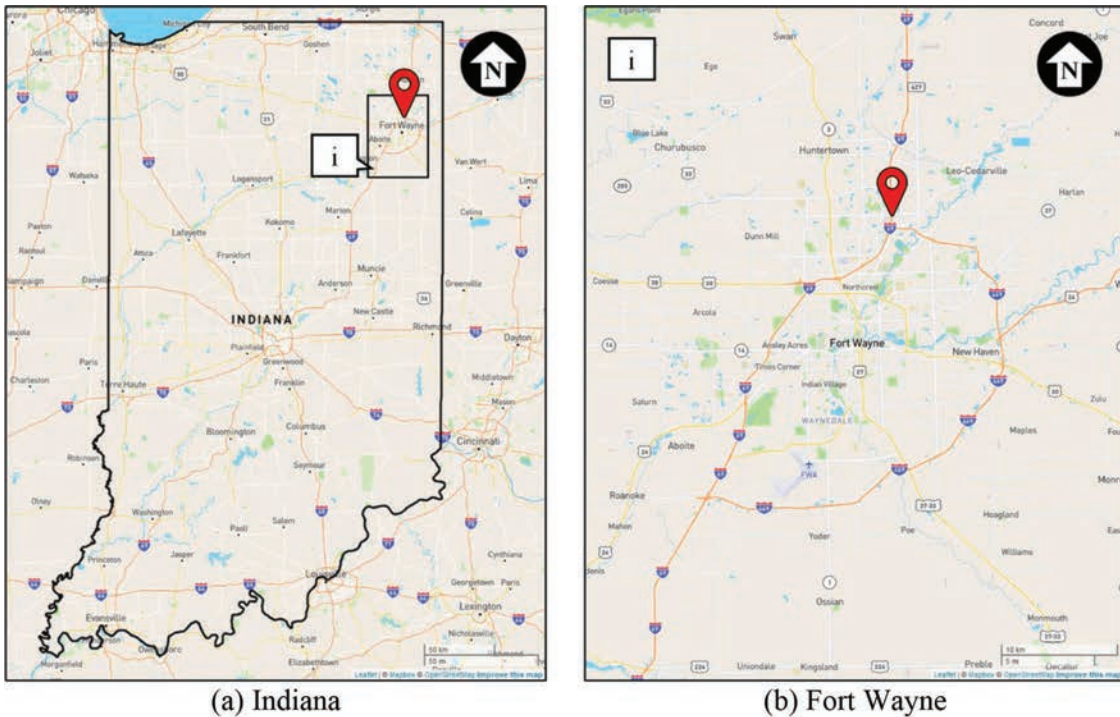


Figure 10.15 Diverging diamond interchange location.

qualitative assessment of progression patterns, and to evaluate queue-length for spillback in the critical interior crossover storage, an EPPD variation that provides information on progression by traffic source is presented.

In this variation of the EPPD, vehicle trajectories coming from the external street and the ramp that share lanes on the crossover storage are superimposed. When doing this, the progression dynamics between signals at the crossover areas 1 and 2 become apparent.

Figure 10.17 shows EPPDs by source for the different movements at the study location from the 16:00 to the 18:00 hrs. between the 7th and 11th of June 2021.

For the EB-through (red) and SB-left (blue) movements (Figure 10.17a), it can be seen that there is a significant number of vehicle trajectories coming from both sources stopping when approaching signal 1 and signal 2 (callout i). Most of the traffic in this figure is from the EB-through approach, from which approximately 50% must stop at signal 2. For the analyzed

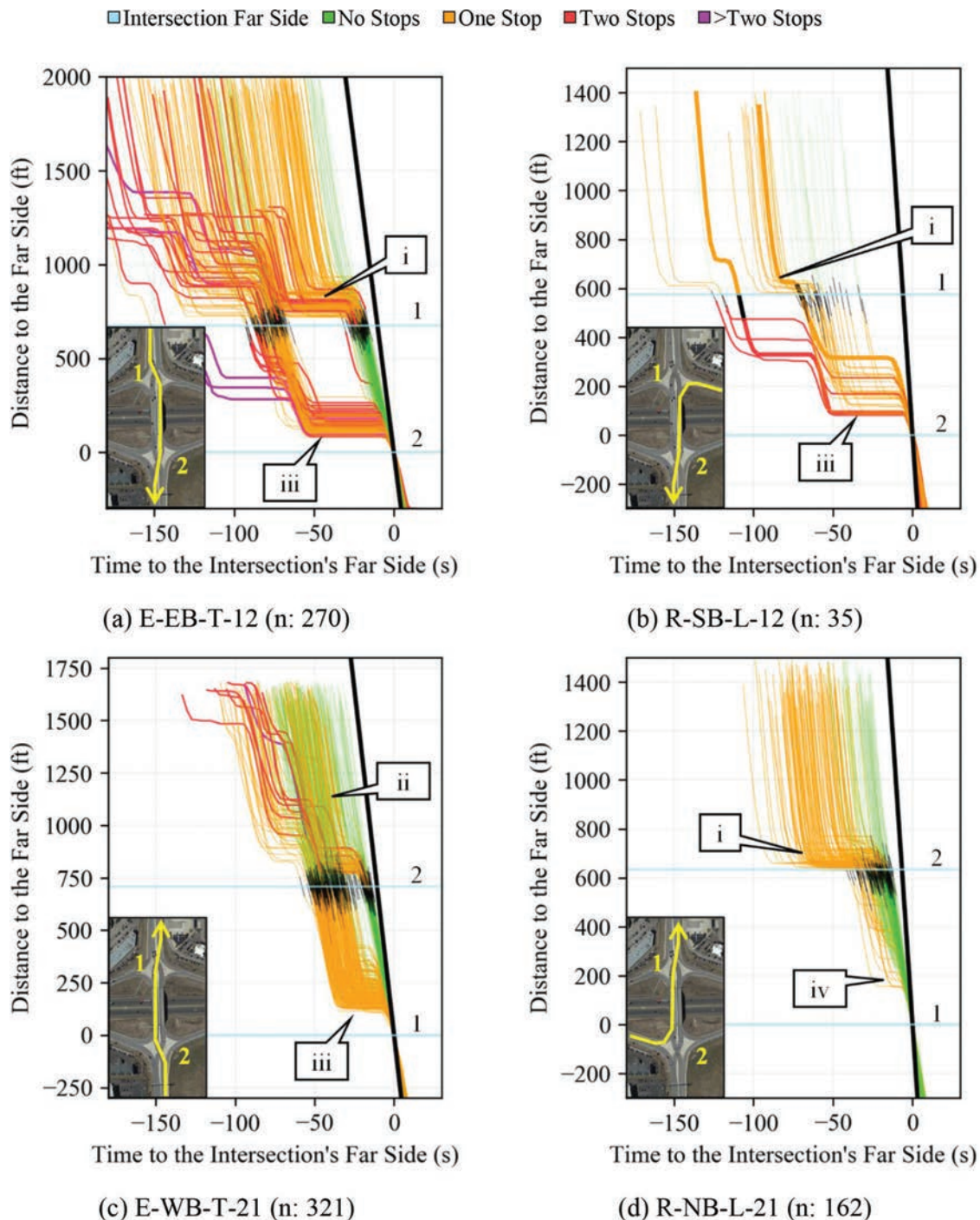


Figure 10.16 DDI EPPDs (map data: Google, IndianaMap Framework Data, Maxar Technologies, U.S. Geological Survey, and USDA Farm Service Agency).

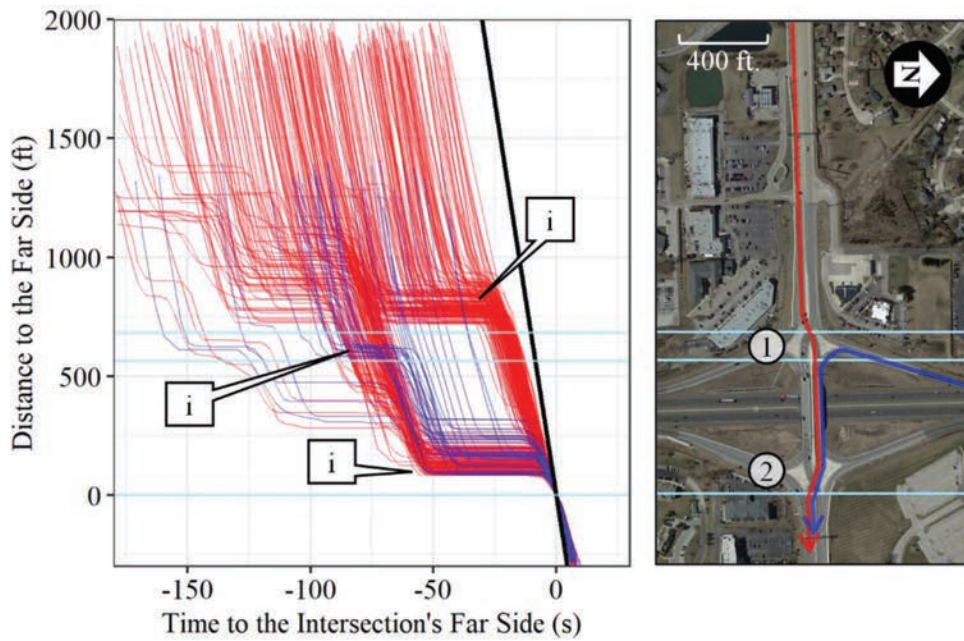
period, 89% of the trajectories traveled EB-through, and only 11% traveled SB-left.

For the WB-through (red) and NB-left (blue) movements (Figure 10.17b), it can be observed that there are some vehicle trajectories from both sources stopping when approaching crossover 1 (callout ii). However, it is shown how most vehicle trajectories coming NB from the ramp can progress without stopping through the signal at 2 (callout iii). This is an indication that the NB-left

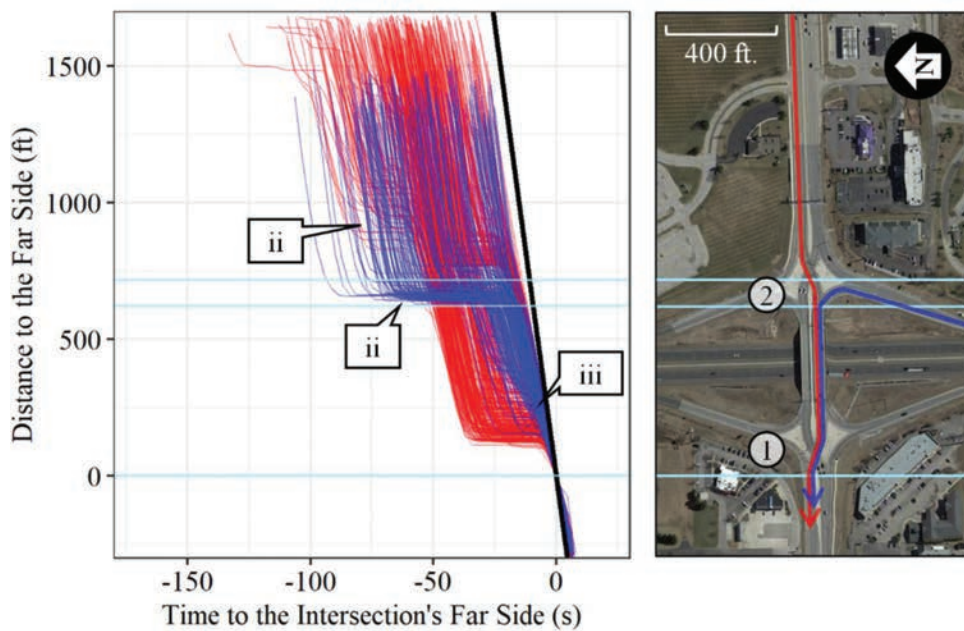
movement at signal 2 has a well-timed offset with signal 1 and vehicles clear the crossover storage area without stopping. For the analyzed period, 66% of the trajectories traveled WB-through and 34% traveled NB-left.

10.2.4 Summary Performance by TOD

Heatmaps summarizing performance measures by TOD, in 15-minute periods, between the 7th and 11th



(a) EB-through (E-EB-T-12) and SB-left (R-SB-L-12) trajectories



(b) WB-through (E-WB-T-21) and NB-left trajectories (R-NB-L-21)

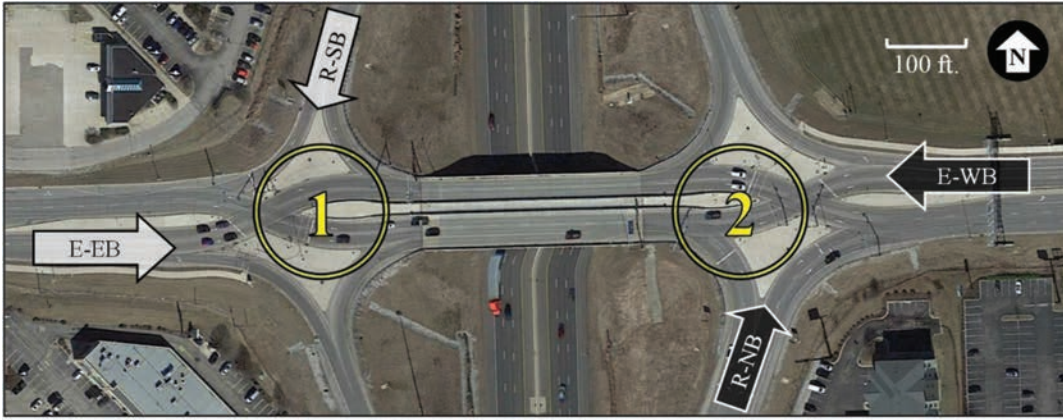
Figure 10.17 Source DDI EPPDs (map data: Google, IndianaMap Framework Data, Maxar Technologies, U.S. Geological Survey, and USDA Farm Service Agency).

of June 2021 are provided in Figures 10.18, 10.19, 10.20, and 10.21. In these graphics, the trajectories' source is specified; further, if individual (1 or 2) or a combination (1 and 2) of traffic signals are analyzed is also indicated. Additional details on how to interpret these graphics are provided as follows.

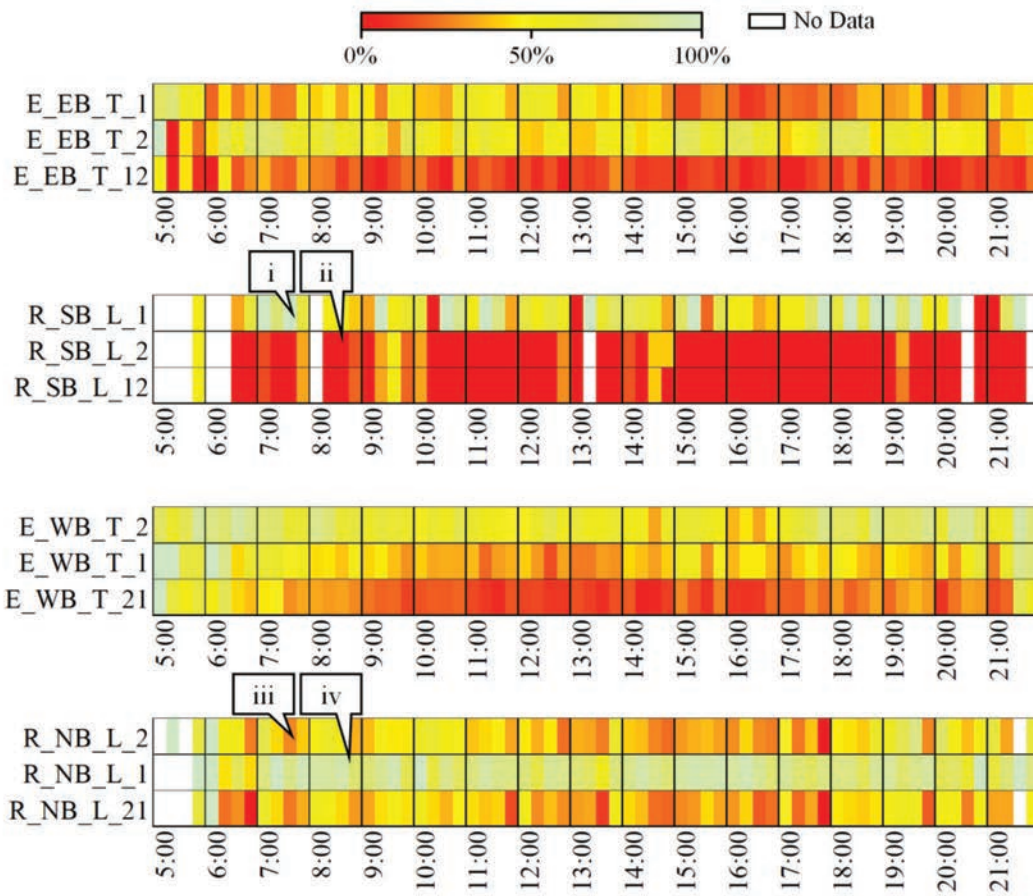
- Figure 10.18: Percentage of sampled vehicles arriving on green. This graphic is useful when assessing the level of

progression. From this figure, it is shown how some vehicles traveling SB from the ramp arrive on green at the signal at 1 (callout i), but virtually none do so at 2 (callout ii). On the other hand, some vehicles traveling NB from the ramp have to stop when approaching 2 (callout iii), but most of them progress without stopping at 1 (callout iv).

- Figure 10.19: Average delay LOS (Table 5.1). Even if this graphic is not specifically useful for operational decisions, it provides practitioners with a standard



(a) Traffic sources (map data: Google, IndianaMap Framework Data, Maxar Technologies, U.S. Geological Survey, and USDA Farm Service Agency)



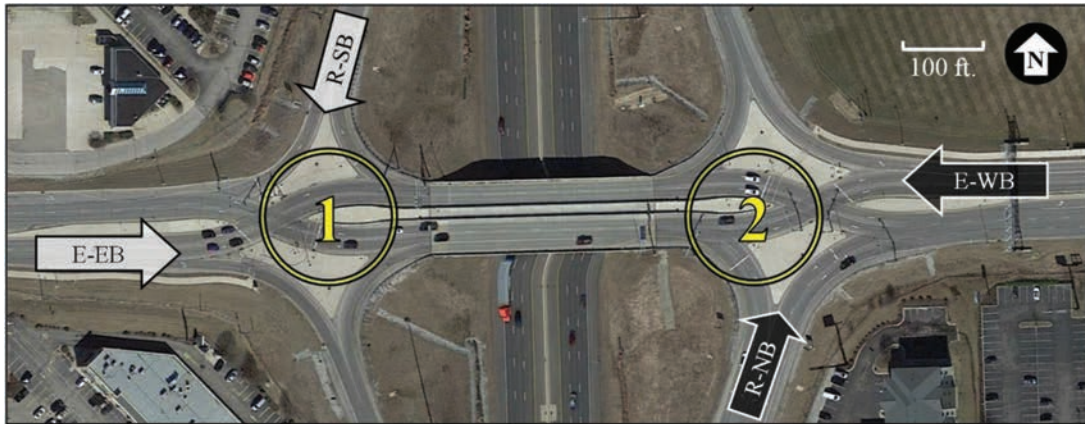
(b) AOG estimations

Figure 10.18 AOG summary results.

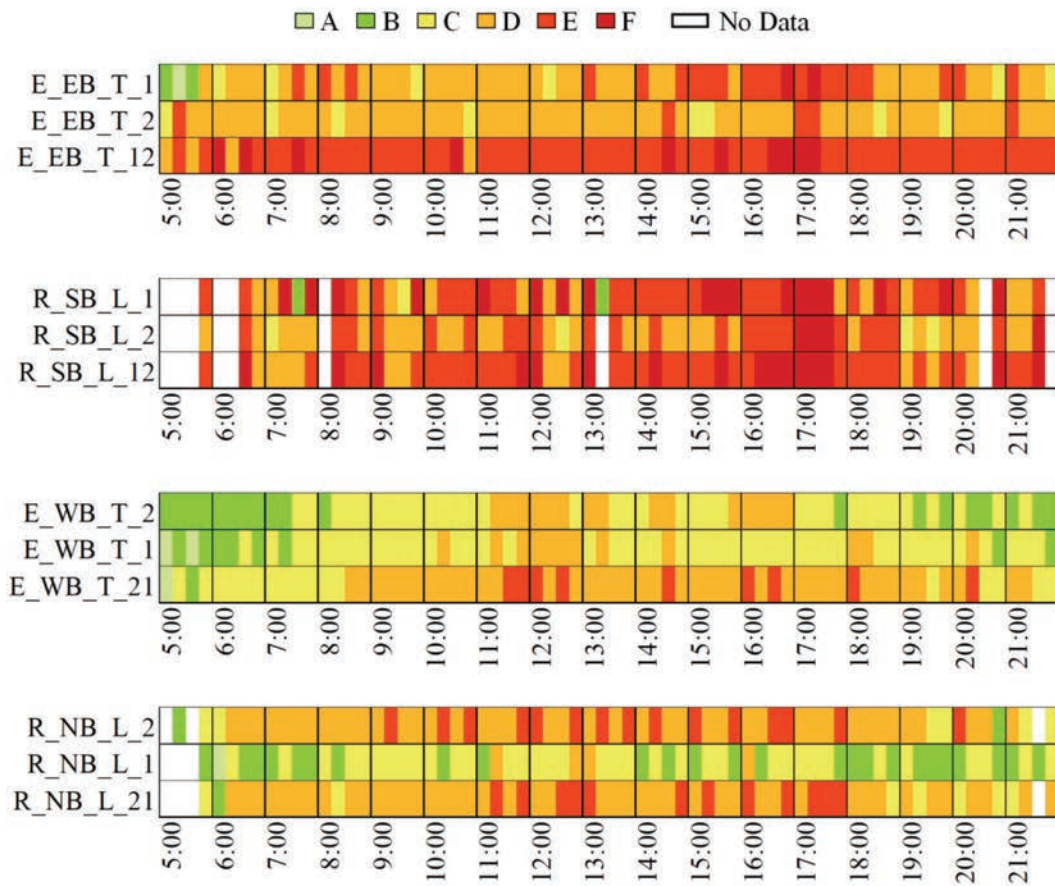
measurement of delay by approach. This graphic can also be adapted to provide alternative numerical scales for delay.

- Figure 10.20: Percentage of sampled vehicles experiencing split failures. This graphic provides an indication of when and where approaches are operating at overcapacity. Those cases may be opportunities to rebalance split time.

For this performance measure, traffic signals need to be analyzed individually as SF intrinsically describes operations at a single traffic signal. Of special concern are the TOD where vehicles traveling EB from the external street and SB from the ramp experience split failures within the crossover storage (callout i), which means that long queues may be forming inside this critical area.



(a) Traffic sources (map data: Google, IndianaMap Framework Data, Maxar Technologies, U.S. Geological Survey, and USDA Farm Service Agency)



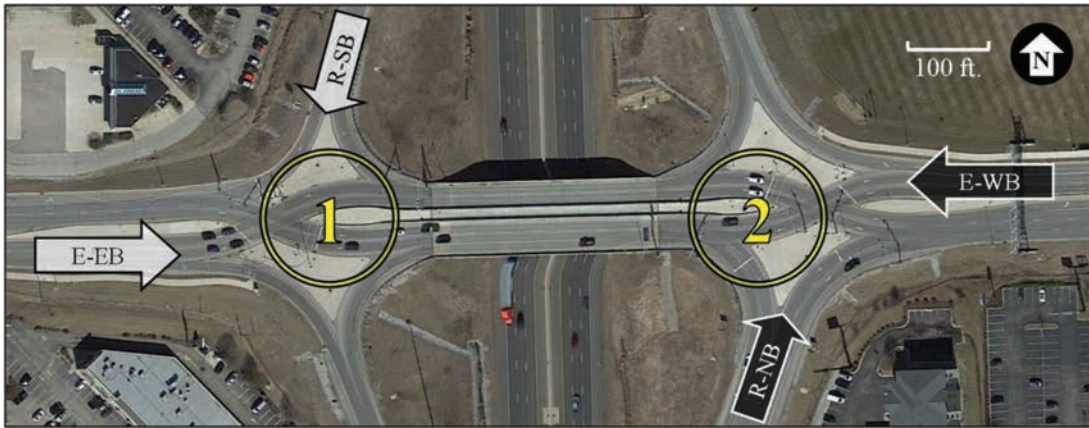
(b) LOS estimations

Figure 10.19 LOS summary results.

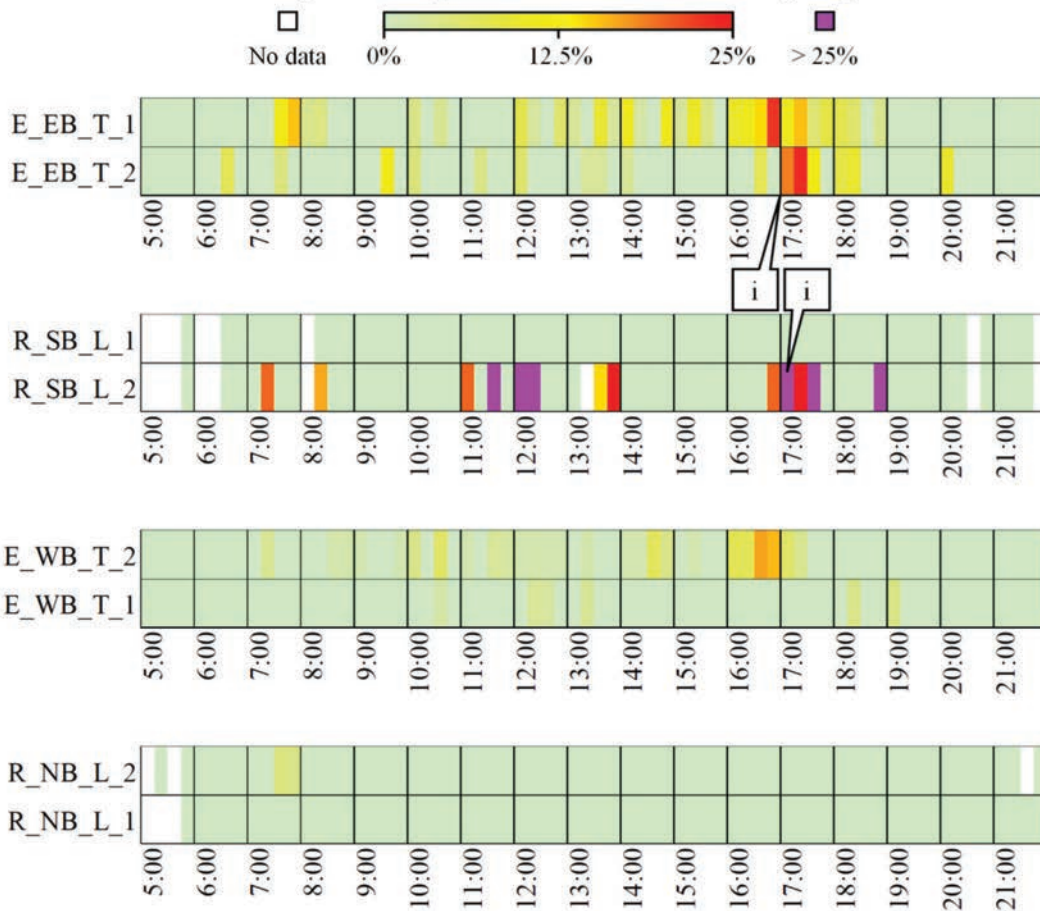
- Figure 10.21: Percentage of sampled vehicles experiencing downstream blockage. This graphic is useful to identify locations that are being affected by a downstream queue. For this performance measure, as for SF, traffic signals need to be analyzed individually. For the studied location, it is shown how the downstream traffic signals are affecting the progression of vehicles entering the DDI traveling SB (callout i) and NB (callout ii).

10.2.5 Discussion

Figure 10.16 to Figure 10.21 provides valuable information on the operational performance at the analyzed DDI. Based on the presented results, vehicles traveling WB-through on the external street and coming NB-left from the interstate ramp traverse the



(a) Traffic sources (map data: Google, IndianaMap Framework Data, Maxar Technologies, U.S. Geological Survey, and USDA Farm Service Agency)



(b) SF estimations

Figure 10.20 SF summary results.

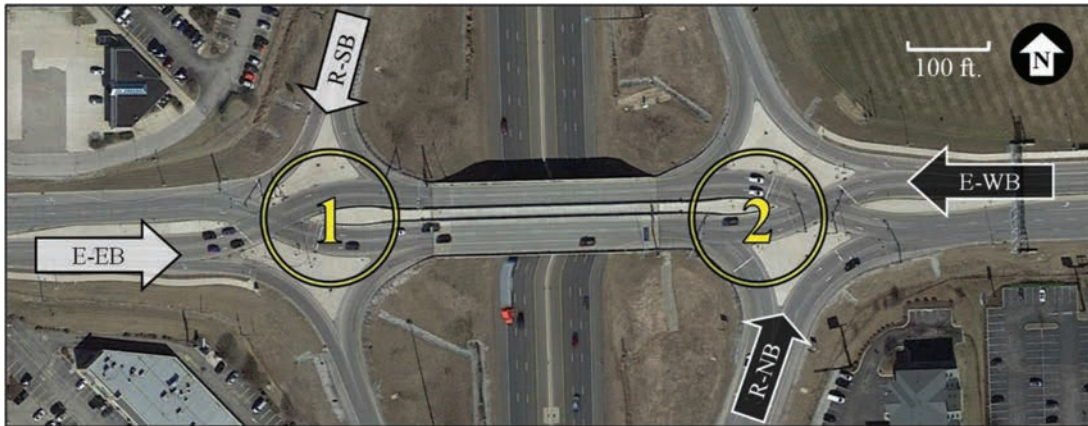
DDI with less delay, have better progression, and is less saturated than the other analyzed movements. The performance can be compared to the agency’s objectives. If operation is not as expected, timing modifications can be implemented.

The framework discussed in this section can be used to assess the performance of any DDI where CV

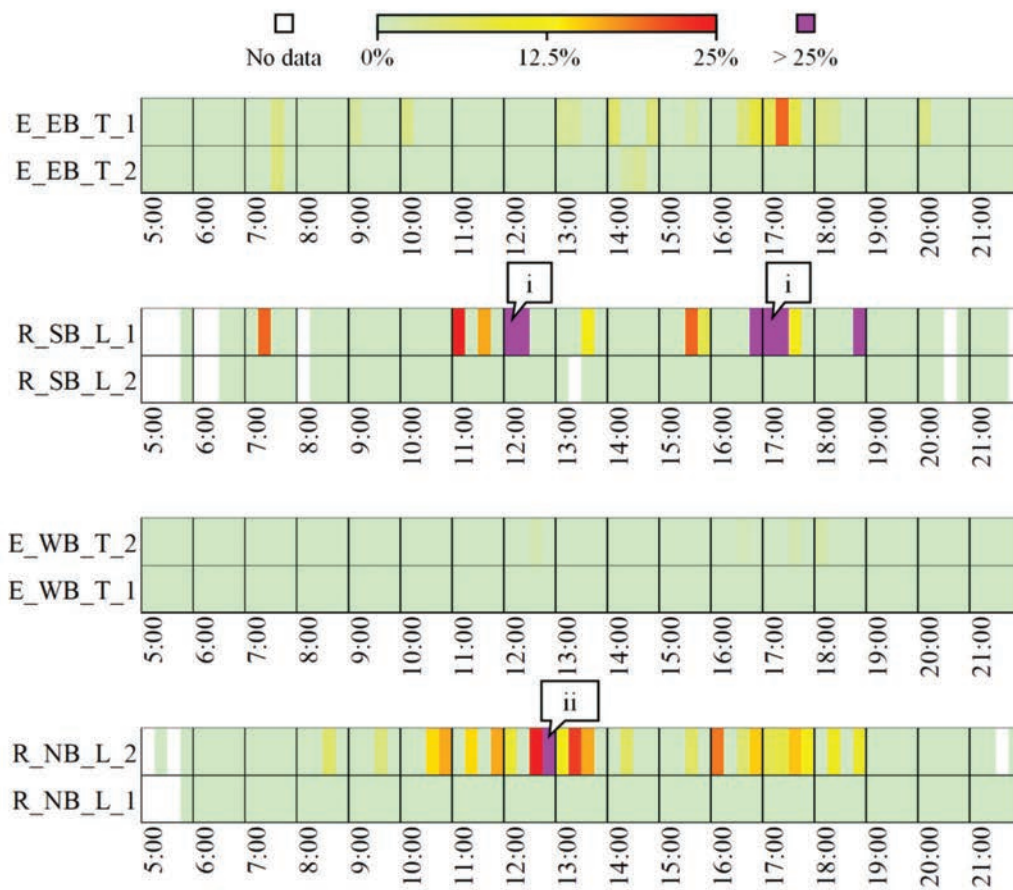
trajectory data is available. As more DDIs are constructed, efficiency evaluations can support their adoption and adjust if necessary.

10.3 Continuous Flow Intersections

Heavy left-turn movements can cause significant operational challenges at conventional signaled inter-



(a) Traffic sources (map data: Google, IndianaMap Framework Data, Maxar Technologies, U.S. Geological Survey, and USDA Farm Service Agency)



(b) DSB estimations

Figure 10.21 DSB summary results.

sections. Some typical solutions are the improvement of alternative routes, widening the right-of-way, lane channelization, and the implementation of special signal phasing. If these techniques cannot be employed or are insufficient, grade separation solutions might be considered. Nevertheless, the cost and construction

time required for grade separated intersections represent major constraints (109).

CFIs, also known as displaced left-turns (DLTs), provide an alternative at-grade intersection design that can improve operations at locations with significant left-turning movements (94, 109). At a CFI, one or

more left-turn movements are displaced to the left of oncoming traffic upstream from the main intersection. Once left-turning vehicles reach the main intersection they can proceed at the same time as opposing through traffic. This approach allows for the reduction of traffic signal phases and conflict points at the main intersection which can improve operations (94, 96).

This section uses CV trajectory data to generate performance measures for a CFI in Utah (14). EPPDs are generated and progression, delay, and split failures at the CFI are evaluated. Additionally, the distribution of stops along relevant approaches is analyzed to characterize the length and location of queues to identify areas of opportunity.

10.3.1 Study Location

Over 4,500 trajectories and 105,000 waypoints are analyzed from August 2021 weekday data to evaluate the performance at the CFI located at Bangerter Highway and 3500 S in West Valley City, Utah (Figure 10.22). This CFI is located in a suburban area and usually serves over 30,000 vehicles approaching the intersection from the north and south, and 14,000 vehicles approaching from the east and west, daily (68).

Figure 10.22c shows an aerial view of the studied intersection. This partial CFI (94) has displaced left-turns only at the major street (Bangerter Hwy, N-S). The system is comprised of the following three signalized intersections.

- North Crossover (NC): This signal controls the flow of vehicles traveling NB-through (light blue) and vehicles traveling SB crossing over (dark blue) that will then turn left at the main intersection. Vehicles traveling SB that continue through at the main intersection are not affected by this signal.
- Main Intersection (MI): This signal controls all the movements that pass through this intersection. Since the major street left-turning vehicles have been crossed to the left of opposing traffic upstream from the MI, all through and left movements on the major street can occur simultaneously unless the adjacent pedestrian walk phases are called.
- South Crossover (SC): This signal controls the flow of vehicles traveling SB-through (light blue) and vehicles traveling NB crossing over (dark blue) that will then turn left at the MI. Vehicles traveling NB that continue through at the MI are not affected by this signal.

By crossing over left-turning vehicles upstream of the MI, the phases required for left-turn movements are not needed; hence, signal efficiency is improved (109). For movements that must traverse two signals, it is imperative to provide efficient progression on the exit (last) signal. This is because storage at the exit signal is limited, and congestion could lead to queue spillback that would significantly affect operations.

10.3.2 Signal Phasing

Figure 10.23 shows conventional signal phasing for partial CFIs (94, 96). All the movements are served in four intervals. For every instance where vehicles flow from the MI towards a crossover (Intervals 1 to 3), both the NC and SC intersections allow for vehicles to travel outbound from the CFI. Only when the minor street through movements traverse the intersection (Interval 4), vehicles cross over upstream of the MI to eventually turn left.

10.3.3 Extended Purdue Probe Diagram

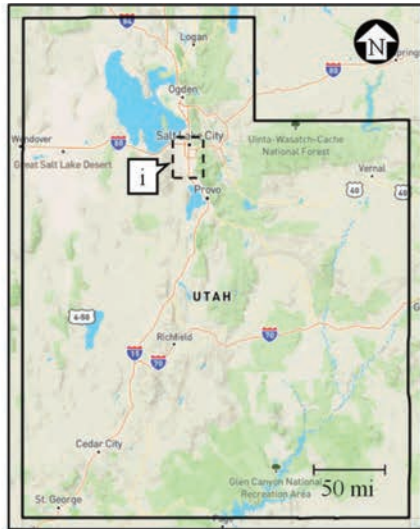
Since the dynamics between the crossover and the main intersection are crucial for the correct operation of CFIs, it is important to provide analytical performance measures and graphics that show operational status for a series of two movements simultaneously. This can be accomplished with EPPDs.

Figure 10.24 shows EPPDs from August 2021 weekdays for the CFI's major street through and displaced-left movements during the PM peak period between the 16:00 and 18:00 hrs. In all four movements some vehicles stop before entering the CFI (above the upmost horizontal blue line), but once in the system (between horizontal blue lines) they effectively progress through the second intersection (callout i) as indicated by high AOG values ranging from 83% to 100%. Well synchronized offsets are important to avoid queue spillback from the limited storage areas inside the CFI. Further, it can be stated that these movements operate in undersaturated conditions as no significant levels of split failures occur.

Figure 10.25 shows PPDs and EPPDs from August 2021 weekdays for the CFI's minor street through and left movements during the PM peak period. The through WB and EB movements (Figure 10.25a and Figure 10.25c, respectively) only have to pass one signalized intersection while the left-turning WB and EB movements (Figure 10.25b and Figure 10.25d, respectively) must traverse two. Similar to the major street movements, the minor street left movements have very efficient progression when exiting the CFI (callout i), with AOG values of 100%. However, all minor street movements show a significant number of vehicles experiencing split failures before entering the intersection, indicating oversaturated conditions.

10.3.4 Summary Performance by TOD

PPDs and EPPDs provide traffic signal performance measures at the movement-level for a defined time period. To assess all movements simultaneously by TOD, a series of heatmaps summarizing performance at 15-minute intervals are provided. This approach permits the prompt identification of operational challenges that can lead to potential improvement opportunities.



(a) Utah (map data: Leaflet, Mapbox, and OpenStreetMap)



(b) Salt Lake City metropolitan area (map data: Leaflet, Mapbox, and OpenStreetMap)



(c) Bangerter Hwy at 3500 S, West Valley City, Utah (map data: Google)

Figure 10.22 Continuous flow intersection location.

Figure 10.26 shows heatmaps indicating the percentage of vehicles experiencing split failures at the three signalized intersections that comprise the analyzed CFI. No significant challenges are observed at the crossovers (Figure 10.26b and Figure 10.26d). However, at the MI (Figure 10.26c), side street movements show high SF during the 14:15–18:30 hrs. period. Since the

movements on the major street do not present any congestion challenges, split rebalance could potentially benefit the minor street left-turn movements (Interval 3 on Figure 10.23). Significant operational improvements of the WB-through (WBT) and EB-through (EBT) movements are difficult as the maximum green time is capped by the travel time from the crossovers

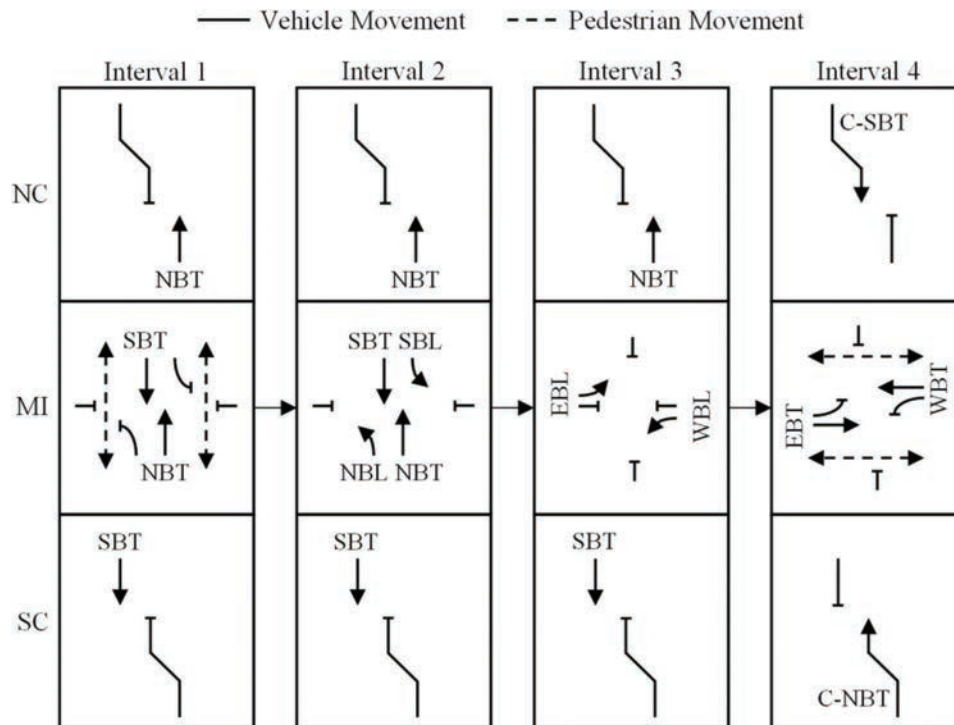


Figure 10.23 Conventional signal phasing for partial CFIs (96).

to the MI of the SB-left (SBL) and NB-left (NBL) movements.

Figure 10.27 shows the percentage of sampled vehicles that arrive on green at each intersection. Some vehicles entering the CFI system (callout i) have to stop and hence present moderate to poor AOG levels. However, once the entry intersection is passed, progression at the exit intersection (callout ii) is efficient and AOG is high. This helps maintain minimal queues on the inner storage areas.

Figure 10.28 shows heatmaps indicating the LOS experienced at each movement. To facilitate the evaluation of the graphic, vehicle movements that enter the system on the major street are indicated with callout i, and vehicle movements that exit with callout ii. From the three metrics, it is evident that the intersection was timed with the objective of minimizing congestion for the north and south approaches during the PM peak period and its shoulder periods, due to their improved AOG and LOS numbers, while the minor street experiences more split failures during the same period.

10.3.5 Stops Distribution

Figure 10.29 shows linear referenced histograms of the location relative to the exit intersections' FS where vehicles first stop while approaching each intersection for movements that pass two signals at the studied CFI during August 2021 weekdays between 16:00 and 18:00 hrs. The distributions are calculated by identifying the

location where vehicles come to a full stop for the first time upstream of each signalized intersection in the system. Then, the recorded values are normalized as a percentage of the total number of sampled vehicles for the evaluated movement.

This analysis can help identify approaches where stops or inefficiencies occur. For example, Figure 10.29 shows how few vehicles stop at the through movements that traverse the crossover intersections (NBT and SBT). In contrast, a significant number of left-turning vehicles stop before entering the CFI. More importantly, for the internal approaches with limited storage, 15% of vehicles traveling NBL stop between MI and SC (callout i), and 17% of vehicles traveling SBL stop between MI and NC (callout ii). Given the distance of the first stops between the MI and the crossovers, it is unlikely that there are any capacity issues as the queues do not extend to the crossovers. However, it might be of interest to investigate further the cause of the stops and whether offset or sequence adjustments can be made to prevent NBL and SBL vehicles from stopping at the MI.

10.3.6 Discussion

As CFIs are deployed, it is important to holistically measure performance across the multiple signals that compose the system. Figure 10.24 to Figure 10.29 have provided valuable information on the operational performance of the analyzed CFI. Based on the presented results, a significant number of vehicles have

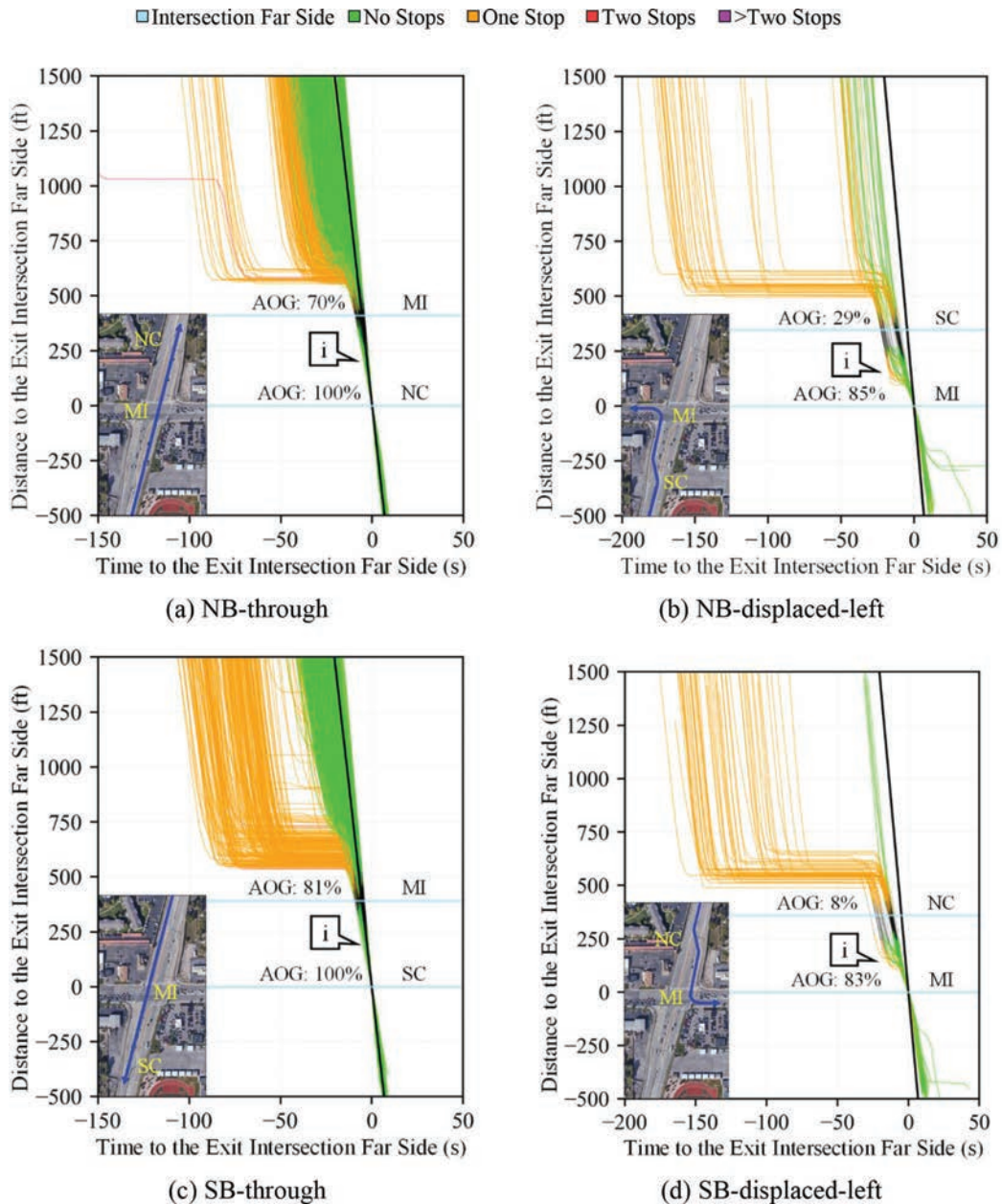


Figure 10.24 EPPDs for major street movements (map data: Google).

to stop before entering the CFI, but once the first signal is passed, progression is mostly unimpeded for the sampled vehicles until they exit the system. This confirms the correct operation of the CFI as it is critical to keep internal storage areas free of long

queues. To further assess queue characteristics at a closely-coupled intersection, visualization such as the one presented in Figure 10.29 can be used to evaluate queue-lengths and the ratio of vehicles that have to stop.

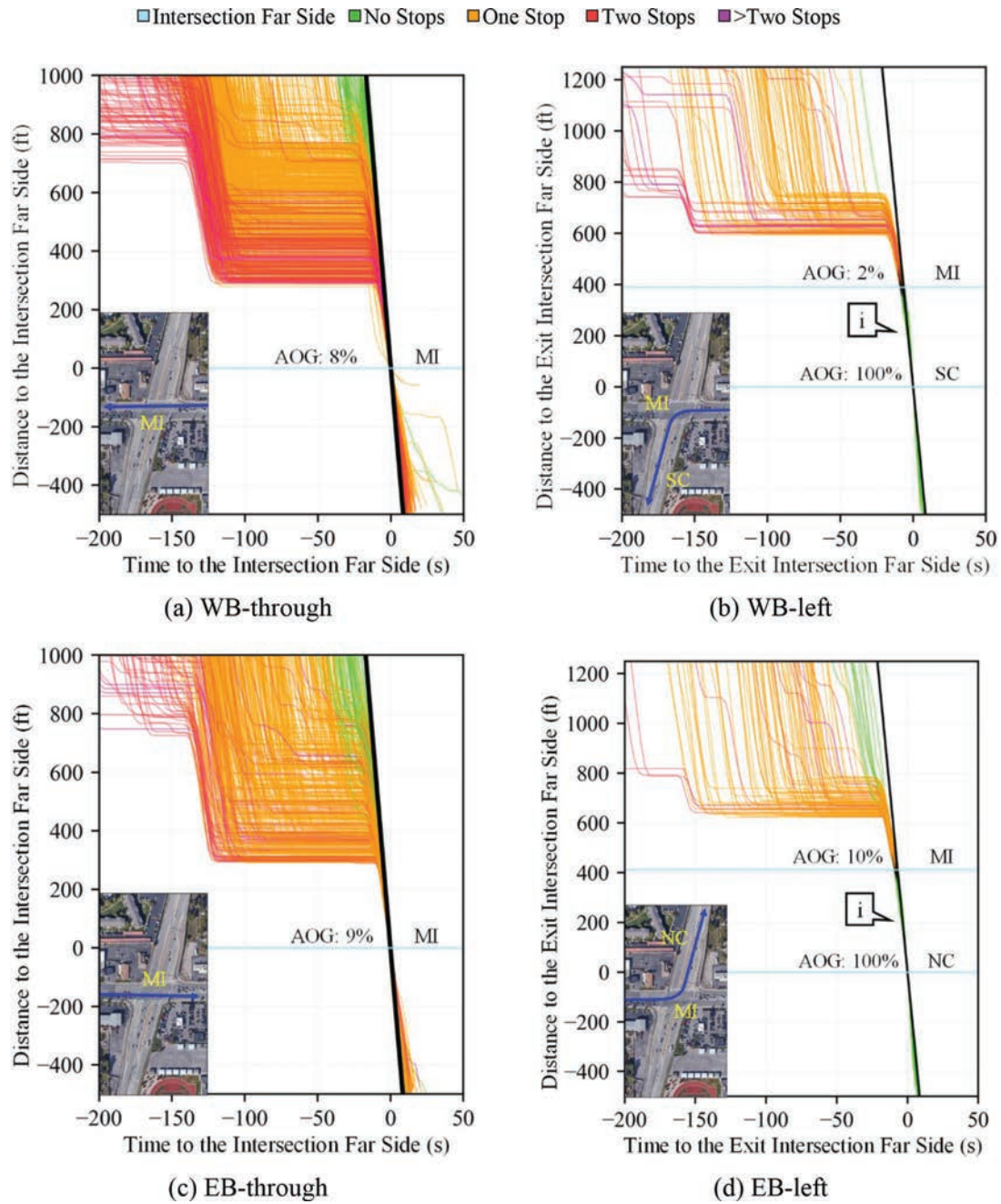


Figure 10.25 PPDs and EPPDs for minor street movements (map data: Google).

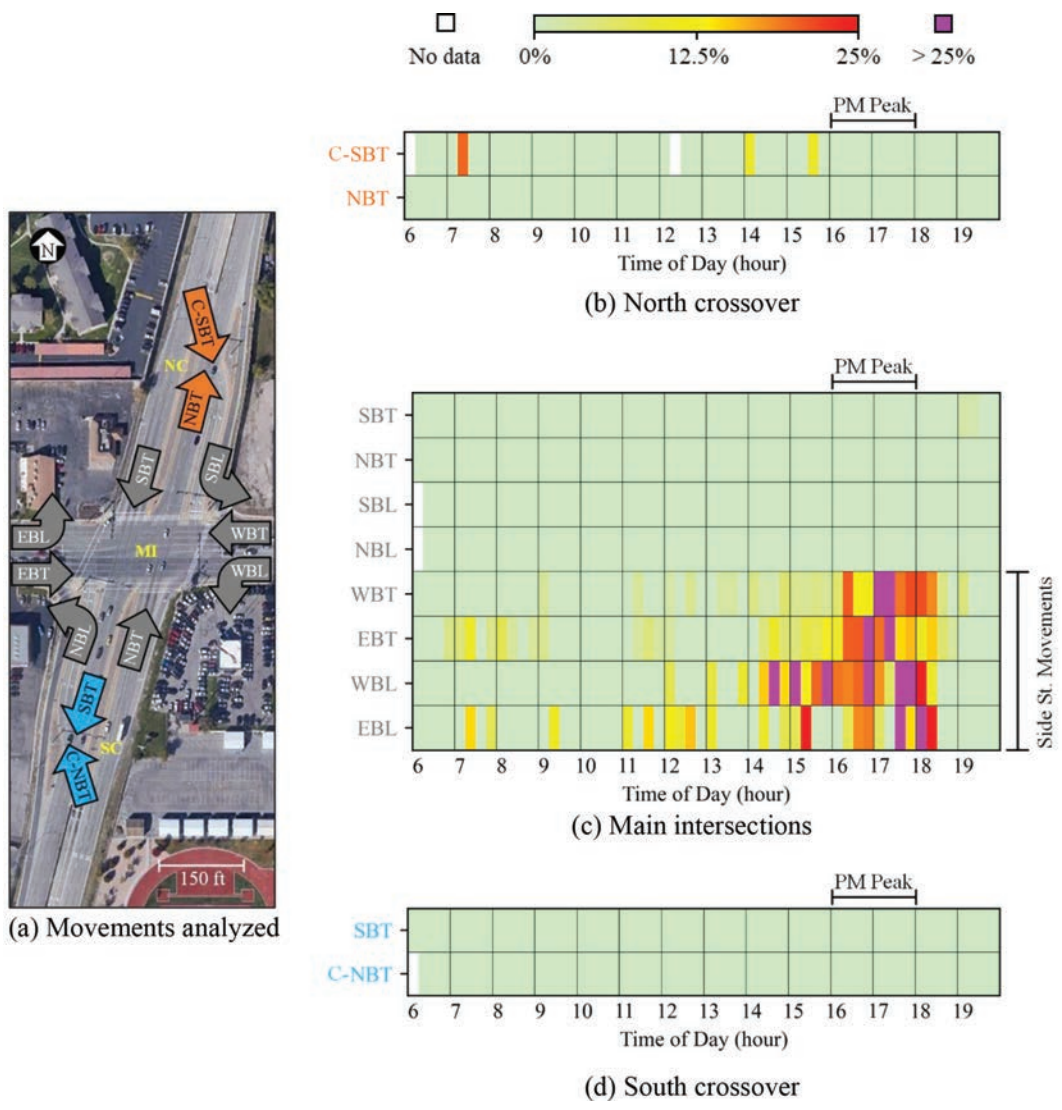


Figure 10.26 SF summary results at all signals at the CFI for August 2021 weekdays (map data: Google).

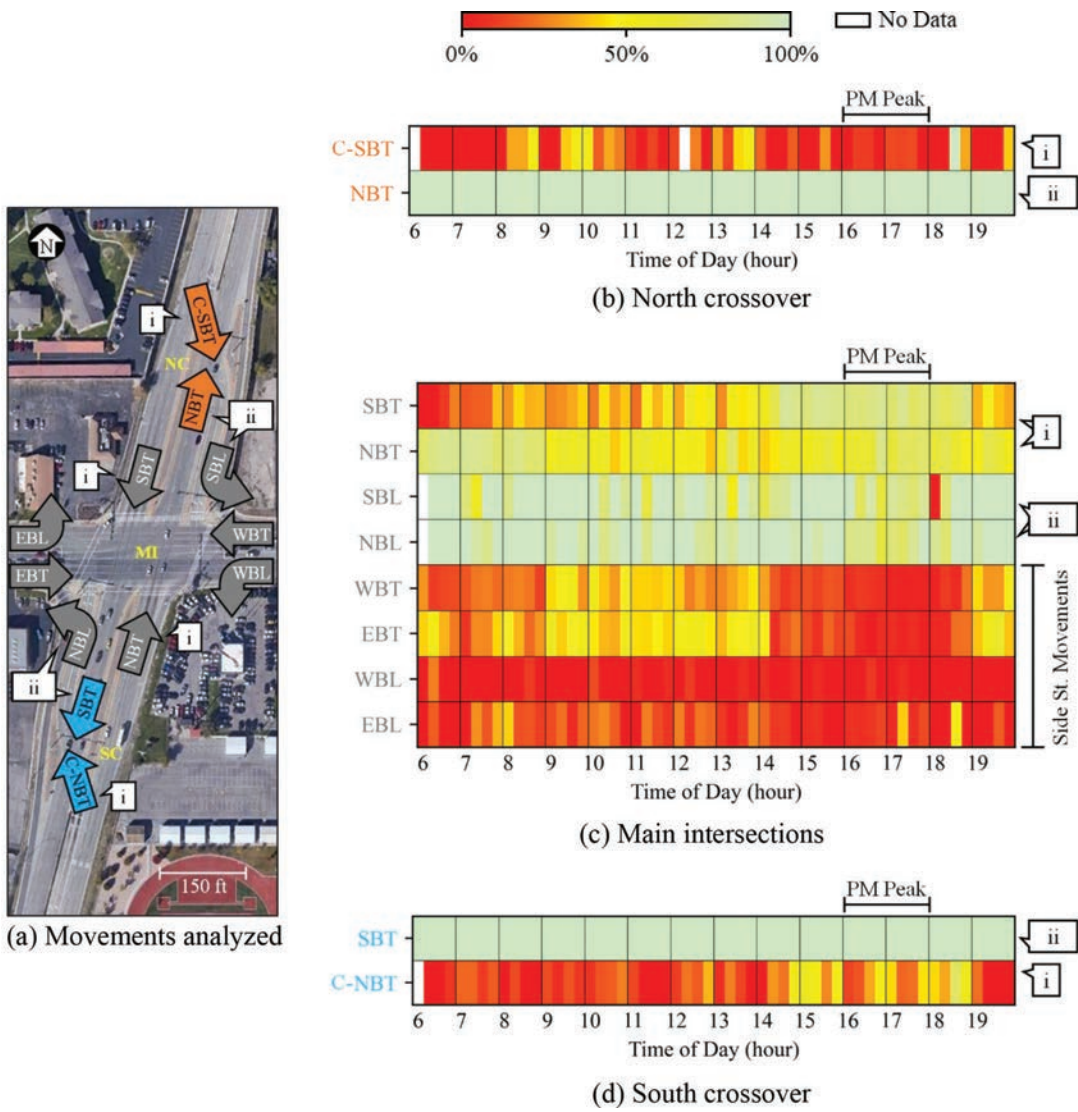


Figure 10.27 AOG summary results at all signals at the CFI for August 2021 weekdays (map data: Google).

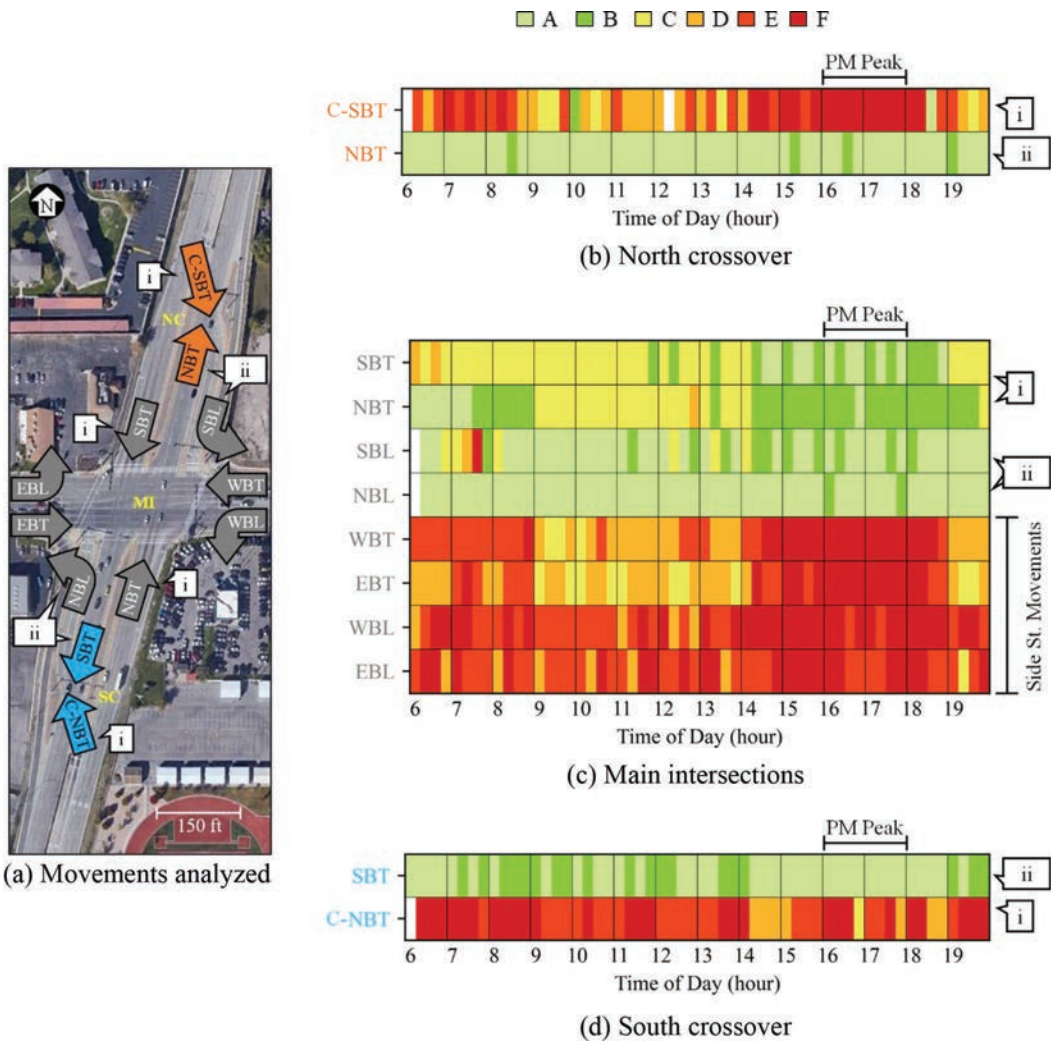


Figure 10.28 LOS summary results at all signals at the CFI for August 2021 weekdays (map data: Google).

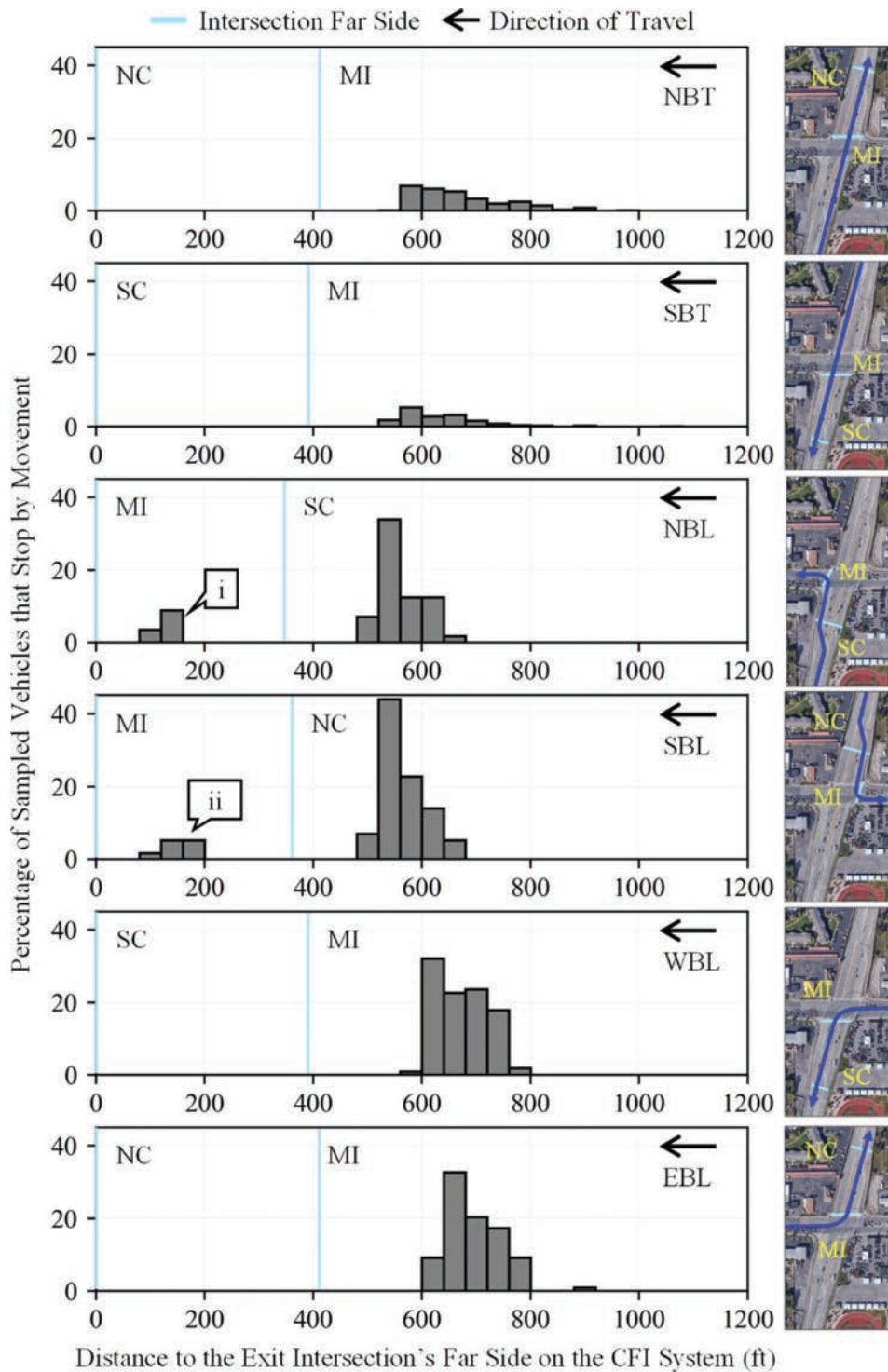


Figure 10.29 Initial stops distribution as a percentage of the total sampled trajectories (map data: Google).

11. ROUNDABOUTS

A roundabout is a type of circular intersection where vehicles travel around an island. Yield control is utilized for entering traffic, there are channelized approaches, and specific geometries are implemented to modulate speeds on the circulatory roadway (110). With over 8,000 roundabouts in the United States (111), this type of intersection has become a popular alternative to traffic signals (112). It is therefore important to develop techniques that allow for a systematic evaluation of roundabouts' efficiency.

Roundabout performance measures focus on the estimation of capacity and operational characteristics, such as delay, LOS, and queue-length. Capacity estimations are generally associated with entrance capacity which estimates the number of vehicles that can be safely accommodated at a roundabout (113–116). The estimations of operational characteristics of roundabouts have been derived from various data sources and methods such as video detection (117), wireless magnetometers (118, 119), Bluetooth probe data (120), modelling (121), and microsimulation (122–124). Further, the HCM defines techniques for estimating control delay, LOS, and queue-length based upon demand volumes (64).

However, applying these techniques agency-wide to assess performance is labor-intensive and costly due to the extensive roundabout count data collection effort required for conducting the engineering analysis or simulation (112). Furthermore, local driver behavior needs to be calibrated for each analysis as it can significantly vary due to the novelty of the design for some users (122–124). These requirements pose significant challenges when trying to scale the analysis.

This chapter presents CV-based techniques to estimate roundabout delay, LOS, queue-lengths, and origin-destination characteristics (15). Eliminating the need to collect turning movement counts dramatically improves the scalability of the analysis. Over 264,000 trajectories and 3.6 million waypoints are analyzed to describe these methodologies and their application is demonstrated by assessing over 100 roundabouts in Carmel, Indiana.

11.1 Control Delay

The HCM proposes LOS as the main performance indicator for both interrupted and uninterrupted flow (64). In the particular case of roundabouts, LOS is based on control delay, and its criteria definition is shown in Table 11.1.

At a roundabout, traffic control is performed by the roundabout itself, its markings, and its signage. Therefore, control delay can be estimated by calculating the difference in travel time through the studied location between a sampled vehicle trajectory and an FFT (Equation 5.2) (4, 63, 112). Thus, the same technique used to estimate control delay for signalized intersections from a PPD, as described in Chapter 5 (Figure 5.2), can be

TABLE 11.1
HCM level of service criteria for roundabouts (64)

LOS	Average Control Delay (s/veh)
A	≤10
B	>10–15
C	>15–25
D	>25–35
E	>35–50
F	>50

applied to calculate control delay at roundabouts. From Table 11.1 and the estimated control delay, individual vehicle trajectories can be assigned a LOS.

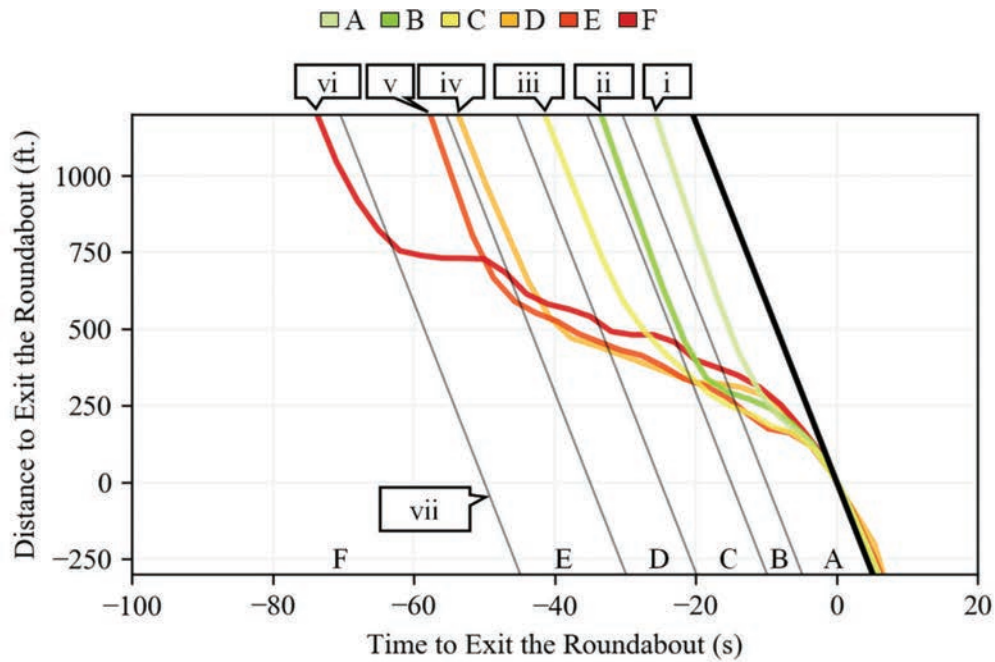
Figure 11.1a shows a PPD for a roundabout, which is referenced to the distance and time when the vehicle exits the intersection. Callouts i–vi are vehicle trajectories approaching the roundabout from the west, traveling EB, at Ditch Rd. and W 96th St. color-coded by their assigned LOS. Delay can be estimated by comparing how far away a particular trajectory is from the FFT. The farther to the left a trajectory is, the greater its delay. Callout vii is a segregation line that helps to visually separate trajectories by their LOS (in this case separating E and F trajectories).

Figure 11.1a is a subset of Figure 11.1b, which shows 38 trajectories sampled between 17:00 and 17:15 hrs. during July 12th to 16th, 2021 at the same roundabout approach. Figure 11.1b also has a pie chart that shows the percentage of trajectories categorized with the estimated LOS. Over 30% of trajectories have a LOS F, and only 8% have a LOS A.

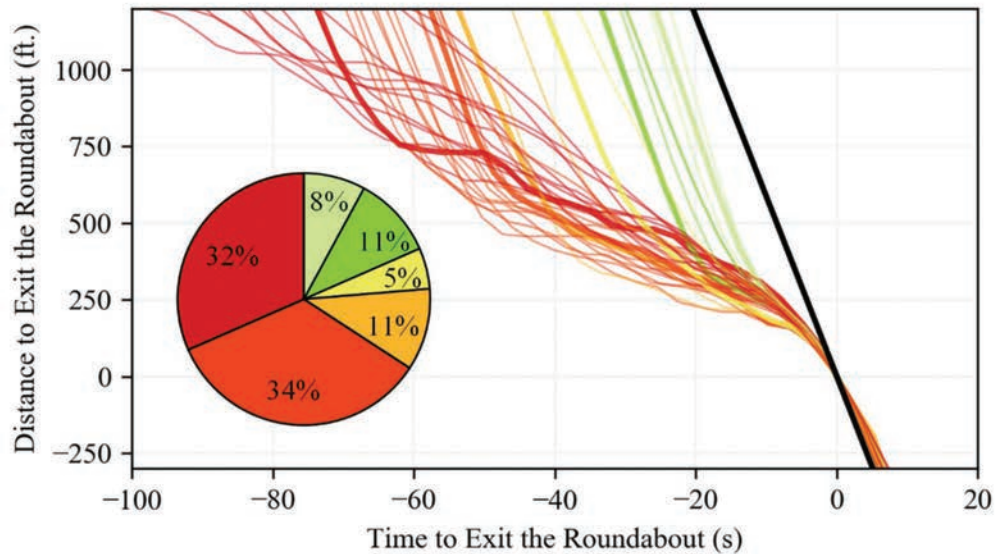
Roundabout PPDs, such as Figure 11.1b, can be systematically generated for all the approaches at a roundabout to quantify approach delay. Approach delay is the delay experienced by vehicles entering from the same approach regardless of exit choice. Figure 11.2 shows PPDs for all four approaches at Ditch Rd. and W 96th St. during the same peak 15-minute period as Figure 11.1 over five days. The SB direction of travel, callout i, is the most efficient approach with most of the vehicles experiencing a LOS B. On the other hand, vehicles traveling WB, callout ii, present the highest proportion of vehicles having a LOS F.

By averaging the control delay experienced by each sampled vehicle over the studied approach and time period, each approach can be assigned a LOS. For the analysis shown in Figure 11.2, the average control delay (and LOS) for the SB, WB, NB, and EB approaches is 16 s/veh (C), 67 s/veh (F), 41 s/veh (E), and 44 s/veh (E), respectively. In contrast, Figure 11.3 shows PPDs for all approaches at the same location during an off-peak 15-minute period. In this case, the average control delay (and LOS) for the SB, WB, NB, and EB approaches is 10 s/veh (A), 18 s/veh (C), 16 s/veh (C), and 14 s/veh (B), respectively.

A noteworthy benefit of using CV data is the ability to cover most hours of the day to characterize temporal variations in performance. Figure 11.4 shows the LOS



(a) Six trajectories with different LOS



(b) All 38 trajectories during the TOD period

Figure 11.1 Vehicle trajectories traveling EB at Ditch Rd. and W 96th St. during a peak 15-minute period.

change by 15-minute periods for the four approaches at Ditch Rd. and W 96th St. Callout i represents the time-period and approach analyzed in Figure 11.1 and Figure 11.2d. This visualization provides an efficient performance summary for a single location that helps identify direction of travel and TOD where the roundabouts are congested.

11.2 Data Aggregation and Visualization Graphics

Figure 11.2 to Figure 11.4 describe the performance at a single roundabout. However, agencies are typically interested in systemwide assessment of all their approaches, as well as the average of all approaches of each roundabout.

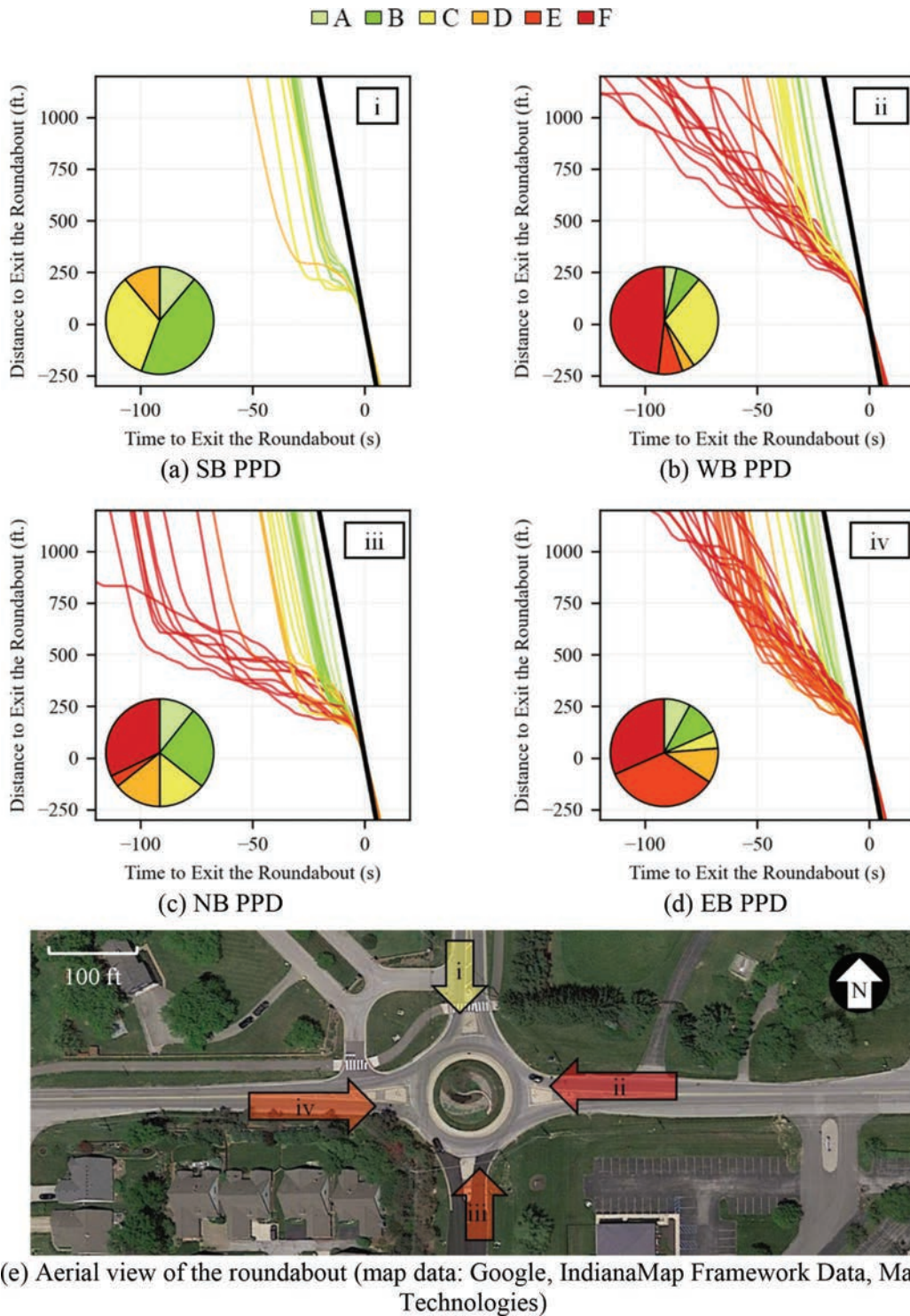


Figure 11.2 Ditch Rd. and W 96th St. trajectories by approach and estimated LOS during a peak 15-minute period between July 12th–16th, 2021.

Figure 11.5 shows pareto-sorted bar-graphs of the average control delay by hour experienced by each approach on over 100 roundabouts in Carmel, Indiana. LOS thresholds are shown with blue dashed lines for reference. Only approaches with at least 10 sampled vehicles during the analysis period are considered.

As demand fluctuates throughout the day, the number of approaches with 10 sampled vehicles or more also changes.

These visualizations are particularly useful when assessing the quantity of approaches experiencing congestion (LOS F or E) and identifying peak periods

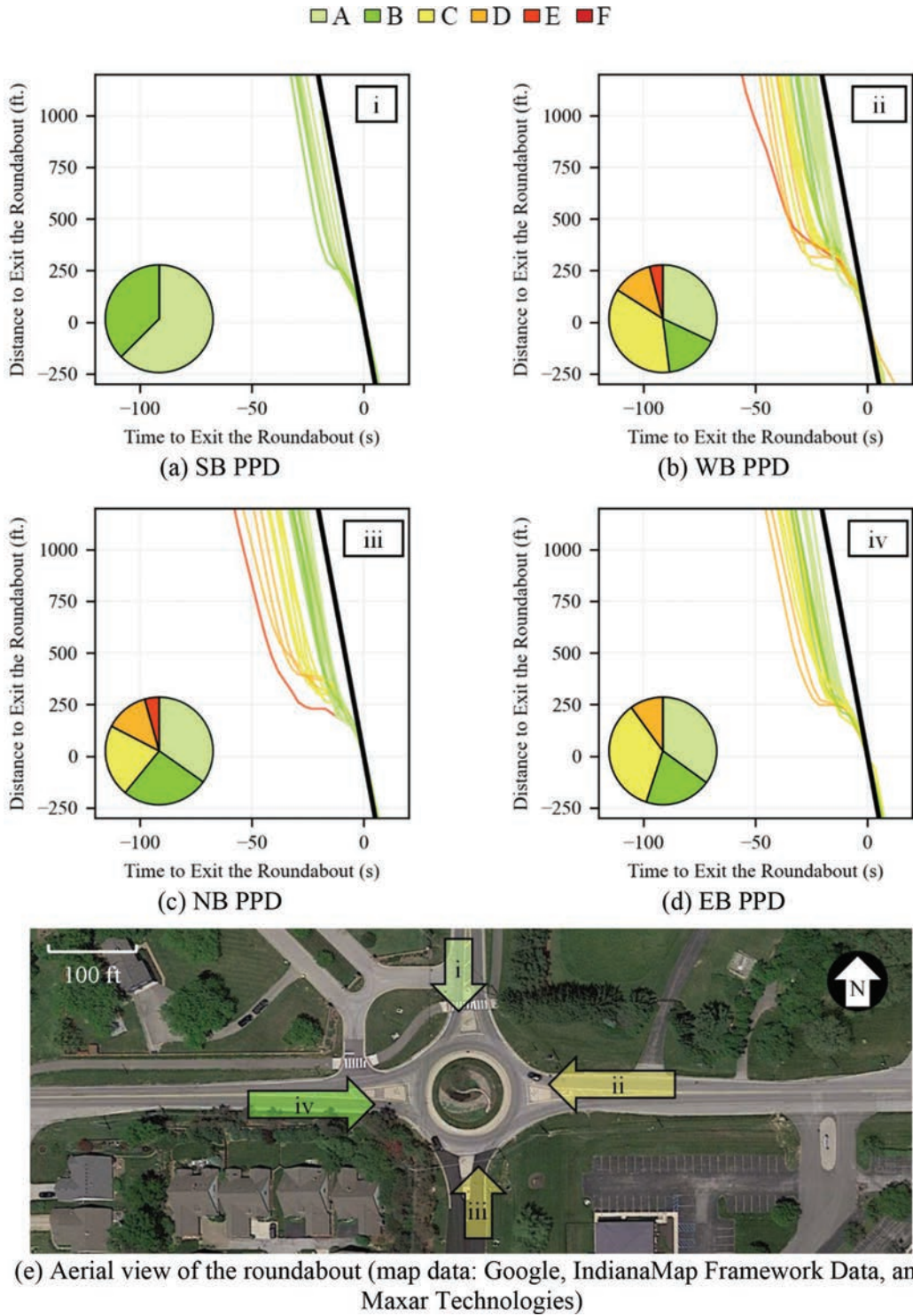


Figure 11.3 Ditch Rd. and W 96th St. trajectories by approach and estimated LOS during an off-peak 15-minute period between July 12th–16th, 2021.

(time with most C or worse LOS approaches). Additionally, locations in which vehicles travel faster than the posted speed limit (negative delay) can also be identified.

Figure 11.6a shows a pareto-sorted bar-graph of the average control delay experienced on every approach in

the system during the 15-minute period with the most approaches with a LOS C or worse (17:00–17:15 hrs.). From this graph, the locations with the highest delays can easily be identified for further analysis. Figure 11.6b shows the 10 approaches with the highest estimated control delay. Callout i, corresponding to the

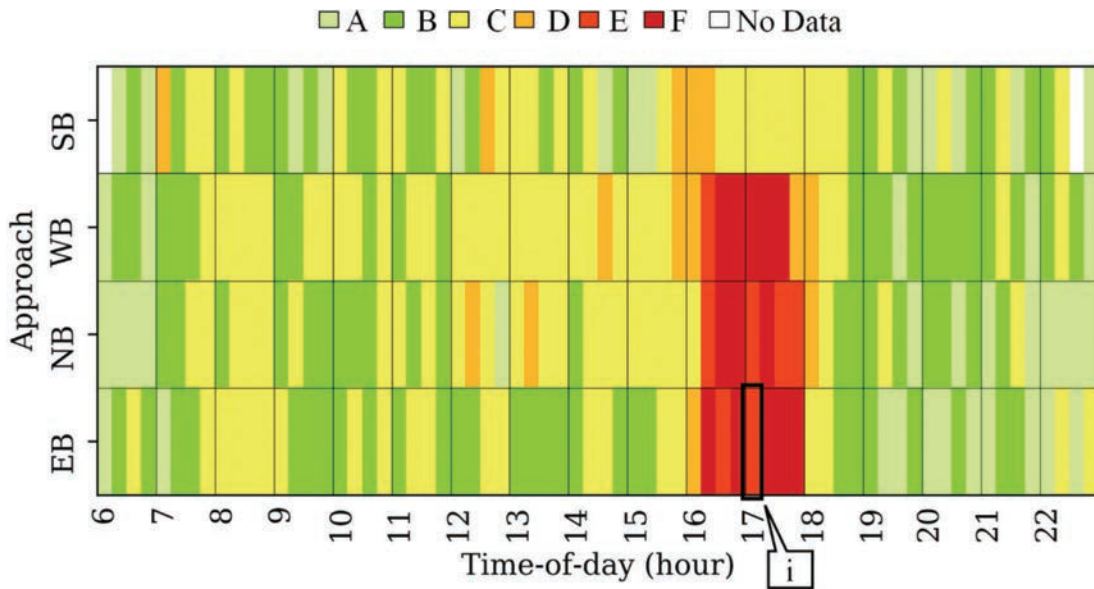


Figure 11.4 LOS by TOD at Ditch Rd. and W 96th St. between July 12th–16th, 2021.

NB movement of Roundabout 1 (Keystone Pkwy at 116th St. E), has a control delay of 276 seconds (the y-axis is truncated at 120 s/veh).

Additionally, a geographical representation of the results can provide practitioners with insights on the effects that certain roundabouts may have on adjacent locations. Figure 11.7a shows all the analyzed roundabouts color-coded by their highest-delay approach's LOS. Callouts reference the roundabouts' ID and direction of travel (SB, EB, NB, or WB) presented in Figure 11.6b.

Roundabout 3 has two approaches that are within the 10 highest approach delays in the system during the study period. Vehicles traveling EB have the highest delay at Roundabouts 6 and 7. Given Roundabouts' 6 and 7 proximity to each other (Figure 11.7a), it is possible that the poor performance at Roundabout 7 is propagating to Roundabout 6.

Additionally, studied locations can be color-coded by the LOS based on the average control delay from all the approaches (Figure 11.7b), instead of only focusing on the highest-delay approach. If a location has poor LOS based on the highest-delay approach, but a good LOS based on all the approaches, it is an indication that few approaches in that roundabout are under-performing. In contrast, if a location shows poor LOS in both visualizations (Figure 11.7a and Figure 11.7b), it indicates that most of the entering vehicles have high control delay.

Table 11.2 shows the 10 highest estimated control delays by approach (Figure 11.6b and Figure 11.7a). Further, the average for the entire roundabout is also provided.

11.3 Queue-Length

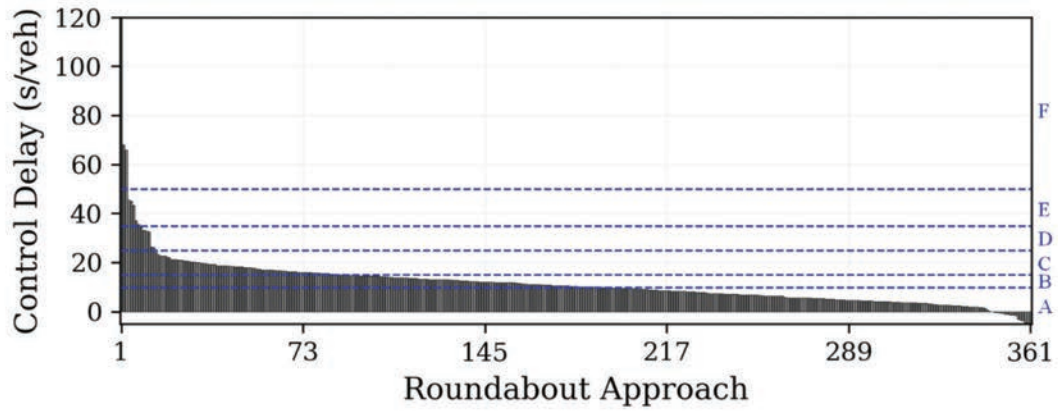
The HCM provides a technique to compute 95th percentile queue-lengths at roundabouts based on

volume-to-capacity ratios, lane capacities, and study time periods (64). From CV trajectory data, queue-length can be estimated as the distance to the center of the roundabout when a vehicle first stops during its approach. Then, queue-lengths from several days can be aggregated over various TOD periods to estimate the 95th percentile.

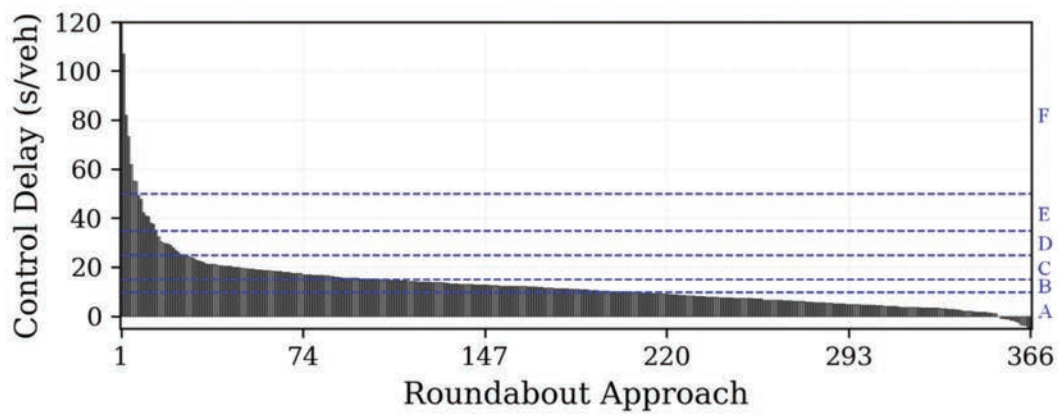
Figure 11.8 shows the estimated 95th percentile queue-length, as used by the HCM (64), at Ditch Rd. and W 96th St. from data sampled during all the weekdays in July 2021. As expected, the delay presented in Figure 11.4 relates to the queue-lengths in Figure 11.8, since the highest delays occur during the time with the longest queues (from the 16:00 to the 18:00 hrs. for approaches WB, NB, and EB).

11.4 Origin-Destination Characteristics

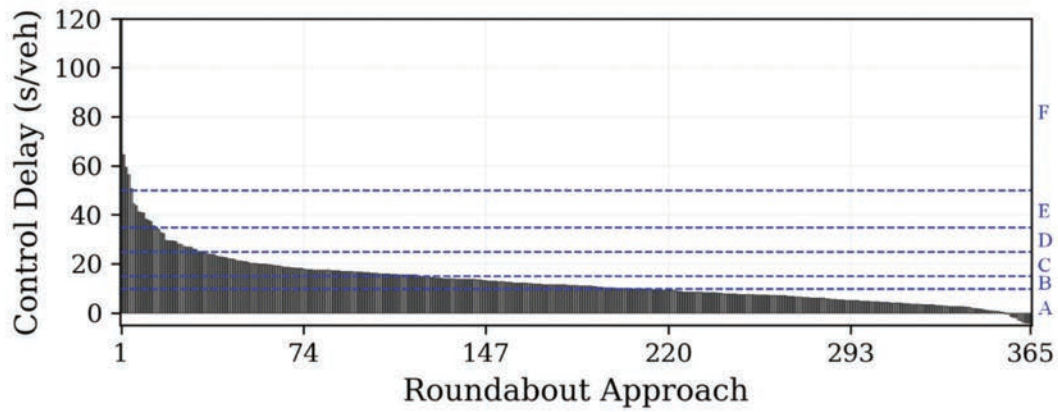
The technique presented in Chapter 4 to automatically identify vehicle turning movements from trajectory data can provide valuable information on the origin-destination characteristics at roundabouts and the variation over time (3). Table 11.3 shows July 2021 weekdays vehicle turning counts at Ditch Rd. and W 96th St. (ID 2). From this table, the movements with higher demands can be identified for each 15-minute segment during the AM and PM peak periods. Even though the counts shown are a sample of all the vehicles that proceed through the roundabout, valuable insight can be obtained from the demand distribution that can help practitioners understand traffic trends. These values can then be used to scale approach volumes to estimate absolute movement volume by time period.



(a) 15:00–16:00 hrs.

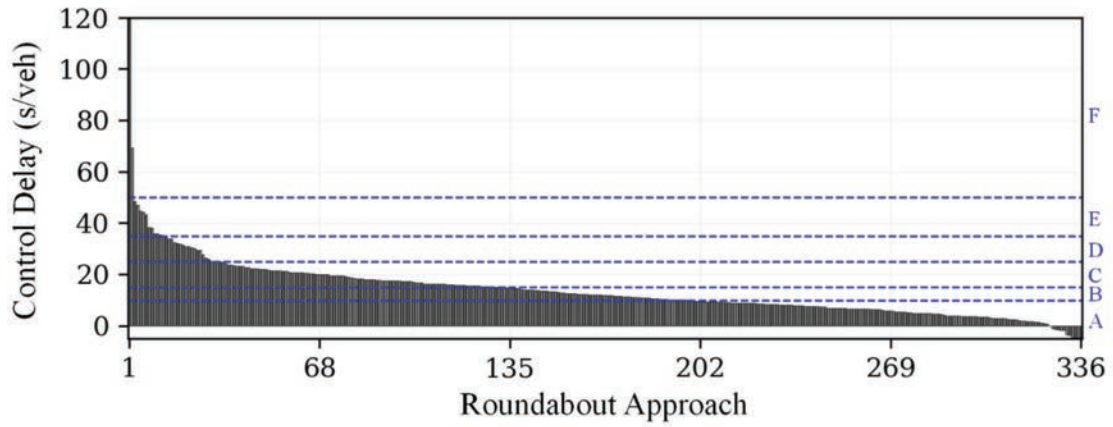


(b) 16:00–17:00 hrs.

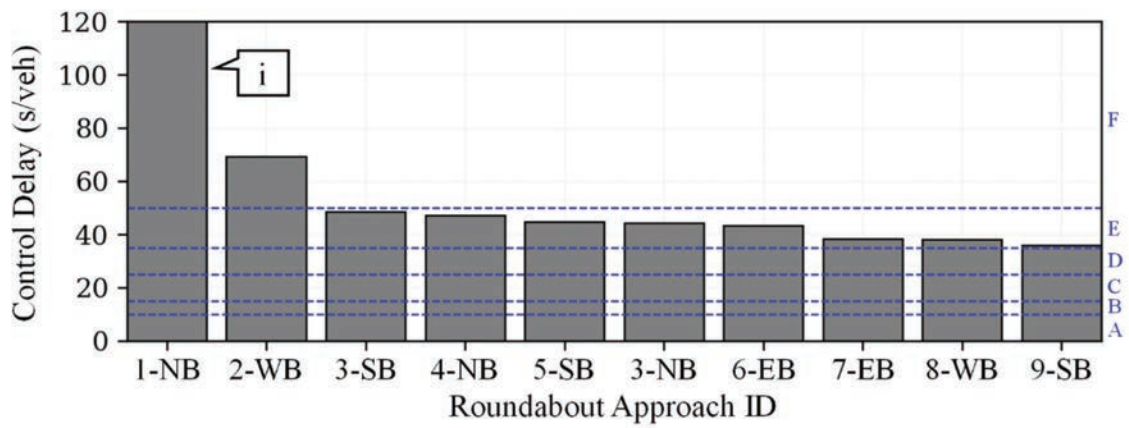


(c) 17:00–18:00 hrs.

Figure 11.5 LOS system visualization by approach for all the weekdays in July 2021.

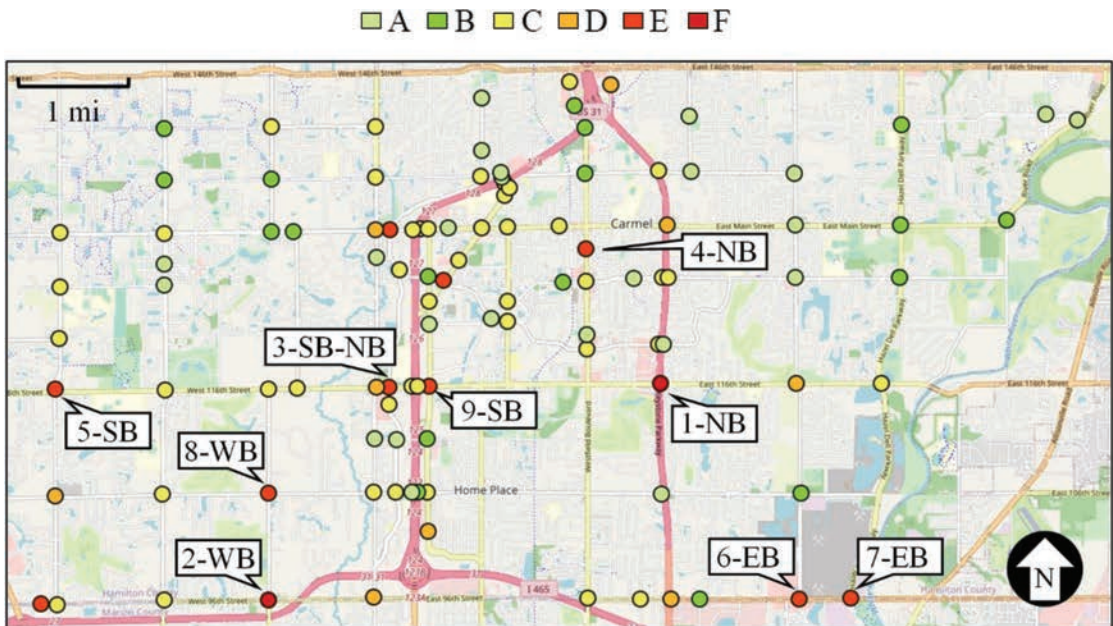


(a) All 336 analyzed approaches

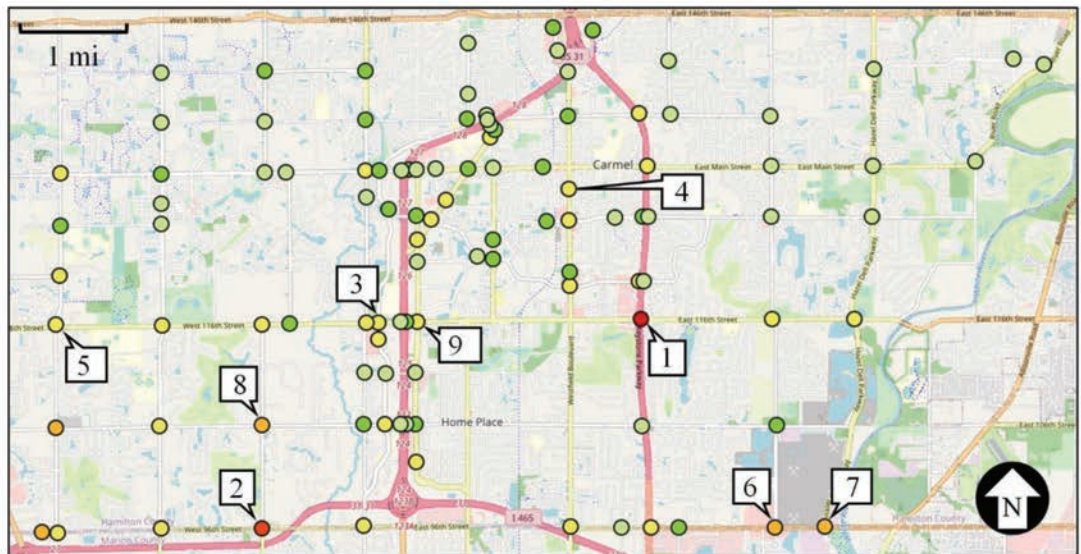


(b) 10 highest delays by approach with their location ID

Figure 11.6 LOS system visualization by approach for all the weekdays in July 2021 during the most congested 15-minute period.



(a) Highest delay approach



(b) Average by roundabout

Figure 11.7 LOS system visualization from the 17:00 to the 17:15 hrs. for all the weekdays in July 2021 (map data: OpenStreetMap).

TABLE 11.2
Highest control delays by approach between 17:00 and 17:15 hrs.

ID	Name	NB Delay (s/veh)	EB Delay (s/veh)	SB Delay (s/veh)	WB Delay (s/veh)	Average (s/veh)
1	Keystone Pkwy at 116th St. E	276	N/A	N/A	9	75
2	96th St. at Ditch Rd.	34	30	20	69	42
3	116th St. at Illinois St.	44	24	49	21	25
4	Rangeline Rd. at 4th St. SW	47	8	14	N/A	17
5	116th St. at Shelborne Rd.	26	15	45	18	23
6	96th at Gray Rd.	35	43	20	12	32
7	96th at Hazel Dell Pkwy	N/A	38	20	9	27
8	106th St. at Ditch Rd.	17	18	15	38	26
9	116th St. at Pennsylvania St.	28	12	36	23	21

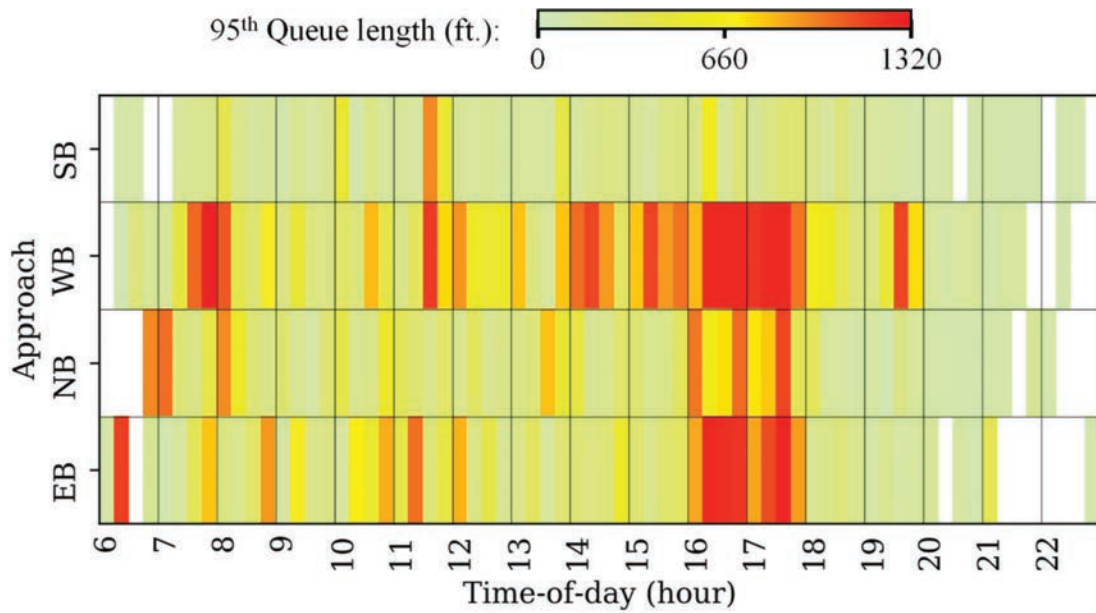


Figure 11.8 Estimated queue-length by TOD at Ditch Rd. and W 96th St. (ID 2) for weekdays in July 2021.

TABLE 11.3
 July 2021 weekday sampled vehicle turning counts at Ditch Rd. and W 96th St. (ID 2)

Start Time	Southbound			Westbound			Northbound			Eastbound		
	L	T	R	L	T	R	L	T	R	L	T	R
6:00	0	5	0	24	6	0	1	13	7	0	22	2
6:15	0	19	0	30	18	0	2	0	21	0	16	2
6:30	2	34	2	67	48	0	14	4	31	1	16	3
6:45	3	8	0	87	47	3	8	3	54	1	33	1
7:00	0	12	0	46	38	0	4	6	38	1	47	1
7:15	0	36	1	87	61	0	7	9	49	0	36	6
7:30	3	45	1	72	44	3	12	32	66	3	87	8
7:45	3	56	4	61	58	1	10	44	75	5	52	16
8:00	8	40	7	65	44	1	22	19	28	6	47	20
8:15	2	45	2	35	31	3	16	26	40	8	62	16
8:30	9	24	4	34	33	2	7	21	32	8	61	7
8:45	2	29	7	45	50	7	12	23	43	7	48	5
15:00	3	32	6	28	55	8	16	28	49	5	90	14
15:15	4	25	3	32	70	4	6	32	33	5	65	13
15:30	1	43	10	45	76	7	12	37	55	3	65	15
15:45	2	28	13	37	97	1	17	41	45	6	81	18
16:00	7	37	5	56	75	4	17	45	41	7	73	18
16:15	2	28	7	42	106	2	25	34	58	12	85	28
16:30	5	53	6	49	87	4	33	56	51	11	88	27
16:45	2	50	6	34	91	5	26	57	38	13	77	22
17:00	3	33	16	39	87	3	35	39	51	9	82	35
17:15	3	46	16	43	93	8	24	39	46	9	96	35
17:30	4	30	13	42	96	7	15	35	29	7	80	22
17:45	2	22	8	28	73	0	11	38	32	5	67	15

Note: L = left, T = through, and R = right.

12. SAFETY EVALUATION

Previous chapters have presented different uses of CV trajectory data to assess intersection performance. However, agencies not only have the objective of maintaining efficient systems, but also to provide safe mobility to users. This chapter discusses the usage of CV event data at signalized intersections to do the following.

- Correlate HB events and crashes to provide a proactive approach for evaluating safety (16).
- Assess driver behavior change by analyzing HA event occurrences after implementing a new type of mainline left-turn phasing (17).

12.1 Hard-braking Events as Surrogate for Crashes

Agencies usually screen signalized intersections and approaches for safety improvements by utilizing crash data from the previous 3–5 years (125, 126). Due to the relative infrequency of crashes at many locations, this multi-year analysis of data is needed to ensure the validity and accuracy of statistical models. However, this method is considered reactive as agencies must wait for a substantial crash history to develop as evidence for proceeding with safety improvement projects. There is a growing interest in the industry to replace this historical method with surrogate events to reduce the time between data collection and the implementation of safety improvements.

Since the 1960s, there have been efforts to supplement or replace crash counts with traffic conflicts (127). Conflicts occur more frequently than crashes and are caused by the same failures that result in crashes (128). The higher number of conflicts combined with their similar causations to crashes make them attractive to agencies trying to statistically determine opportunities for safety improvements. However, conflicts can be difficult to observe and document, require trained personnel, and can be dependent on the subjective ratings of the observer.

In July 2019, there were over 6 million sampled HB events in Indiana. In contrast, during the same month, there were only 17,652 crashes in the state, which represent 0.3% of the total number of sampled HB events. This section evaluates the validity of using CV HB events at a signalized corridor for the safety screening of intersections and approaches by providing a comparison with rear-end crashes. This could allow for the implementation of mitigation measures addressing emerging problems much quicker than typical practices that rely on 3–5 years of crash data.

12.1.1 Study Corridor

HB data collected between July 1st and July 31st, 2019, at eight signalized intersections along SR-37, located south of Indianapolis, Indiana, is used (Figure 12.1). The corridor is a 4- to 6-lane principal arterial

with a speed limit of 55 mph. The volume along the corridor varies between 64,000 VPD at the northernmost intersection, 49,000 VPD in the middle of the corridor, and 38,000 VPD at the southernmost intersection.

Indianapolis commuters living south of the city use this corridor to travel NB in the morning and SB in the evening. The studied intersections (Figure 12.1c), in north to south order, are Thompson Rd., Harding St., Epler Ave., Southport Rd., Wicker Rd., County Line Rd., Fairview Rd., and Smith Valley Rd. These intersections run actuated-coordinated operation, most of them with a cycle length of 120 seconds, across four different weekday TOD plans.

- AM peak (AM): 05:00–09:15 hrs.
- Midday (MD): 09:15–14:30 hrs.
- PM peak (PM): 14:30–19:00 hrs.
- Evening (EV): 19:00–22:00 hrs.

In addition to showing the location for SR-37 in Indiana, Figure 12.1 shows the locations of the over 6 million July 2019 HB events in the state (Figure 12.1a). Of the 6 million HB events, almost 16,000 occurred along the 6.5-mile corridor (Figure 12.11c).

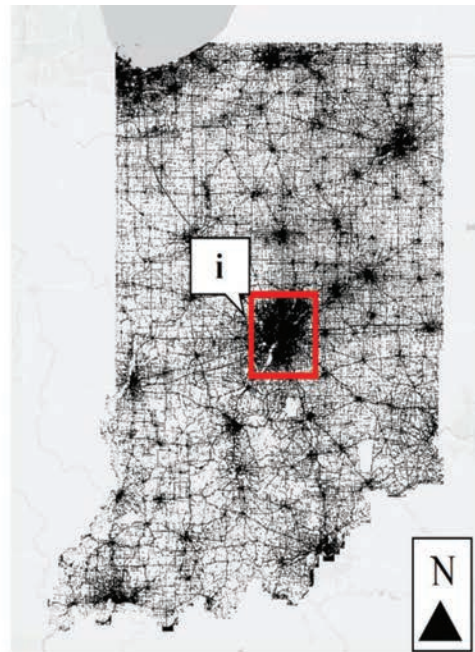
12.1.2 Hard-braking Events

The CV HB event data is explained in Chapter 2 and Chapter 3.

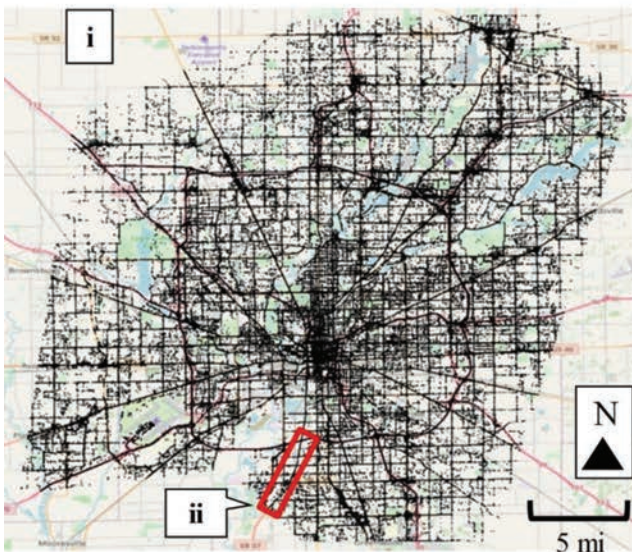
12.1.2.1 Methodology. The HB events analyzed are sorted by intersection, distance from stop bar, and vehicle speed when the event occurred. To obtain relevant HB events, geofence regions are drawn upstream along the through lanes for each approach. These geofences begin parallel to the opposing direction's stop bar and end 1,320 ft. (1/4 mi.) upstream. HB events that occur within those regions are retrieved, and the location of each event is compared to the intersection's stop bar to calculate the distance from the stop bar.

Figure 12.2a shows the HB events for an area along the study corridor. Figure 12.2b shows the upstream geofence regions and the retrieved HB events color-coded by speed. The 400 ft. boundary, relative to the stop bar, roughly corresponds to the location of the advance detectors at this intersection (129, 130).

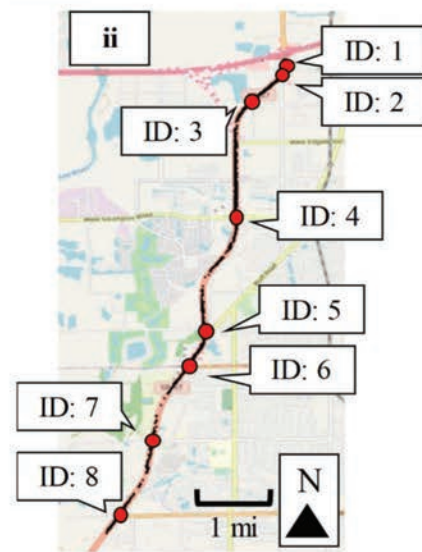
12.1.2.2 Analysis: hard-braking events by intersection. The impact of dilemma zone (129, 130) and queuing on HB needs to be further studied. Type II dilemma zone has been defined in previous literature as the road segment where there is a 10%–90% probability of a vehicle stopping at onset of yellow (129). The occurrence of HB events less than 400 ft. upstream from the stop bar (location of advance detector at 55 mph speed limit zones) at lower speeds are possibly due to vehicles stopping for the red light, whereas such occurrences at higher speeds could be due to dilemma zone issues. HB events occurring at distances greater



(a) 6,172,453 HB events in Indiana



(b) 1,687,533 HB events in Indianapolis



(c) 15,863 HB events along SR-37

Figure 12.1 Studied signalized corridor and July 2019 HB data (map data: OpenStreetMap).

than 400 ft. from the stop bar are potentially due to long queues during congested conditions.

Figure 12.3 shows the number of weekday HB events occurring at each intersection, stacked by distance from the stop bar, aggregated over the month of July 2019. For both NB and SB approaches, most of the HB events occur within 400 ft. of the stop bar. However, there are a few intersections (4 and 5 in SB, and 8 in NB) where over 40% of HB events occurred more than 400 ft. from the stop bar. To understand the temporal nature of the HB events and their distances from the stop bar, heatmaps of the event counts are generated.

Figure 12.4 illustrates heatmaps of the number of HB events on the NB approach by 30-minute periods across two distance categories: less than 400 ft. (Figure 12.4a) and more than 400 ft. (Figure 12.4b). For the less than 400 ft. category, most HB events occur during the AM, MD, and PM periods, with no clear patterns or trends. For the 400–1,320 ft. range, there are fewer HB events, except for Intersection 8 during the PM plan.

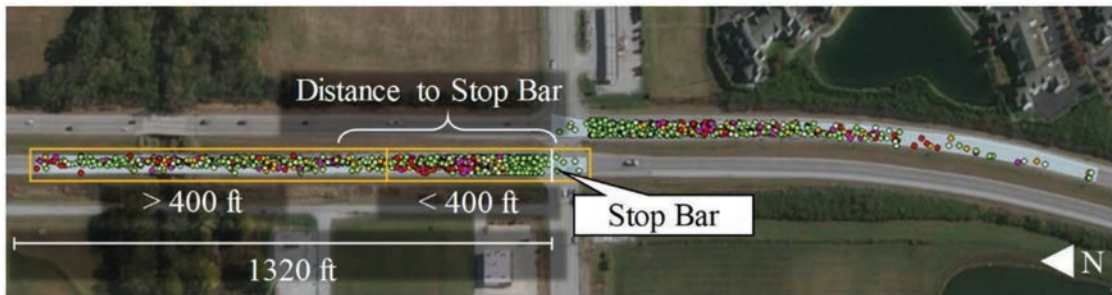
Figure 12.5 shows a heatmap similar to Figure 12.4, for the SB approach. HB events within 400 ft. of the intersection (Figure 12.5a) are generally higher for the PM plan, especially at intersection 8, Smith Valley Rd.

● Hard-braking event



(a) ~3,000 HB events around Southport Rd. (Intersection 4)

< 30 mph
 30 – 35 mph
 35 – 40 mph
 40 – 45 mph
 > 45 mph



(b) ~1,600 HB events captured by the NB and SB upstream geofence regions

Figure 12.2 HB event processing (map data: Google).

Figure 12.5b, which is comprised of events occurring beyond 400 ft., shows a different pattern than the NB approaches. Intersection 4 (Southport Rd.) and 5 (Wicker Rd.) experience a large number of HB events during the PM plan. This could be indicative of HB that occurs at the back of long queues during the PM peak period.

12.1.2.3 Analysis: hard-braking patterns by approach.

To further investigate the pattern of HB events, histograms stacked by speeds are plotted for different TOD plans over their distance from the stop bar. Figure 12.6 shows the HB events at the SB approach of Intersection 4, Southport Rd. During the PM time plan (Figure 12.6b), HB events occur consistently for the entirety of the evaluated area, with very few of those HB events occurring at speeds over 45 mph. The aerial image in Figure 12.6a shows that there are no driveways or bus stops in the region that could be contributing to these HB events; therefore, it can be assumed that these HB events are due to long-queues.

Figure 12.7 shows the HB events at the SB approach of Intersection 8, Smith Valley Rd. The PM plan (Figure 12.7b) stands out as having numerous HB events within the 0–400 ft. region. In some of the bins around 250 ft. upstream of the intersection, over 60% of those HB events occur at speeds above 45 mph, likely due to the occurrence of dilemma zone issues. Dilemma zone protection is often difficult on coordinated movements with heavy minor movements as more phases

compete for green time and coordinated phases are forced-off.

12.1.3 Crash Events

12.1.3.1 Crash data. Crash counts are aggregated by intersection using information gathered from Indiana’s online crash repository. Using the provided GPS information, crashes that are located along the corridor within 1,320 ft. of an intersection are assigned to that intersection. Crashes that are missing geolocation information are manually assigned to intersections on the study corridor, if applicable, by reading through the crash report’s narrative.

In Indiana, during July 2019, 17,652 crashes were reported, of which 24 occurred along the roughly 6.5-mile study corridor. Ten of those 24 crashes occurred in the vicinity of an intersection. To perform a statistical correlation test, the crash time frame is increased to a 4.5-year period between January 1st, 2016, and July 9th, 2020. This increases the intersection crash count to 551 crashes, of which 391 were weekday crashes and 261 of those were marked as rear-end collisions.

12.1.3.2 Distribution of crashes among intersections.

Figure 12.8 shows stacked bar graphs of the number of crashes categorized by manner of collision that occurred adjacent to the eight intersections along SR-37 on weekdays during the 4.5-year study period. The SB approach of Intersection 4 (Southport Rd.) stands

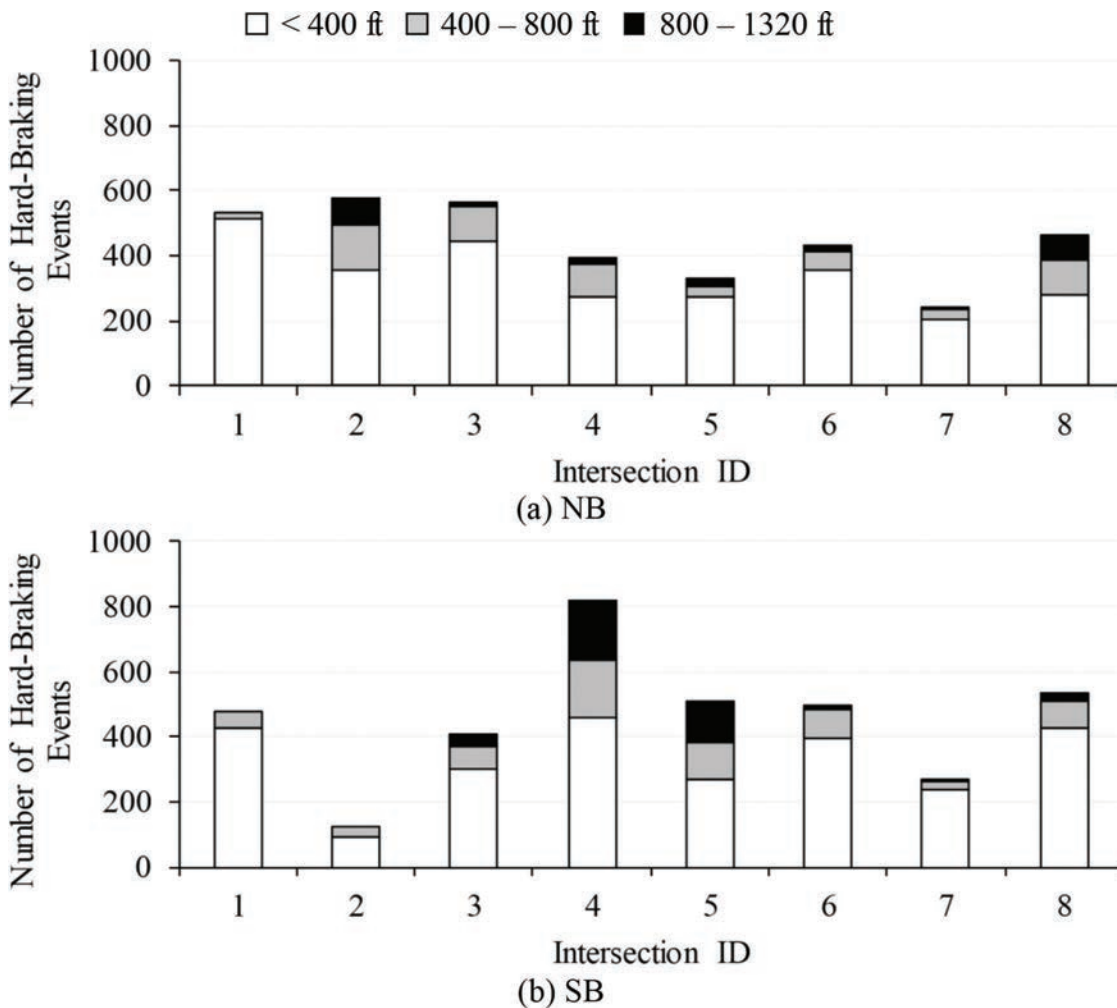


Figure 12.3 Number of weekday HB events by intersection and distance to the stop bar.

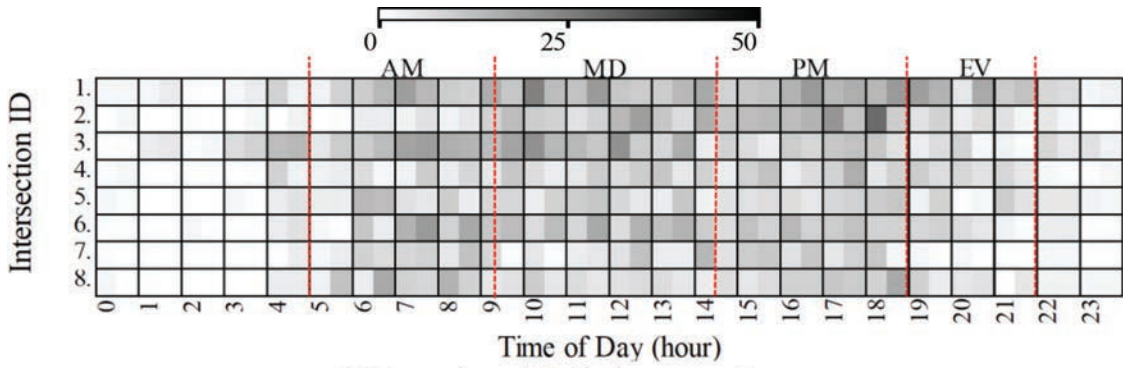
out as having the most crashes (71 crashes). Of those 71 crashes, 70% are rear-end collisions. Likewise, the second and third highest crash count approaches, SB Intersection 5 (Wicker Rd.) and NB Intersection 8 (Smith Valley Rd.), have 75% and 65%, respectively, of their total crash count as rear-end crashes. Overall, 65% of the 391 recorded weekday crashes on this corridor are rear-end collisions.

12.1.3.3 Methodology. Similar to the HB events, crashes are filtered by their different attributes. Crashes are characterized by their recorded manner of collision, distance from stop bar, and TOD. Finally, a statistical analysis is completed. The Spearman’s rank-order correlation (131), Pearson’s correlation (132), and Kendall’s correlation (133) tests are applied to the HB event and crash data for each intersection. Additionally, a sensitivity analysis is performed, and a preliminary model is presented. Rear-end crashes represented the largest group of crashes among the eight intersections; therefore, the statistical analysis focuses on the comparison between HB events and rear-end crashes.

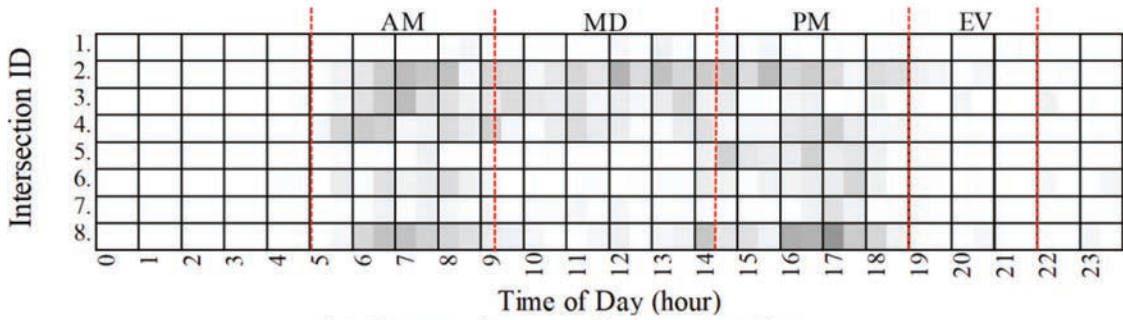
12.1.3.4 Analysis: crashes by TOD. Figure 12.9 presents a heatmap of weekday crashes aggregated over the study period. Crashes are binned by 30-minute periods and assigned to their respective intersections. In the SB approach (Figure 12.9b), Intersection 4 (Southport Rd.) and Intersection 5 (Wicker Rd.) stand out in the PM time frame as having a relatively large number of crashes. Visually, this is similar to Figure 12.5b, where Southport Rd. and Wicker Rd. also stood out as having a larger number of HB events at a distance larger than 400 ft. from the stop bar.

12.1.4 Correlation Between Hard-braking Events and Crashes

12.1.4.1 Correlation tests. In addition to the graphical visualizations highlighting similar patterns between crashes and HB events, several correlation tests are performed to determine if linear correlation is present. The aggregated July 2019 weekday HB events occurring over a 30-minute period are compared with the aggregated 4.5-year period rear-end crashes occurring over the same 30-minute period. First, a simple Spearman

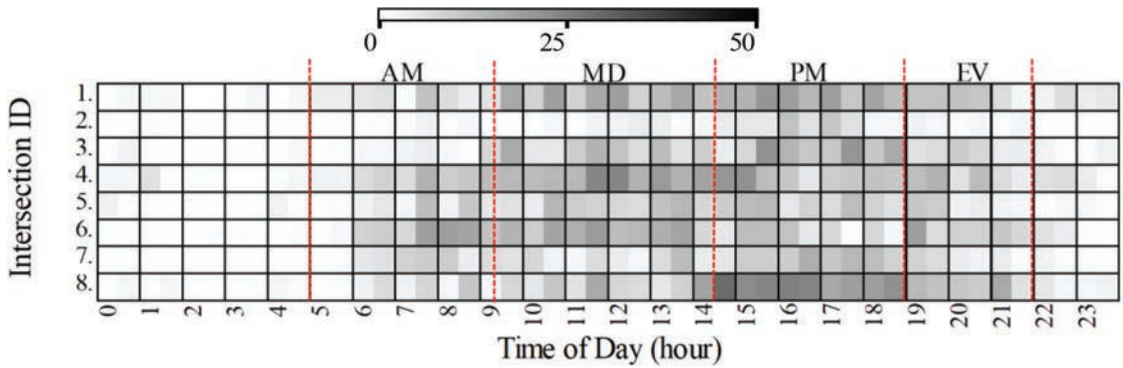


(a) Less than 400 ft. from stop bar

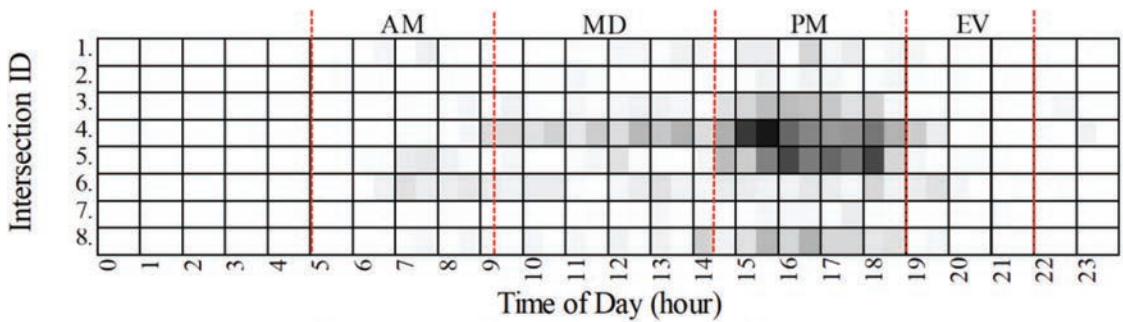


(b) Greater than 400 ft. from stop bar

Figure 12.4 Heatmap of NB weekday HB events by intersection in July 2019.



(a) Less than 400 ft. from stop bar

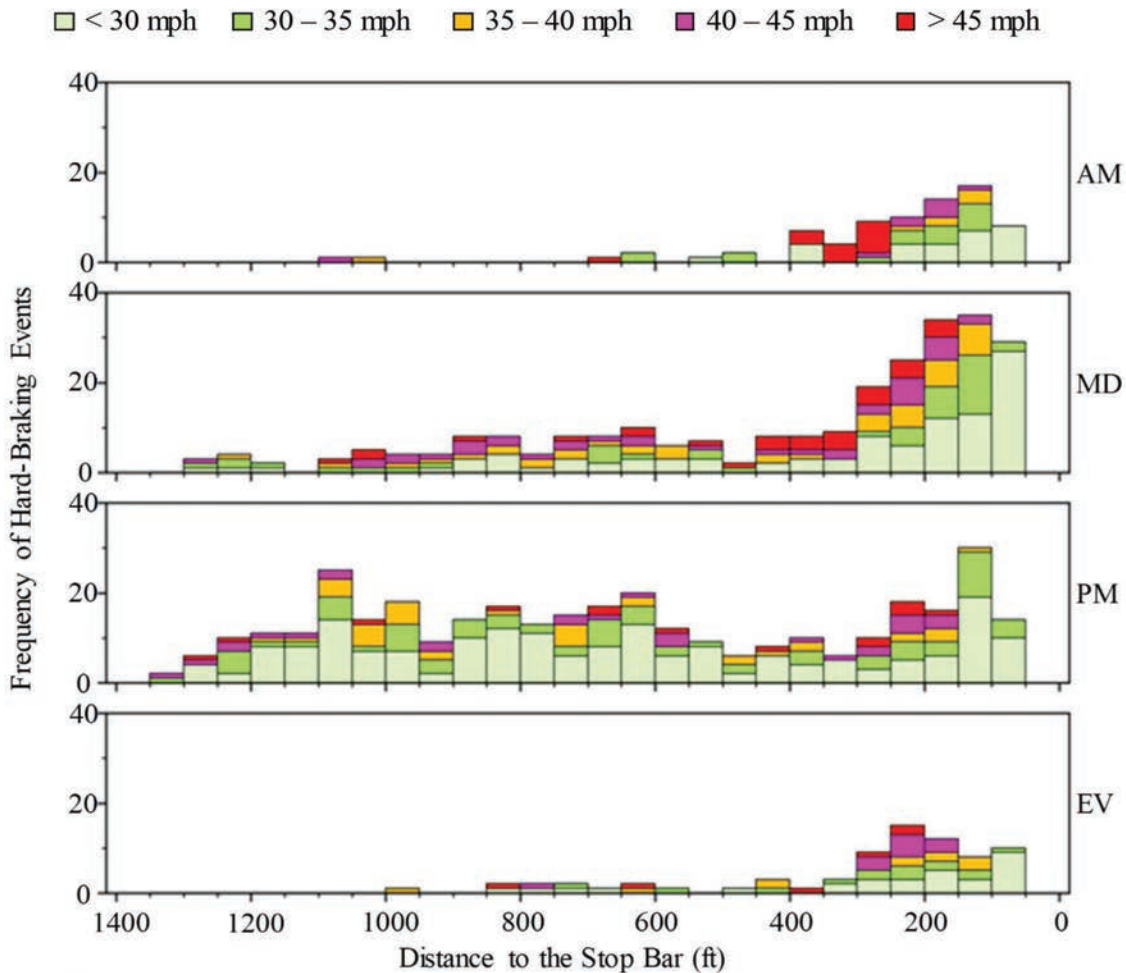


(b) Greater than 400 ft. from stop bar

Figure 12.5 Heatmap of SB weekday HB events by intersection in July 2019.



(a) Aerial view of the approach (map data: Google)



(b) Frequency of HB events by distance to the stop bar and speed for weekdays, July 2019

Figure 12.6 SB approach at Southport Rd. (Intersection 4).

rank-order correlation test (131) is conducted to evaluate the monotonic relationship between a pair of data. The correlation coefficient, r_s , represents the strength of that relationship. There are many interpretations in the literature (134, 135) for coefficient thresholds, but a conservative interpretation suggested by (136) is utilized and is presented in Table 12.1.

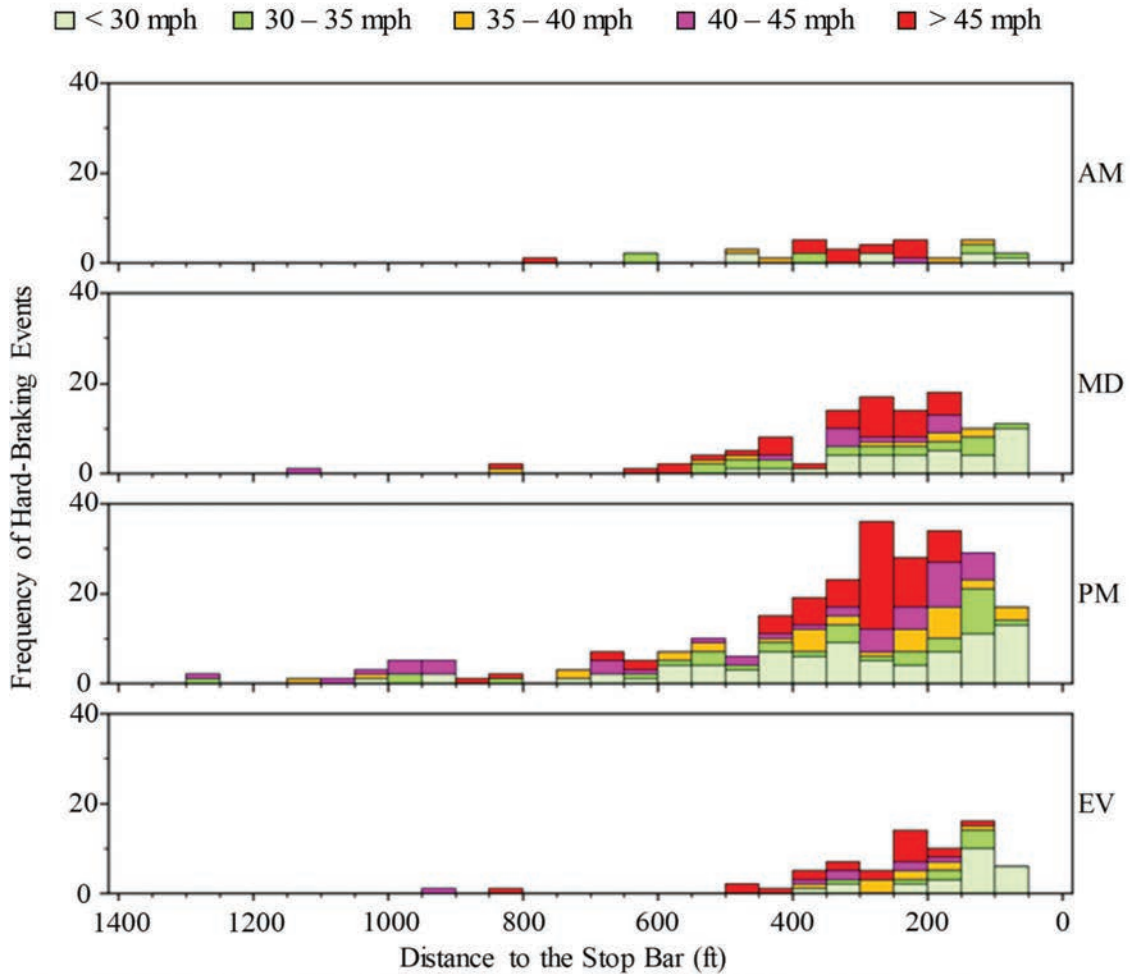
Table 12.2 and Table 12.3 show the results of the Spearman test conducted at 95% and 99% confidence levels (CL) and highlights intersections with a strong

correlation, for NB and SB, respectively. Results indicate a strong correlation between rear-end crashes and HB events past 400 ft. of the stop bar at NB Intersection 8 (Smith Valley Rd.), and SB Intersection 4 (Southport Rd.) and 5 (Wicker Rd.). A check in the strong correlation box is used if the r_s value exceeds the 0.6 threshold shown in Table 12.1.

Interestingly, while SB Intersection 8 (Smith Valley Rd.) experienced a high number of high-speed HB events within 250 ft. of the stop bar (Figure 12.7b), this



(a) Aerial view of the approach (map data: Google)



(b) Frequency of HB events by distance to the stop bar and speed for weekdays, July 2019

Figure 12.7 SB approach at Smith Valley Rd. (Intersection 8).

location does not exhibit a strong correlation to rear-end crashes as suggested by prior conflict models (137).

Along with the Spearman's rank-order correlation test, Pearson's (132) and Kendall's (133) correlation tests are performed. Table 12.4 presents the coefficient interpretations used for these tests (138).

The results for the Pearson's and Kendall's correlation test in SB direction are shown in Table 12.5 and Table 12.6, respectively. The two SB intersections that are shown by the Spearman's correlation test to have a

strong correlation are also shown to have a moderate correlation by the Pearson's and Kendall's correlation tests. In addition to those intersections, the Pearson's correlation test also identifies SB Intersections 1 (Thompson Rd.) and 4 (Southport Rd.) as having a moderate correlation between number of HB events and rear-end crashes in the under 400 ft. region.

12.1.4.2 Sensitivity analysis. To determine if 1 month of HB event data is sufficient to suggest a reasonable

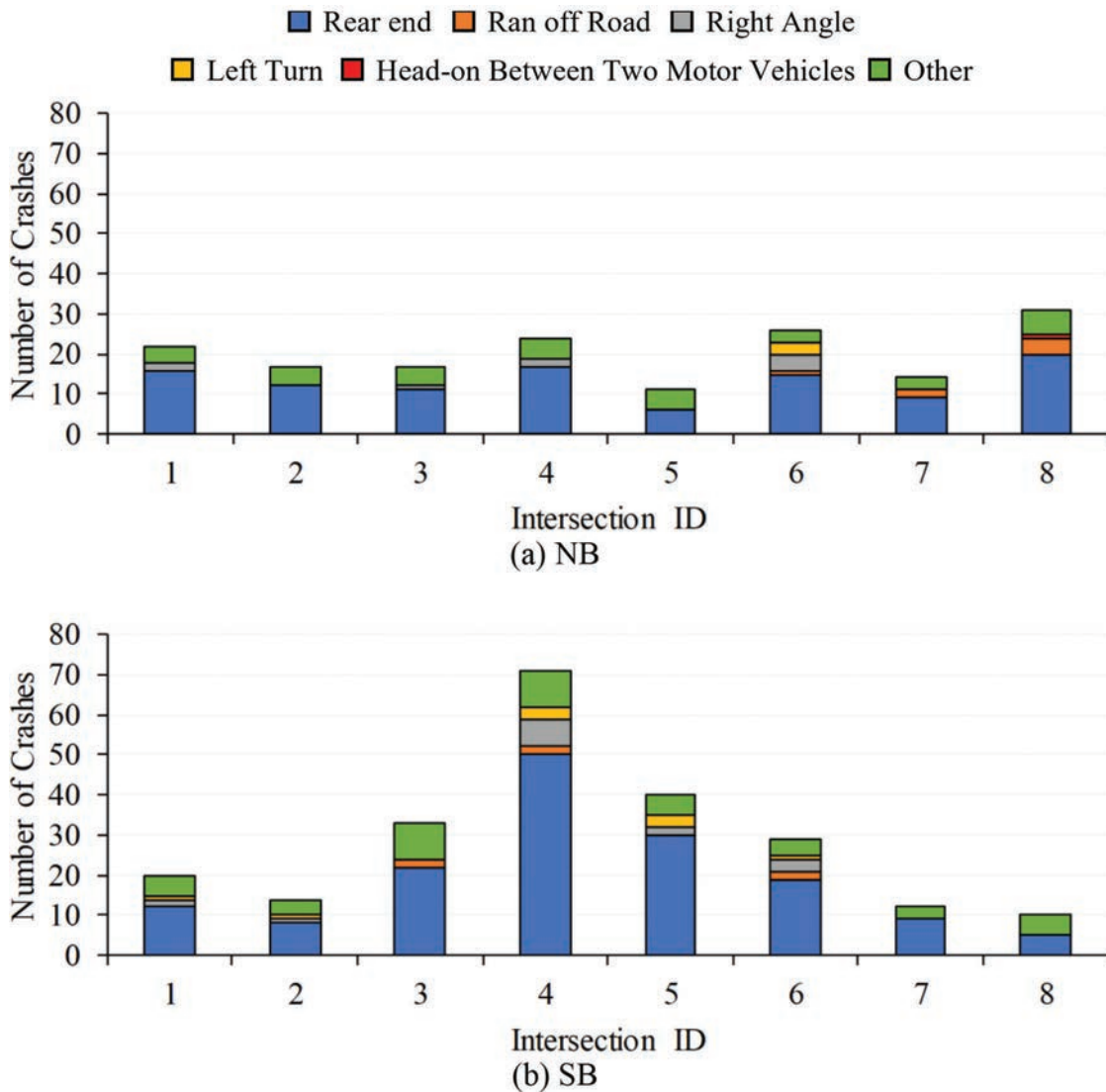


Figure 12.8 Number of weekday crashes by intersection and type on SR-37, between January 1st, 2016, and July 9th, 2020.

correlation between HB events and crashes, a sensitivity analysis using Spearman’s correlation is performed. While this evaluation primarily uses 1 month of HB data collected from July 2019, the sensitivity analysis also includes data from July and August 2019. Figure 12.10 shows the results of this assessment. The two plots in Figure 12.10 show that the r_s values plateau around 4 weeks’ worth of data. This suggests that 1 month of HB data is sufficient to result in a reliable correlation with over 4.5 years’ worth of crash data.

12.1.5 Statistical Modelling

To explore the relationship between number of HB events, volumes, and other intersection attributes and the number of crashes, a statistical model is developed. The response variable in this study, the number of

crashes across the eight intersections by 30-minute bins, is a discrete, nonnegative integer which is typically modeled by a count data model. Commonly, these count data models are either a Poisson model or a negative binomial regression model (139).

The Poisson model, which is often used to model rare-event count data, like crashes, requires the mean and variance of the response variable to be equal. Further, the Poisson model assumes that the response variable y has a Poisson distribution, and that the logarithm of expected values can be modeled as linear. The Poisson probability density function is given by

$$Pr\{Y = y_i\} = \frac{e^{-\mu}\mu^{(y_i)}}{y_i!} \quad (\text{Eq. 12.1})$$

where μ is the Poisson parameter. When $\mu > 0$, the mean and variance are equal to the expected number

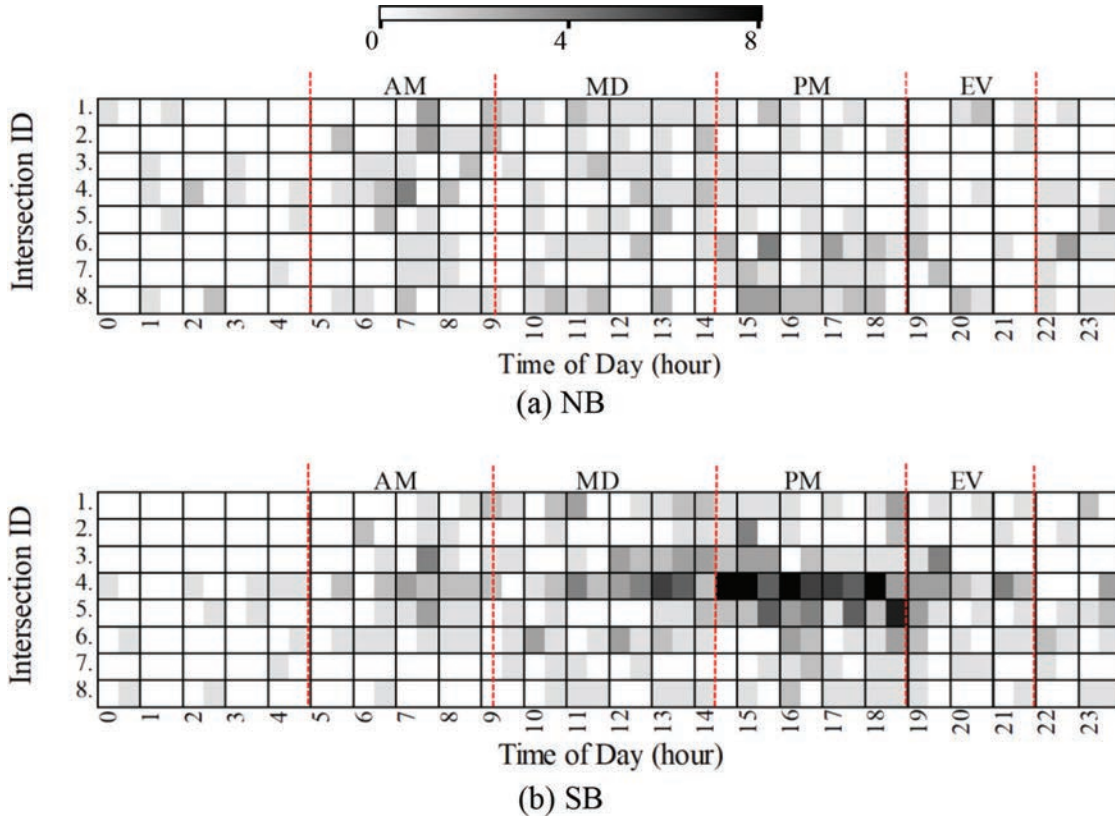


Figure 12.9 Frequency heatmap of weekday crashes between January 1st, 2016, and July 9th, 2020.

TABLE 12.1
Interpretation of correlation coefficient–Spearman

Correlation Coefficient	Correlation Significance
0.80–1.0	Very strong
0.60–0.79	Strong
0.40–0.59	Moderate
0.20–0.39	Weak
0.00–0.19	Very weak

$E(Y)$. Typically, the relationship between the explanatory variables and the Poisson parameter is a log-linear model,

$$\mu = e^{\beta X_i} \quad (\text{Eq. 12.2})$$

where X_i is a vector of explanatory variables and β is a vector of estimable parameters.

The data is considered over-dispersed when the variance of the response variable is larger than its mean. This can typically be modeled using a negative binomial model, which can be derived from Equation 12.2. For each observation i

$$\mu_i = e^{(\beta X_i + \varepsilon_i)} \quad (\text{Eq. 12.3})$$

where e^{ε_i} is a Gamma-distributed disturbance term with a mean of 1 and a variance of α (139). The added

disturbance term allows the variance and the mean to differ as shown below

$$VAR[y_i] = E[y_i][1 + \alpha E[y_i]] + \alpha E[y_i]^2 \quad (\text{Eq. 12.4})$$

The probability density function for the negative binomial model is defined as

$$P(y_i) = \frac{\Gamma((1/\alpha) + y_i)}{\Gamma(1/\alpha) + y_i!} \left(\frac{(1/\alpha)}{(1/\alpha) + \mu_i} \right)^{1/\alpha} \left(\frac{\mu_i}{(1/\alpha) + \mu_i} \right)^{y_i} \quad (\text{Eq. 12.5})$$

The Poisson model is a special case of the negative binomial model for when α , also known as the over-dispersion parameter, is considered to be equal to zero. The generalized linear model of the mean μ on the predictor vector X_i is formulated as

$$L(\mu) = \beta_i X_i^T \quad (\text{Eq. 12.6})$$

Table 12.7 shows the descriptive statistics for the model variables. The Poisson and negative binomial models are considered. The variance of the response variable is larger than the mean of the response variable indicating the data may be over-dispersed and favoring a negative binomial model. However, under the negative binomial model the over-dispersion parameter is not significant. Therefore, the Poisson model is selected.

TABLE 12.2

Spearman's correlation between intersection rear-end crash counts and number of HB events by distance for NB SR-37

Int. ID	0–400 ft.			400–1,320 ft.		
	r_s	p value	Strong Correlation	r_s	p value	Strong Correlation
1	0.23	0.11		0.21	0.15	
2	0.10	0.52		0.44 ¹	0.002	
3	0.25	0.09		0.33 ²	0.02	
4	0.16	0.28		0.28	0.06	
5	-0.15	0.31		0.33 ²	0.02	
6	0.20	0.18		0.2	0.19	
7	0.34 ²	0.02		0.15	0.32	
8	0.42 ¹	<0.001		0.65 ¹	<0.001	✓

¹Significant at 99% CL.²Significant at 95% CL.

TABLE 12.3

Spearman's correlation between intersection rear-end crash counts and number of HB events by distance for SB SR-37

Int. ID	0–400 ft.			400–1,320 ft.		
	r_s	p value	Strong Correlation	r_s	p value	Strong Correlation
1	0.54 ¹	<0.001		0.15	0.32	
2	0.15	0.3		0.08	0.58	
3	0.55 ¹	<0.001		0.57 ¹	<0.001	
4	0.53 ¹	<0.001		0.72 ¹	<0.001	✓
5	0.44 ¹	0.002		0.61 ¹	<0.001	✓
6	0.46 ¹	0.001		0.31 ²	0.03	
7	0.12	0.14		0.22	0.13	
8	0.33 ²	0.022		0.23	0.11	

¹Significant at 99% CL.²Significant at 95% CL.

TABLE 12.4

Interpretation of correlation coefficient—Pearson and Kendall

Correlation Coefficient	Correlation Significance
0.90–1.0	Very high positive correlation
0.70–0.90	High positive correlation
0.50–0.70	Moderate positive correlation
0.30–0.50	Low positive correlation
0.00–0.30	Negligible correlation

Table 12.8 presents the results of the data. Of the seven variables, only two, HB and volume, are found to be significant. The McFadden ρ^2 is an indicator of the overall fit of the model and is given by

$$\rho^2 = 1 - \frac{LL(\beta)}{LL(0)} \quad (\text{Eq. 12.7})$$

where $LL(\beta)$ is the log-likelihood at convergence with a parameter vector β and $LL(0)$ is the initial log-likelihood.

Varying between zero and 1, a ρ^2 closer to one indicates a better model. The ρ^2 statistic for the given model is estimated to be 0.19, pointing to the preliminary nature of this model and the limited nature of the HB event data set. The parameters show that the

number of rear-end crashes increase significantly with an increase in HB event counts, which is fairly intuitive. Additionally, it also follows naturally that an increase in volumes will lead to an increase in rear-end crash counts according to the model's parameters.

12.1.6 Discussion

Crash data over a period of 4.5 years at eight signalized intersections are compared with 1 month of HB data to determine if there is a statistical relationship. Graphical illustrations comparing aggregated HB events and crashes (Figure 12.4, Figure 12.5, and Figure 12.9) demonstrate a visual relationship between the two data sets. Statistical tests show that three intersections (8 NB, 4 SB, and 5 SB) have a strong correlation between rear-end crashes and HB events occurring past 400 ft. from the stop bar (Table 12.2 and Table 12.3). The same three intersections show high HB counts, farther away than 400 ft. from the stop bar, in comparison with the rest of the corridor (Figure 12.4b and Figure 12.5b). This could indicate that the HB and rear-end crashes correlation is stronger at locations where vehicles hard-brake far away from the stop bar (perhaps due to long queues).

TABLE 12.5
Pearson’s correlation between intersection rear-end crash counts and number of HB events by distance for SB SR-37

Int. ID	0–400 ft.			400–1,320 ft.		
	r_s	p value	Moderate Correlation	r_s	p value	Moderate Correlation
1	0.54	<0.001	✓	0.06	0.68	
2	0.07	0.63		0.06	0.67	
3	0.42	0.00		0.40	0.00	
4	0.51	<0.001	✓	0.66	<0.001	✓
5	0.43	0.00		0.62	<0.001	✓
6	0.44	0.00		0.26	0.07	
7	0.08	0.57		0.12	0.41	
8	0.34	0.02		0.23	0.12	

TABLE 12.6
Kendall’s correlation between intersection rear-end crash counts and number of HB events by distance for SB SR-37

Int. ID	0–400 ft.			400–1,320 ft.		
	r_s	p value	Moderate Correlation	r_s	p value	Moderate Correlation
1	0.45	<0.001		0.14	0.32	
2	0.14	0.28		0.08	0.58	
3	0.44	<0.001		0.48	<0.001	
4	0.40	<0.001		0.61	<0.001	✓
5	0.36	0.00		0.53	<0.001	✓
6	0.39	0.00		0.28	0.03	
7	0.11	0.40		0.21	0.13	
8	0.28	0.02		0.21	0.11	

Results from the sensitivity analysis showed that a sample size of at least 4 weeks of HB events is needed to result in reliable correlation with crash data (Figure 12.10). Finally, results from the statistical modelling illustrated that the number of crashes can significantly increase with higher number of HB events and volume (Table 12.8).

The correlation shown between rear-end crashes and HB events is particularly beneficial to agencies because statistically valid data can be collected in a month or two, instead of waiting the traditional 3–5 years for a significant number of crashes to occur. Histograms like the one shown in Figure 12.6 and Figure 12.7, can provide agencies with a high-fidelity perspective on exactly where those events may be clustered to assess potential mitigation measures. Additionally, the techniques described are also scalable to larger numbers of intersections and corridors. Agencies could implement this method to assess all traffic signals within an urban area or an entire state.

Furthermore, HB events could potentially be used to assess safety at a variety of scenarios and locations other than signalized intersections; for example, at interstate work zones (140). These capabilities can provide agencies with proactive data-driven tools to evaluate safety concerns that enable the prompt implementation of solutions.

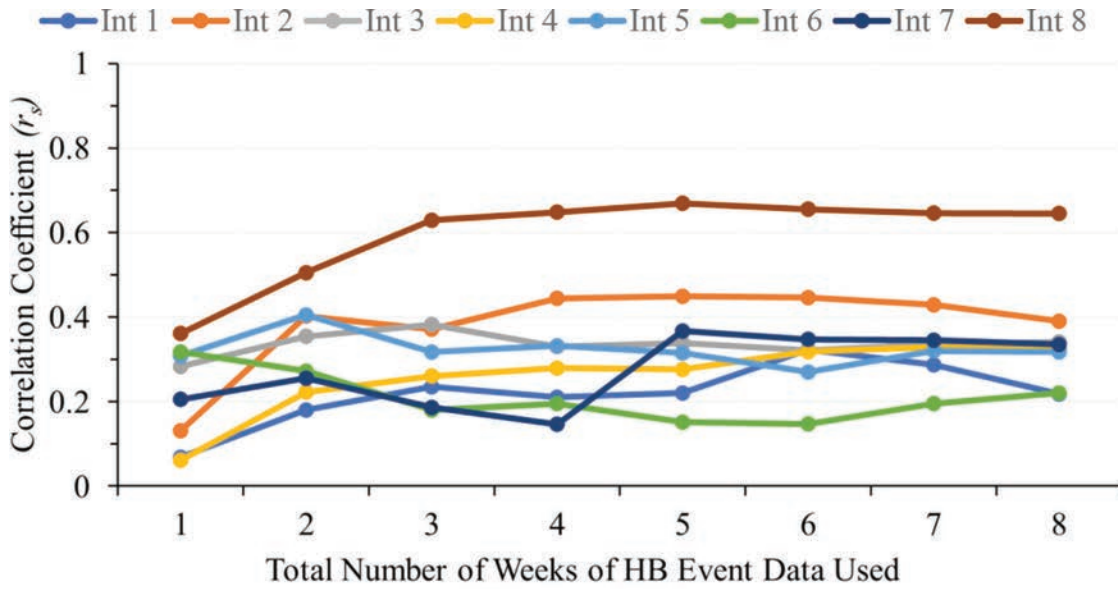
The contents presented in this section are based on (16), which is an Open Access article published under a [Creative Commons Attribution 4.0 International License](#).

12.2 Driver Behavior Assessment After Changing Left-Turn Phasing

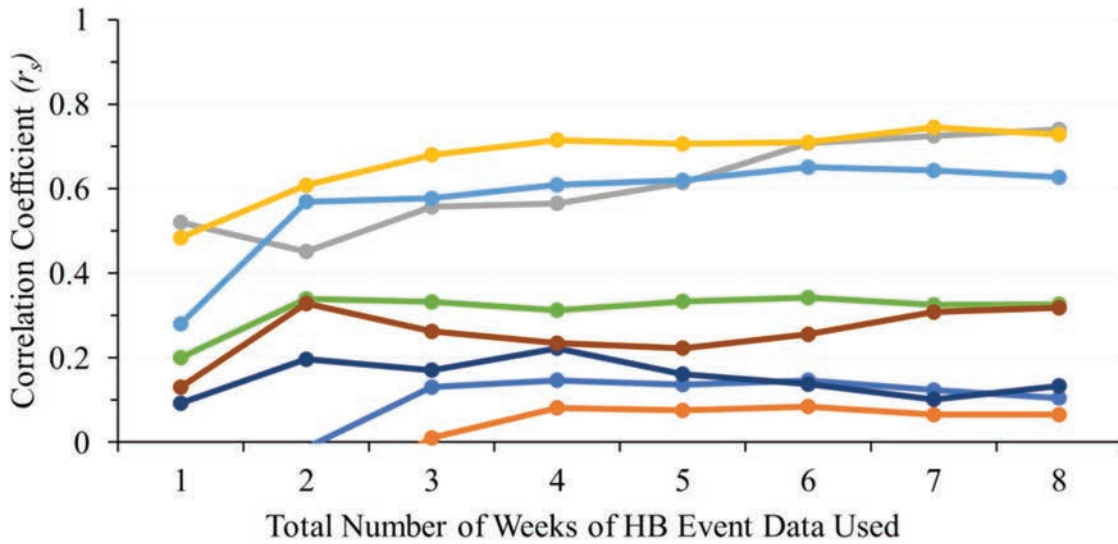
There are three different types of left-turn traffic signal phasing used in the United States: protected, permitted (or permissive), and protected-permitted. Protected-only left-turns, in which only a static green arrow is shown at the traffic signal, are usually considered the safest phasing type since it eliminates driver gap acceptance decisions. However, this usually results in vehicles having to wait for longer periods that increase delay. On the other hand, protected-permitted left-turns increase efficiency by not only providing a static green arrow, but also a flashing yellow arrow (FYA) where drivers must assess if there is a sufficient gap for them to safely make a left-turn (141–144).

Traditionally, a combination of crash data, traffic volumes, and engineering judgement are used to select the type of left-turn operation. This approach often takes several years to accumulate statistically significant crash data and engineering judgement can vary considerably.

This section utilizes CV data sets to evaluate driver behavior and signal performance by analyzing the change in HA, delay, progression, and saturation before and after a left-turn phasing type change (17). This provides a framework to assess left-turn phase changes without the need for long data collection periods, provides quicker feedback than traditional crash studies, and is more objective than engineering judgement.



(a) NB 400–1,320 ft.



(b) SB 400–1,320 ft.

Figure 12.10 Sensitivity analysis for Spearman correlation between HB events and rear-end crashes for 8 weeks in July and August 2019.

12.2.1 Protected-Permitted to Protected-Only Transition

The effects on vehicle behavior and signal performance after changing the EB-left turn phasing at the intersection of US-40 and German Church Rd., located east of Indianapolis, are analyzed. The movement on Figure 12.11a was changed from a FYA protected-permitted (Figure 12.11b, callout i) to a three-section protected-only (Figure 12.11c, callout ii) on June 24th, 2020. The EB approach at this intersection has four lanes: a dedicated left-turn, two through lanes, and a dedicated right-turn. The objective of the change was to improve safety for the left-turn due to crash occurrences during the FYA permitted phase.

12.2.2 Evaluation of Driver Acceleration at the Traffic Signal

Driver behavior can be significantly affected based on the type of traffic signal phasing implemented. When a driver is waiting for a gap to make a left-turn during a FYA, they may decide to aggressively accelerate through a small gap. The HAs typically occur after the stop bar (Figure 12.11a, callout iii) while waiting for a gap in oncoming traffic. These events are a potential indication of risk since vehicles have to hard-accelerate to make it through an opening.

Figure 12.12 shows the percentage of sampled vehicles turning left that hard-accelerated from a 3-

TABLE 12.7
Descriptive statistics for model variables

Variable Name	Description	Mean	Std. Dev
Crash	Crash count by 30-minute bins	0.34	0.71
Hard-braking	Hard-braking event count totaled for July	2.41	4.87
Volume	Volumes by 30-minute bins	1,042.58	631.80
Lanes	Number of lanes	4.25	0.43
Barrels	Barrel median present (1 = “yes”, 0 = “no”)	0.19	0.39
Cement	Cement median present (1 = “yes”, 0 = “no”)	0.19	0.39
Right	Exclusive right present (1 = “yes”, 0 = “no”)	0.88	0.33
Left	Exclusive left present (1 = “yes”, 0 = “no”)	0.94	0.24

TABLE 12.8
Estimation results

Variable Name	Estimate	P-value
Hard-braking ¹	0.50	<0.0001
Volume ¹	0.0012	<0.0001
Number of observations	768	–
Restricted log-likelihood (contestant only)	-602.34	–
Log-likelihood at convergence	-490.64	–
Chi-squared	223.40	–
McFadden ρ^2	0.19	–

¹Significant at 99% CL.

week period before (Figure 12.12a, ~1,500 samples) and after (Figure 12.12b, ~1,600 samples) the phasing change, as well as their difference (Figure 12.12c). The percentages are organized by the distance to the stop bar where the events occurred (negative values being downstream of the stop bar) and color-coded based on the vehicle’s speed at the time the event was recorded.

During the 3 weeks analyzed before the phasing change (Figure 12.12a), over 5.5% of the sampled vehicles turning left hard-accelerated after crossing the stop bar. Even though most of the HA events lie within the first 15 meters (49 ft.) after the stop bar, there are events still occurring even after 25 meters (82 ft.) past the stop bar (callout i).

In contrast, during the three weeks analyzed after the phasing change (Figure 12.12b), less than 3.4% of the sampled vehicles turning left had to hard-accelerate after crossing the stop bar. The highest percentage decrease occurred between 10 and 15 meters past the stop bar (callout ii vs. iii), and HA events 25 meters after the stop bar completely disappeared (callout i vs. iv). A small increase between 20 and 25 meters past the stop bar (callout v) could indicate a possible rise of yellow/red-light-running. The left-turn phasing change impact on traffic signal performance is assessed below.

12.2.3 Evaluation of Traffic Signal Efficiency

12.2.3.1 PPD assessment. Besides the effects on hard-acceleration, traffic signal performance can also be notably impacted by a change on a left-turn phasing

type. PPDs are used to calculate HCM LOS (64), AOG, and SF at the evaluated movement.

Figure 12.13 shows PPDs of vehicle trajectories that traveled EB-left at US-40 and German Church Rd. before (June 15th–19th, 2020, Figure 12.13a) and after (July 13th–17th, 2020, Figure 12.13b) the phasing change. It can be observed how vehicles tend to inch forward after the stop bar when having a protected-permitted phase (Figure 12.13a, callout i) while with a protected-only control they tend to stay static until being given a green light (Figure 12.13b, callout ii).

Figure 12.13a shows how most of the trajectories with the longest delay approach the intersection approximately 70 seconds behind the FFT (callout iii). In comparison, Figure 12.13b shows that the trajectories with most delay have around a 90 second difference compared to the FFT (callout iv), signifying an increase on delays and a deterioration of the LOS.

For the time periods analyzed in Figure 12.13, the percentage of sampled vehicles having a LOS F went from 6% to 25% after implementing the protected-only left-turn phasing. This is not surprising since green time for left-turning vehicles is effectively reduced, but the combination of these graphics and objective quantitative measurements of change in delay are valuable information for traffic engineers and illustrate the value of the CV data sets.

Further, after a left-turn phasing type change from protected-permitted to protected-only, AOG is expected to decrease since vehicles usually have a shorter period in which they are allowed to proceed through the intersection. A vehicle that arrives during the permitted phase and stops to wait for a gap is not considered AOG. For the time periods analyzed in Figure 12.13, AOG went from 27% to 25% after implementing the protected-only left-turn phasing.

Split failures are identified from CV trajectories turning left when a vehicle stops more than once before exiting the intersection and it has an approach delay longer than one stop trajectories for the same 30-minute TOD period. This is necessary to eliminate the effects of additional stops while waiting for a gap during a permitted phase. Figure 12.13a shows a trajectory that stops twice before exiting the intersection (callout v) but is not categorized as having experienced a split failure since its delay is not greater than other one stop



(a) Aerial view



(b) Protected-permitted signalization at the study location



(c) Protected-only signalization at the study location

Figure 12.11 Left-turn change from protected-permitted to protected-only at US-40 and German Church Rd. (map data: Google, IndianaMap Framework Data, Maxar Technologies, and USDA Farm Service Agency).

trajectories that occurred during the same 30-minute TOD period. Therefore, it is assumed that the second stop occurred during the permitted phase. For the time periods analyzed in Figure 12.13, there is no SF change.

12.2.3.2 Temporal comparison of traffic signal performance measures. To provide a holistic view on the impact of the implementation of protected-only left-turn on traffic signal performance, Figure 12.14 shows changes on SF, AOG, and LOS by TOD before (June 15th–19th, 2020) and after (July 13th–17th, 2020) the phasing change.

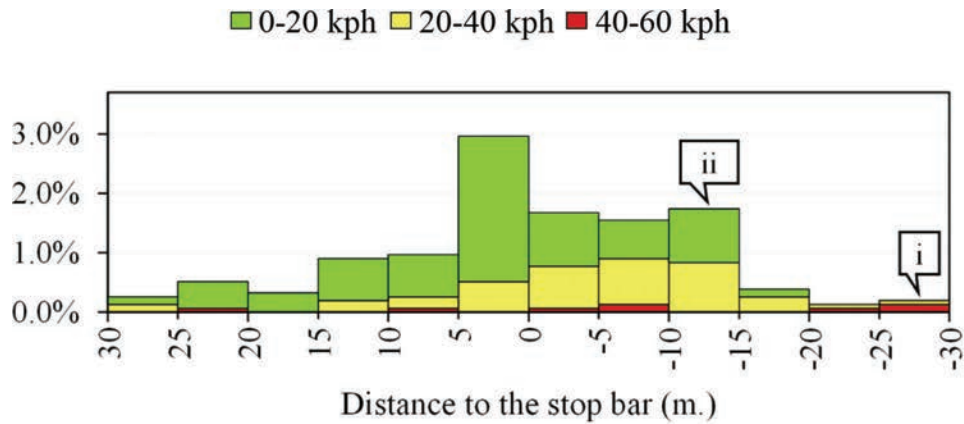
- SF: The percentage of sampled vehicles experiencing split failures does not have a notable change.
- AOG: There is a significant decrease in arrivals on green, especially during the morning (07:00–11:00) and evening (19:00–22:00) hours.
- LOS: There is a substantial increase in LOS E and F throughout the day.

12.2.4 Results and Discussion

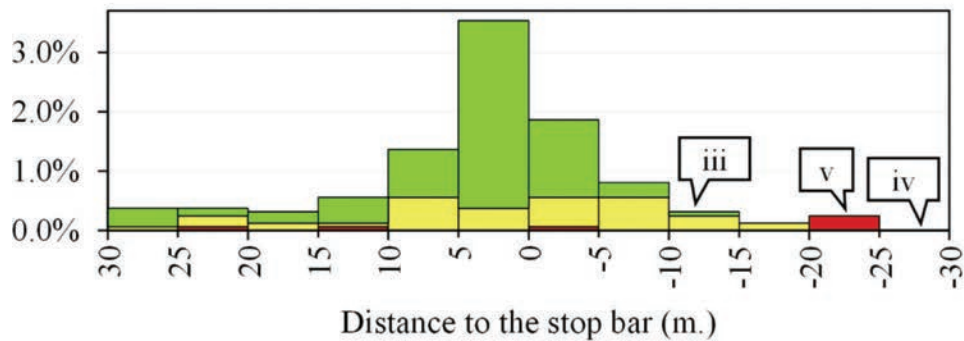
To evaluate the impact of changing the left-turn phasing at US-40 and German Church Rd. from protected-permitted to protected-only, HA events are assessed, and traffic signal performance calculated for all the weekdays in January, June, and July 2020. In total, over 7,000 individual trajectories, 172,000 way-points, and 700 HA events are analyzed.

Table 12.9 shows the HA counts and the percentage of sampled vehicles turning left that hard-accelerate within a 30-meter (98 ft.) distance before and after the stop bar. A 14% decrease (from 101 to 87) on HA events after the stop bar is calculated between January and July 2020. This change is likely due to the fact that drivers did not have to evaluate oncoming traffic for sufficient gaps and accelerate from a stop to cross traffic.

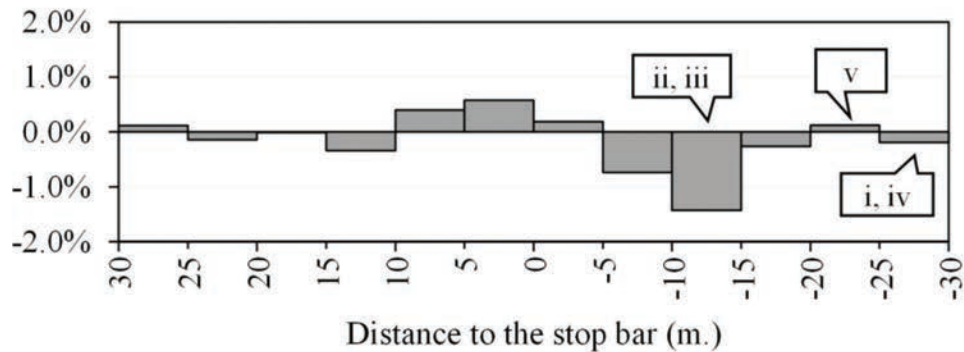
Table 12.10 shows the calculated SF, AOG, and average control delay. There are no significant changes



(a) Weekdays with protected-permitted phasing: 1st–19th June, 2020



(b) Weekdays with protected phasing: 13th–31st July, 2020



(c) Difference between (a) and (b)

Figure 12.12 Percentage of sampled vehicles turning left that hard-accelerate.

in SF; however, AOG decreased from 44% in January to 17% in July, and the average control delay rose 28 seconds (from LOS C to E) during the same period. These results are expected as the protected phasing reduces the effective green time that a left-turning vehicle has.

The discussed methodology to assess efficiency and surrogate safety measures can be systematically scaled,

which is particularly valuable for agencies that want to evaluate the effect that different control techniques have on performance and driver behavior.

Although the fixed threshold of 8.76 ft/s^2 used to define HB and HA events showed promising results in this chapter, it is anticipated that alternative thresholds may provide improved correlation with crash data and better describe driver behavior.

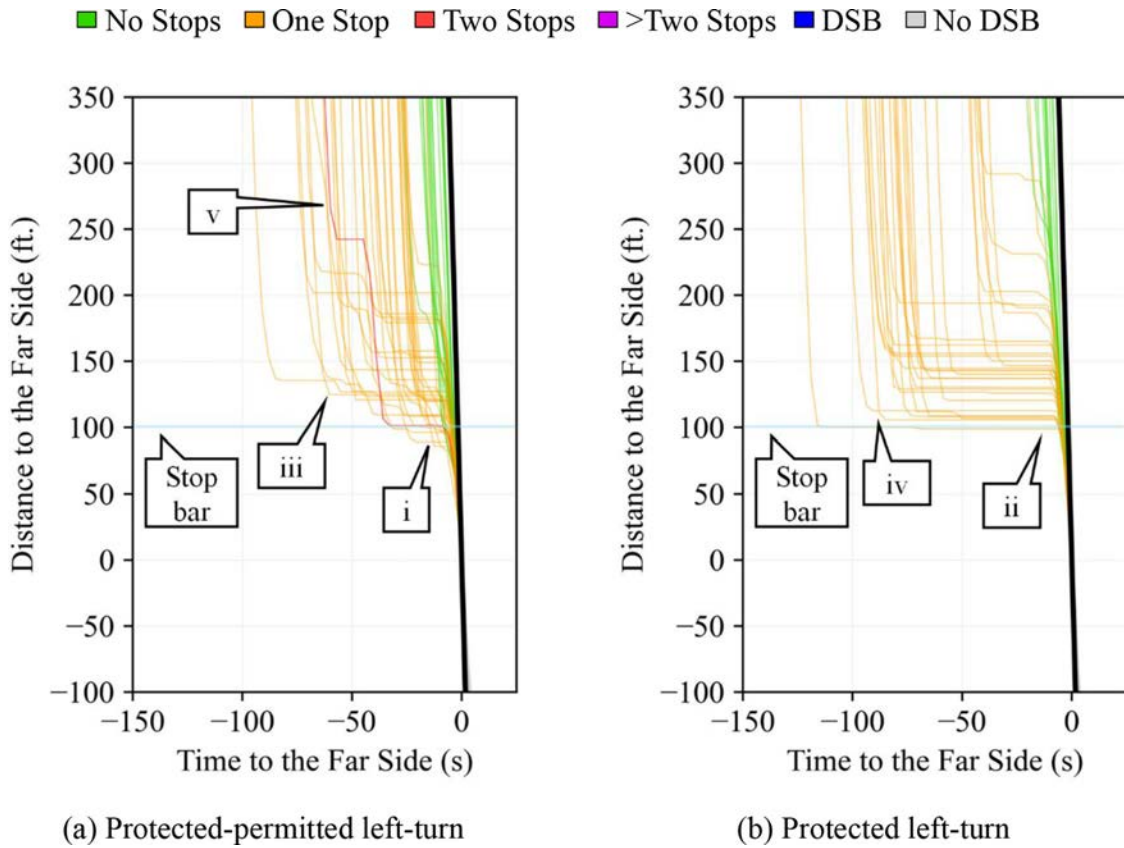
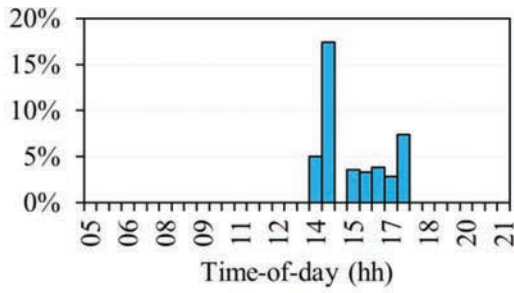


Figure 12.13 PPDs of vehicle trajectories traveling EB-left between 11:00 and 13:00 hrs.

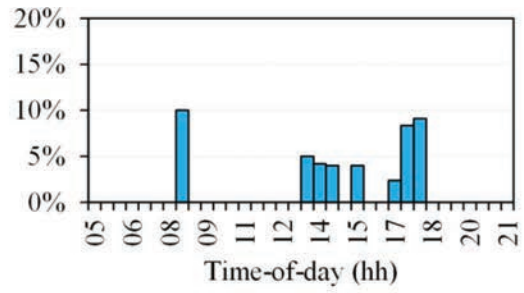
TABLE 12.9
2020 monthly weekday EB left-turn HA

Month	HA Count	HA Pct. (%)	HA Count ASB	HA Pct. ASB (%)
January	210	9	101	4
June ¹	280	12	131	6
July	253	10	87	3

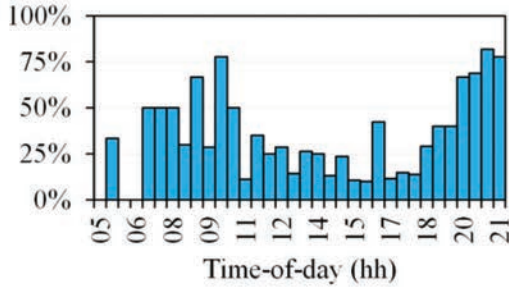
¹Protected left-turn implementation on June 24th.
Note: ASB = after-stop-bar.



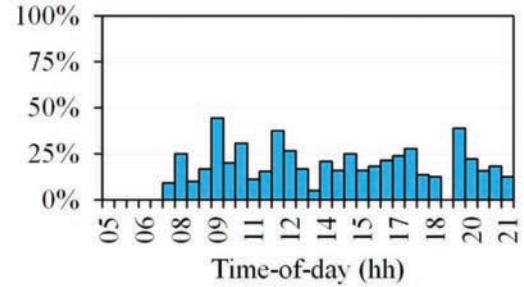
(a) SF before the transition



(b) SF after the transition

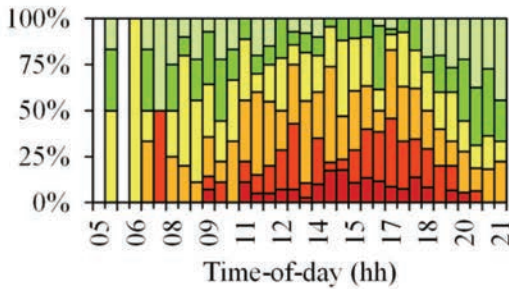


(c) AOG before the transition

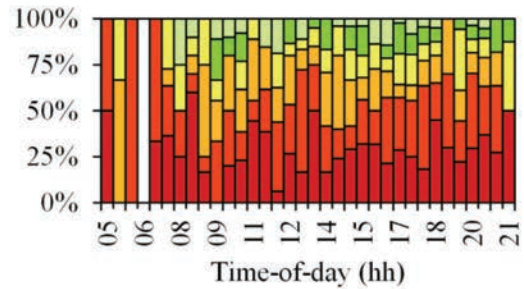


(d) AOG after the transition

Legend: A (light green), B (green), C (yellow), D (orange), E (red), F (dark red)



(e) Percentage of sampled vehicles by LOS before the transition



(f) Percentage of sampled vehicles by LOS after the transition

Figure 12.14 EB left-turn traffic signal performance measures before and after the phasing transition.

TABLE 12.10
2020 monthly weekday EB left-turn traffic signal performance measures

Month	SF (%)	AOG (%)	Average Control Delay (s/veh)
January	1	44	34
June ¹	2	31	45
July	1	17	62

¹Protected left-turn implementation on June 24th.

13. SCALABILITY

One of the main benefits of generating CV-based traffic signal performance measures is that analyses are easily scalable due to the ubiquity of the data. For example, Figure 13.1 shows over 160,000 trajectory waypoints collected during a 30-minute period in Indiana and around Indianapolis. Even with samples collected over such a small period, significant network coverage is provided. Further, since most CV studies do not require labor-intensive field data collection or cost-prohibiting detection and communication equipment, signal evaluation techniques can be implemented anywhere.

During this project, the performance of thousands of signals was evaluated, and a web dashboard called “PM Heatmap” was developed to facilitate the reporting of results.

13.1 PM Heatmap Web Dashboard

In the PM Heatmap, traffic signal performance is estimated with PPDs (Chapter 5) generated from the linear referencing and data-driven movement detection techniques presented in Chapter 3 and Chapter 4. Therefore, the only manual effort required to evaluate the performance at a traffic signal is the identification of the intersection’s center and retrieval radius needed to assign vehicle movements. This manual task usually

takes less than 5 minutes and hands-off processing of 1 month of CV trajectory data for an intersection is on average completed in under 1 hour at a cost of \$0.09 following the data management suggestions discussed in Chapter 2.

Figure 13.2 shows the PM Heatmap web dashboard. Users of the platform can individually select the intersections (callout i) and time periods of interest (callout ii). For the signals selected, AOG, SF, DSB, and LOS results are available (callout iii) for all the left-, through-, and right-turns (callout iv). Performance measures are presented in heatmap format (callout v), as discussed in Chapter 7, to facilitate the identification of challenges by TOD and the development of before-after studies (Chapter 8).

Similar results can be accomplished by any agency that uses CV trajectory data to estimate traffic signal performance measures following the techniques and recommendations presented in this report. Figure 13.3 and Figure 13.4 show dashboard-derived performance heatmaps for signalized corridors in Frisco, TX, and Cincinnati, OH, respectively.

Thus far, over 4,700 traffic signals, 910 million trajectories, and 14 billion waypoints in all 50 states and Washington, D.C., have been analyzed and included in the PM Heatmap. Figure 13.5 shows the location of the evaluated intersections and Figure 13.6 illustrates the data analyzed by state.

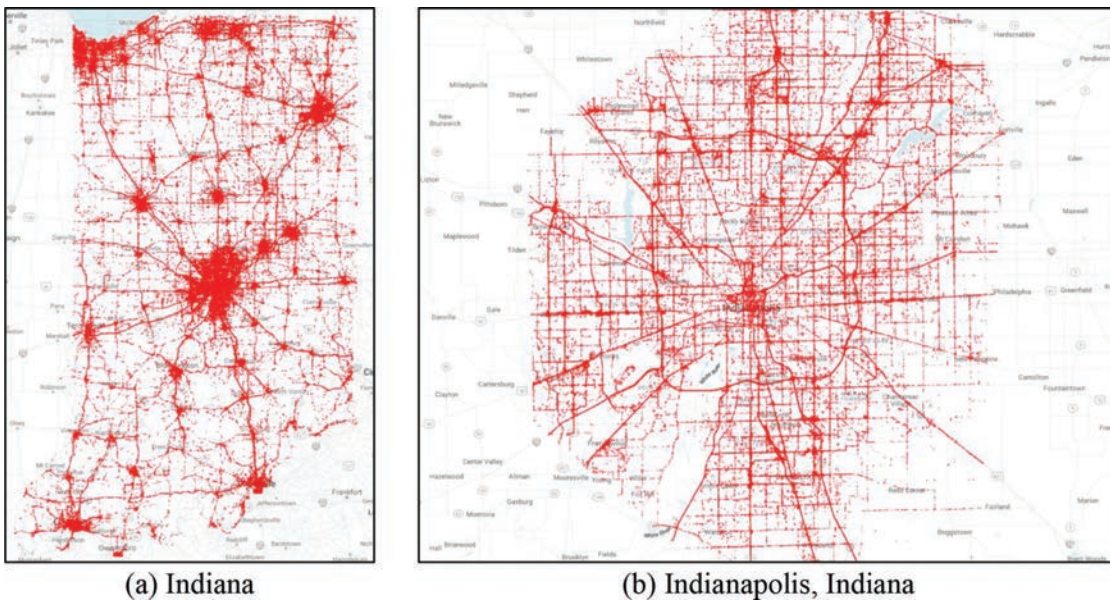


Figure 13.1 Trajectory waypoints collected during a 30-minute period in January 2020 (map data: Google).

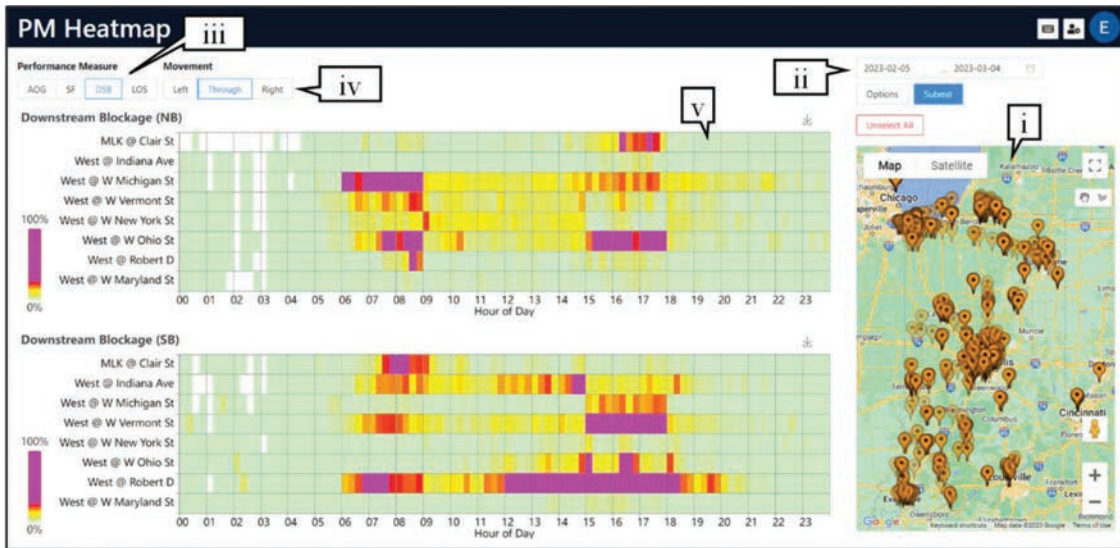


Figure 13.2 PM Heatmap web dashboard.



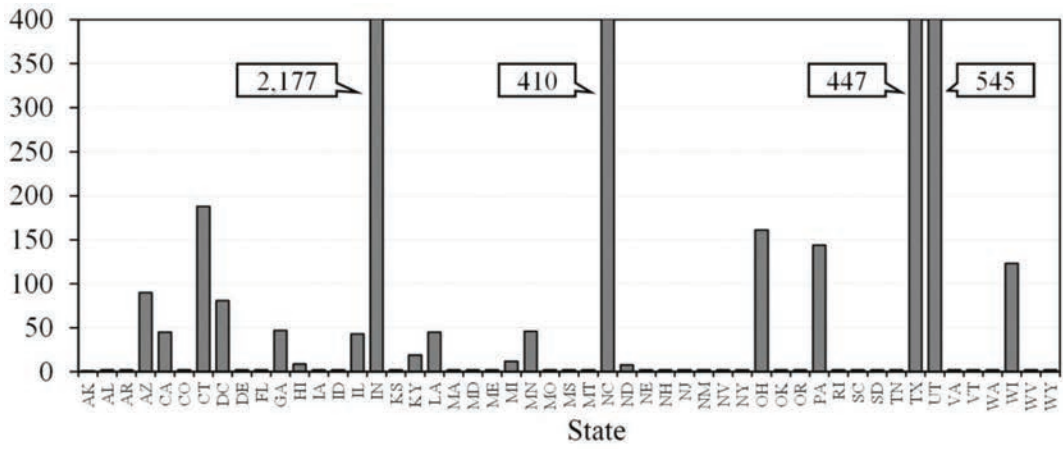
Figure 13.3 PM Heatmap web dashboard showing AOG results for a 9-intersection corridor in Frisco, TX.



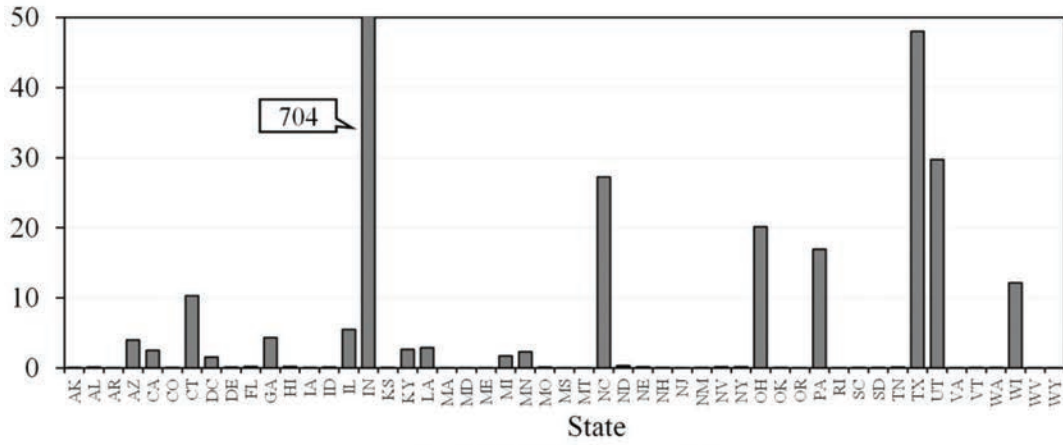
Figure 13.4 PM Heatmap web dashboard showing SF results for a 22-intersection corridor in Cincinnati, OH.



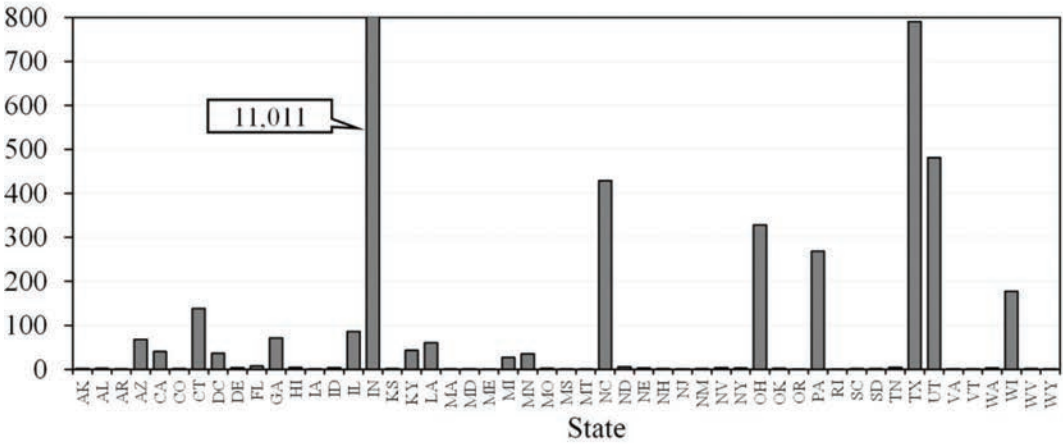
Figure 13.5 Traffic signals included in the PM Heatmap web dashboard.



(a) Intersection count



(b) Trajectory count (millions)



(c) Waypoint count (millions)

Figure 13.6 Data evaluated in the PM Heatmap web dashboard.

14. SUMMARY

CV data provides opportunities to systematically evaluate transportation infrastructure in a scalable manner, without the need for detection or communication equipment, or the deployment of personnel to the field. This report presents an overview of CV-based techniques used to evaluate traffic signal performance at the movement-, approach-, intersection-, arterial-, and system-levels.

Chapter 2 introduced the CV data sets and approaches to efficiently store and manage them. Chapter 3 provided geographical representations of event and trajectory data by their attributes as well as methodologies to linear reference vehicle progression through intersections. Chapter 4 discussed techniques to assign intersection movements to passing vehicles.

14.1 Traffic Signal Performance Measures

Chapters 5 through 11 presented techniques and frameworks on how to use trajectory data to evaluate signal performance. Chapter 5 introduced performance concepts in relation to vehicle trajectories at the movement-level focused on the Purdue Probe Diagram (PPD). Chapter 6 discussed techniques to evaluate arterial travel times. Chapter 7 proposed visualizations to evaluate performance at the arterial- and system-levels. Chapter 8 presented case-studies that illustrate frameworks to evaluate diversions and retiming impacts on signalized corridors. Chapter 9 provided a methodology based on SF and DSB estimations to identify locations where signal retiming is likely to improve operations. Chapter 10 discussed methodologies to evaluate performance at closely-coupled intersections by analyzing the complete progression of vehicles through each system. Chapter 11 presented techniques to systematically evaluate delay and queue-lengths at roundabout approaches. Even though roundabouts are not signalized, they are often used adjacent to traffic signals and the ubiquity of CV data allows these techniques to be inclusive of this alternative intersection design.

14.2 Intersection Safety and Driver Behavior Evaluation

Chapter 12 evaluated the use of CV HB event data to assess safety at signalized intersections. This approach is particularly beneficial to agencies because statistically valid data can be collected in just a month or two, instead of the usual 3- to 5-year period required to obtain significant crash data. Additionally, the change in driver behavior is assessed after modifying the type of control at a traffic signal by analyzing HA events. Although the fixed threshold of 8.76 ft/s² used to define HB and HA events showed promising results, it is anticipated that alternative thresholds may provide improved correlation with crash data and better describe driver behavior.

HA and HB events are recorded as soon as a vehicle's on-board accelerometer experiences an acceleration (or deceleration) greater in magnitude than 8.76 ft/s² (0.272 g), as defined by the data supplier. The range of heading values is (0°, 360°), where 0° is the true north and it increases clockwise.

14.3 Scalability

Chapter 13 discussed the scalability and replicability possibilities of using ubiquitous CV trajectory data to evaluate signal performance. It described how just under 5 minutes of manual labor is usually required to evaluate an intersection with data processing costs under \$0.10 for a month-long analysis. Furthermore, a developed web dashboard that interactively provides users performance estimations on over 4,700 signals was presented.

14.4 Future Opportunities

Even though significant progress has been accomplished in the use of CV data sets to evaluate signal performance, there are still important areas of opportunities that will need to be explored. Some of these opportunities are the following.

- As CV data sets start to include additional attributes than those discussed in Chapter 2, such as traction control or lane keep assist, opportunities will arise to evaluate different infrastructure characteristics and identify locations where maintenance is needed (145, 146).
- Performance measure analysis techniques could be updated to not only include passenger cars, but also commercial vehicles. This would improve the current understanding of how heavy vehicles affect signal operations.
- Enhance performance measures by including multi-modal analysis by combining CV passenger and commercial vehicle data sets with transit (147), bicycle, and pedestrian data.
- Design performance measures derived from entire vehicle trajectories that also integrate signal event high-resolution information. As CV data sets do not count with signal state information, and since various agencies already count with signal controller high-resolution event data, these two data sets could be incorporated to provide more detailed performance measures. For example, this will aid in identifying root cause as either vehicle demand or detector failures when split failures are identified by CV data.
- The manual labor required to generate CV-based traffic signal performance measures could be further reduced by automating the intersection center detection and waypoint retrieval radiuses. In general, the techniques presented in this document can be used with OpenStreetMap signal locations, but this should be approached with caution to ensure that atypical intersections are properly interpreted. There is no substitute for an engineer individually reviewing each intersection's configuration to ensure confidence in CV analyses.

REFERENCES

- Day, C. M., Bullock, D. M., Li, H., Remias, S. M., Hainen, A. M., Freije, R. S., Stevens, A. L., Sturdevant, J. R., & Brennan, T. M. (2014). *Performance measures for traffic signal systems: An outcome-oriented approach*. West Lafayette, IN: Purdue University. <https://doi.org/10.5703/1288284315333>
- Day, C. M., Bullock, D. M., Li, H., Lavrenz, S. M., Smith, W. B. B., & Sturdevant, J. R. (2015). *Integrating traffic signal performance measures into agency business processes*. West Lafayette, IN: Purdue University. <https://doi.org/10.5703/1288284316063>
- Saldivar-Carranza, E. D., Li, H., & Bullock, D. M. (2021b). Identifying vehicle turning movements at intersections from trajectory data. *2021 IEEE Intelligent Transportation Systems* (pp. 4043–4050). <https://doi.org/10.1109/ITSC48978.2021.9564781>
- Saldivar-Carranza, E., Li, H., Mathew, J., Hunter, M., Sturdevant, J., & Bullock, D. M. (2021). Deriving operational traffic signal performance measures from vehicle trajectory data. *Transportation Research Record: Journal of the Transportation Research Board*, 2675(9), 1250–1264. <https://doi.org/10.1177/03611981211006725>
- Saldivar-Carranza, E. D., Li, H., Gayen, S., Taylor, M., Sturdevant, J., & Bullock, D. M. (2023). Comparison of arrivals on green estimations from vehicle detection and connected vehicle data. *Transportation Research Record: Journal of the Transportation Research Board*. <https://doi.org/10.1177/03611981231168116>
- Desai, J., Mathew, J. K., Li, H., & Bullock, D. M. (2022). Leveraging connected vehicle data to assess interstate exit utilization and identify charging infrastructure investment allocation opportunities. *World Electric Vehicle Journal*, 13(9), 167. <https://doi.org/10.3390/wevj13090167>
- Desai, J., Scholer, B., Mathew, J. K., Li, H., & Bullock, D. M. (2022). Analysis of route choice during planned and unplanned road closures. *IEEE Open Journal of Intelligent Transportation Systems*, 3, 489–502. <https://doi.org/10.1109/OJITS.2022.3183928>
- Saldivar-Carranza, E. D., Li, H., Mathew, J. K., Gayen, S., Malackowski, H., & Bullock, D. M. (2023). *Reporting framework for arterial-level traffic signal performance measures estimated from connected vehicle trajectory data*. West Lafayette, IN: Purdue University. <https://doi.org/10.5703/1288284317617>
- Saldivar-Carranza, E. D., Hunter, M., Li, H., Mathew, J., & Bullock, D. M. (2021). Longitudinal performance assessment of traffic signal system impacted by long-term interstate construction diversion using connected vehicle data. *Journal of Transportation Technologies*, 11(4), 644–659. <https://doi.org/10.4236/jtts.2021.114040>
- Saldivar-Carranza, E., Li, H., Mathew, J., Fisher, C., & Bullock, D. M. (2022). Signalized corridor timing plan change assessment using connected vehicle data. *Journal of Transportation Technologies*, 12(3), 310–322. <https://doi.org/10.4236/jtts.2022.123019>
- Saldivar-Carranza, E. D., Li, H., Platte, T., & Bullock, D. M. (2023). Systemwide identification of signal retiming opportunities with connected vehicle data to reduce split failures. *Transportation Research Record: Journal of the Transportation Research Board*. <https://doi.org/10.1177/03611981231168844>
- Saldivar-Carranza, E., Rogers, S., Li, H., & Bullock, D. M. (2022). Diamond interchange performance measures using connected vehicle data. *Journal of Transportation Technologies*, 12(03), 475–497. <https://doi.org/10.4236/jtts.2022.123029>
- Saldivar-Carranza, E. D., Li, H., & Bullock, D. M. (2021a). Diverging diamond interchange performance measures using connected vehicle data. *Journal of Transportation Technologies*, 11(4), 628–643. <https://doi.org/10.4236/jtts.2021.114039>
- Saldivar-Carranza, E., Li, H., Taylor, M., & Bullock, D. M. (2022). Continuous flow intersection performance measures using connected vehicle data. *Journal of Transportation Technologies*, 12(04), 861–875. <https://doi.org/10.4236/jtts.2022.124047>
- Saldivar-Carranza, E., Mathew, J. K., Li, H., & Bullock, D. M. (2022). Roundabout performance analysis using connected vehicle data. *Journal of Transportation Technologies*, 12(01), 42–58. <https://doi.org/10.4236/jtts.2022.121003>
- Hunter, M., Saldivar-Carranza, E., Desai, J., Mathew, J., Li, H., & Bullock, D. M. (2021). A proactive approach to evaluating intersection safety using hard-braking data. *Journal of Big Data Analytics in Transportation*, 3, 81–94. <https://doi.org/10.1007/s42421-021-00039-y>
- Saldivar-Carranza, E. D., Mathew, J. K., Li, H., Hunter, M., Platte, T., & Bullock, D. M. (2021). Using connected vehicle data to evaluate traffic signal performance and driver behavior after changing left-turns phasing. *2021 IEEE International Intelligent Transportation Systems Conference (ITSC)*, 4028–4034. <https://doi.org/10.1109/ITSC48978.2021.9564654>
- Saldivar-Carranza, E., Li, H., Mathew, J. K., Gayen, S., Malackowski, H., & Bullock, D. M. (2023). *Trajectory-based arterial traffic signal performance measures reports*. West Lafayette, IN: Purdue University. <https://doi.org/10.5703/1288284317633>
- INRIX. (2022). *INRIX to showcase newest features and improvements in signal analytics at ITS world congress*. <https://inrix.com/press-releases/signal-analytics-trajectory-plots/>
- Leitner, D., Meleby, P., & Miao, L. (2022). Recent advances in traffic signal performance evaluation. *Journal of Traffic and Transportation Engineering (English Edition)*, 9(4), 507–531. <https://doi.org/10.1016/j.jtte.2022.06.002>
- Dobrota, N., Stevanovic, A., Mitrovic, N., Alshayeb, S., & Zlatkovic, M. (2023). Development and evaluation of performance measures for capacity utilization of traffic signals. *Transportation Research Record: Journal of the Transportation Research Board*, 2677(1), 1337–1355. <https://doi.org/10.1177/03611981221104460>
- Novat, N. (2022). *Utilizing simulated vehicle trajectory data from connected vehicles to characterize performance measures on an arterial after an impactful incident* [Master's thesis, Cleveland State University]. OhioLINK. http://rave.ohiolink.edu/etdc/view?acc_num=csu1673902978713825
- Nazari Enjedani, S., & Khanal, M. (2023). Development of a turning movement estimator using CV data. *Future Transportation*, 3(1), 349–367. <https://doi.org/10.3390/futuretransp3010021>
- Mohammadnazar, A., Patwary, A. L., Moradloo, N., Arvin, R., & Khattak, A. J. (2022). Incorporating driving volatility measures in safety performance functions: Improving safety at signalized intersections. *Accident Analysis & Prevention*, 178, 106872. <https://doi.org/10.1016/j.aap.2022.106872>

25. ITE/NOCoe. (2019). *2019 Traffic signal benchmarking and state of the practice report*. <https://transportationops.org/trafficsignals/benchmarkingreport>
26. National Academies of Sciences, Engineering, and Medicine. (2020). *Performance-based management of traffic signals* (NCHRP Research Report 954). <https://doi.org/10.17226/25875>
27. Sunkari, S. R. (2004). The benefits of retiming traffic signals. *ITE Journal-institute of Transportation Engineers*, 74(4), 26–29.
28. National Transportation Operations Coalition. (2012). *National traffic signal report card*. http://www.ite.org/reportcard/technical_reportfinal.pdf%5Cnhttp://www.ite.org/reportcard/TechnicalReport.pdf
29. FHWA. (2019). *Every day counts: An innovation partnership with states* (Report No. FHWA-19-CAI-013, EDC-4 Final Report). Federal Highway Administration. https://www.fhwa.dot.gov/innovation/everydaycounts/reports/edc4_final/#
30. Sturdevant, J. R., Overman, T., Raamot, E., Deer, R., Miller, D., Bullock, D. M., Day, C. M., Brennan T. M., Jr., Li, H., Hainen, A., & Remias, S. M. (2012). *Indiana traffic signal hi resolution data logger enumerations*. <https://doi.org/10.4231/K4RN35SH>
31. Lattimer, C. R. (2020). *Automated traffic signals performance measures* (Report No. FWHA-HOP-20-002). Federal Highway Administration. <https://ops.fhwa.dot.gov/publications/fhwahop20002/fhwahop20002.pdf>
32. Liu, H. X., Ma, W., Hu, H., Wu, X., & Yu, G. (2008). SMART-SIGNAL: Systematic monitoring of arterial road traffic signals. *2008 11th International IEEE Conference on Intelligent Transportation Systems* (pp. 1061–1066). <https://doi.org/10.1109/ITSC.2008.4732638>
33. Day, C., O'Brien, P., Stevanovic, A., Hale, D., & Matout, N. (2020). *A methodology and case study: Evaluating the benefits and costs of implementing automated traffic signal performance*. Leidos. <https://ops.fhwa.dot.gov/publications/fhwahop20003/fhwahop20003.pdf>
34. FHWA. (2021). *Every day counts: Innovation for a nation on the move* (Report No. FHWA-21-CAI-020, EDC-4 F Final Report). Federal Highway Administration.
35. Remias, S. M., Hainen, A. M., Day, C. M., Brennan, T. M. Jr., Li, H., Rivera-Hernandez, E., Sturdevant, J. R., Young, S. E., & Bullock, D. M. (2013). Performance characterization of arterial traffic flow with probe vehicle data. *Transportation Research Record: Journal of the Transportation Research Board*, 2380(1), 10–21. <https://doi.org/10.3141/2380-02>
36. Remias, S., Brennan, T., Grimmer, G., Cox, E., Horton, D., & Bullock, D. (2012). *2011 Indiana interstate mobility report—Full version*. <https://doi.org/10.5703/1288284314680>
37. Kamyab, M., Remias, S., Najmi, E., Hood, K., Al-Akshar, M., & Ustun, I. (2019). Evaluation of interstate work zone mobility using probe vehicle data and machine learning techniques. *Transportation Research Record: Journal of the Transportation Research Board*, 2673(2), 811–822. <https://doi.org/10.1177/0361198119827936>
38. Remias, S. M., Day, C. M., Waddell, J. M., Kirsch, J. N., & Trepanier, T. (2018). Evaluating the performance of coordinated signal timing: Comparison of common data types with automated vehicle location data. *Transportation Research Record: Journal of the Transportation Research Board*, 2672(18), 128–142. <https://doi.org/10.1177/0361198118794546>
39. Poddar, S., Chakraborty, P., Sharma, A., Knickerbocker, S., & Hawkins, N. (2022). Massively parallelizable approach for evaluating signalized arterial performance using probe-based data. *Journal of Intelligent Transportation Systems* (pp. 1–15). <https://doi.org/10.1080/15472450.2022.2069497>
40. Mathew, J. K., Desai, J. C., Sakhare, R. S., Kim, W., Li, H., & Bullock, D. M. (2021). Big data applications for managing roadways. *ITE Journal*, 91(2), 28–35. <https://www.nxtbook.com/ygsreprints/ITE/ite-journal-february-2021/index.php#/p/28>
41. University of Michigan: Center for Sustainable Systems. (2022, September). *Personal transportation factsheet* (Publication No. CSS01-07). https://css.umich.edu/sites/default/files/2022-09/Personal%20Transportation_CSS01-07.pdf
42. ITSdigest. (2018, February 16). 470 million connected vehicles on the road by 2025. <https://www.itsdigest.com/470-million-connected-vehicles-road-2025>
43. SAE International. (2016). *J2735D: Dedicated short range communications (DSRC) message set dictionary*.
44. Abernethy, B., Andrews, S., & Pruitt, G. (2012). *Signal phase and timing (SPaT) applications, communications requirements, communications technology potential solutions, issues and recommendations* (Report No. FHWA-JPO-13-002). Federal Highway Administration.
45. Waddell, J. M., Remias, S. M., & Kirsch, J. N. (2020). Characterizing traffic-signal performance and corridor reliability using crowd-sourced probe vehicle trajectories. *Journal of Transportation Engineering, Part A: Systems*, 146(7), 1–11. <https://doi.org/10.1061/JTEPBS.0000378>
46. Day, C. M., Li, H., Richardson, L. M., Howard, J., Platte, T., Sturdevant, J. R., & Bullock, D. M. (2017). Detector-free optimization of traffic signal offsets with connected vehicle data. *Transportation Research Record: Journal of the Transportation Research Board*, 2620(1), 54–68. <https://doi.org/10.3141/2620-06>
47. Argote-Cabañero, J., Christofa, E., & Skabardonis, A. (2015). Connected vehicle penetration rate for estimation of arterial measures of effectiveness. *Transportation Research Part C: Emerging Technologies*, 60, 298–312. <https://doi.org/10.1016/j.trc.2015.08.013>
48. FHWA. (2022, December). *Traffic monitoring guide*. Federal Highway Administration. <https://www.fhwa.dot.gov/policyinformation/tmguid/>
49. Hunter, M. (2022). *An assessment of connected vehicle data: The evaluation of intersections for elevated safety risks and data representativeness* [Master's thesis, Purdue University]. <https://doi.org/10.25394/PGS.19661028.v1>
50. Sakhare, R. S., Hunter, M., Mukai, J., Li, H., & Bullock, D. M. (2022). Truck and passenger car connected vehicle penetration on Indiana roadways. *Journal of Transportation Technologies*, 12(4), 578–599. <https://doi.org/10.4236/jtts.2022.124034>
51. Siegel, J. E., Erb, D. C., & Sarma, S. E. (2018). A survey of the connected vehicle landscape—Architectures, enabling technologies, applications, and development areas. *IEEE Transactions on Intelligent Transportation Systems*, 19(8), 2391–2406. <https://doi.org/10.1109/TITS.2017.2749459>
52. Saavedra, M. Z. N. L., & Yu, W. E. S. (2017). A comparison between text, parquet, and PCAP formats for use in distributed network flow analysis on hadoop. *Journal of Advances in Computer Networks*, 5(2), 59–64. <https://doi.org/10.18178/JACN.2017.5.2.241>

53. Shyam, R., Ganesh, H. B. B., Kumar S S., Poornachandran, P., & Soman K P. (2015). Apache spark a big data analytics platform for smart grid. *Procedia Technology*, 21, 171–178. <https://doi.org/10.1016/j.protcy.2015.10.085>
54. BigQuery Google Cloud. (n.d.). *How BigQuery pricing works*. Retrieved February 28, 2023, from <https://cloud.google.com/bigquery/#section-5>
55. Crane, K., Livesu, M., Puppo, E., & Qin, Y. (2020). A survey of algorithms for geodesic paths and distances. *ArXiv*. <https://doi.org/10.48550/arXiv.2007.10430>
56. Geopy. (2022). *Geopy* (2.3.0) [Computer software]. <https://geopy.readthedocs.io/en/stable/#module-geopy.distance>
57. Pebesma, E. (2018). Simple features for R: Standardized support for spatial vector data. *The R Journal*, 10(1), 439–446. <https://doi.org/10.32614/RJ-2018-009>
58. Li, H., Platte, T., Mathew, J., Smith, W. B., Saldivar-Carranza, E., & Bullock, D. M. (2020). *Using connected vehicle data to reassess dilemma zone performance of heavy vehicles*, 2675(5). <https://doi.org/10.1177/0361198120914606>
59. Savolainen, P. T., Sharma, A., & Gates, T. J. (2016). Driver decision-making in the dilemma zone – Examining the influences of clearance intervals, enforcement cameras and the provision of advance warning through a panel data random parameters probit model. *Accident Analysis and Prevention*, 96, 351–360. <https://doi.org/10.1016/j.aap.2015.08.020>
60. Urbanik, T., Tanaka, A., Lozner, B., Lindstrom, E., Lee, K., Quayle, S., Beard, S., Tsoi, S., Ryus, P., Gettman, D., Sunkari, S., Balke, K., & Bullock, D. (2015). *Signal timing manual - Second Edition* (NCHRP Report 812). <https://doi.org/10.17226/22097>
61. Reclus, F., & Drouard, K. (2009). Geofencing for fleet and freight management. *2009 9th International Conference on Intelligent Transport Systems Telecommunications, (ITST)* (pp. 353–356). <https://doi.org/10.1109/ITST.2009.5399328>
62. Bajorski, P. (2011). *Statistics for imaging, optics, and photonics*. John Wiley & Sons.
63. Quiroga, C. A., & Bullock, D. (1999). Measuring control delay at signalized intersections. *Journal of Transportation Engineering*, 125(4), 271–280. [https://doi.org/10.1061/\(ASCE\)0733-947X\(1999\)125:4\(271\)](https://doi.org/10.1061/(ASCE)0733-947X(1999)125:4(271))
64. Transportation Research Board (TRB). (2010). *Highway capacity manual 2010*. National Research Council (NRC).
65. Day, C. M., Brennan, T. M., Jr., Premachandra, H., Sturdevant, J. R., & Bullock, D. M. (2011). Analysis of peer data on intersections for decisions about coordination of arterial traffic signal. *Transportation Research Record: Journal of the Transportation Research Board*, 2259(1), 23–36. <https://doi.org/10.3141/2259-03>
66. Emtenan, A. M. T., & Day, C. M. (2020). Impact of detector configuration on performance measurement and signal operations. *Transportation Research Record: Journal of the Transportation Research Board*, 2674(4), 300–313. <https://doi.org/10.1177/0361198120912244>
67. Young, S. E., Day, C. M., Bullock, D. M., & Fong, D. S. T. (2017). *Visualizations of arterial traffic performance measures: A picture book approach*. <https://doi.org/10.5703/1288284316562>
68. Utah Department of Transportation. (2022, August). *Automated traffic signal performance measures version 4.3.1*. <https://Udottraffic.Utah.Gov/ATSPM>
69. Freije, R. S., Hainen, A. M., Stevens, A. L., Li, H., Smith, W. B., Summers, H., Day, C. M., Sturdevant, J. R., & Bullock, D. M. (2014). Graphical performance measures for practitioners to triage split failure trouble calls. *Transportation Research Record: Journal of the Transportation Research Board*, 2439(1), 27–40. <https://doi.org/10.3141/2439-03>
70. Haseman, R. J., Wasson, J. S., & Bullock, D. M. (2010). Real-time measurement of travel time delay in work zones and evaluation metrics using Bluetooth probe tracking. *Transportation Research Record*, 2169(1), 40–53. <https://doi.org/10.3141/2169-05>
71. Rahmani, M., Jenelius, E., & Koutsopoulos, H. N. (2015). Non-parametric estimation of route travel time distributions from low-frequency floating car data. *Transportation Research Part C: Emerging Technologies*, 58, 343–362. <https://doi.org/10.1016/j.trc.2015.01.015>
72. Angel, A., Hickman, M., Mirchandani, P., & Chandnani, D. (n.d.). Methods of traffic data collection, using aerial video. *The IEEE 5th International Conference on Intelligent Transportation Systems* (pp. 31–36). <https://doi.org/10.1109/ITSC.2002.1041184>
73. Kazagli, E., & Koutsopoulos, H. N. (2013). Estimation of arterial travel time from automatic number plate recognition data. *Transportation Research Record: Journal of the Transportation Research Board*, 2391(1), 22–31. <https://doi.org/10.3141/2391-03>
74. Martchouk, M., Mannerling, F., & Bullock, D. (2011). Analysis of freeway travel time variability using Bluetooth detection. *Journal of Transportation Engineering*, 137(10), 697–704. [https://doi.org/10.1061/\(ASCE\)TE.1943-5436.0000253](https://doi.org/10.1061/(ASCE)TE.1943-5436.0000253)
75. Nishii, K., Kondo, K., & Kitamura, R. (1988). Empirical analysis of trip chaining behavior. *Transportation Research Record: Journal of the Transportation Research Board*, 1203, 48–59.
76. Primerano, F., Taylor, M. A. P., Pitaksringkarn, L., & Tisato, P. (2007). Defining and understanding trip chaining behaviour. *Transportation*, 35(1), 55–72. <https://doi.org/10.1007/s11116-007-9134-8>
77. Currie, G., & Delbosc, A. (2011). Exploring the trip chaining behaviour of public transport users in Melbourne. *Transport Policy*, 18(1), 204–210. <https://doi.org/10.1016/j.tranpol.2010.08.003>
78. Hensher, D. A., & Reyes, A. J. (2000). Trip chaining as a barrier to the propensity to use public transport. *Transportation*, 27(4), 341–361. <https://doi.org/10.1023/A:1005246916731>
79. Purdue Traffic Lab. (2021a). *LOS weighted average control delay by time-of-day - Indianapolis Downtown, IN* [Video]. YouTube. <https://tinyurl.com/controlDelayIndyDowntown>
80. Desai, J., Saldivar-Carranza, E., Mathew, J. K., Li, H., Platte, T., & Bullock, D. (2021). Methodology for applying connected vehicle data to evaluate impact of interstate construction work zone diversions. *2021 IEEE International Intelligent Transportation Systems Conference (ITSC)* (pp. 4035–4042). <https://doi.org/10.1109/ITSC48978.2021.9564873>
81. Schrank, D., Albert, L., Eisele, B., & Lomax, T. (2021). *2021 Urban mobility report*. Texas A&M Transportation Institute. <https://static.tti.tamu.edu/tti.tamu.edu/documents/mobility-report-2021.pdf>
82. FHWA Office of Operations. (2017, February 22). *Making work zones work better*. https://ops.fhwa.dot.gov/aboutus/one_pagers/wz.htm

83. Lochrane, T. W. P., Al-Deek, H., Paracha, J., & Scriba, T. (2013). *Understanding driver behavior in work zones*, 76(5). <https://www.fhwa.dot.gov/publications/publicroads/13marapr/04.cfm>
84. Indiana Department of Transportation. (n.d.). *North split upgrades driving progress: FAQs* [Webpage]. Retrieved February 21, 2023, from <https://northsplit.com/faqs/>
85. Purdue Traffic Lab. (2021b). *Split failure event* [Video]. YouTube. <https://tinyurl.com/splitFailure>
86. Day, C. M., & Bullock, D. M. (2011). Computational efficiency of alternative algorithms for arterial offset optimization. *Transportation Research Record: Journal of the Transportation Research Board*, 2259(1), 37–47. <https://doi.org/10.3141/2259-04>
87. ODOT. (n.d.). *Traffic monitoring management system (TMMS)*. Ohio Department of Transportation. Retrieved January 19, 2022, from <https://www.transportation.ohio.gov/wps/portal/gov/odot/programs/technical-services/traffic-monitoring/tmms>
88. Denney, R. W., Head, L., & Spencer, K. (2008, November 1). *Signal timing under saturated conditions* (Publication No. FHWA-HOP-09-008). Booz Allen Hamilton Holding Corporation.
89. Day, C. M., Li, H., Sturdevant, J. R., & Bullock, D. M. (2018). Data-driven ranking of coordinated traffic signal systems for maintenance and retiming. *Transportation Research Record: Journal of the Transportation Research Board*, 2672(18), 167–178. <https://doi.org/10.1177/0361198118794042>
90. Li, H., Richardson, L. M., Day, C. M., Howard, J., & Bullock, D. M. (2017). Scalable dashboard for identifying split failures and heuristic for reallocating split times. *Transportation Research Record: Journal of the Transportation Research Board*, 2620(1), 83–95. <https://doi.org/10.3141/2620-08>
91. Campbell, R., & Skabardonis, A. (2014). Issues affecting performance of adaptive traffic control systems in over-saturated conditions. *Transportation Research Record: Journal of the Transportation Research Board*, 2438(1), 23–32. <https://doi.org/10.3141/2438-03>
92. NCHRP. (2010). *Traffic signal retiming practices in the United States*. National Cooperative Highway Research Program. <https://doi.org/10.17226/22915>
93. Singleton, P. A., & Runa, F. (2021). Pedestrian traffic signal data accurately estimates pedestrian crossing volumes. *Transportation Research Record: Journal of the Transportation Research Board*, 2675(6), 429–440. <https://doi.org/10.1177/0361198121994126>
94. Hughes, W., Jagannathan, R., Sengupta, D., & Hummer, J. (2010, April). *Alternative intersections/interchanges: Informational report (AIIR)* (Publication No. FHWA-HRT-09-060). <https://www.fhwa.dot.gov/publications/research/safety/09060/09060.pdf>
95. National Academies of Sciences, Engineering, and Medicine. (2021). *Diverging diamond interchange informational guide, second edition* (NCHRP Research Report 959). <https://doi.org/10.17226/26027>
96. Steyn, H., Bugg, Z., Ray, B., Daleiden, A., Jenior, P., & Knudsen, J. (2014, August). *Displaced left turn intersection: Informational guide* (Report No. FHWA-SA-14-068). Kittelson & Associates, Inc. <https://safety.fhwa.dot.gov/intersection/crossover/fhwasa14068.pdf>
97. Alzoubaidi, M., Molan, A. M., & Ksaibati, K. (2021). Comparing the efficiency of the super diverging diamond interchange to other innovative interchanges. *Simulation Modelling Practice and Theory*, 106. <https://doi.org/10.1016/j.simpat.2020.102174>
98. Hunter, M., Guin, A., Anderson, J., & Park, S. J. (2019). Operating performance of diverging diamond interchanges. *Transportation Research Record: Journal of the Transportation Research Board*, 2673(11), 801–812. <https://doi.org/10.1177/0361198119855341>
99. Dhattrak, A., Edara, P., & Bared, J. G. (2010). Performance analysis of parallel flow intersection and displaced left-turn intersection designs. *Transportation Research Record: Journal of the Transportation Research Board*, 2171(1), 33–43. <https://doi.org/10.3141/2171-04>
100. Yang, X., Cheng, Y., & Chang, G.-L. (2016). Operational analysis and signal design for asymmetric two-leg continuous-flow intersection. *Transportation Research Record: Journal of the Transportation Research Board*, 2553(1), 72–81. <https://doi.org/10.3141/2553-08>
101. Abdelrahman, A., Abdel-Aty, M., Lee, J., Yue, L., & Al-Omari, M. M. A. (2020). Evaluation of displaced left-turn intersections. *Transportation Engineering*, 1. <https://doi.org/10.1016/j.treng.2020.100006>
102. Hainen, A. M., Stevens, A. L., Day, C. M., Li, H., Mackey, J., Luker, M., Taylor, M., Sturdevant, J. R., & Bullock, D. M. (2015). Performance measures for optimizing diverging interchanges and outcome assessment with drone video. *Transportation Research Record: Journal of the Transportation Research Board*, 2487(1), 31–43. <https://doi.org/10.3141/2487-03>
103. Chang, M.-S., & Messer, C. J. (1985). Volume guidelines for signalization of diamond interchanges. *Transportation Research Record: Journal of the Transportation Research Board*, 1010, 29–37.
104. Hainen, A. M., Li, H., Stevens, A. L., Day, C. M., Sturdevant, J. R., & Bullock, D. M. (2015). Sequence optimization at signalized diamond interchanges using high-resolution event-based data. *Transportation Research Record: Journal of the Transportation Research Board*, 2487(1), 15–30. <https://doi.org/10.3141/2487-02>
105. Messer, C. J., & Chang, M.-S. (1987). Traffic operations of basic traffic-actuated control systems at diamond interchanges. *Transportation Research Record: Journal of the Transportation Research Board*, 1114, 54–62.
106. Venglar, S. P., Koonce, P., & Urbanik, T. II. (1998). *Passer III-98 application and user's guide*. Texas Transportation Institute.
107. Nelson, E. J., Bullock, D., & Urbanik, T. (2000). Implementing actuated control of diamond interchanges. *Journal of Transportation Engineering*, 126(5), 390–395. [https://doi.org/10.1061/\(ASCE\)0733-947X\(2000\)126:5\(390\)](https://doi.org/10.1061/(ASCE)0733-947X(2000)126:5(390))
108. FDOT. (2020, October 30). *D217 diverging diamond interchanges*. Florida Department of Transportation. <https://fdotwww.blob.core.windows.net/sitefinity/docs/default-source/roadway/fdm/ddc/ddc-217-ddi-2020-10.pdf>
109. Goldblatt, R. B., Mier, F., & Friedman, J. (1994). Continuous flow intersections. *Institute of Transportation Engineers*, 64(7), 35–42.
110. Robinson, B. W., Rodegedts, L., Scarborough, W., Kittelson, W., Troutbeck, R., Brilon, W., Bondzio, L., Courage, K., Kyte, M., Mason, J., Flannery, A., Myers, E., Bunker, J., & Jacqemart, G. (2000, June). *Roundabouts: An informational guide* (Report No. FWA-RD-00-067). Federal Highway Administration. <https://www.fhwa.dot.gov/publications/research/safety/00067/00067.pdf>

111. Taylor, K., & Rodegerdts, L. (n.d.). *How many roundabouts are in the United States?* Retrieved November 10, 2021, from [https://www.kittelson.com/ideas/how-many-roundabouts-are-in-the-united-states/#:~:text=Thanks to the database's growth,through 2020 is about 7%2C900](https://www.kittelson.com/ideas/how-many-roundabouts-are-in-the-united-states/#:~:text=Thanks%20to%20the%20database's%20growth,through%2020%20is%20about%207%2C900)
112. NCHRP. (2010). *Roundabouts: An informational guide, second edition* (NCHRP Report 672). National Cooperative Highway Research Program. <https://nacto.org/docs/usdg/nchrprpt672.pdf>
113. Özuysal, M., Çalışkanelli, S. P., Tanyel, S., & Baran, T. (2009). Capacity prediction for traffic circles: applicability of ANN. *Proceedings of the Institution of Civil Engineers - Transport*, 162(4), 195–206. <https://doi.org/10.1680/tran.2009.162.4.195>
114. Ren, L., Qu, X., Guan, H., Easa, S., & Oh, E. (2016). Evaluation of roundabout capacity models: An empirical case study. *Journal of Transportation Engineering*, 142(12). [https://doi.org/10.1061/\(ASCE\)TE.1943-5436.0000878](https://doi.org/10.1061/(ASCE)TE.1943-5436.0000878)
115. Dahl, J., & Lee, C. (2012). Empirical estimation of capacity for roundabouts using adjusted gap-acceptance parameters for trucks. *Transportation Research Record: Journal of the Transportation Research Board*, 2312(1), 34–45. <https://doi.org/10.3141/2312-04>
116. Xu, F., & Tian, Z. Z. (2008). Driver behavior and gap-acceptance characteristics at roundabouts in California. *Transportation Research Record: Journal of the Transportation Research Board*, 2071(1), 117–124. <https://doi.org/10.3141/2071-14>
117. Flannery, A., Elefteriadou, L., Koza, P., & McFadden, J. (1998). Safety, delay, and capacity of single-lane roundabouts in the United States. *Transportation Research Record: Journal of the Transportation Research Board*, 1646(1), 63–70. <https://doi.org/10.3141/1646-08>
118. Hainen, A. (2016). Investigating mixed logit analysis of critical headways at a single-lane instrumented roundabout. *Journal of the Transportation Research Forum*, 55. <https://doi.org/10.5399/osu/jtrf.55.3.4391>
119. Hainen, A. M., Rivera-Hernandez, E. M., Day, C. M., McBride, M. T., Grimmer, G., Loehr, A. J., & Bullock, D. M. (2013). Roundabout critical headway measurement based on high-resolution event-based data from wireless magnetometers. *Transportation Research Record: Journal of the Transportation Research Board*, 2389(1), 51–64. <https://doi.org/10.3141/2389-06>
120. Day, C. M., Hainen, A. M., & Bullock, D. M. (2013). *Best practices for roundabouts on state highways* (Joint Transportation Research Program No. FHWA/IN/JTRP-2013/14). West Lafayette, IN: Purdue University. <https://doi.org/10.5703/1288284315216>
121. Flannery, A., Kharoufeh, J. P., Gautam, N., & Elefteriadou, L. (2005). Queuing delay models for single-lane roundabouts. *Civil Engineering and Environmental Systems*, 22(3), 133–150. <https://doi.org/10.1080/10286600500279949>
122. Praticò, F. G., Vaiana, R., & Gallelli, V. (2012). Transport and traffic management by micro simulation models: Operational use and performance of roundabouts. *WIT Transactions on the Built Environment*, 128, 383–394. <https://doi.org/10.2495/UT120331>
123. Ghanim, M., Kharbeche, M., Hannun, J., Hannun, J., & Shamiyeh, K. (2020). Safety and operational performance of signalized roundabouts: A case study in Doha. *Procedia Computer Science*, 170, 427–433. <https://doi.org/10.1016/j.procs.2020.03.085>
124. Valdez, M., Cheu, R. L., & Duran, C. (2011). Operations of modern roundabout with unbalanced approach volumes. *Transportation Research Record: Journal of the Transportation Research Board*, 2265(1), 234–243. <https://doi.org/10.3141/2265-26>
125. INDOT. (2012). *Indiana design manual 2012, Chapter 5: Engineering assessment* (pp. 90–128). https://www.in.gov/indot/design-manual/files/IDM_Complete_2012.pdf
126. Golembiewski, G. A., & Chandler, B. (2011). *Road safety information analysis: A manual for local rural road owners* (Report No. FHWA-SA-11-10). Science Applications International Corporation. https://safety.fhwa.dot.gov/local_rural/training/fhwasa1210/lrro_data.pdf
127. Perkins, S., & Harris, J. (1968). Traffic conflict characteristics-accident potential at intersections. *Highway Research Record*, 225, 35–43.
128. Tarko, A. P. (2020). Traffic conflicts as crash surrogates. In *Measuring Road Safety Using Surrogate Events* (pp. 31–45). Elsevier Ltd.
129. Parsonson, P. S. (1978). Signalization of high speed isolated intersections. *Transportation Research Record*, 681, 34–42. http://books.google.com/books/about/Signalization_of_High_Speed_Isolated_Int.html?id=73v-GwAACAAJ&pgis=1
130. Zeeger, C. V., & Deen, R. C. (1978). *Green-extension systems at high-speed intersections* (Kentucky Transportation Center Research Report 834). <https://doi.org/10.13023/KTC.RR.1978.496>
131. Spearman, C. (1904). The proof and measurement of association between two things. *The American Journal of Psychology*, 15(1), 72–101. <https://doi.org/10.2307/1412159>
132. Pearson, K. (1895). Note on regression and inheritance in the case of two parents. *Proceedings of the Royal Society of London*, 58(347-352), 240–242.
133. Kendall, M. G., & Gibbons, J. D. (1990). *Rank correlation methods* (5th ed.). E. Arnold.
134. Dancy, C., & Reidy, J. (2007). *Statistics without maths for psychology*. Pearson Education.
135. Chan, Y. H. (2003). Biostatistics 104: correlation analysis. *Singapore Medical Journal*, 44(12), 614–619.
136. Evans, J. D. (1996). *Straightforward statistics for the behavioral sciences*. Thomson Brooks/Cole Publishing Co.
137. Sharma, A., Bullock, D., & Peeta, S. (2011). Estimating dilemma zone hazard function at high speed isolated intersection. *Transportation Research Part C: Emerging Technologies*, 19(3), 400–412. <https://doi.org/10.1016/j.trc.2010.05.002>
138. Mukaka, M. M. (2012). Statistics corner: A guide to appropriate use of correlation coefficient in medical research. *Malawi Medical Journal*, 24(3), 69–71.
139. Washington, S. P., Karlaftis, M. G., & Mannering, F. L. (2010). *Statistical and econometric methods for transportation data analysis*. Chapman and Hall/CRC.
140. Desai, J., Li, H., Mathew, J. K., Cheng, Y.-T., Habib, A., & Bullock, D. M. (2021). Correlating hard-braking activity with crash occurrences on interstate construction projects in Indiana. *Journal of Big Data Analytics in Transportation*, 3, 27–41. <https://doi.org/10.1007/s42421-020-00024-x>
141. Harwood, D. W., Bauer, K. M., Potts, I. B., Torbic, D. J., Richard, K. R., Rabbani, E. R., Hauer, E., Elefteriadou, L., & Griffith, M. S. (2003). Safety effectiveness of intersection left- and right-turn lanes. *Transportation Research Record: Journal of the Trans-*

- portation Research Board*, 1840(1), 131–139. <https://doi.org/10.3141/1840-15>
142. Chen, L., Chen, C., & Ewing, R. (2015). Left-turn phase: Permissive, protected, or both? A quasi-experimental design in New York City. *Accident Analysis & Prevention*, 76, 102–109. <https://doi.org/10.1016/j.aap.2014.12.019>
143. Srinivasan, R., Council, F., Lyon, C., Gross, F., Lefler, N., & Persaud, B. (2008). Safety effectiveness of selected treatments at urban signalized intersections. *Transportation Research Record: Journal of the Transportation Research Board*, 2056(1), 70–76. <https://doi.org/10.3141/2056-09>
144. Li, X., Weber, A., Cottam, A., & Wu, Y.-J. (2019). Impacts of changing from permissive/protected left-turn to protected-only phasing: Case study in the City of Tucson, Arizona. *Transportation Research Record: Journal of the Transportation Research Board*, 2673(4), 616–626. <https://doi.org/10.1177/0361198119842108>
145. Mahlberg, J. A., Li, H., Zachrisson, B., Leslie, D. K., & Bullock, D. M. (2022). Pavement quality evaluation using connected vehicle data. *Sensors*, 22(23), 9109. <https://doi.org/10.3390/s22239109>
146. Mahlberg, J. A., Sakhare, R. S., Li, H., Mathew, J. K., Bullock, D. M., & Surnilla, G. C. (2021). Prioritizing roadway pavement marking maintenance using lane keep assist sensor data. *Sensors*, 21(18), 6014. <https://doi.org/10.3390/s21186014>
147. Mathew, J. K., Li, H., Saldivar-Carranza, E., Duffy, M., & Bullock, D. M. (2022). Integrated performance measures for bus rapid transit system and traffic signal systems using trajectory data. *Journal of Transportation Technologies*, 12(04), 833–860. <https://doi.org/10.4236/jtts.2022.124046>
148. Day, C. M., & Bullock, D. M. (2020). Optimization of traffic signal offsets with high resolution event data. *Journal of Transportation Engineering, Part A: Systems*, 146(3). <https://doi.org/10.1061/jtepbs.0000309>

APPENDIX A. REPORTING FRAMEWORK FOR ARTERIAL-LEVEL TRAFFIC SIGNAL PERFORMANCE MEASURES

This appendix provides a system level corridor visualization framework (8) to assess performance by TOD and location to quickly identify periods of a day where individual movements experience operational challenges (46, 69, 148).

The framework is shown in Figure 7.4 and summarizes HCM LOS (Figure 5.2), AOG (Figure 5.3), SF (Figure 5.7), and DSB (Figure 5.8) for all relevant movements over 24 hours on an arterial. Table 7.2

explains the information included in Figure 7.4. This approach provides an at-a-glance summary of up to 3,072 measures per intersection since it gives information for eight different movements and four performance measures for 96 fifteen-minute periods.

To further demonstrate implementation, 14 reports with the discussed framework, displaying performance estimations for 12 corridors, located in 11 different states, are provided. Table A.1 provides details on these reports.

Additionally, (18) expands on (8) by providing 58 arterial-level performance reports of corridors located in 14 different states.

TABLE A.1
Corridor-wide performance report provided

Figure No.	State	Corridor	No. Signals	Description
A.1	CA	RTE-83	13	Segment in Chino between SR-60 and Pine Ave.
A.2	CT	CT-10	10	Segment in Southington between Town Line Rd. and Loper St.
A.3	GA	SR-247	23	Segment in Warner Robins between I-75 and Oak Ave.
A.4	IN	West St.	11	Segment in downtown Indianapolis before North Split closure (9)
A.5	IN	West St.	11	Segment in downtown Indianapolis during North Split closure (9)
A.6	MN	Hennepin Ave.	5	Effects of SR-53 bridge closure on Hennepin Ave. between 2nd St. and University Ave.
A.7	NC	US-70	12	Segment in Powhatan between Town Center Blvd. and Gordon Rd.
A.8	OH	US-27	22	Segment north of Cincinnati before implementing adaptive control (10)
A.9	OH	US-27	22	Segment north of Cincinnati running on adaptive control (10)
A.10	PA	US-30	11	Segment in Lancaster between Oakview Rd. and SR-896
A.11	TX	Texas Ave.	13	Segment in College Station between University Dr. and Deacon Dr.
A.12	TX	Eldorado	9	Segment in Frisco between Legacy Dr. and Preston Rd.
A.13	UT	SR-175	20	Segment south of Salt Lake City between 4000 W and 1700 E
A.14	WI	WI-96	8	Segment in Appleton between Casaloma Dr. and N Perkins St.

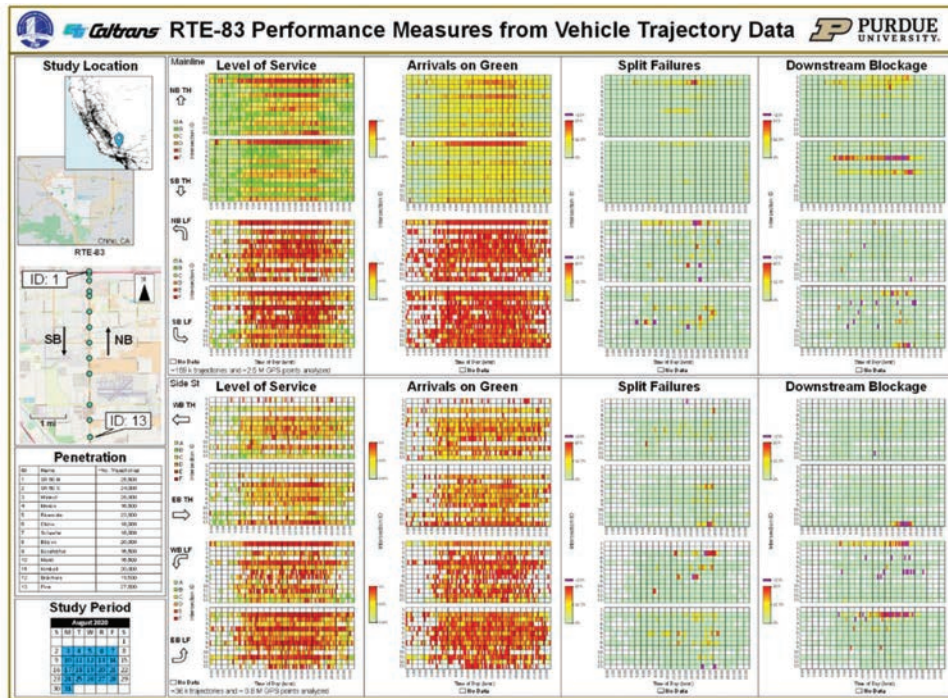


Figure A.1 RTE-83 in CA between SR-60 and Pine Ave.

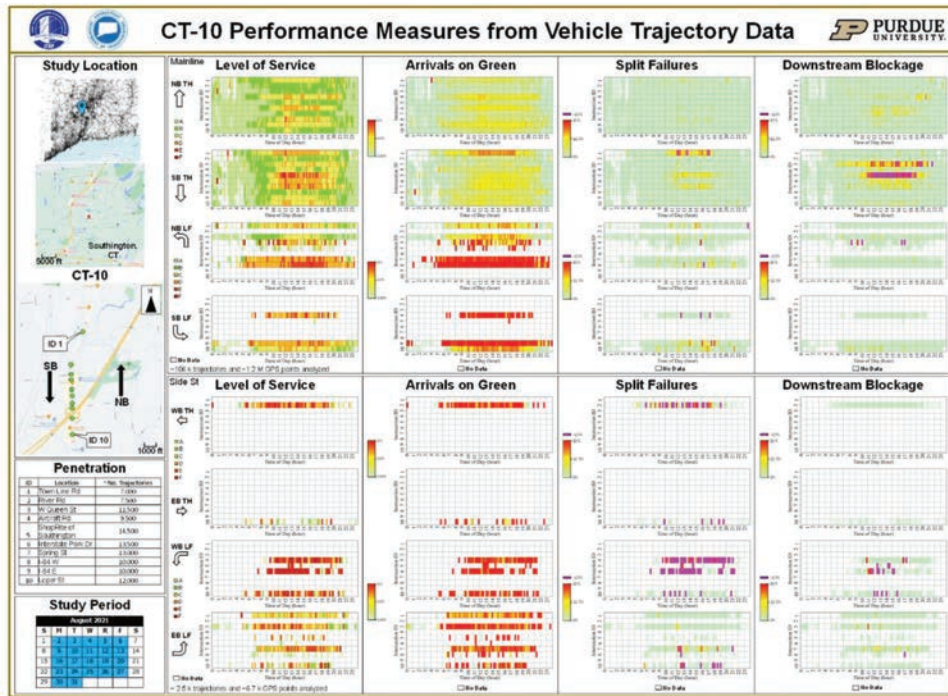


Figure A.2 CT-10 in CT between Town Line Rd. and Loper St.

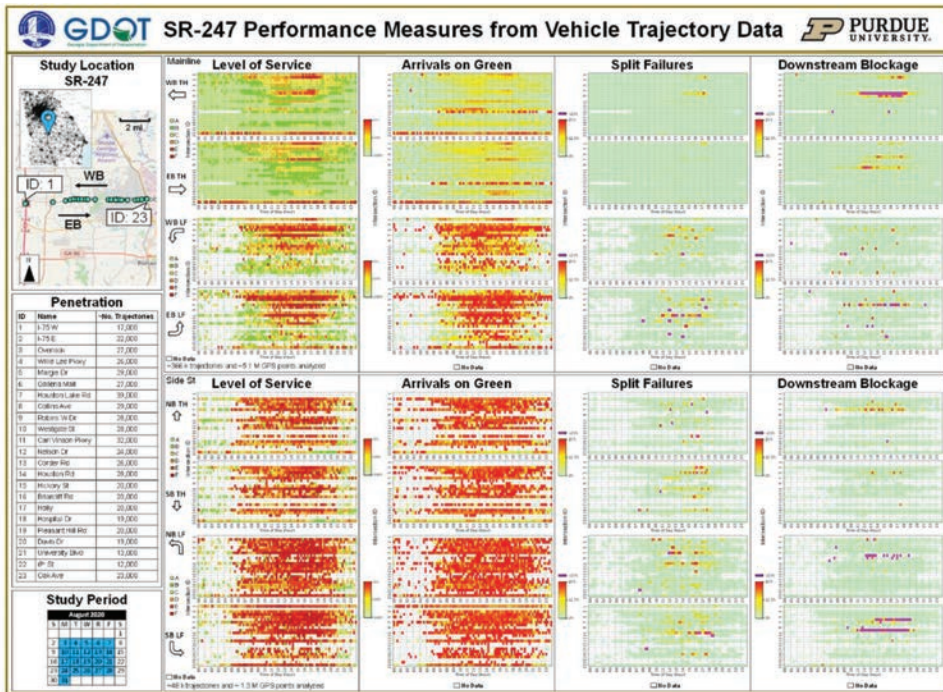


Figure A.3 SR-247 in GA between I-75 and Oak Ave.

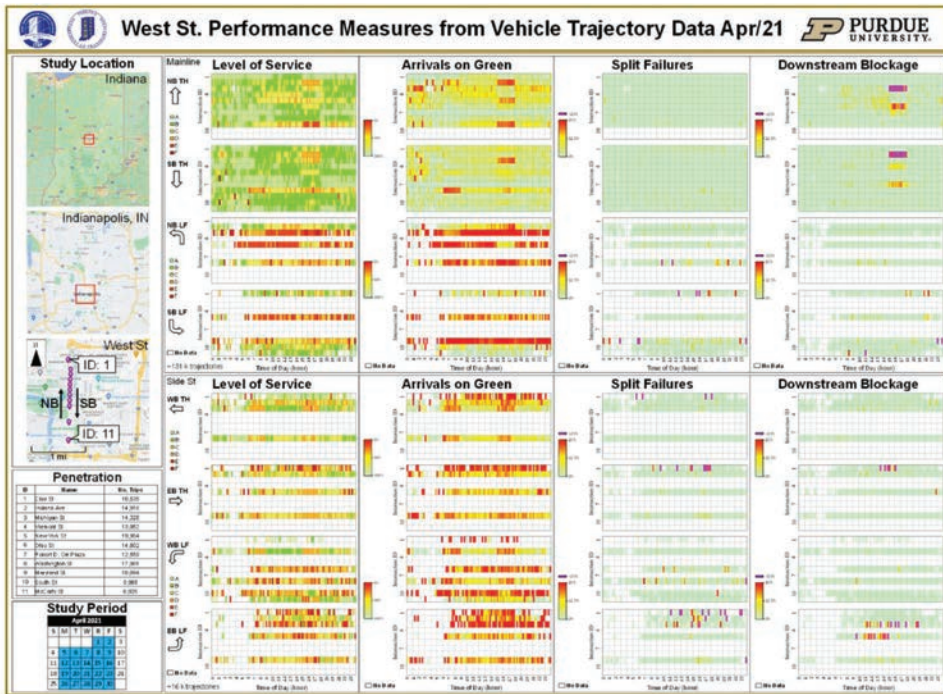


Figure A.4 West St. in IN before the North Split closure (9).

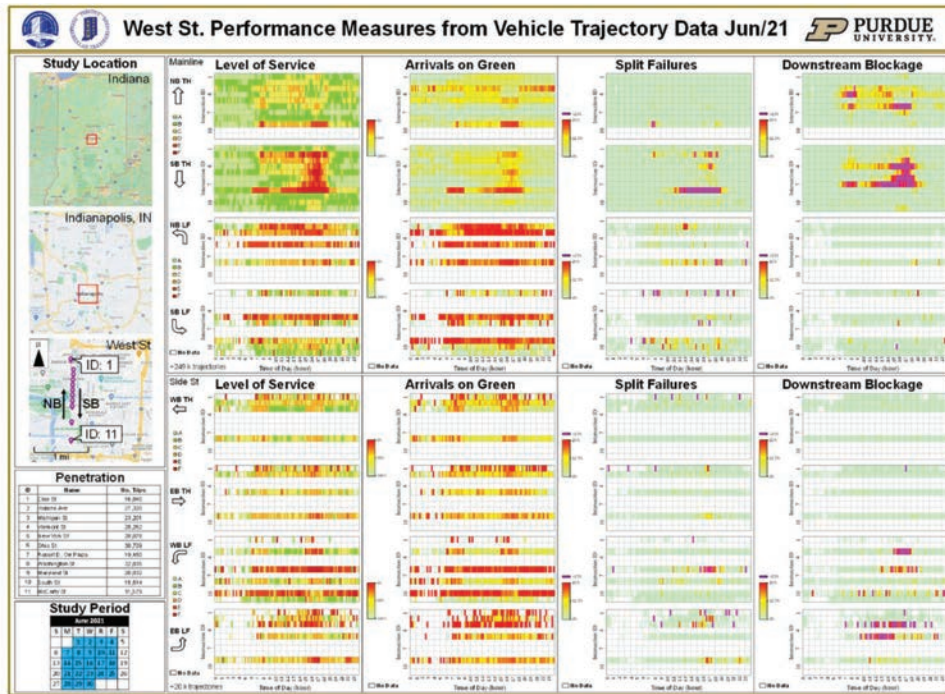


Figure A.5 West St. in IN after the North Split closure (9).

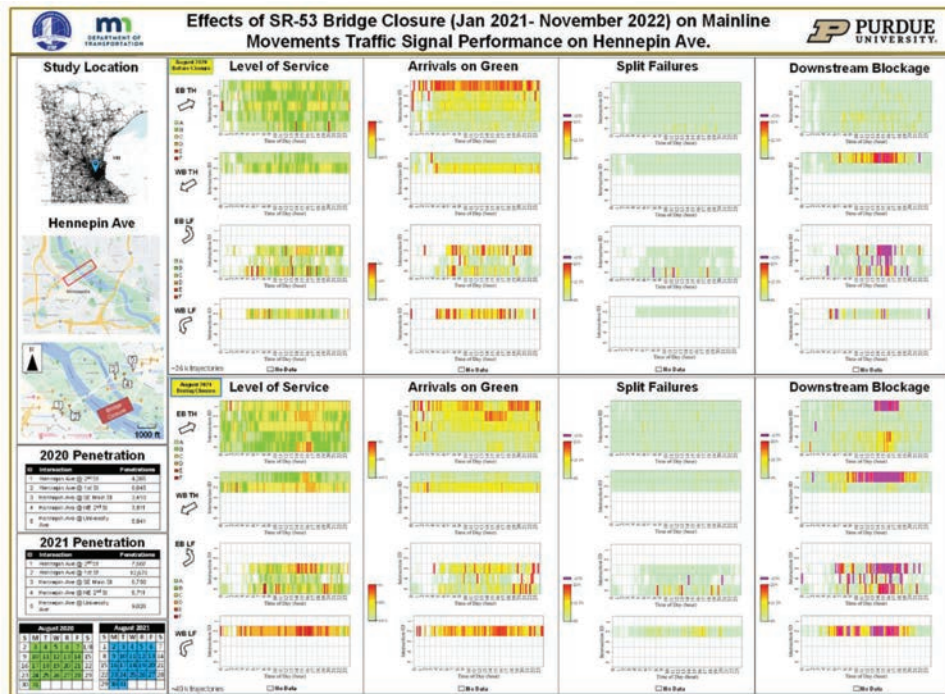


Figure A.6 SR-53 bridge closure effects on Hennepin Ave. in MN between 2nd St. and University Ave.

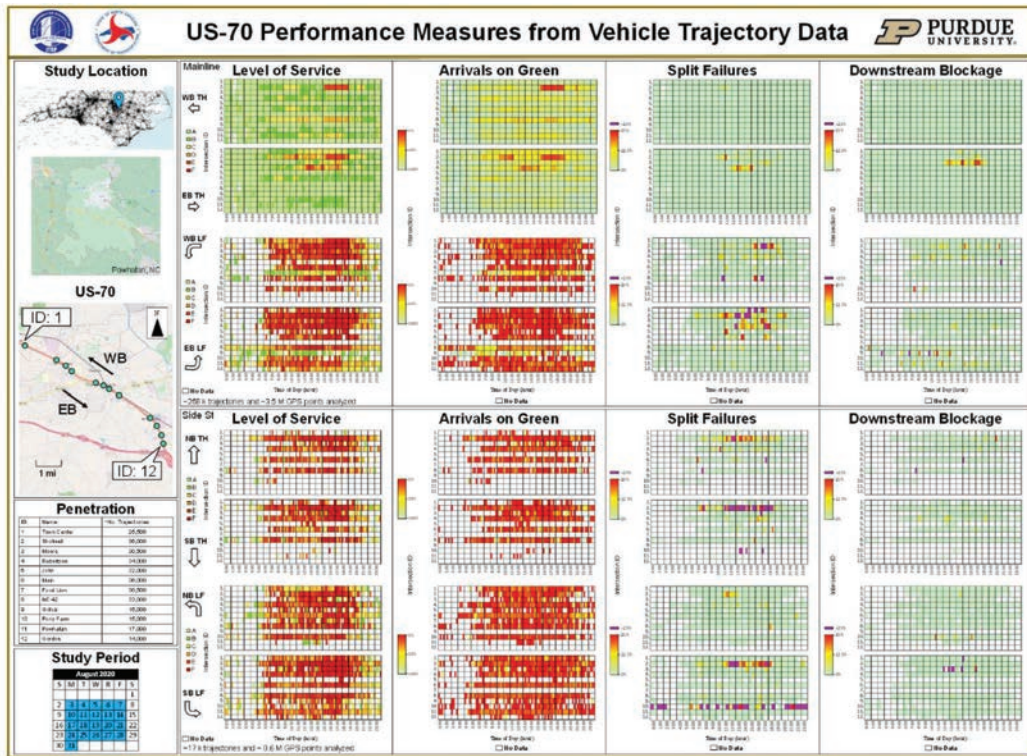


Figure A.7 US-70 in NC between Town Center Blvd. and Gordon Rd.

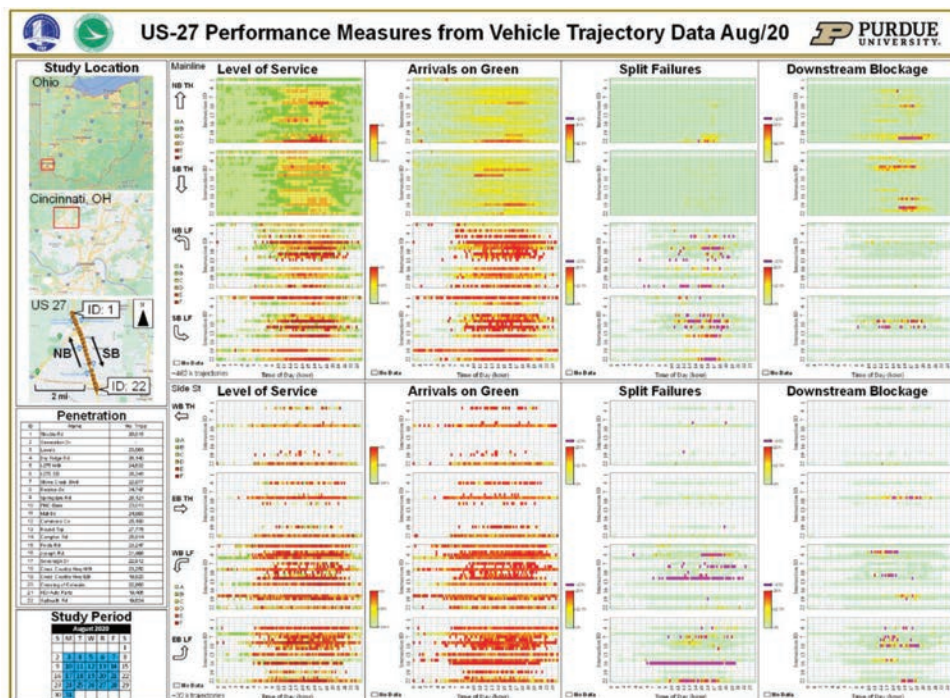


Figure A.8 US-27 in OH before implementing adaptive control (10).

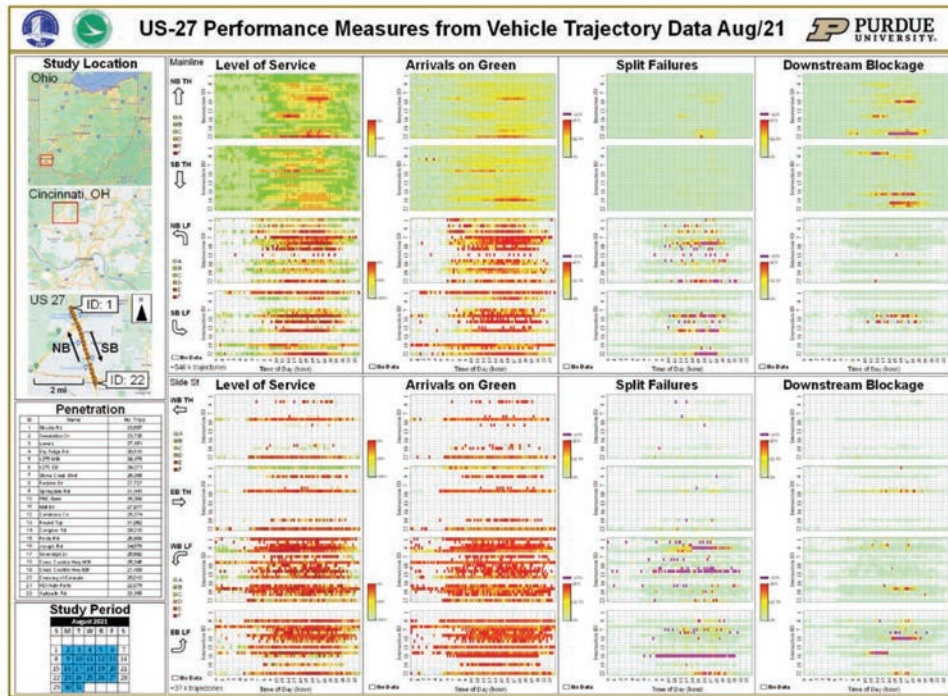


Figure A.9 US-27 in OH running on adaptive control (10).

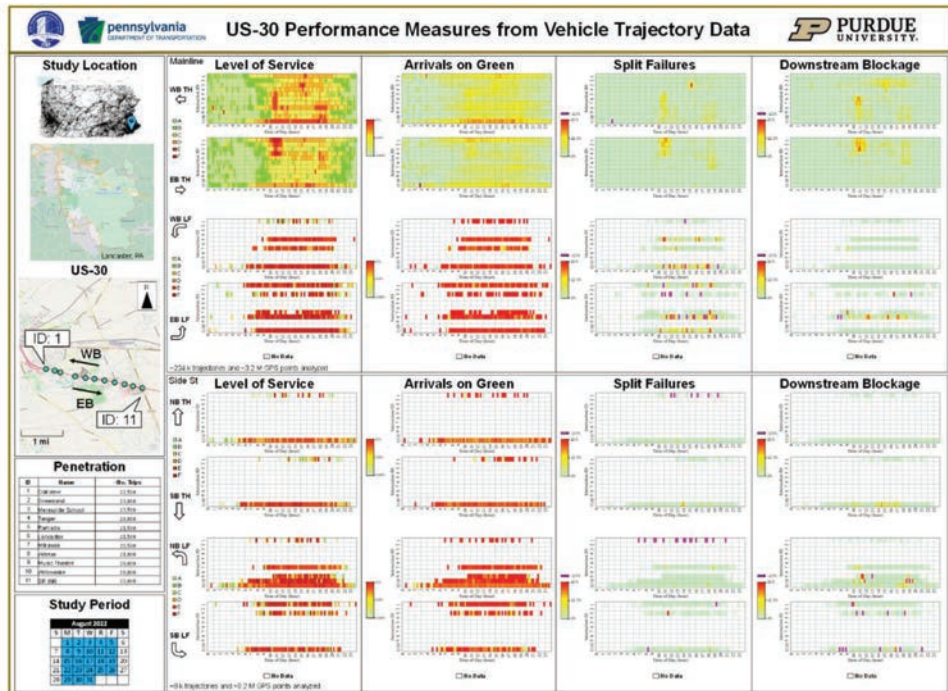


Figure A.10 US-30 in PA between Oakview Rd. and SR-896.

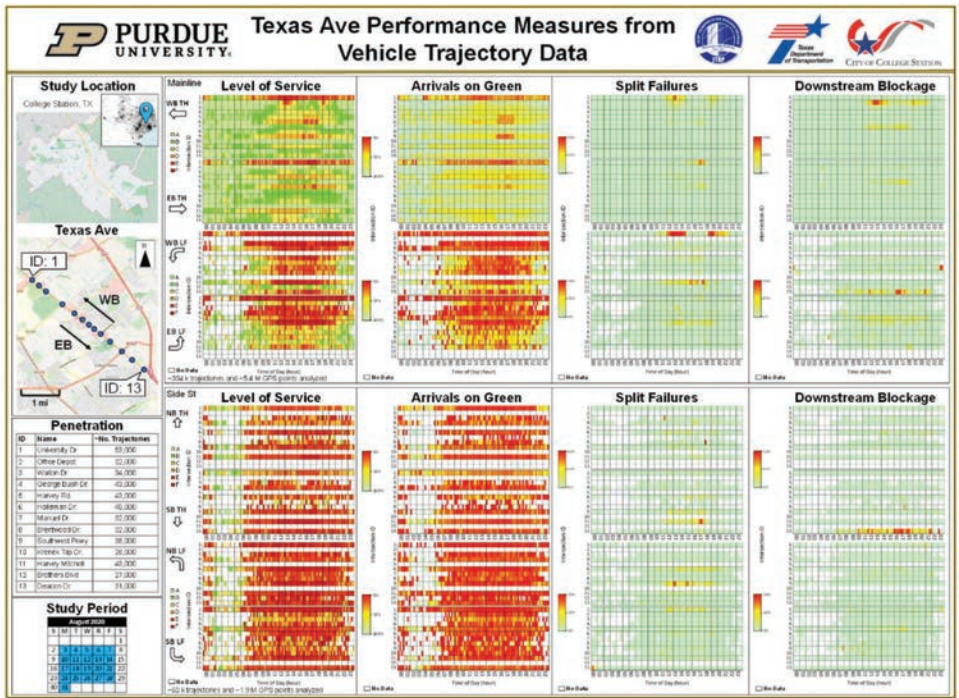


Figure A.11 Texas Ave. in College Station, TX, between University Dr. and Deacon Dr.

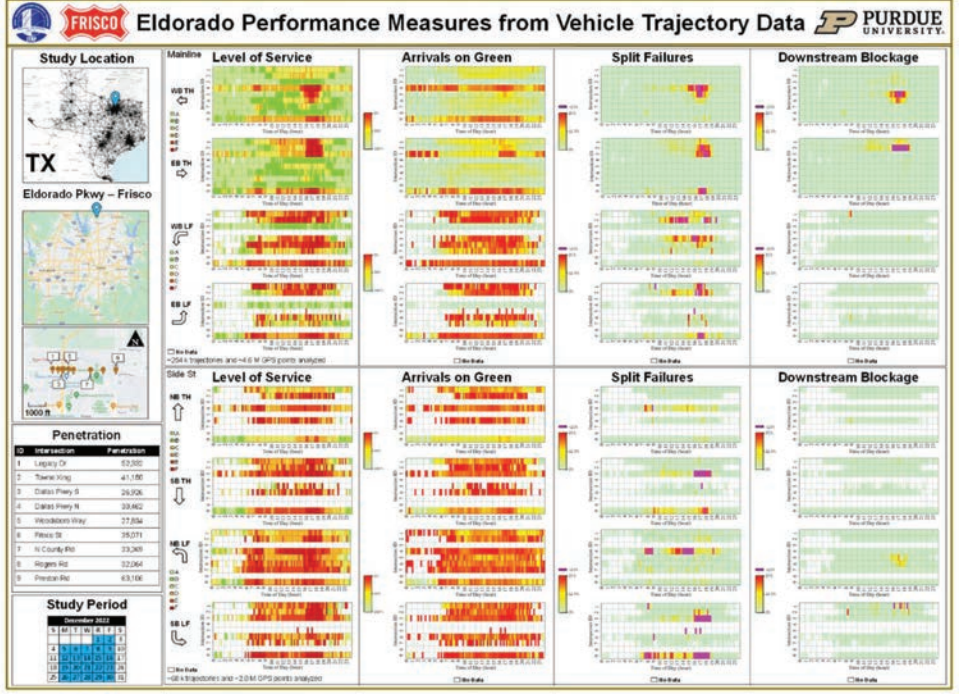


Figure A.12 Eldorado Pkwy. in TX between Legacy Dr. and Preston Dr.

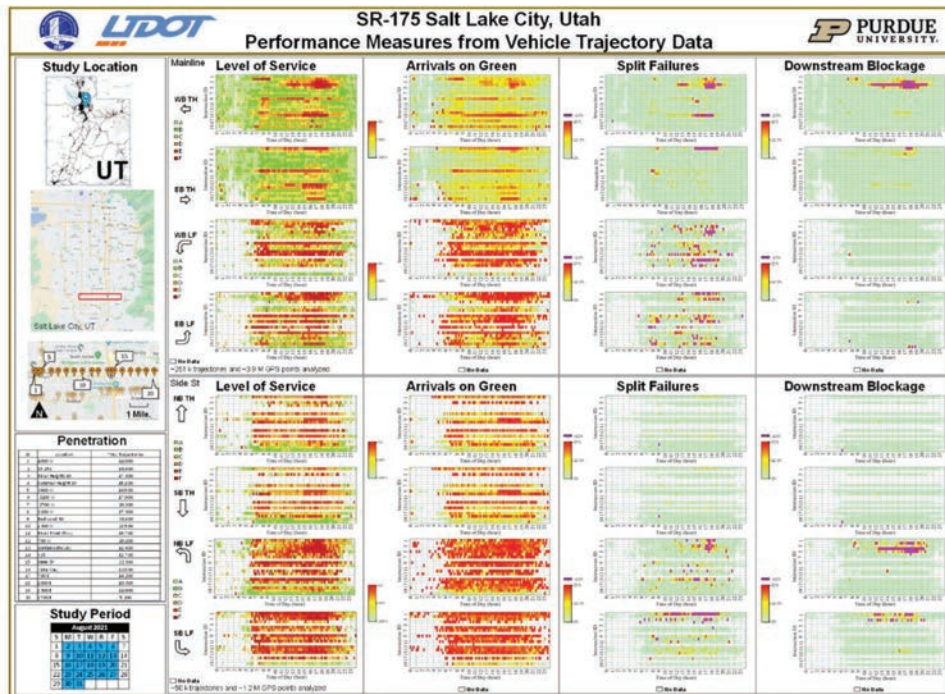


Figure A.13 SR-175 in UT between 4000 W and 1700 E.

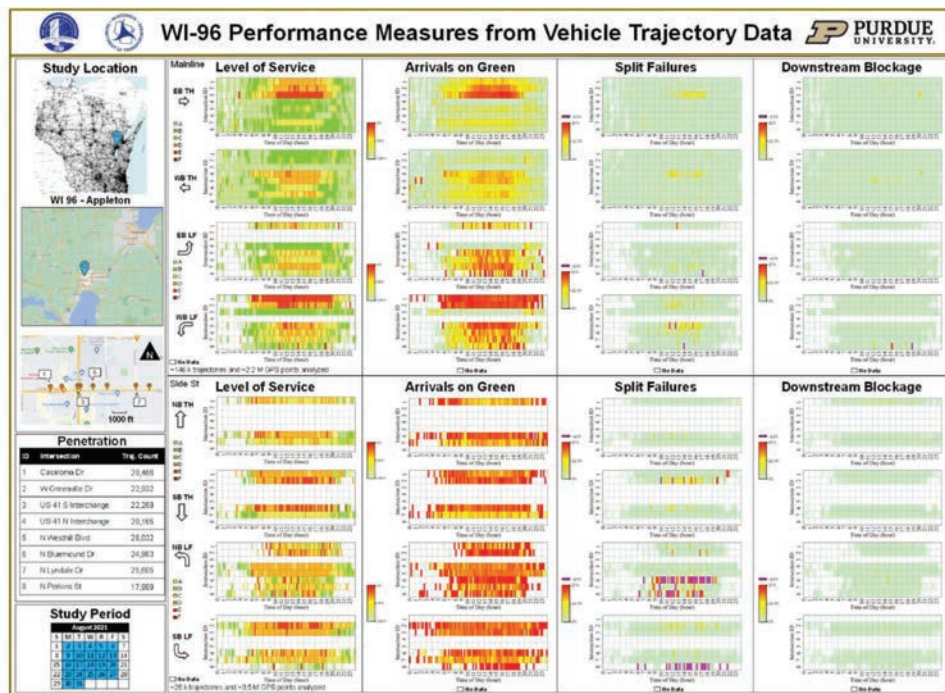


Figure A.14 WI-96 in WI between Casaloma Dr. and N Perkins St.

APPENDIX B. RELEVANT MEDIA

Throughout the development of the project, the team has created diverse visualization materials to explain research concepts, evaluate signal operations, and

better understand traffic conditions. Table B.1 provides a list of some of the most relevant videos produced for the different studies.

TABLE B.1
Relevant media description and access

Description	Video Link	Video QR Code
Travel times of vehicles passing through a roundabout affected by crossing pedestrians.	https://tinyurl.com/roundaboutTravelTimes	
Vehicle experiencing an arrival on green.	https://tinyurl.com/arrivalOnGreen	
Vehicle experiencing an arrival on red.	https://tinyurl.com/arrivalOnRed	
Vehicle experience a split failure.	https://tinyurl.com/splitFailure	
Occurrence of downstream blockage for vehicles proceeding through an upstream intersection.	https://tinyurl.com/downstreamBlockage	
Lack of downstream blockage for vehicles proceeding through an upstream intersection.	https://tinyurl.com/noDownstreamBlockage	

TABLE B.1
(Continued)

Description	Video Link	Video QR Code
LOS based on average control delay at intersections in downtown Indianapolis, Indiana.	https://tinyurl.com/controlDelayIndyDowntown	
LOS based on average control delay at intersections in Indianapolis, Indiana.	https://tinyurl.com/controlDelayIndy	
LOS based on average control delay at intersections in Indiana.	https://tinyurl.com/controlDelayIndiana	
LOS based on average control delay at intersections south of Salt Lake City, Utah.	https://tinyurl.com/controlDelaySaltLakeCity	
LOS based on average control delay at intersections in Charlotte, North Carolina.	https://tinyurl.com/controlDelayCharlotte	
Corridor-wide CV trajectories by time-of-day at SR-37 south of Indianapolis, Indiana.	https://tinyurl.com/corridorWideTrajectories	
Operational conditions at US-421 at W 116th St. before the signal retiming suggested in Chapter 9.	https://tinyurl.com/conditionsBeforeRetiming	

TABLE B.1
(Continued)

Description	Video Link	Video QR Code
Operational conditions at US-421 at W 116th St. after the signal retiming suggested in Chapter 9.	https://tinyurl.com/conditionsAfterRetiming	
LOS based on average control delay at roundabouts in Carmel, Indiana.	https://tinyurl.com/roundaboutControlDelayCarmel	

Project Partners

This work was supported in part by the Joint Transportation Research Program and Pooled Fund Study (TPF-5(377)) led by the Indiana Department of Transportation (INDOT) and supported by the state transportation agencies of California, Connecticut, Georgia, Minnesota, North Carolina, Ohio, Pennsylvania, Texas, Utah, Wisconsin, plus the City of College Station, Texas, and the Federal Highway Administration Operations Technical Services Team.



Mitch Daniels Blvd, West Lafayette, Indiana.

This monograph summarizes advances in traffic signal performance measures derived from commercially available connected vehicle data. The authors also wish to thank the many agencies, practitioners, and colleagues we have collaborated with during the development of the project.

The contents of this report reflect the views of the authors, who are responsible for the facts and the accuracy of the data presented herein, and do not necessarily reflect the official views or policies of the sponsoring organizations. These contents do not constitute a standard, specification, or regulation.

Publication

This report was published in collaboration with the Joint Transportation Research Program and Purdue University. The full content of this technical report is available for download at <https://doi.org/10.5703/1288284317625>.

Open Access and Collaboration with Purdue University

The Indiana legislature established the Joint Highway Research Project in 1937. In 1997, this collaborative venture between the Indiana Department of Transportation and Purdue University was renamed as the Joint Transportation Research Program (JTRP) to reflect state and national efforts to integrate the management and operation of various transportation modes. Since 1937, the JTRP program has published over 1,800 technical reports. In 2006, the JTRP partnered with the Purdue University Libraries to incorporate these technical reports in the University's open access digital repository and to develop production processes for rapidly disseminating new research reports via this repository. Affiliated publications have also been added to the collection. As of 2023, the JTRP collection has over 3.5 million downloads, with some particularly popular reports having over 35,000 downloads.